Quantifying salt marsh resilience to anthropogenic disturbance and climate change:

an integrated field and numerical investigation

Thesis submitted in accordance with the requirements of the University of Liverpool for the degree of

Doctor in Philosophy

by

Natascia Pannozzo

School of Environmental Science

Department of Geography and Planning

June 2023

Declaration

This thesis is the result of my own work and includes nothing which is the outcome of work done in collaboration except where specifically indicated in the text. It has not been previously submitted, in part or whole, to any university or institution for any degree, diploma, or other qualification.

In accordance with The University of Liverpool guidelines, this thesis does not exceed 100,000 words.

Signed: N. Pannozzo

Date: 01.06.2023

Abstract

Salt marshes are significant ecosystems whose survival largely depends upon the equilibrium between sea-level variations and sediment availability. With changing climate and increasing human disturbance influencing sediment transport within intertidal systems, it is unclear whether salt marshes will be able to retain their resilience. This study aims to i) investigate salt marsh resilience to embankment construction and changes in sea-level and storm activity and ii) develop a new luminescence-based approach, which is independent of stratigraphy and sediment composition, for the detection of storm activity across intertidal environments. The Ribble Estuary, North-West England, was used as a test case and the response of the system to embankment construction, sea-level rise and storm activity was investigated using an integration of numerical modelling and field analyses (paleoenvironmental reconstruction and monitoring). Results showed that the construction of embankments along an estuary shoreline can promote ebb dominance in the intertidal system and intensify sediment export, threatening marsh accretion, although this is negligible in a system characterised by high rates of marine sediment supply. Sea-level rise can also threaten estuary and marsh stability by promoting ebb dominance and triggering sediment export, but an increase in storm intensity has the potential to counteract the decrease in sediment budget caused by sea-level rise by promoting flood dominance and triggering sediment import. However, while storms enhance salt marsh vertical accretion, especially benefitting the marsh interior, the majority of the storm sediment supplied to the salt marsh platform are generated by an increase in erosion and resuspension of mudflat and tidal creek sediments, with implications for marsh lateral retreat. Results also demonstrated that luminescence signals of K-feldspar can diagnose differential modes of deposition across intertidal settings and can, therefore, successfully detect storm activity across intertidal environments. Overall, this study offers new perspectives and tools that can benefit both coastal research development and coastal management.

Acknowledgements

I would like to acknowledge the support of the School of Environmental Sciences, University of Liverpool, which funded my PhD project and my supervisors Prof. Nicoletta Leonardi, Dr. Rachel Smedley and Dr. Iacopo Carnacina for guiding me during my PhD journey. I also would like to acknowledge the EPRSC for supporting the supervision of Prof. Nicoletta Leonardi (EP/V056042/1), the RGS-IBG for funding part of the field campaign and laboratory measurements (project titled ‘Building coastal resilience one sediment grain at the time: field measurements and community engagement on nature-based solutions for coastal protection’, PI Prof. Nicoletta Leonardi, RGS-IBG Environment and Sustainability Research Grant), the Liverpool luminescence laboratory (managed by Dr. Rachel Smedley) for allowing me to perform the luminescence analyses, and all the organisations that have funded my attendance to conferences which allowed me to present this work to the scientific community (Liverpool luminescence laboratory, BSG, QRA and IGCP639). I further would like to acknowledge the RSPB for allowing the field work campaign in the Ribble Estuary, the Physical Geography and luminescence laboratories and their technicians and students (Jennifer Bradley, Luke Glascott, Mike O’Connor, Joshua Hicks, Richard Clark, Grace Skirrow and Molly Spater) for their support with equipment, field work and laboratory analyses, Dr. Xiaorong Li who developed the original model for the Ribble Estuary as part of the projects ‘Adaptation and Resilience of Coastal Energy Supply (ARCoES)’ and ‘Physical and biological dynamic coastal processes and their role in coastal recovery (BLUE-coast)’, Prof. Richard Chiverrell and Prof. Andy Plater for their contributions to two of the thesis chapters, and all the editors, anonymous reviewers and colleagues that have helped me improve my work.

Table of Contents

List of Figures

List of Tables

Thesis structure

Chapter 1. Investigating salt marsh resilience: background and rationale

Chapter 1 outlines the context and motivation behind this study as well as the main research goals. First, the ecosystem services provided by salt marshes are reviewed. Then, the importance of sediment availability for salt marsh survival and the contribution of tides to sediment supply are evaluated. Lastly, the climate and anthropogenic forcings that influence salt marsh stability and the current rate of salt marsh loss are examined, identifying the gaps in the current state of knowledge that defined the thesis aims.

Authors' contribution:

N. Pannozzo: principal investigator and author, conceptualisation and figures production.

Chapter 2. Study site and methodological approach

Chapter 2 outlines the rationale behind the choice of the Ribble Estuary as case study and the combination of numerical modelling and field analyses as a methodological approach. The practical and scientific reasons behind the choice of the study site are first outlined. Then, the benefits of using numerical modelling in integration with field analyses are evaluated for the study of estuary and marsh response to climate forcings and anthropogenic disturbance at multiple spatial and temporal scales. Lastly, a review of the main features of the numerical model used (Delft3D) and the field techniques implemented (geochemical, particle size and luminescence analyses) is provided.

Authors' contribution:

N. Pannozzo: principal investigator and author, conceptualisation and figures production.

Chapter 3. An integration of numerical modelling and paleoenvironmental analysis reveals the effects of embankment construction on long-term salt marsh accretion

Published paper: Pannozzo, N., Smedley, R.K., Chiverrell, R.C., Carnacina, I., Leonardi, N., 2022. Journal of Geophysical Research: Earth Surface, 127, e2021JF006524. https://doi.org/10.1029/2021JF006524

Chapter 3 uses an integration of numerical modelling and paleoenvironmental analyses to investigate the contribution of embankment construction to long-term salt marsh accretion. Accretion rates derived using optically stimulated luminescence (OSL) dating are combined with a multi-proxy paleoenvironmental investigation on sediment cores extracted from Hesketh Out Marsh, the mobile seafloor of the central Irish Sea and the Ribble catchment area. The paleoenvironmental analyses are then compared to simulations conducted using the hydrodynamic model Delft3D to investigate the effects of embankment construction on the estuary hydrodynamics and morphodynamics over the period constrained by the OSL dating.

The model-data integration shows that embankments are responsible for an overall intensification of the ebb currents in the system which promotes sediment export, although this did not compromise the long-term resilience of the Ribble marshes because of the high rates of marine sediment supply and the 60 years of river dredging, which enhanced the flood dominance of the tide near the tidal flat.

Authors' contribution:

N. Pannozzo: principal investigator and author, conceptualisation, field/laboratory analysis, model setup, data processing and analysis, and figures production.

R. K. Smedley: conceptualisation, investigation, manuscript development, and advice on experimental design, field/laboratory analysis, data processing and analysis and figures production.

R. C. Chiverrell: investigation, provision of the Irish Sea cores, manuscript development, and advice on experimental design, field/laboratory analysis, data processing and analysis and figures production.

I. Carnacina: conceptualisation, investigation, manuscript development, and advice on experimental design, model setup, data processing and analysis, and figures production.

N. Leonardi: conceptualisation, investigation, provision of the original Ribble model, and advice on experimental design, model setup, data processing and analysis, and figures production.

Chapter 4. Salt marsh resilience to sea-level rise and increased storm intensity

Published paper: Pannozzo, N., Leonardi, N., Carnacina, I., Smedley, R.K., 2021. Geomorphology, 389 (4), 107825. https://doi.org/10.1016/j.geomorph.2021.107825

Chapter 4 uses numerical modelling to investigate salt marsh resilience under the combined impact of sea-level rise and increased storm intensity. The hydrodynamic model Delft3D is employed to explore the change in estuary and marsh sediment budget under various simulated storm surge and sea-level scenarios.

The analysis shows that storm surges can positively contribute to the resilience of the marsh and estuarine system by promoting flood dominance and triggering a net import of sediment, while sea-level rise can threaten the stability of the salt marsh and the estuary by promoting ebb dominance and triggering a net export of sediment. Results also show that storm surges have a general tendency to counteract the decrease in sediment budget caused by sea-level rise.

Authors' contribution:

N. Pannozzo: principal investigator and author, conceptualisation, model setup, data processing and analysis, and figures production.

N. Leonardi: conceptualisation, investigation, provision of the original Ribble model, and advice on experimental design, model setup, data processing and analysis, and figures production.

I. Carnacina: investigation, manuscript development, and advice on experimental design, model setup, data processing and analysis, and figures production.

R. K. Smedley: investigation, manuscript development, and advice on experimental design, data processing and analysis and figures production.

Chapter 5. Storm sediment contribution to salt marsh accretion and expansion

Published paper: Pannozzo, N., Leonardi, N., Carnacina, I., Smedley, R.K., 2022. Geomorphology, 108670. https://doi.org/10.1016/j.geomorph.2023.108670

Chapter 5 uses field analyses from an eight-month field campaign to understand the influence of storms on the sediment supply to different marsh areas and whether storms can deliver new material onto the salt marsh platform, which would otherwise not be sourced in fair-weather conditions.

Field data from sediment traps indicates that storm activity causes an increase in inorganic sediment supply to the whole salt marsh platform, especially benefitting the marsh interior. Furthermore, the majority of the sediment supplied to the salt marsh platform during the stormy periods results to be generated by an increase in erosion and resuspension of mudflat and tidal creek sediments, while only a minimal contribution is given by the sediments transported from outside the intertidal system. This suggests that, in the long term, storms will promote salt marsh vertical accretion but might simultaneously reduce the overall larger-scale sediment availability with implications for the marsh lateral retreat.

Authors' contribution:

N. Pannozzo: principal investigator and author, conceptualisation, field/laboratory analysis, data processing and analysis, and figures production.

N. Leonardi: conceptualisation, investigation, and advice on experimental design, field/laboratory analysis, data processing and analysis, and figures production.

I. Carnacina: investigation, manuscript development, and advice on experimental design, data processing and analysis, and figures production.

R. K. Smedley: investigation, manuscript development, and advice on experimental design, data processing and analysis and figures production.

Chapter 6. Novel luminescence diagnosis of storm deposition across intertidal environments

Published paper: Pannozzo, N., Smedley, R.K., Plater, A.J., Carnacina, I. Leonardi, N., 2023. Science of the Total Environment, 867, 161461. https://doi.org/10.1016/j.scitotenv.2023.161461

Chapter 6 explores the use of luminescence approaches to detect storm deposition across intertidal environments. Sediment cores collected from the salt marsh are used to test whether luminescence properties of sand-sized K-feldspar grains could diagnose the differential modes of deposition across intertidal settings (i.e., sandflat, mudflat and salt marsh) in the longer-term sediment records by detecting the variability in sediment bleaching potential between settings (i.e., sediment exposure to sunlight), thus establishing a framework for the interpretation of luminescence properties of intertidal sediments. Modern sediment samples collected before and after a storm event are then used to test whether such properties could diagnose changes in sediment processing (i.e., bleaching potential) of mudflat sediments caused by storm activity, despite no changes in sediment composition being recorded by geochemical and particle size distribution analyses.

The analysis shows that luminescence can diagnose the differential modes of deposition across intertidal settings and can, therefore, successfully detect storm deposits across intertidal environments providing a new approach that can be applied to longer-term sediment records to reveal (and date) changes in the environment of deposition and/or depositional dynamics where there is no obvious stratigraphic evidence of such.

Authors' contribution:

N. Pannozzo: principal investigator and author, conceptualisation, field/laboratory analysis, data processing and analysis, and figures production.

R. K. Smedley: conceptualisation, investigation, manuscript development, and advice on experimental design, field/laboratory analysis, data processing and analysis and figures production.

A. J. Plater: investigation, manuscript development, and advice on experimental design, data processing and analysis and figures production.

I. Carnacina: investigation, manuscript development, and advice on experimental design, data processing and analysis, and figures production.

N. Leonardi: investigation, manuscript development, and advice on experimental design, data processing and analysis, and figures production.

Chapter 7. Conclusions

Chapter 7 summarises the key findings of this study and identifies the implications of such findings. After outlining the advances that this study made both in the understanding of salt marsh responses to climate forcings and anthropogenic disturbance and in the development of new tools that can help to more accurately unravel how climate forcings drive coastal change, the implications of these findings are evaluated in the light of scientific advances needed in the research of coastal processes and essential information required for the assessment of coastal management measures.

Authors’ contribution:

N. Pannozzo: principal investigator and author, conceptualisation and figures production.

Chapter 1

Investigating salt marsh resilience: background and rationale

1.1 Salt marsh functioning

Salt marshes are vegetated wetlands, typical of mid and high latitudes (mangroves are their tropical counterpart), distributed within the upper intertidal zone of low-energy shorelines, such as estuaries, deltas, bays and lagoons (Townend et al., 2011). They and are found on every continent with the exception of Antarctica (Figure 1 a; Mcowen et al., 2017), including some of the most populated coastlines (Figure 1 b; NASA, 2020). Salt marshes developed through the Holocene, owed to a deceleration in relative sea-level rise that allowed the infilling of low-energy coastal zones with marine and riverine sediments (Engelhart and Horton, 2012). It is estimated that the current worldwide extension of marshland could reach ca. 40 Mha (Pendleton et al. 2012), although only 5,495,089 hectares in 43 countries have been mapped so far (Mcowen et al., 2017).

Salt marshes develop when tidal flats, formed through the infilling of accommodation spaces, reach a threshold elevation relative to sea level that allows vegetation growth (Figure 2 a; Morris et al., 2002). Tidal flats increase in elevation through the delivery of fine sediments from rivers and the sea, which are transported over the intertidal platform during flood tide (Figures 3 and 5; Reed, 1990). Once vegetation colonises the tidal flats (Figure 2 b), it supports marsh growth and stability through organogenic production, particle capture by plant stems, and enhanced particle settling caused by a reduction in turbulent kinetic energy of the water flow through the plant canopy (Morris et al. 2002; Neumeier and Ciavola, 2004; Mudd et al., 2010). As the vegetated platform continues to accrete vertically and expand horizontally, marsh portions with higher elevation start experiencing shorter and less frequent inundation, leading to a succession from pioneer marshes, which are characterised by low elevations and populated by macrophytes and aquatic fauna, through to mature marshes, which are characterised by high elevations and populated by halophytic shrubs and terrestrial fauna, generating a wide range of habitats (Figure 2 c; Bertness et al., 2002; Pratolongo et al., 2019).

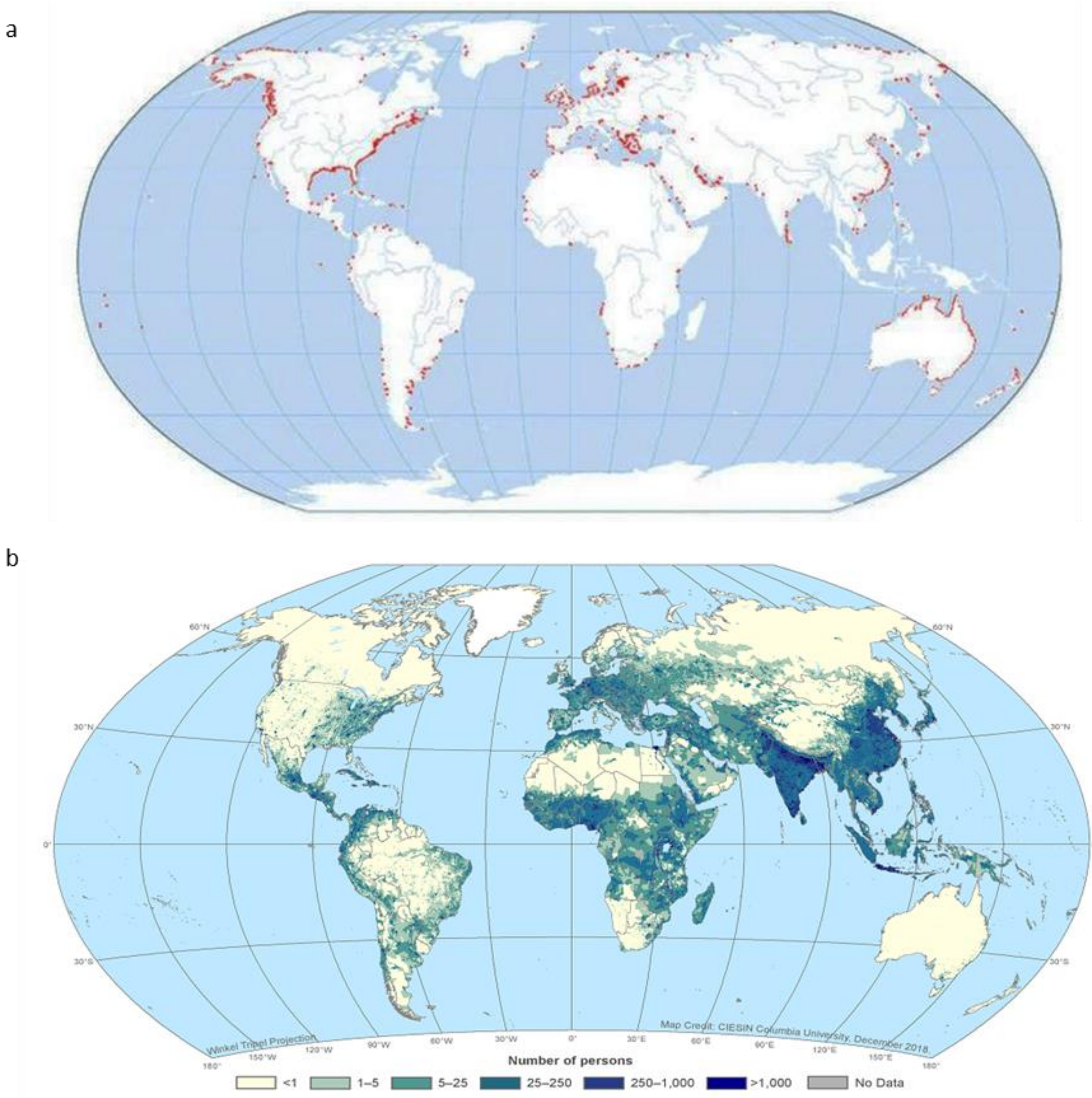

Figure 1. Maps of the worldwide salt marsh (© Mcowen et al., 2017) (a) and human population (© NASA, 2020) (b) distributions.

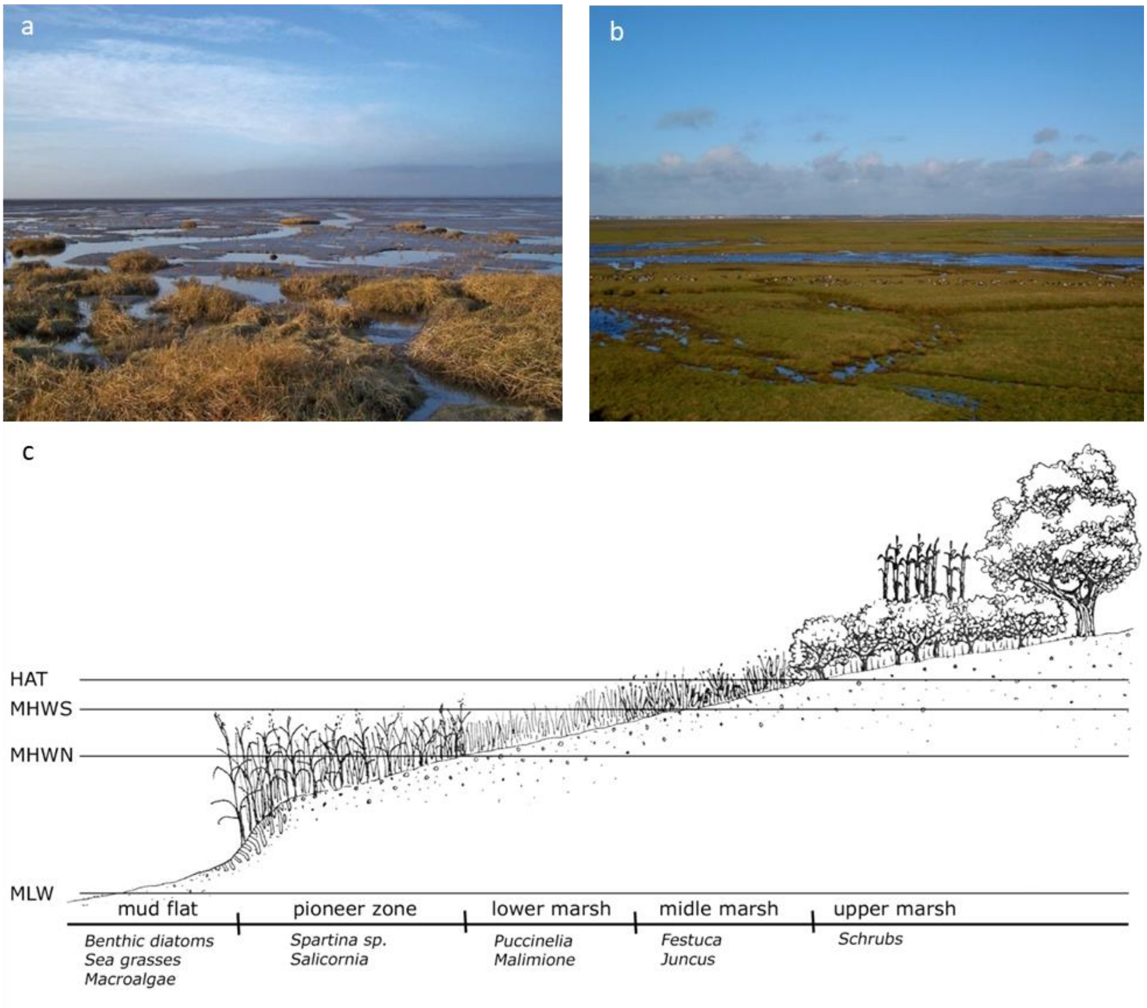

Figure 2. Photos showing salt marsh formation (a) and maturing salt marsh (b) at Hesketh Bank (Ribble Estuary, UK) and diagram showing salt marsh zonation (© Bertness et al., 2002) (c).

The high levels of primary productivity that characterise salt marsh vegetation also allow nutrient removal and high rates of carbon sequestration at geological time scales (Zedler and Kercher, 2005; Barbier et al., 2011). Salt marshes also have the ability to buffer storm surges and waves - as vegetation increases the surface roughness, increasing the frictional drag and slowing down the water flow - and to stabilise sediments through the binding action of plant roots, thus protecting the coastline against flooding and erosion (Möller et al. 1999; Feagin et al., 2009).

1.2 The importance of sediment availability for marsh survival

Being located at the land-sea interface, salt marsh survival largely depends on the equilibrium between sea-level variations and sediment availability (Mariotti and Carr, 2014; Ma et al., 2014; Mitchell et al., 2017). Salt marshes are generally resilient to sea-level rise when sediment supply and organogenic production are high enough to allow salt marshes to accrete and expand at the same pace as sea-level rise (Kirwan et al., 2010). Sediment supply to the salt marsh platform primarily depends on the availability of suspended sediment concentrations within the intertidal zone (Temmerman et al., 2004; Kirwan et al., 2010; Willemsen et al., 2021). The availability of suspended sediment in the water column is controlled by current velocities and wave energy, responsible for sediment resuspension (Figure 3; Rose and Thorne, 2001; Zhang et al., 2019). According to Kirwan et al. (2010), the amount of suspended sediment concentrations available within the intertidal area has to be at least ~20 mg/L to allow marsh survival under current rate of sea-level rise. Currents and waves are also responsible for sediment transport across the intertidal system and for the sediment supply to the salt marsh platform (Figure 3; Rose and Thorne, 2001; Zhang et al., 2019). Sediment deposition is positively correlated with duration and frequency of tidal inundation (i.e. hydroperiod) (Reed, 1990); the capacity of salt marsh surfaces to trap these sediments, however, depends on the age of the marsh, with young low marsh surfaces trapping sediments at a high rate until they reach an equilibrium level with mean high water, whereas high old marsh surfaces accrete at a slower rate comparable to the rate of sea-level rise (Temmermann et al., 2004).

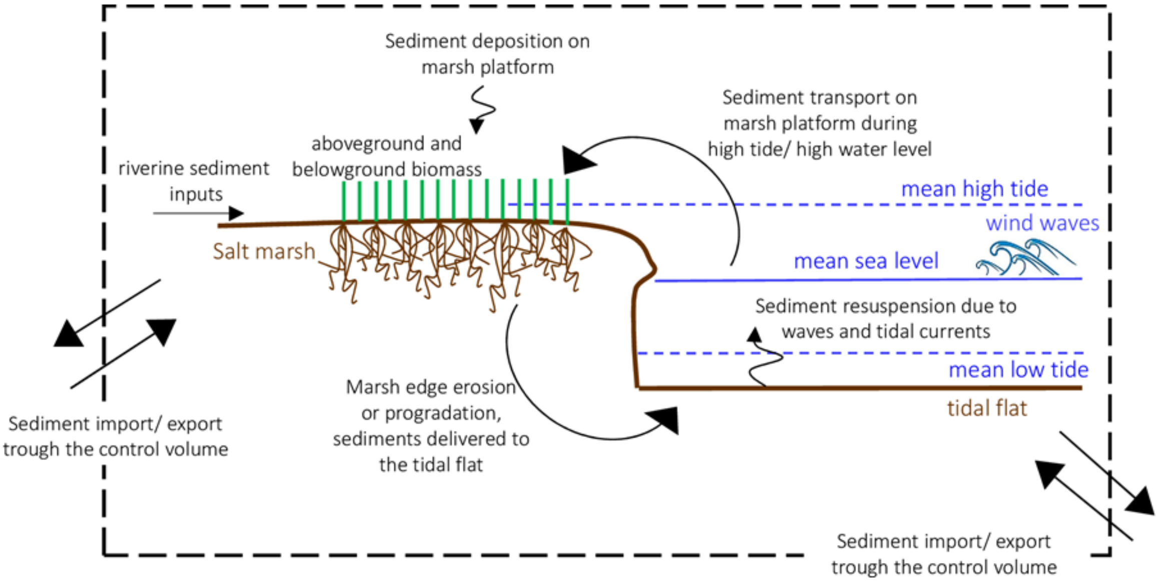

Figure 3. Diagram showing marine and riverine sediment inputs to an intertidal system and the contribution of waves and tidal currents to sediment resuspension from the tidal flat and transport over the salt marsh platform (© Leonardi et al., 2018).

1.3 Tides contribution to sediment supply

As sediments are delivered to salt marsh platforms during flood tide, the amount of sediment that can reach salt marshes depends on the quantity of sediment entering and exiting the system during each tidal cycle (Guo et al., 2016; Palazzoli et al., 2020). Sediment transport within intertidal systems is primarily influenced by tidal asymmetry and distortion. When there is a flood dominance (flood phase shorter and more intense than ebb phase), flood velocities are sufficiently high to resuspend sediment and promote landward sediment import while, in the case of ebb dominance (ebb phase shorter and more intense than flood phase), ebb velocities transport suspended sediment out of the systems enhancing sediment export (Van Dongeren and de Vriend, 1994; Lanzoni and Seminara, 2002).

The distortion and asymmetry of a tidal signal are usually analysed using the principal lunar semi-diurnal constituent M2, which is the dominant astronomical tidal constituent, and the largest shallow water constituent M4, which is the pure second harmonic (or overtide) of the constituent M2 that forms in shallow water due to non-linear processes (Friedrichs and Aubrey, 1988; Blanton et al., 2002). The distortion is calculated using the ratio $A_{4-2}=A_{M4}/A_{M2}$ where A is the amplitude of the tidal height and the asymmetry is calculated using the relationship $\Delta\theta=2\theta_{M2}-\theta_{M4}$ where θ is the phase of the tidal height (Friedrichs and Aubrey, 1988; Blanton et al., 2002). When Δθ is between 0° and 180° the flood phase dominates, whereas when it is between 180° and 360° the ebb phase dominates; the magnitude of A_{4-2} is representative of the significance of the dominance (Figures 4 a, b; Friedrichs and Aubrey, 1988).

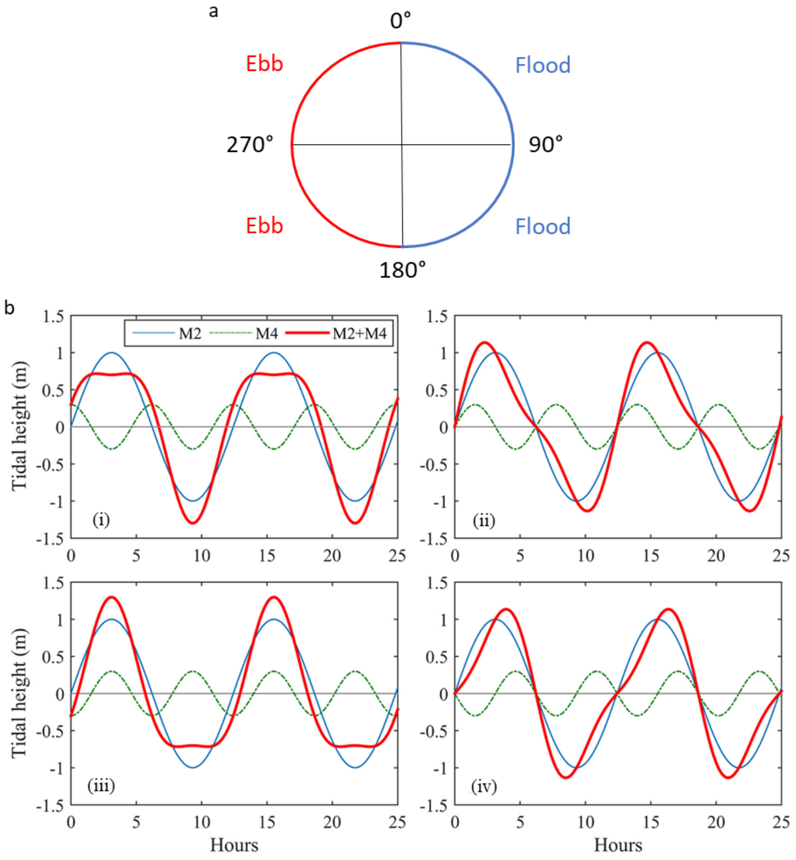

Figure 4. Diagram showing flood and ebb dominance with respect to the phase difference $\Delta\theta=2\theta_{M2}-\theta_{M4}$ (i.e. tidal asymmetry - when Δθ is between 0° and 180° the flood phase dominates, whereas when it is between 180° and 360° the ebb phase dominates) (a); graph showing the height of the principal lunar semi-diurnal constituent M2, the largest shallow water constituent M4, and M2+M4 with a phase difference $\Delta\theta=2\theta_{M2}-\theta_{M4}$ of 0° (i), 90° (ii), 180° (iii) and 270° (iv) and an amplitude ratio $A_{4-2}=A_{M4}/A_{M2}$ of 0.3 (© Guo et al., 2016) (b).

1.4 Climate forcings and anthropogenic activities influencing salt marsh stability

Encroachment and survival of salt marshes are only possible if marsh vertical accretion and lateral expansion can keep pace with sea-level rise (Mariotti and Carr, 2014; Ma et al., 2014; Mitchell et al., 2017). Vertical accretion and lateral expansion are determined by sediment supply and organogenic production (Kirwan et al., 2010, 2016; Donatelli et al., 2020), but sediment supply to marsh platforms is affected by several external forcings, which can either enhance marsh stability or threaten it (Figure 5).

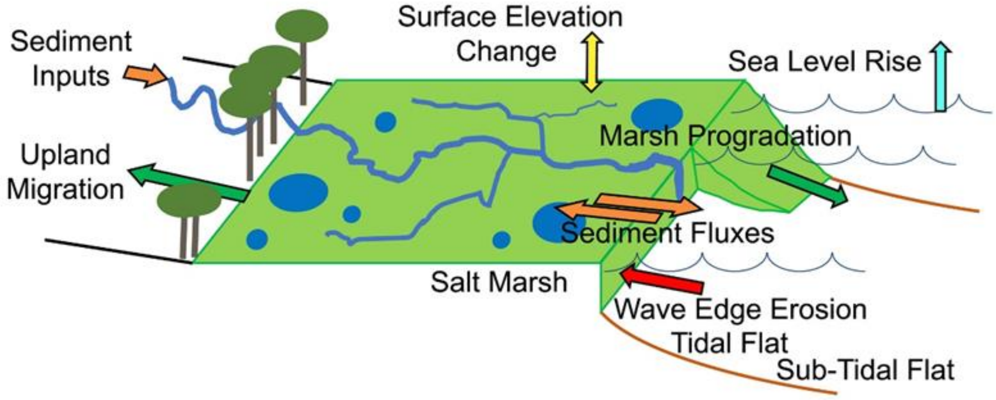

Figure 5. Diagram showing marine and riverine sediment inputs to an intertidal system, salt marsh advance, retreat and change in elevation, and the influence of sea-level rise and wind waves on such processes (© Fagherazzi et al., 2020).

Increasing rates of sea-level rise (Figure 6; Masson-Delmotte et al., 2018) can lead to marsh drowning and lateral retreat, as sea-level rise creates new accommodation space, increasing the amount of sediment input required to guarantee marsh stability (FitzGerald et al., 2008; Kirwan et al., 2010; Ganju et al., 2017; Leonardi et al., 2018; Fagherazzi et al., 2020), and, in some locations, promotes near-shore ebb dominance, enhancing sediment export from the intertidal system (Carrasco et al., 2018; Zhang et al., 2020). Wind waves triggered by storms can also threaten marsh stability as wave overtopping is responsible for erosion of the marsh scarp, which in the long-term causes the collapse of the marsh platform edge (Marani et al., 2011; Fagherazzi et al., 2013; Leonardi and Fagherazzi, 2014; Leonardi et al., 2016; Leonardi et al., 2018; Li et al., 2019). However, while some studies have shown that storm waves can contribute to marsh erosion, others have observed that storm waves can resuspend sediments from the seabed, which can then be transported into the estuarine system by tidal currents, thus contributing to sediment supply to the salt marsh (Fernández-Mora et al., 2015; Brooks et al., 2017). Furthermore, there is evidence that overwash by storm surges delivers considerable amount of sediments to marsh platforms, supporting marsh growth (Turner et al., 2006; Walters and Kirwan, 2016; Castagno et al., 2018) and potentially contributing to salt marsh resilience to sea-level rise (Schuerch et al., 2013).

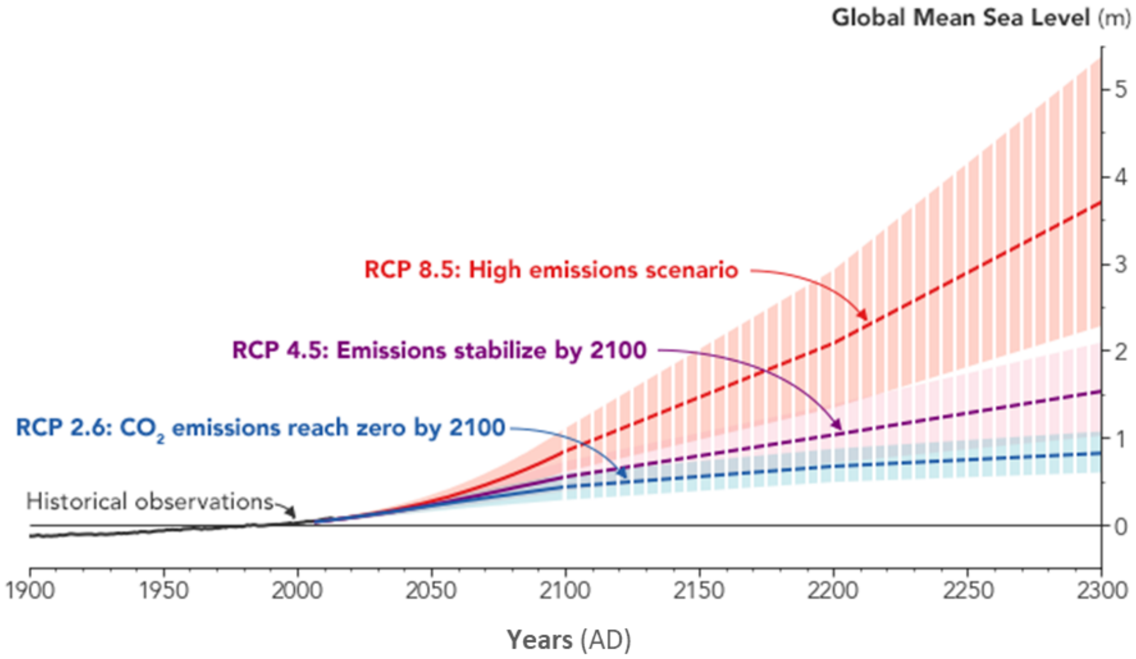

Figure 6. Projections of mean sea level change relative to 1900 according to different emission scenarios (© Masson-Delmotte et al., 2018).

Anthropogenic activities that interfere with sediment supply to the coast can also have an impact on salt marsh resilience. For instance, in coastal systems where sediment input is predominantly riverine, the vulnerability of salt marshes to increasing sea levels is further exacerbated by river dredging and damming, which cause a shortage of seawards sediment supply (Ganju et al., 2017; Donatelli et al., 2018). Sea defences have also the potential to affect sediment supply to marsh platforms. When salt marshes and tidal flats are embanked, tidal inundation is prevented or reduced, thus limiting the amount of marine sediment that can reach the marsh platform (e.g., Kiesel et al., 2020; Kiesel et al., 2022). Furthermore, several studies around the world have observed that the presence of embankments along an estuary alters tide propagation (e.g., Pelling et al., 2013; Holleman and Stacey, 2014; Carless et al., 2016), therefore changing the sediment transport dynamics within an intertidal system (Guo et al., 2016; Palazzoli et al., 2020). Consequently, in systems which are largely filled with marine sediments, the implementation of sea defences could either aggravate marsh vulnerability by enhancing sediment export or support marsh growth by promoting the infilling of intertidal areas (Van Dongeren and de Vriend, 1994; Lanzoni and Seminara, 2002). Similarly, other coastal management interventions that change the geometry of the intertidal basin (e.g., dredging) can affect tidal asymmetry (Zhu et al. 2015; Van Maren et al. 2015), hence sediment supply to salt marsh platforms (Donatelli et al., 2020). Ultimately, direct alteration of salt marsh morphology (e.g., construction of ditches for drainage purposes), can change the natural hydrodynamics of salt marshes, affecting marsh platforms elevation, with consequences also for habitats zonation (Tonjes et al., 2013). Indeed, extensive salt marsh areas have been lost in the last centuries due to a combination of anthropogenic activities and sea-level rise (e.g., Bakker et al., 1993; Kennish et al., 2001).

Due to their recognised ecological and economic value, numerous projects around the world have been conducted to create new salt marshes and/or restore lost salt marshes to provide long-term and low-cost coastal protection while preserving ecological productivity and contributing to achieving net-zero goals (Temmerman et al., 2013). Nevertheless, despite the global effort in protecting these ecosystems, increasing rates of salt marsh loss have been recorded worldwide, with 1,453 km^2 lost globally only over the last 20 years (Campbell et al., 2022).

1.5 Research gaps and thesis aims

Despite the numerous insightful studies investigating the impact of climate forcings and anthropogenic disturbance on salt marsh dynamics, there are still many uncertainties over the extent to which these forcings affect long-term salt marsh resilience (Fagherazzi et al., 2020).

G1. First of all, the impact of coastal management interventions (e.g., embankment construction, dredging) on marine sediment supply to salt marsh platforms is still very poorly understood. In fact, while the effects of these activities on tidal propagation have been widely observed, there is yet a lack of studies investigating how the changes in tidal dynamics caused by such interventions affect salt marsh sediment budget and whether they are significant enough to affect long-term salt marsh stability. Due to the popular employment of hard sea defences for the protection of coastal areas (Floerl et al., 2021), it is especially necessary to understand the effects of embankment construction on salt marsh accretion.

G2. Secondly, although the separate effects of storms and sea-level rise on salt marsh stability have been widely investigated, few studies have explored the combined impact of changing storm activity and sea-level rise on the sediment budget of a salt marsh and their combined effect on sediment transport within an intertidal system has yet not been discussed (e.g., Schuerch et al., 2013). Hence, a comprehensive view on the extent to which storms can counteract the impact of sea-level rise on salt-marsh accretion is still missing.

G3. There are then uncertainties on the degree to which storms contribute sediments to different areas of marsh platforms (e.g., outer marsh vs marsh interior) and on the sediment sources that storms draw on (e.g., offshore vs nearshore). Indeed, although the hydrodynamics influence on sediment supply to different areas of marsh platforms is well understood (Rose and Thorne, 2001; Zhang et al., 2019), the extent to which storms can affect suspended sediment availability across salt marshes is still unknown. Nonetheless, determining how storm sediment supply affects different areas of the marsh platform is crucial for understanding to what extent salt marsh vertical accretion can benefit from storm activity (Reed et al., 1990; Roberts and Plater, 2005). Determining the provenance of sediments supplied by storms, instead, allows to understand whether storms can also benefit marsh lateral expansion (Mariotti and Fagherazzi, 2013; Fagherazzi et al., 2013) by delivering to the marsh platform sediments from outside the intertidal system (Cahoon et al., 1995) or whether they can further reduce the overall sediment availability to the salt marsh (Roner et al., 2021) by enhancing the erosion of the adjacent mudflats and tidal creeks (Grant et al., 1997; Wesselman et al., 2017; Brooks et al., 2017). However, the few studies that have explored storm sediment provenance provide inconsistent results (e.g., Cahoon et al., 1995; Grant et al., 1997; Wesselman et al., 2017; Brooks et al., 2017).

G4. A further issue is represented by the shortage of long-term data which are necessary for validating and informing long-term modelling studies upon which the assessment coastal management measures rely (Capotondi et al., 2019). While numerous long-term records of human activity and sea level derived from well-established proxies are available from around the world (e.g., Lepofsky et al., 1996; Stefani and Vincenzi, 2005; Engelhart et al., 2011; Shennan et al., 2018), there are still inconsistencies in long-term storm activity records, as traditional paleoenvironmental techniques rely on abrupt changes in stratigraphy and composition for the reconstruction of extreme events, which do not always occur during storm activity (Grant et al., 1997; Wesselman et al., 2017; Brooks et al., 2017). Nevertheless, several studies have outlined how storm frequency needs to be considered when investigating storm contribution to long-term salt marsh resilience (e.g., McCloskey and Liu, 2012; Schuerch et al., 2013; Walters and Kirwan, 2016; Bianchette et al., 2022); hence, it is a fundamental goal to provide a new approach to diagnosing storm activity in the geological record that does not rely solely upon a change in sediment composition and stratigraphy.

To address these knowledge gaps, this study aims to:

i) better understand salt marsh resilience to changes in climate forcings and sea defences implementation, by

O1. investigating the effects of embankment construction on long-term salt marsh accretion (Chapter 3),

O2. exploring estuarine and salt marsh response to the combined impact of sea-level rise and increased storm intensity (Chapter 4),

O3. quantifying storm sediment contribution to different areas of marsh platforms and determining the sediment sources that storms draw on (Chapter 5);

ii) develop a new luminescence-based approach for the detection of storm activity across intertidal environments which is stratigraphy and sediment composition independent (Chapter 6), by

O1. testing whether luminescence signals can diagnose differential modes of deposition across intertidal settings,

O2. testing whether these signals can detect storm activity across intertidal environments that remain undetectable with existing techniques that depend on sediment composition.

Chapter 2

Study site and methodological approach

2.1 The choice of the study site

The Ribble Estuary, located on the Lancashire coast, North-West England (Figure 7 a), was chosen as a case study for this project because of its environmental (Natural England, 2019; RSPB, 2019) and economic (Tovey et al., 2009) importance, in addition to its exposure to escalating climate hazards (e.g., increasing rates in sea-level rise; PSMSL, 2019) and extensive anthropogenic interventions (e.g., embankment construction and dredging; van der Wal et al., 2002), which make it suitable for the investigation of salt marsh response to climate and anthropogenic forcings.

The Ribble Estuary is a Site of Special Scientific Interest (SSSI), which extends for c.a. 9,226 ha, and it is home to the Ribble Marshes National Nature Reserve, which extends for c.a. 2,302 ha (Natural England, 2019). The estuary and its marshes - covered predominantly by *Puccinellia maritima* and *Spartina townsendii* - host c.a. 250,000 migrating water birds and thousands of nesting birds belonging to twelve different species, while the sand dunes on both sides of the estuary and the mosses behind the dunes and marshes host one of the most diverse vegetation found in the UK and a wide range of rare and declining wildlife (RSPB, 2019). Hesketh Out Marsh (Figure 7 b), one of the most extensive salt marshes within the Ribble Marshes National Nature Reserve, faced a multi-million two-phase scheme implemented between 2007 and 2017 to restore the intertidal habitat, reclaimed for agricultural purposes in 1980, with the goal to enhance the protection of coastal infrastructures against flooding and restore the habitats loss during the period of reclamation (Tovey et al., 2009). The management and protection of this site is, therefore, crucial from both an environmental and an economic perspective.

The Ribble Estuary is a funnel shaped, tidally dominated and macrotidal estuary (Wakefield et al., 2011). The extensive tidal flats and salt marshes lying along the riverbanks (Figure 7 b) are thought to have formed through the combination of infilling of sandy sediments from the bed of the Irish Sea and the deposition of silt and clay-sized sediments coming from the River Ribble, with the sea influencing the sediment supply to the estuary in a much more significant quantity than the river (Wright et al., 1971; van der Wal et al., 2002), and tidal pumping being the main process introducing sediments into the estuary, especially during storms (Lyons, 1997). The bed of the central Irish Sea is, in fact, characterised by waves of mobile sediments that move up to 70 m per year (Van Landeghem et al., 2012), which are a legacy of large sediment volumes deposited by ice retreating northwards up the Irish Sea during the last deglaciation (Van Landeghem and Chiverrell, 2020; Scourse et al., 2021). Glacial Isostatic Adjustment (GIA) models and geological sediment records show a long-term decrease in the rate of relative sea-level rise in North West England for the past 2000 years (Tooley, 1974; Shennan et al., 2018). However, sea level reconstructions and historical tidal gauge records show that, for the past ca. 240 years, the rate of sea-level rise has been increasing again (from ca. 0.39 mm yr^{-1} to ca. 2 mm yr^{-1}), thus causing an increase in the accommodation space (Plater et al., 1993; Woodworth et al., 1999; PSMSL, 2019). In 1810, the intertidal areas started to be reclaimed for agricultural purposes, and dredging operations were conducted between 1847 and 1910 to facilitate navigation through the channel that was experiencing infilling (van der Wal et al., 2002; Parsons et al., 2013a). As the survival of this intertidal system is thought to largely depend on long-term marine sediment supply and storm sediment inputs, the stability of the Ribble marshes could be highly susceptible to the potential impacts of climate change and anthropogenic disturbance on sediment dynamics. Nevertheless, owed to the wealth of natural and anthropogenic forcings that the Ribble Estuary is exposed to, this site represents a living laboratory that can be exploited to better understand to what extent human interference and changes in climate forcings can affect marsh resilience.

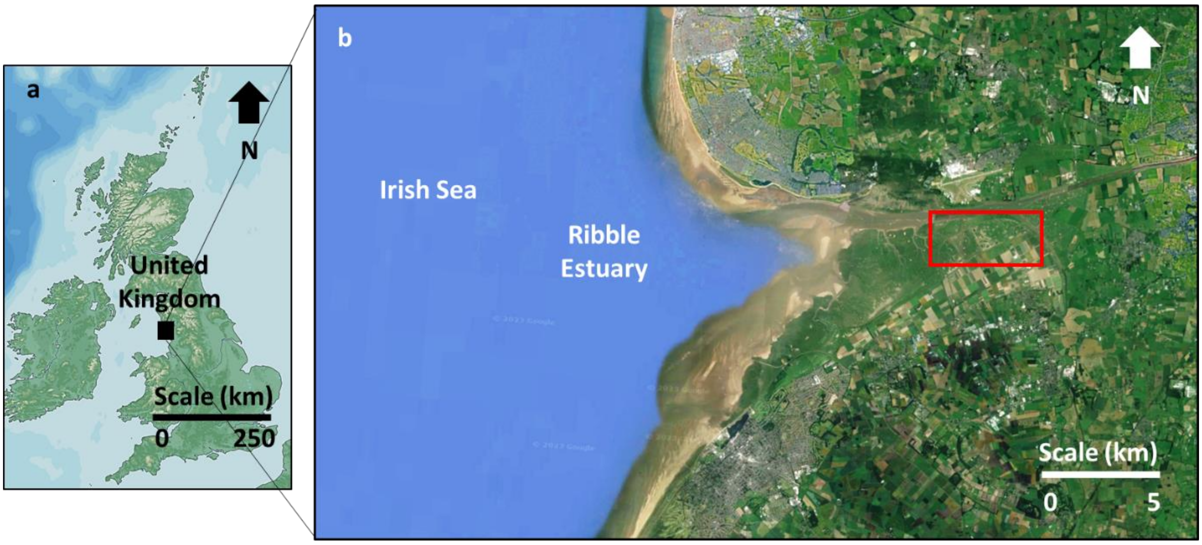

Figure 7. Location (a) and map (b) of the Ribble Estuary and its extensive tidal flats and salt marshes (© Google Earth Pro, 2022). The red rectangle outlines the salt marsh area involved in the 2007-2017 restoration scheme (Hesketh Out Marsh).

2.2 Quantifying salt marsh resilience: estimating sediment budgets and tracing sediment transport pathways

As salt marsh survival largely depends on sediment availability and dynamics, to fully evaluate long-term marsh resilience, it is necessary to quantify all sediment fluxes in and out of the intertidal system, which are a direct measure of sediment availability within the system, and to assess all sediment dynamics within the tidal flat-salt marsh complex, which help determine how such sediments are delivered to and retained by the salt marsh platform (Fagherazzi et al., 2020). Two useful metrics to evaluate these processes are sediment budgets (Ganju et al., 2015) and sediment transport pathways (Pearson et al., 2020). Sediment budgets result from the balance of sediment inputs and outputs for a defined system and time period, and can therefore be employed to determine whether a system has an overall surplus or deficit of material (Slaymaker, 2003). Sediment budgets have been extensively used to evaluate the life-span of tidal flats and salt marshes as an overall surplus of sediment is generally associated with the accretion of a system, while an overall sediment deficit is associated with erosion (Ganju et al., 2015). When sediment budgets are quantified for a whole tidal flat, they can help understand sediment fluxes in and out of the intertidal system and determine the overall resilience of the system (e.g., Li et al., 2018), while estimating sediment budgets for a salt marsh platform can help determine how sediments move between the tidal flat and the marsh platform and determine the resilience of the marsh platform (e.g., Donatelli et al., 2018). However, although sediment budgets can help diagnose sediment movement, to fully understand marsh resilience it is also necessary to trace sediment transport pathways and determine what are the sediment sources and sinks within and outside an intertidal system and how sediments move between those (Pearson et al., 2020). Determining sediment sources and sinks can help understand the sediment trapping capacity of different tidal flat and salt marsh areas, thus providing an estimate on the degree of resilience that certain tidal flat and salt marsh areas might have with respect to others (e.g., Zhang et al., 2019). This study uses a combination of sediment budget studies and analyses of sediment sources and sinks to fully understand the degree of resilience that salt marshes have with respect to anthropogenic disturbance and climate change.

2.3 The benefits of using a multidisciplinary approach

Numerical models are widely employed for the investigation of intertidal systems to climate forcing and anthropogenic disturbance, as they are able to simulate hydrodynamic-morphodynamic feedbacks at multiple spatial and temporal scales relatively quickly and without the deployment of resources necessary to run field campaigns that are able to cover the same time and spatial extents (Fagherazzi et al., 2012). The most popular ones are finite-different hydrodynamic and transport models – e.g., Delft3D, COAWST – which compute unsteady shallow water equations in two (depth-averaged) or three dimensions and can therefore be used to investigate the effects of currents and waves on sediment transport and morphology, while also exploring how currents and waves adjust to morphological changes (Lesser et al., 2004; Warner et al., 2010), with the capacity to simulate scenarios that span from days to centuries with a spatial resolution ranging from meters to kilometres (e.g., Veeramony et al., 2017; Fernández-Fernández et al., 2019; Elmilady et al., 2021). These features allow to use the outputs of numerical simulations for a variety of purposes, including sediment budgets and sediment tracing analyses (e.g., Li et al., 2018; Donatelli et al, 2018; Zhang et al., 2019).

Despite their advantages, however, numerical models cannot be used as a stand-alone method of investigation of coastal processes. First of all, to produce realistic scenarios, models have to be forced with hydrodynamic, meteorological, topographic and sediment data derived either from other models (for forecasting simulations) or from field campaigns and remote sensing observations (for simulations of present-day scenarios or hindcasting simulations) (Lesser et al., 2004; Warner et al., 2010). Secondly, to assess the performance of a model, calibration and validation protocols have to be followed, which imply the comparison of model outputs with data derived from direct measurements (e.g., Elias et al., 2012; Leonardi et al., 2013). There are then some performance-related limitations that need to be considered. Hydrodynamic and transport models can face challenges in accurately simulating scenarios that span beyond a few centuries or in simulating processes at a spatial resolution higher than a few meters, due to instabilities that the models start experiencing at such scales (Stelling, 1984). Conversely, field measurements (e.g., of topography, vegetation coverage, suspended sediment concentrations) and field and laboratory analyses of sediment properties (e.g., biogeochemical composition, particle size, magnetism) that are proxies for hydrological, meteorological and sedimentary processes, can provide fairly accurate hydrodynamic and morphodynamic measurements at high spatial resolution (e.g., Grant et al., 1997; Tognin et al., 2021). In addition, when applied to sediment cores, such field and laboratory analyses allow to investigate these dynamics at time scales ranging from centuries to millennia (e.g., Madsen et al., 2007a; Plater et al., 2007; Gunnell et al., 2013). Through direct measurements or the analyses of sediment properties, field and laboratory tools also allow to perform sediment budget and sediment tracing studies (e.g., Madsen et al., 2005; Hazermoshar et al., 2016).

To provide a comprehensive understanding of the sediment dynamics that characterise intertidal systems at multiple temporal and spatial scales, it is therefore necessary to adopt a multidisciplinary approach (e.g., Hopkinson et al., 2018). To assess salt marsh resilience to anthropogenic disturbance and climate change, this study integrates numerical simulations, direct topographic, hydrodynamic and suspended sediment measurements, and geochemical, particle size and luminescence analyses performed on both surface sediments and sediment cores.

2.4 Numerical modelling

Numerical simulations for this study were performed using the finite-difference model Delft3D, which computes unsteady shallow water equations in two (depth-averaged) or three dimensions on a curvilinear, boundary fitted grid or spherical coordinates (Lesser et al., 2004). The model is composed of three principal modules. The FLOW module is a hydrodynamic and transport simulation programme which calculates non-steady flow phenomena and suspended and bed total load transport processes of multiple cohesive and non-cohesive sediment fractions, resulting from tidal and meteorological forcings. It computes non-linear topographic effects on the flow and the exchange of sediments between the bed and the flow, accounting for vertical diffusion of sediments due to turbulent mixing and sediment settling due to gravity. The WAVE module is based on the spectral wave model SWAN (Booij et al., 1999) and computes the non-steady propagation of short-crested waves considering nonlinear wind action, wave-wave interaction, energy dissipation due to bottom friction, wave breaking, refraction (due to bottom topography, water levels and flow fields), shoaling and directional spreading. The FLOW and WAVE modules are forced at an open boundary with observed or modelled data and can be used in combination to realistically integrate flow and wave propagation. The MOR module computes suspended and bed total load transport and morphological changes for cohesive and non-cohesive sediment fractions, and feedbacks with the FLOW and WAVE modules to simulate the effects of currents and waves on sediment transport and morphology, while allowing the flows and waves to adjust themselves to the local bathymetry (Figure 8).

The MOR module can also be adapted to simulate these processes on any time scale from days to centuries at various spatial resolutions, it can keep track of the bed composition to build a stratigraphic record, and it can be extended to include features that simulate damming, dredging and dumping scenarios. Additional features can be incorporated to simulate the vegetation presence on the intertidal platform and its effect on the flow and wave fields. As numerous studies around the globe have successfully demonstrated, these features allow simulation of the effects of climate forcings and anthropogenic activities on hydrodynamic-morphodynamic feedbacks at multiple spatial and temporal scales rather accurately (e.g., Veeramony et al., 2017; Castagno et al., 2018; Fernández-Fernández et al., 2019; Zhang et al., 2020; Elmilady et al., 2021). A detailed description of Delft3D and the FLOW, WAVE and MOR modules can be found in Deltares (2019 a, b).

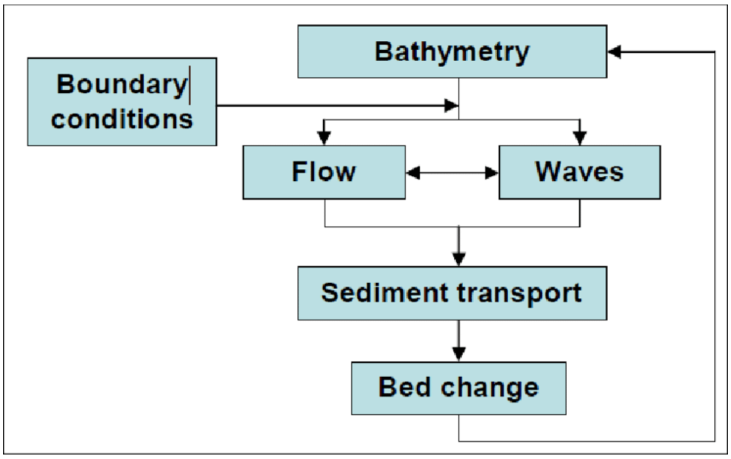

Figure 8. Schematics of Delft3D work flow for a single time step (© Hillen, 2009).

2.5 Field analyses

2.5.1 Geochemistry and particle size

Geochemical and particle size analyses are widely employed for the study of sediment dynamics that are directly associated with changes in energy levels or changes in sediment composition and, in intertidal settings, they have been often used to reconstruct environmental transitions (e.g., Plater et al., 2007; Kolditz et al., 2012) and infer sediment provenance (e.g., Plater et al., 2000; Hazermoshar et al., 2016).

As observed by Stupples and Plater (2007) and by Rahman and Plater (2014), the different energy levels found across intertidal settings are associated with differential modes of deposition that characterise each type of setting and, consequently, with different particle size distributions: (i) sandflats, which experience high energy currents, are characterised by coarse, well sorted to moderately sorted, positively skewed to symmetrical distributed, meso- to leptokurtic sediments which are transported as traction load by the fast tidal flow velocities (i.e., during the flood phase) and deposit through infilling; (ii) salt marshes, which experience very slow currents, are characterised by very fine, poorly sorted, near-symmetrical distributed and platykurtic sediments which are transported as suspended load and deposit through settling during the turn of the tide (i.e., during the ebb phase); (iii) mudflats, which are transitional environments, are characterised by fine, very poorly sorted, positively skewed to symmetrical distributed, meso- to platykurtic sediments which experience mixed transport conditions (Figure 9). Hence, particle size analyses can be employed to investigate transitions from one intertidal setting to another (Plater et al., 2007). As particle size distributions are indicative of different levels of energy, they also have the potential to be used to speculate on the distance travelled by sediments before deposition.

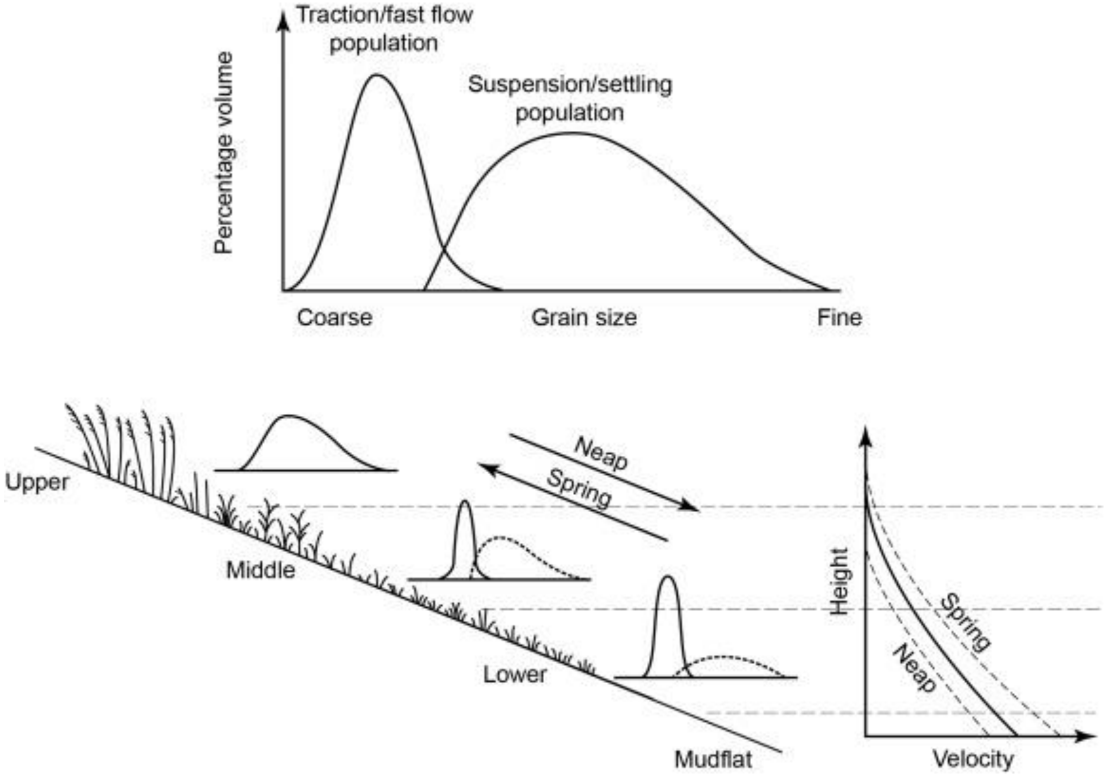

Figure 9. Particle size distribution profiles of intertidal sediments as a function of elevation relative to tidal height and flow velocity (© Stupples and Plater, 2007).

Similarly, as observed by Plater et al. (2007), Kolditz et al. (2012) and Hazermoshar et al. (2016), sediment composition can also differ between intertidal environments: (i) sandflats are rich in Si (sand content indicator), Ca and Sr (shell content indicators), and Na (salt water indicator); (ii) silt-mudflats are rich in Zr, K, Al, Ti, Rb, Nb (silt and clay mineral indicators); (iii) salt marshes are rich in K, Al, Ti, Rb, Nb (clay mineral indicators) and LOI, S, Br (organic content indicators). Geochemical analyses can therefore be used as an additional proxy to investigate environmental transitions within an intertidal system. Geochemical properties of sediments, however, are generally inherited from parent material and are therefore predominantly used to investigate sediment provenance (e.g., Figure 10; Garzanti et al., 2020). In the study of intertidal settings, geochemical properties of sediments have often been analysed to infer the marine or riverine provenance of the intertidal sediments (e.g., Plater et al., 2000; Hazermoshar et al. 2016).

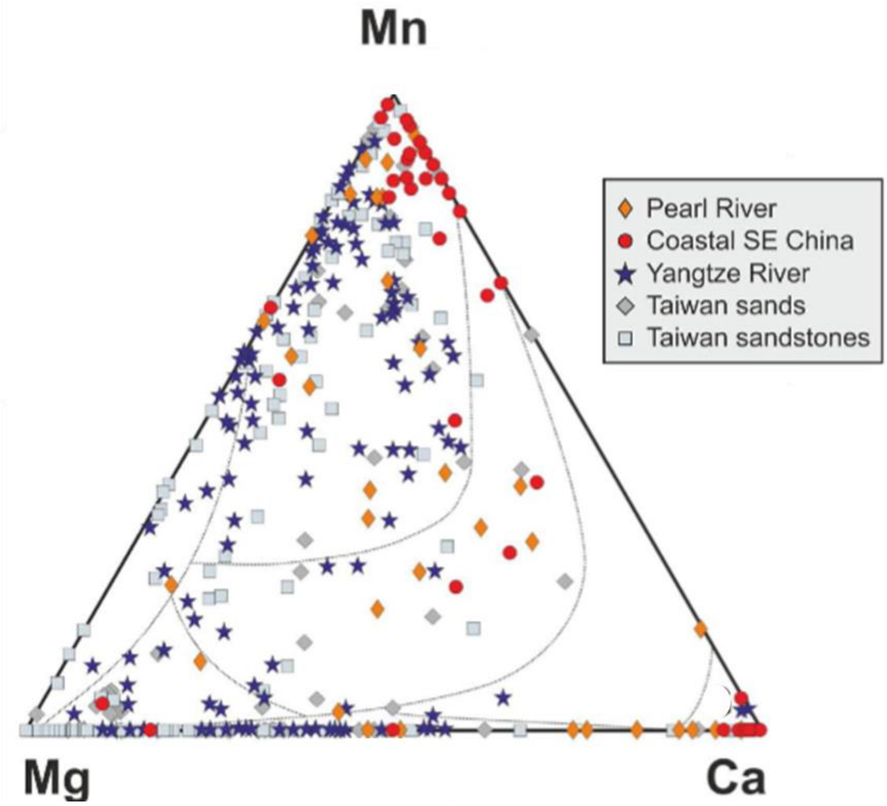

Figure 10. Geochemical characterisation of sediments collected from two river catchments (Pearl River and Yangtze River) in South-East, the coast of South-East China and the western Taiwan sand and sandstones used to infer the provenance of the western Taiwan sandstones (© Garzanti et al., 2020).

2.5.2 Luminescence

Luminescence is a technique based upon the principle that, when minerals such as quartz and feldspars are stimulated by light, heat or pressure, electrons that were stored in the crystal lattice of the minerals are released but, when buried, the minerals are exposed for a period of time to natural radiation (environmental dose-rate) which re-traps electrons within the crystal lattice (Aitken, 1985). The movement of electrons into different energetic states produces a signal called luminescence. When electrons are released due to external stimulations (e.g., sunlight exposure during transport and deposition), the luminescence signal is reset (or bleached); when minerals are buried (and shielding from external stimulation), the signal re-accumulates and can be stored during burial from a few minutes to millions of years (Figure 11; Duller, 2008). During the bleaching process, when all the mineral grains in a sediment sample are heated or exposed to sunlight for sufficient periods of time to completely zero the signals from all grains (e.g., a few seconds for quartz and a few hours for feldspar), the grains are said to be well-bleached (e.g., in aeolian environments). When the opportunity for sunlight exposure is limited (e.g., in turbulent water columns), the luminescence signals of some individual grains in a population of a sample might never or only partially be reset and the grains are said to be partially bleached. By exposing the mineral grains to an external stimulus, light or heat, in a laboratory, it is possible to measure how much energy was stored during burial (e.g., Murray et al., 2021). This stimulus excites the electrons trapped within the crystal lattices and causes the emission of a photon of light. The measured is termed thermoluminescence (TL) if the mineral is thermally stimulated, or if it is light stimulated, it is termed optically stimulated luminescence (OSL) for quartz and infrared stimulated luminescence (IRSL) for feldspar. The measured luminescence signal emitted from a mineral can then be compared to signals resulting from known radiation doses delivered in the laboratory to the same sample, to interpolate the intensity of the signal emitted from the mineral (i.e., equivalent dose or D_e).

The luminescence properties of sediment grains can be exploited for a variety of applications. The most common application is sediment burial dating. Assuming that the environmental dose rate is constant over time, it is possible to determine the time elapsed since the mineral was last exposed to light, heat or pressure prior to burial. The date at which the sediment was buried is obtained by dividing the equivalent dose (or D_e) by the environmental dose rate (e.g., Smedley, 2018). Luminescence of quartz and feldspars has been successfully applied to intertidal sediments dating to constrain both long-term accretion rates (e.g., Madsen et al., 2007a) and deposition of sediments derived from high energy events – i.e. storms and tsunamis (e.g., Madsen et al., 2009; Davis et al., 2010). Hence, luminescence dating can be employed in combination with paleoenvironmental proxies to investigate the impact of climate and anthropogenic forcings on salt marsh formation and accretion and, compared to other dating proxies commonly employed to investigate marshland settings (e.g., ^{210}Pb, ^{137}Cs), it can be applied to a broad range of organic and inorganic materials and can retrieve ages spanning from present days to hundred thousand years ago (Madsen et al., 2005).

Since the equivalent dose is indicative of how well-bleached the mineral grains were before they were buried, luminescence can also be exploited to infer the nature of the bleaching environment (e.g., the presence or absence of sediment processing) (Gray et al., 2019). It has been deployed in a few studies to date as a sediment tracer to identify sediment sources and transport pathways in both coastal and fluvial settings (Sawakuchi et al., 2011, 2012, 2018; Ahmed et al., 2014; Haddadchi et al., 2016; Gray et al. 2017, 2018). In intertidal settings, the differential degrees of bleaching could be potentially used to infer the intertidal sediment dynamics which are associated with differential modes of deposition (e.g., sediment transport and deposition occurring during fair-weather conditions and during stormy conditions).

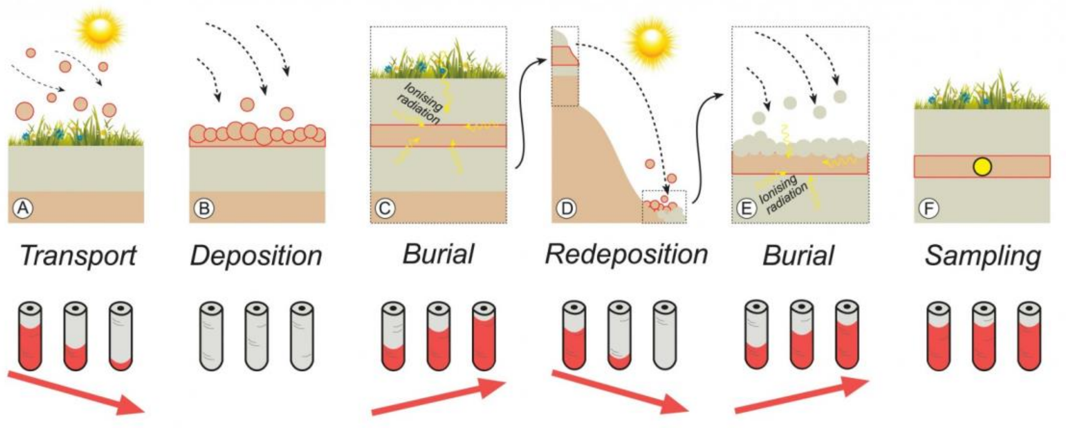

Figure 11. Diagram illustrating the luminescence signal as charge of a rechargeable battery, which resets when sediment grains are exposed to heat or sunlight (during transport and deposition) and re-accumulates after burial (© Duller, 2008).

Chapter 3

An integration of numerical modelling and paleoenvironmental analysis reveals the effects of embankment construction on long-term salt marsh accretion

3.1 Preface

Despite the popular implementation of hard sea defences for the protection of coastal areas, their impact on marine sediment supply to salt marsh platforms is still very poorly understood. However, there is evidence that embankments can affect tidal propagation, hence they are likely to also affect sediment transport. This chapter investigates the effects of embankment construction on salt marsh accretion using a combination of short-term modelled scenarios and long-term paleoenvironmental reconstructions. Paleoenvironmental reconstructions allow to investigate any potential shifts in the long-term accretion of a salt marsh platform and correlate such potential changes with the historical record of estuary management interventions. Short-term modelling, on the other hand, is useful to understand how embankments change tidal and sediment transport dynamics within the intertidal system, hence sediment supply to the salt marsh. Used in combination, these analyses can provide a complete picture on the effects of sea defences on long-term marsh accretion.

3.2 Abstract

There are still numerous uncertainties over the influence of anthropogenic interventions on salt marsh dynamics. This study uses the Ribble Estuary as a test case and an integrated approach of numerical modelling and paleoenvironmental analysis to investigate the contribution of embankment construction to long-term marsh accretion. Accretion rates derived using optically stimulated luminescence dating (OSL) were combined with a multi-proxy paleoenvironmental investigation on sediment cores extracted from the salt marsh, the mobile seafloor of the central Irish Sea and the river catchment area. These analyses provided a first evolutionary perspective on the Ribble Estuary preceding any management interventions. The paleoenvironmental analyses were then compared to simulations conducted using the hydrodynamic model Delft3D to investigate the effects of embankment construction on estuarine hydrodynamics and

morphodynamics of the salt marsh over the period constrained by the OSL. The numerical simulations showed that embankments were responsible for an overall intensification of the ebb currents in the system which promoted sediment export. The paleoenvironmental analyses showed that the marsh has been accreting at a rate of 4.61 to 0.86 cm yr^{-1} over the last ca. 190 years and that the high sedimentation rate was caused by a naturally high rate of sediment supply. The model-data integration showed that the effects of the embankment construction on sediment transport did not compromise the long-term resilience of the salt marsh because of the high rates of sediment supply and the river dredging which enhanced the flood dominance of the tide near the tidal flat.

3.3 Introduction

Salt marshes are ecosystems of high environmental and economic value that provide a variety of services, including nutrient removal, habitat provision and high rates of carbon sequestration at geological time scales (Zedler and Kercher, 2005; Barbier et al., 2011). As a result of their ability to buffer storm waves, they also provide coastal protection against flooding (e.g., Möller et al. 1999; Leonardi et al., 2018), which led to a worldwide effort to create new salt marshes and/or restore salt marshes that were previously reclaimed for anthropogenic activities to provide long-term and low-cost coastal protection (Temmerman et al., 2013).

Salt marshes form when tidal flats increase in elevation with respect to sea-level, through the delivery of fine sediment from rivers and the sea to estuarine accommodation space, which creates newly exposed surfaces that become colonised by vegetation (Reed, 1990). The resilience of salt marshes to sea-level rise is thought to be dependent upon sediment availability and rate of sediment supply to the estuarine accommodation space (FitzGerald et al., 2008; Kirwan et al., 2010, 2016; Ganju et al., 2017) and the effects of anthropogenic interventions for shoreline management on the hydrodynamic and morphodynamic feedbacks of the system (Pontee, 2014; Lee et al., 2017; Palmer et al., 2019; Li et al., 2020).

Salt marshes are generally resilient to sea-level rise when sediment supply and organogenic production are high enough to allow marsh accretion (Kirwan et al., 2010) or when salt marshes can migrate inland (Kirwan et al., 2016). Increasing suspended sediment concentrations promotes the long-term resilience of salt marshes by enhancing both vertical accretion (Temmermann et al., 2004) and lateral expansion (Willemsen et al., 2021). Willemsen et al. (2021) observed that, during mild weather, salt marshes that would experience retreat due to exposure to higher wave energy (between 0.10 m and 0.15 m), are able to switch from a retreating to an expansional behaviour with an increase in sediment supply. However, the accumulation of such sediments on salt marsh surfaces depends on the age of the marsh, with young low marsh surfaces trapping sediments at a high rate until they reach an equilibrium level with mean high water, whereas high old marsh surfaces accrete at a slower rate comparable to the rate of sea-level rise (Temmermann et al., 2004). The minimum amount of suspended sediment concentrations to allow marsh survival under current rate of sea-level rise has been estimated to be ~20 mg/L (Kirwan et al., 2010). Increasing rates of sea-level rise can compromise the stability of estuaries and salt marshes by causing marsh drowning and lateral retreat, as new accommodation space is created and, as a result, the amount of sediment inputs required to preserve marsh stability increases (FitzGerald et al., 2008; Kirwan et al., 2010, 2016; Ganju et al., 2017).

Coastal management can significantly influence the accretion and expansion of salt marshes. Several studies around the world found that the presence of embankments alters the way sea-level rise affects the tidal signal by changing the resonance properties of the coastline (e.g., Pelling et al., 2013; Holleman and Stacey, 2014; Carless et al., 2016). These changes in the tidal signal affect sediment transport dynamics in estuaries and, consequently, sediment supply to coastal marshes (Guo et al., 2016; Palazzoli et al., 2020). It has also been observed that the construction of embankments can channelise sediments towards the estuarine accommodation space, inducing siltation of intertidal areas (Pontee, 2014; Lee et al., 2017).

Salt marshes in the Ribble Estuary, North-West England, have an extremely important environmental and economic value, as they are one of Europe's largest salt marsh systems (~2,302 ha) and have been restored through managed realignment to provide flood protection (Tovey et al., 2009). Previous investigations undertaken in the estuary using bathymetric charts suggested that a very rapid accretion characterised the system in the 19th century, triggered by embankment construction started in 1810 AD, whereas a more natural accretion characterised the estuary in the 20th century following a stabilization of the system (van der Wal et al., 2002). Van der Wal et al. (2002) suggested that the construction of embankments caused an infilling of the estuary and accelerated the natural rate of accretion, concluding that anthropogenic interventions have outstripped those of changes in natural forcing on the morphological development in the area. There is no evidence of the direct effect of embankments on the hydrodynamics and morphodynamics of the system and there is no bathymetric data available for the period that precedes 1847, therefore no shift from a slower natural to a faster unusual accretion has been detected in the system through field data in the available literature (van der Wal et al., 2002). The sediment supply to the Ribble Estuary is thought to be predominantly marine (Lyons, 1997). The central Irish Sea is characterised by waves of mobile sediments that move up to 70 m per year (Van Landeghem et al., 2012). This high amount of mobile sediment has been linked to the legacy of sediments discharged through the melting and retreat of the Irish Sea Glacier (Van Landeghem and Chiverrell, 2020; Scourse et al., 2021) and Wright et al. (1971) suggested that these sediments are the major source of sediment supply to the Ribble estuary. Therefore, considering the great availability of sediment that can potentially reach the estuary, the infilling of the estuary and rapid accretion of the system might have alternatively been natural and been caused by a surplus of sediments available that infilled the estuary until the system reached equilibrium.

Despite numerous insightful studies on the subject, there are still many uncertainties over the effects of embankment construction on long-term salt marsh accretion with respect to natural sediment availability. This study uses the Ribble Estuary as a case study and an integrated approach of paleoenvironmental reconstruction and hydrodynamic modelling to investigate the effects that embankment construction undergoing in the estuary since 1810 AD had on the long-term accretion of Hesketh Out Marsh with respect to the high rates of natural sediment supply. It specifically assesses how the embankments have affected the long-term sediment delivery to and accumulation on the salt marsh platform and whether they caused any changes in the long-term marsh accretion rate since the beginning of the formation of the tidal flat. The Ribble Estuary has been chosen as a test case because of the establishment of extensive tidal flats and marsh areas since the 19th century, high quantity of natural sediment availability and existing embankments. Hesketh Out Marsh has been chosen as a sampling site due to the environmental and economic importance of this site, as it has been managed realigned, after being reclaimed in 1980 AD, to provide more resilience to the coast against flooding (Tovey et al., 2009), making it essential to understand the factors that can influence the resilience of this site in the long term.

Sediment cores from Hesketh Out Marsh, located in the centre of the estuary, were recovered and analysed spanning the evolution from sand-flat to salt marsh, with time scales and accretion rates secured by optically stimulated luminescence dating (OSL). Sediment geochemistry (X-Ray fluorescence) was analysed for the marsh cores, for samples collected from the Ribble catchment and for cores extracted from the adjacent seafloor of the Irish Sea to test a hypothesis that the sand-flat/marsh materials are predominantly Irish Sea in provenance. Changes in sediment accretion rates alongside down-core changes in particle size distribution, geochemistry and organic content were used to detect changes or shifts in sedimentation processes and depositional environment. A record of estuary management was then used to determine whether any change in accretion and sedimentation processes might be chronologically linked to the beginning of embankment construction. The hydrodynamic model Delft3D was employed to simulate sediment accumulation within the tidal flat-salt marsh system in scenarios that include i) the existing embankments and ii) zero anthropogenic disturbance, to investigate the hydrodynamic and morphodynamic feedbacks that might cause changes in sedimentation when embankments are present, and further understand whether the presence of embankments might be responsible for a significant change in sedimentation. The evolutionary profile of the marsh was then compared to the rate of accretion, revealing whether any change in accretion rate can be connected to the natural evolution and stabilisation of the system and related changes in the mode of sediment supply.

3.4 Study site

The Ribble Estuary is located on the Lancashire coast of North-West England (Figure 12 a). The estuary is funnel-shaped, tidally dominated and macro-tidal (Wakefield et al., 2011). Owing to the waves generated in the Irish Sea basin, the estuary experiences moderate wave energy (Pye and Neal, 1994). Lyons (1997) suggested that sediments are introduced into the estuary mostly by tidal pumping, especially during high storm surges. The formation of the extensive intertidal sand-silt flats and salt marshes lying along the riverbanks (Figure 12 b) is thought to have resulted from the combination of infilling of sandy sediments from the bed of the Irish Sea and deposition of the silt and clay-sized sediments coming from the River Ribble, with the sea influencing the sediment supply to the estuary in a much more significant quantity than the river (van der Wal et al., 2002). The accretion of the intertidal flat and salt marsh platform might have been further aided by the moderate wave climate characterising the estuary insufficient to cause significant lateral erosion (van der Wal et al., 2002). Glacial Isostatic Adjustment models show a long-term decrease in relative sea-level in North-West England for the past 2000 years (Tooley, 1974; Shennan et al., 2018), but historical tidal gauge records show that this was followed by an average increase in mean sea-level of 2 mm yr^{-1} since the beginning of the measurements in 1858 AD (Woodworth et al., 1999; PSMSL, 2019). Plater et al. (1993) also suggested that a secular rise in sea-level characterised the area, increasing the accommodation space. In 1810 AD, land reclamation of the estuary begun, and embankments were built along the northern bank of the estuary first, from Lytham to Preston, and along the southern bank later, north of Southport (van der Wal et al., 2002; Parsons et al., 2013a). Between 1847 AD and 1910 AD the channel began to be dredged as the inner estuary was experiencing an infilling (van der Wal et al., 2002; Parsons et al., 2013a). Hesketh Marsh and Hesketh New Marsh were reclaimed respectively in 1859 AD and 1883 AD for agricultural purposes (Figure 12 c, d, e, f), while Hesketh Out Marsh was only reclaimed in 1980 AD (Figure 12 g), but a managed realignment project that restored Hesketh Out Marsh was conducted between 2007 AD and 2017 AD (Figure 12 h; Tovey et al., 2009).

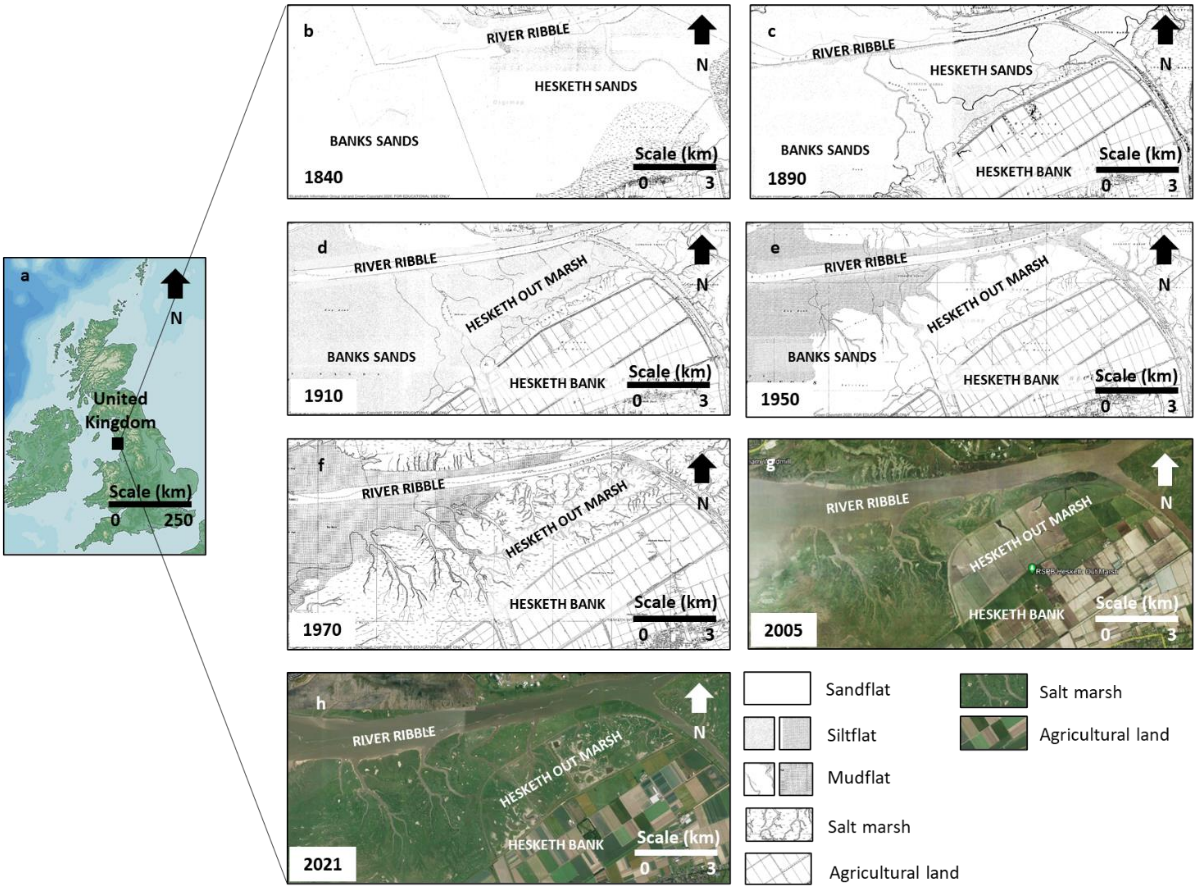

Figure 12. Location of the Ribble Estuary (a); reconstruction of Hesketh Out Marsh evolution through historic and aerial maps: in 1840 AD (b) Hesketh Out Marsh area was occupied by a sandflat, between 1890 AD (c) and 1910 AD (d) the sandflat was replaced by a silt flat, in 1950 AD (e) a mudflat was the dominant environment, in 1970 AD (f) a fully formed marsh was visible, in 2005 Hesketh Out Marsh was still reclaimed for agricultural purposes (g), in 2021 the managed realignment scheme was already completed (© Landmark Information Group Ltd and Crown Copyright, 2017; © Google Earth Pro, 2022).

3.5 Methods

3.5.1 Paleoenvironmental reconstruction

To perform the analysis for paleoenvironmental reconstruction, Hesketh Out Marsh was cored using a percussion corer with a gauge 1 m long and 7.5 cm in diameter. Two cores 3.20 m long (HOM19-1 and HOM19-2) were extracted from the middle marsh (Figure 13 h). The middle marsh was chosen as a sampling location because it is characterised by an accumulation rate slow enough to provide a record which more likely extends before embankment construction and is less likely characterised by sediment loss due to wave erosion compared to records that can be recovered by the lower marsh area (Berry and Plater, 1998). Furthermore, it was not enclosed by embankments before 1980 AD (Tovey et al., 2009), therefore it can provide a record of accretion extending more towards present day compared to the higher marsh (Hesketh New Marsh), which was enclosed in 1883 AD. HOM19-1 was cored in the sunlight and used for geochemical, particle size distribution and near-infra red analysis. HOM19-2 was cored using black sleeves to protect the sediments from sunlight exposure and was used for optically stimulated luminescence analysis. Stratigraphic analysis was performed on both cores to ascertain that they contain similar stratigraphic patterns and that the OSL chronology developed for the sediment profile can provide temporal context to the measurements of changing sediment composition (Figure 13 i).

3.5.1.1 Sediment provenance

Geochemistry is widely used as a proxy to reconstruct the provenance of marshland sediments (i.e. marine or riverine). For instance, it was employed by Plater et al. (2000) in the attempt to reconstruct sediment provenance in the Tees estuary, North-West England and by Hazermoshar et al. (2016) to characterize surficial sediments in Eynak Marsh, North of Iran. To investigate the provenance of the marsh sediments, the geochemistry of the salt marsh sediment was compared to that obtained for samples in the likely sediment source areas in the Ribble catchment and the eastern Irish Sea (Liverpool Bay – Sefton Coast). The HOM19-1 core was subsampled into a total of 320 samples at 10 mm continuous intervals. To characterise the river sediments, a set of 15 samples from five different locations (three per location) were collected from the surface sediments of the Ribble catchment; the locations included the lower (Figure 13 g), middle (Figure 13 g) and upper Ribble (Figure 13 d), and the Hodder (Figure 13 e) and the Calder (Figure 13 f) tributaries. Marine sediments are transported from the Irish basin into the estuary from south-west and, to a minor extent, from the southern sand dunes through erosion (Parsons et al., 2013a). Characterising this onshore delivery of sediments to the estuary, samples were taken from coastal aeolian dunes near Southport (n = 3) and the upper 1 m of seafloor sediment ~ 20 km offshore in 28-30 m water depths (Figure 13 b, c). The seafloor samples came from 6 m (max length) vibrocores collected at 2 km spacing across the Irish Sea by a Fugro Geotechnical team during survey cruises for installing the Western High Voltage – Direct Link (HVDL) marine cable (see Pearce et al., 2011). The top 1 m was targeted and subsampled at 0.1 m intervals progressing down three vibrocores (n = 30), with these depths from the more mobile surface sediments of the eastern Irish Sea.

Geochemical data were measured by X-Ray fluorescence (XRF) using a XEPOS 3 Energy-dispersive XRF for all the samples from the Hesketh Out Marsh core - divided into upper core (0-100 cm) and basal core (101-320cm) - and probable source area materials from the Irish Sea, Southport sand dunes and Ribble catchment. All samples were lightly hand ground, pressed and then measured under a He atmosphere under combined Pd and Co excitation radiation and using a high resolution, low spectral interference silicon drift detector. The XEPOS 3 undergoes daily standardisation procedure and has accuracies verified routinely using 18 certified reference materials (Boyle et al., 2015). Light elements were corrected for organic content, using loss-on-ignition (LOI) values measured by heating the samples at 105°C overnight to evaporate all moisture content and then igniting them in a furnace at 450°C for 4.5 hours to combust all organic matter (Boyle, 2000). Principal component analysis was performed using PAST3 (Hammer, 2019) to explore the geochemical compositions of the samples and to assess any association between the salt marsh materials and the offshore and fluvially-sourced sediments. The parameters selected for this PCA were: group 1 formed by silicates indicators (Si (mg/g)); group 2 formed by salt water (Na (mg/g), S (mg/g)) and shell content indicators (Ca (mg/g), Sr (µg/g)); group 3 formed by organic content indicators (LOI (%)), silt/clay mineral indicators (K (mg/g), Al (mg/g), Fe (mg/g), Ti (µg/g), Rb (µg/g), Zr (µg/g), Mn (µg/g), Nb (µg/g),), pollutants (Mg (mg/g), P (mg/g), As (µg/g), Pb (µg/g), Zn (µg/g), Ni (µg/g), Cu (µg/g), V (µg/g), Cr (µg/g), Ga (µg/g), Ge (µg/g), Br (µg/g), Ba (µg/g), I (µg/g)) and the rare elements (Y (µg/g), La (µg/g), Ce (µg/g)). The division in groups was based on the association between parameters performed by the PCA (Figure 15) as well as the geochemical properties of the parameters (Boyle, 2000; Plater et al., 2000).

3.5.1.2 OSL analysis of accretion rates

To date the Hesketh Out Marsh sequence and to quantify sediment accretion rates over time, OSL analysis was performed on coarse quartz grains (90-150) from HOM19-2. Sampling of the core was designed to characterise all visible changes in core stratigraphy; a total of twelve samples were extracted from the core (HOM19-2-1 to HOM19-2-12, see Figure 16 for down-core sampling profile). Quartz grains were used for the analysis because their signal resets rapidly in response to sunlight (Godfrey-Smith et al., 1988), thus they are likely well zeroed in young sediments (Ballarini et al., 2003). The dominant bedrock geology of the area, Triassic desert mud-, silt- and sand-stones, would also likely contribute to provide bright quartz grains with good luminescence signal (Fitzsimmons, 2011).

To isolate the coarse quartz grains for equivalent dose measurement, all samples were treated with a 10% (v/v) dilution of 37% HCl to dissolve carbonates and with a 10% (v/v) dilution of H_2O_2 to remove organic content. Dry sieving was used to extract grains 90 –150 µm in dimeter for samples HOM19-2-2 and HOM19-2-4 and 90-125 µm for the rest of the samples. Density separation using sodium polytungstate was performed to isolate the fraction of grains between 2.62-2.70 g cm^{-3} and remove feldspar and heavy metals grains. The quartz grains were then etched using 40% hydrofluoric acid to remove the outer portion of the grains contaminated by alpha particles and to remove any remaining feldspar grains. Another wash with a 10% dilution of HCl was then performed to remove soluble fluorides produced in the previous step.

Grains were mounted as 2 mm-diameter multiple-grain aliquots on to 9.8 mm-diameter aluminium discs and used for analysis. Forty-eight discs were analysed for each sample except for HOM19-2-4, which only had enough quartz for 14 discs. No coarse quartz was recovered for sample HOM19-2-1. The luminescence measurements were made using an automated RisØ TL/OSL DA-15 reader equipped with a $^{90}Sr/^{90}Y$ source (Bøtter-Jensen et al., 2003), the quartz grains were stimulated with a light source consisting of blue (470 nm) light emitting diodes (LEDs) and the luminescence signals were detected using a 5 mm thick U-340 filter and convex quartz lens beneath a photo-multiplier tube. The signal was recorded at 125°C for a total of 40 s, where the OSL signal was summed for the first 0.6-1.5 s and the background was calculated from 33.6 to 38.5 s of the decay curve. A 1.5% instrument measurement error was incorporated into the curve fitting. Individual aliquots were accepted or rejected from D_e calculation according to their performance during the following screening criteria (considering the associated uncertainties): (1) the response to the test dose was greater than three sigma above the background; (2) the test dose uncertainty was <20%; (3) the recycling ratios and (4) OSL-IR depletion ratios were within the range 0.8-1.2, and (5) recuperation was <5% of the response from the largest regenerative dose (7-8 Gy).

A pre-heat plateau test of 21 aliquots from sample HOM19-2-6 was used to determine the preheat temperature used for OSL analysis. The results show that both the D_e and recuperation values started increasing from 220 °C; thus a pre-heat temperature of 200 °C for 10 s and a cut-heat of 160 °C for 0 s were used for the single aliquot regenerative dose (SAR) protocol (Murray and Wintle, 2000). A dose-recovery test was performed on 24 aliquots from sample HOM19-2-6 using a 4.15 Gy dose suggested that the SAR protocol was appropriate (ratio of 0.97 ± 0.06, and overdispersion value of 5 ± 0 %). The D_e distributions (Figure S1) show asymmetries for all samples. Thus, the minimum age model (MAM; Galbraith and Laslett, 1993) was used for age calculation.

Dosimetry samples were prepared using 20-80 g of bulk sediment. The samples were dried at room temperature, weighted, ground to homogenise the material and stored for four weeks. A high-resolution gamma spectrometer was used to measure the radionuclide concentrations (K, U and Th) for 72 hours. The final water content was estimated calculating the weighted average of the mean water content during the period in which samples were transitioning from surface to depth and the mean water content during the period in which the samples were at depth. Both contents were estimated by calculating the weighted average of the water content during the period in which the samples were saturated (below mean water level) and the water content during the period in which the samples were at field water content (above mean water level). Following the model provided by Roberts and Plater (2005), for the period in which samples were transitioning from surface to depth, it was estimated that they were saturated 75% of the time, and for the period in which they were at depth, it was estimated that they were saturated 90% of the time. The saturated water content was estimated as 45%, while the field water content was measured by weighting the samples before and after drying them at room temperature. Cosmic dose was calculated using Prescott and Hutton (1994) equation that accounts for altitude, latitude, longitude and depth below ground level of each sample. Th, U and K concentrations were converted into beta and gamma dose-rates using Guerin et al. (2011) conversion factors and attenuated for grain size and etching (Guerin et al., 2012). The outer coating of the quartz grains was removed by hydrofluoric acid etching and so alpha dose-rates were negligible. The sum of the three beta dose rates and the three gamma dose rates was then calculated and corrected for water content and combined with the cosmic dose to determine the total dose-rate (Table S1). Dose-rates were calculated using the Dose Rate Age Calculator (DRAC; Durcan et al. 2011). Th:U was calculated to check whether it was in equilibrium (3<Th:U<4) or in disequilibrium due to the presence of saltwater (Aitken, 1985). The age of each sample was calculated by dividing the D_e by the dose rate and presented with total uncertainties (± 1 sigma); the present age used is 2019 (Table S2).

All OSL ages were then modelled using the Bayesian package 'OxCal' - version 4.4, which constructs age–depth sequences by integrating the IntCal20 calibration curve with statistical models (Bronk Ramsey, 1995, 2009; Reimer et al., 2020). The OSL ages were entered in the model as a P-sequence, in which sediment deposition is modelled as a Poisson (random) process, and where a parameter (k) determines the extent to which sedimentation rates are allowed to vary. A uniformly distributed prior was used for k such that $k_0=1$, and $\log_{10}(k/k_0)$ U(−2, 2); this allows k to vary between 0.01 and 100. The final probability distributions with ranges incorporating 68.2%, 95.4% and 99.7% of the total area of the distributions with the highest probability density were modelled using a Markov Chain Monte Carlo (MCMC) sampling routine. Outliers were handled as a student-T distribution using a general outlier model. A boundary was inserted at 120 cm, where the core exhibits a neat stratigraphic change and stops being sand dominated (Figure 13 i). The final accretion profile uses the probability weighted mean age and 95.4% uncertainties from the Bayesian age-depth model.

3.5.1.3 Particle size distribution analysis

Particle size distributions (PSDs) can be used to infer whether sediment deposition is driven by accretion or infilling. According to the particle size distribution model developed by Rahman and Plater (2014), fine-skewed to near-symmetrical distributions characterised by well-sorted sand-sized sediment, typical of traction load delivered by the faster tidal flow velocities (i.e. during flood phase), are attributable to infilling; near-symmetrical distributions characterised by fine to very fine, poorly sorted silts, typical of the suspension load that settles during the turn of the tide (i.e. during ebb phase), is attributable to gradual accretion. PSDs were measured for HOM19-1 at 10 mm intervals using a Coulter LS 13 320 Single-Wavelength Laser Diffraction Particle Size Analyser that determines the dimensions of individual particles 0.375-2000 µm. Subsamples were digested in 6% concentrated H_2O_2 (50 ml of H_2O_2 per 10 ml of sample) to remove any organic component, with the samples then dispersed and sonicated in $Na_6O_{18}P_6$ and analysed under sonicating measurement conditions. The resulting PSDs are the average of three repeats after elimination of outliers. The Coulter LS 13 320 undergoes regular calibration checks using samples with known size distributions. End-member modelling analysis (EMMA) was conducted using the EMMAgeo R package to statistically derive the most recurrent modes that explain the variance in the PSDs down-core profile (Dietze et al., 2012). End-member modelling analysis has been successfully applied to sediment deposits in salt marsh settings by Clarke et al. (2014). Clarke et al. (2014) identified six main modal peaks occurring in consistent particle size ranges that account for more than 98.5% of the explained cumulative variance in PSDs, which agree with the six fixed particle size windows identified by Clarke et al. (2013) through the estimate of the particle size ranges deposited through settling, saltation and traction processes. Hence, the maximum number of end-members that the model could detect in the down-core PSD profile was set as seven. Particle size categories with several zero values were combined to enable end-member analysis of the entire data set. A robustness test was performed to check on each end-member (Figure S2 a). The model showed that 86% of the variance in the PSDs present in the HOM19-1 core could be explained by four PSD end-members (Figure S2 b). The loading of the end-members explaining most of the variance was plotted to observe what depositional processes (i.e., infilling or accretion) could be correlated with the PSDs in the core. The down-core profile of the end-members scores were then plotted to observe changes in distribution along the core and attribute whether possible changes in accretion over time detected by the OSL in HOM19-2 were attributable to infilling or gradual accretion.

3.5.1.4 Evolution of Hesketh Out Marsh

3.5.1.4.1 Particle size distributions

Plater et al. (2007) interpretation of grain size properties of sandflat, mudflat and salt marsh sediments was then used to reveal whether any change in accretion rate can be connected to changes in the mode of sediment supply connected with the natural evolution and stabilisation of the system. Salt marsh environments are characterised by very slow currents and sediments are fine, poorly sorted, near-symmetrical distributed and platykurtic. Mudflat sediments are deposited with low energy conditions and characterised by fine, very poorly sorted, positively skewed to symmetrical distributed, meso- to platykurtic sediments. Sand flats sediments are deposited by high energy currents and are instead characterised by coarse, well-sorted to moderately sorted, positively skewed to symmetrical distributed, meso- to leptokurtic sediments. GRADISTAT 8.0v (Blott and Pye, 2001) was used for the statistical analysis of the PSDs measured for each sample of HOM19-1 to calculate D50, D90, standard deviation, skewness and kurtosis (geometric results).

3.5.1.4.2 X-Ray fluorescence analysis

To provide a more robust paleoenvironmental reconstruction, PSD statistical analysis was integrated with geochemical proxies. The geochemical composition of sediments is thought to be directly correlated with changes in stratigraphy and has been used in various case studies for the investigation of environmental transitions in marshland settings. Plater et al. (2007) used changes in the geochemical composition of the sediments as a proxy for stratigraphical changes to reconstruct the evolution of Romney Marsh/Dungeness Foreland depositional complex. Kolditz et al. (2012) implemented the same approach to study the environmental transitions in a marshland setting during sea-level rise in North-West Germany, and Hazermoshar et al. (2016) used it in a multi-proxy study that aimed to characterize surficial sediments in Eynak Marsh in North of Iran. The X-Ray Fluorescence (XRF) measurements for all HOM19-1 samples were used to produce the profiles of the following geochemical proxies: Si/K (silicates normalised towards mineral matter as sand indicator), Ca/K (calcium normalised towards mineral matter as shell content indicator), Fe/Mn (redox indicator), Rb (silt/clay mineral indicator); LOI was added to the list of geochemical proxies as organic content indicator (Plater et al., 2007).

3.5.1.4.3 Near-infra red spectra analysis

The XRF analysis was supplemented by near-infrared (NIR) spectra derived sediment composition. NIR spectra were measured by diffuse reflectance for all HOM19-1 samples using an integrating sphere on a Bruker MPA Fourier-Transform NIRS, with NIR spectra based on combining 24 scans collected at 8 cm^{-1} intervals across the range 3595-12500 cm^{-1} (Russell et al., 2019). NIR spectra were converted to 1st derivatives, calculated using a centrally weighted Savitzky-Golay smoothing algorithm minimising spectral noise (Russell et al., 2019). The NIR spectra were interrogated using multiple regression of known end-member spectra onto the spectra derived for the unknown sediment samples (Russell et al. 2019). NIR spectra for the unknown samples are a conservative mixture of the spectra of component materials, and by using appropriate end-member spectra the multiple regression process can unmix the proportions of the components (Russell et al. 2019). The multiple regression analysis was undertaken in R using the (LM) function in R (R Core Team, 2013), using mineral matter (powdered quartz SiO_2), $CaCO_3$ shell material and organic matter (International Humic Substances Society (IHSS) humic/fulvic acid standards); the output concentrations for these components are reported as weight percent (Figure S3).

3.5.1.4.4 Cluster analysis

A classical hierarchical clustering routine was run on all the components of the PSD, XRF and NIRS analysis using PAST3 (Hammer, 2019) to produce a dendrogram showing how data points can be clustered and statistically identify any change in the depth-profile. The unweighted pair-group average (UPGMA) algorithm, which joins clusters based on the average distance between all members in the groups, with a stratigraphic constraint, was applied with a Euclidean similarity index.

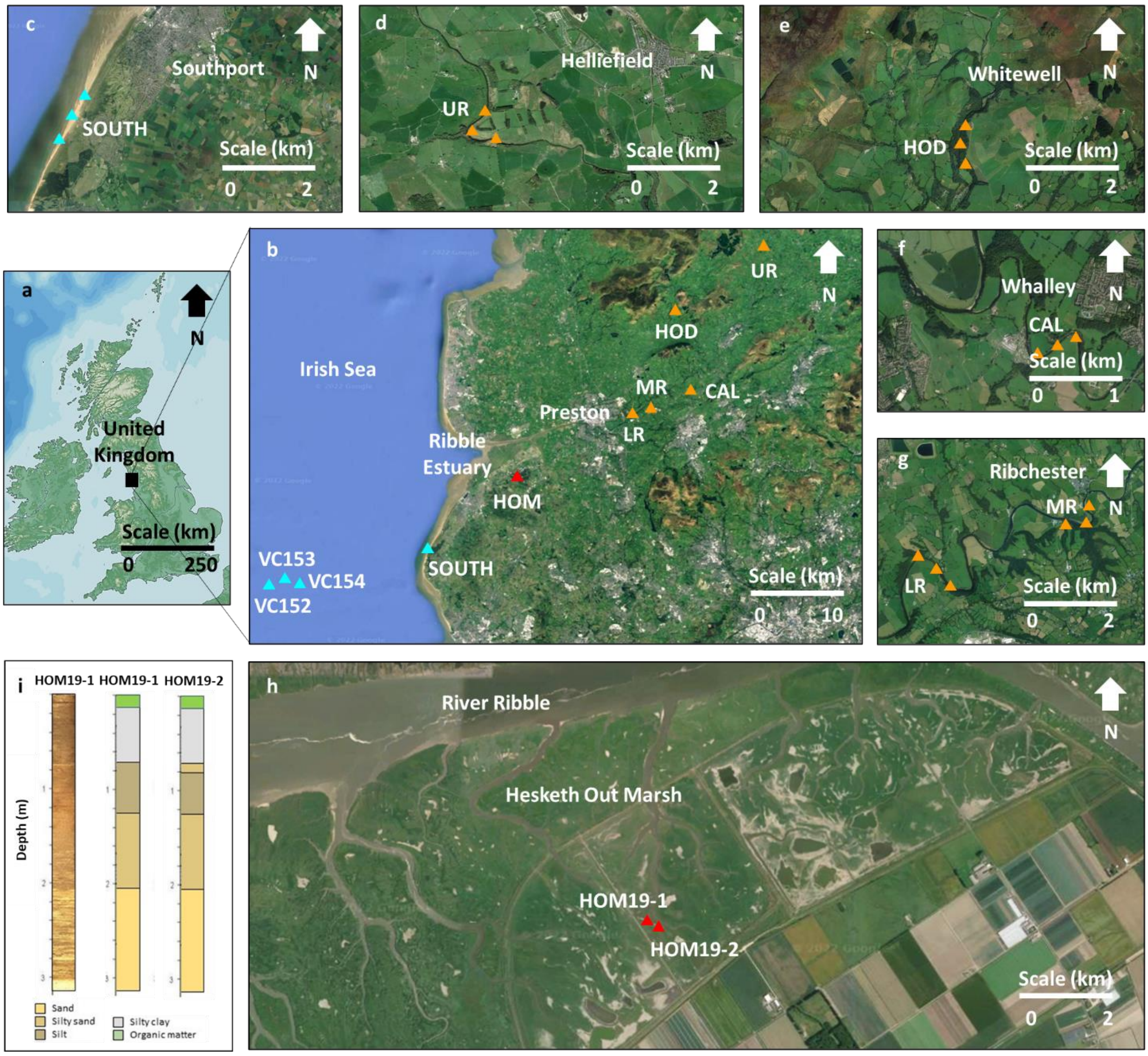

Figure 13. Location of the Ribble Estuary (a); low resolution map showing location of the cores collected from the Irish Sea (blue triangles - VC152, VC153, VC154), the samples collected from the Southport sand dunes (blue triangle - SOUTH), the samples collected from the Ribble catchment (orange triangles - UR, HOD, CAL, MR, LR) and the cores collected from Hesketh Out Marsh (red triangle - HOM) (b); high resolution maps showing location of the sampling along the Southport sand dunes (SOUTH) (c), upper Ribble (UR) (d), Hodder (HOD) (e), Calder (CAL) (f), middle (MR) and lower (LR) Ribble (g), and coring at Hesketh Out Marsh (HOM19-1 and HOM19-2) (h); stratigraphic analysis of HOM19-1 and HOM19-2 (i) (© Google Earth Pro, 2022).

3.5.2 Numerical modelling

To investigate the accretion and evolution of the marsh in scenarios with no anthropogenic disturbance and with the addition of embankments, the FLOW module of the numerical finite-difference model Delft3D was used to simulate the hydrodynamics and sediment transport of the system. The model calculates non-steady flow and transport phenomena using Navier-Stokes and transport equations (Deltares, 2019a). The model set-up for this study accounts for suspended-load, evaluated through the advection-diffusion equation, of multiple cohesive sediment fractions; erosion and deposition for cohesive sediments are computed using the Partheniades–Krone formulations (Partheniades, 1965). It also accounts for vertical diffusion of sediments due to turbulent mixing and sediment settling due to gravity.

The original design of the domain and the set-up and calibration of the model for this study were performed by Li et al. (2018, 2019). The domain consists of a grid of 344 x 80 cells in the east to west and north to south direction (Figure 14 a), and three equally spaced vertical layers. The cell size is approximately 20x20 m within the river, 70x70 m across the intertidal area (including the marsh platform) and 300x300 m in the outer estuary. Simulations with and without embankments presence were conducted using bathymetries from 1847 AD and 2008 AD (Table 1; van der Wal et al., 2002; Parsons et al., 2013a). The 1847 AD bathymetry is the oldest with data availability within the timeframe of the dates produced by the OSL analysis (Table S2) and it offers the opportunity to simulate the presence of an accommodation space before the formation of the intertidal flat and before the beginning of the channel dredging (Figure 14 b). The 2008 AD bathymetry was used to simulate an established intertidal flat and salt marsh platform and completed channel dredging (Figure 14 c). Between 1847 AD and 1910 AD the channel began to be dredged as the inner estuary was experiencing an infilling, with dredge spoils disposed off the mouth of the estuary until 1905 and offshore after then, and the depth of the channel increased approximately by 1 m when it was at its deepest (van der

Wal et al., 2002; Parsons et al., 2013a). It has been observed that channel dredging can modify tidal asymmetry (Zhu et al., 2015; Van Maren et al., 2015). To understand how channel dredging interfered with the effects of embankment construction on the sediment transport, a simulation was run using the 1847 AD bathymetry with a channel depth increased by 1 m (Figure 14 d); this allowed to investigate the sole effect of channel dredging without considering the morphological evolution of the intertidal flat and the construction of further embankments that occurred during the period of the historical dredging. The bathymetric data for 1847 AD was obtained by digitising the maps provided by van der Wal et al. (2002) with reference Above Ordnance Datum Newlyn (AODN). Since the data provided by van der Wal et al. (2002) covered a restricted area of the domain (53.59° N to 53.89° N, -3.13° E to -2.83° E), to provide a domain large enough to stabilize the model, this was integrated with present data obtained from the combination of two datasets: the bathymetry data for the open sea collected from EDINA DIGIMAP and the LiDAR data for the coastal regions downloaded from the Environment Agency's LiDAR data archive. The elevation of the inland terrain model and very offshore areas is, on average, of the same order of magnitude to that presented in van der Wal et al. (2002). The choice of integrating the digitised bathymetry with present bathymetric data was based on limitations in terms of data availability for that period and the assumption that changes in the most offshore bathymetry and inland terrain elevation (where the marsh is already well formed) would affect the analyses and calculations performed on the salt marsh platform and within the intertidal area to a minor extent compared to the long-term changes of the river, inner and outer estuary bathymetry. The bathymetry influences the propagation of the tidal currents (e.g., Van Maren et al., 2015; Li et al., 2018; Palmer et al., 2019), therefore this choice could cause limitations such as an overall overestimation or underestimation of the net sediment transport within the estuary and of the final sediment budget of the salt marsh. The bathymetric data for 2008 AD was obtained directly by combining the bathymetry data for the open sea collected from EDINA DIGIMAP and the LiDAR data for the coastal regions downloaded from the Environment Agency's LiDAR data archive. Since the two datasets have different vertical reference levels, Low Astronomical Tide (LAT) and Above Ordnance Datum Newlyn (AODN) respectively, they were adjusted and referred to Mean Sea Level (MSL) following the spatially varying Vertical Offshore Reference Frame (VORF) corrections provided by the UK Hydrographic Office prior to combining. The model is constrained within two open boundaries, one 20 km offshore and one across the River Ribble. The model was successfully calibrated by Li et al. (2018, 2019) using the 2008 AD bathymetry and 2008 AD time-series for both river discharge and offshore water level. Data for the offshore boundary was provided by the Extended Area Continental Shelf Model fine grid (CS3X), which has approximately 12 km resolution, covers an area from 53.55° N to 53.92° N and from -3.33° E to -2.75° E. Data for the river boundary was collected from the National River Flow Archive and consists of a time series of daily-averaged river discharge values; a constant discharge of 44 m^3 s^{-1} was estimated using the mean discharge for the simulated period. Each simulation was run for one year. To simulate past ocean boundary conditions, 10 tidal harmonics (M2, S2, N2, K2, O1, P1, Q1, K1, M4 and S1) were derived for the Ribble Estuary using the global tidal model GOT-e 4.10c (Ray 1999; Zaron and Elipot, 2021). To ascertain that the tidal harmonics would allow for the modelling of realistic hydrodynamic for the simulated years, the water level at ocean boundary for the 2008 AD scenario forced with tidal harmonics was compared to the water level for the 2008 AD scenario forced with water level time-series (Figure S4). Since the river contribution to sediment delivery in the intertidal area is minimal (Figure 15; Lyons, 1997; van der Wal et al., 2002) and no time-series for river discharge are available for 1847 AD, the time-series for river discharge from 2008 AD were used to force the river boundary of the 1847 AD scenarios as well. The Ribble Estuary experiences moderate wave energy (Pye and Neal, 1994). However, for simplicity, the effects of wind waves have been neglected in this study to investigate exclusively the effects of embankments on the sediment transport. A uniform and not erodible initial bed composition was applied, to avoid feedbacks between hydrodynamics and the initial bathymetry. This is because the focus of the study was the investigation of the redistribution of input sediments and deposition within the estuarine accommodation space with and without embankments, rather than the modelling of the morphological evolution of the estuary. The initial suspended sediment input and the sediment input at river and ocean boundaries were simulated using cohesive erodible sediments. The suspended sediment input at the river boundary was calculated as an average for the year 2008 in proportion to the river discharge, using the Wright-Parker formulation (without stratification) for the suspended load, which estimated a mean value of 0.002 kg m^{-3}. The input at the ocean boundary for the suspended load and the initial suspended sediment concentration in the domain were given using the value measured by Silva et al. (2016) in 2011 (0.001 kg m^{-3}). To simulate the presence of embankments, thin dams were imposed, and the position of the dams was chosen based on the position of the embankments at the time of each bathymetric survey (Table 1; van der Wal et al., 2002; Parsons et al., 2013a).

To quantify the contribution of embankment construction on the accretion of the tidal flat-salt marsh, the sediment budget of Hesketh Out Marsh platform was calculated at the end of the simulated year for each scenario by multiplying the cumulative deposition of each cell for the cell area and summing them (Ganju et al., 2015). Tidal asymmetry has been recognised as one of the main factors controlling the net import/export of sediments and the large-scale morphological evolution of estuaries (Guo et al., 2016; Palazzoli et al., 2020; Donatelli et al., 2018) and there is evidence that the presence of embankments alters the way sea-level rise affects the resonance properties of the coastline, modifying the tidal signal and changing the sediment supply to coastal marshes (e.g., Pelling et al., 2013; Holleman and Stacey, 2014; Carless et al., 2016). To investigate the effect of embankment construction on the tidal signal, Fourier analysis was conducted for each scenario for an entire monthly tidal cycle. The MATLAB package T-TIDE was used to conduct the analysis (Pawlowicz et al., 2002). The distortion and asymmetry of the tidal signal were analysed using the principal lunar semi-diurnal constituent M2 and the largest shallow water constituent M4; the distortion was calculated using the ratio $A_{4\text{-}2}=A_{M4}/A_{M2}$ where A is the amplitude of the tidal height and the asymmetry was calculated using $\Delta\theta=2\theta_{M2}-\theta_{M4}$ where θ is the phase of the tidal height (Friedrichs and Aubrey, 1988; Blanton et al., 2002). When $\Delta\theta$ is between 0° and 180° the flood phase dominates, whereas when it is between 180° and 360° the ebb phase dominates; the magnitude of $A_{4\text{-}2}$ is representative of the significance of the dominance (Friedrichs and Aubrey, 1988). The harmonic analysis was not performed on dry cells and on salt marsh or tidal flat cells intermittently covered by water.

Table 1. List of simulated scenarios indicating name and description of the simulations. Records of channel dredging and embankment construction are provided by van der Wal et al. (2002) and Parsons et al. (2013a).

Simulation name	**Simulation description**
1847 AD	● Oldest bathymetry available ● Accommodation space preceding the formation of the intertidal flat and the beginning of the channel dredging ● Embankment scenario includes embankments built between 1810 AD and 1847 AD
2008 AD	● Present day bathymetry ● Established intertidal flat and salt marsh platform and completed channel dredging ● Embankment scenario includes only embankments left after 2017 AD
1847 AD (simulated dredging)	● 1847 bathymetry modified to simulate channel dredging ● Channel depth increased by 1 m to simulate dredging ● Embankment scenario includes embankments built between 1810 AD and 1847 AD

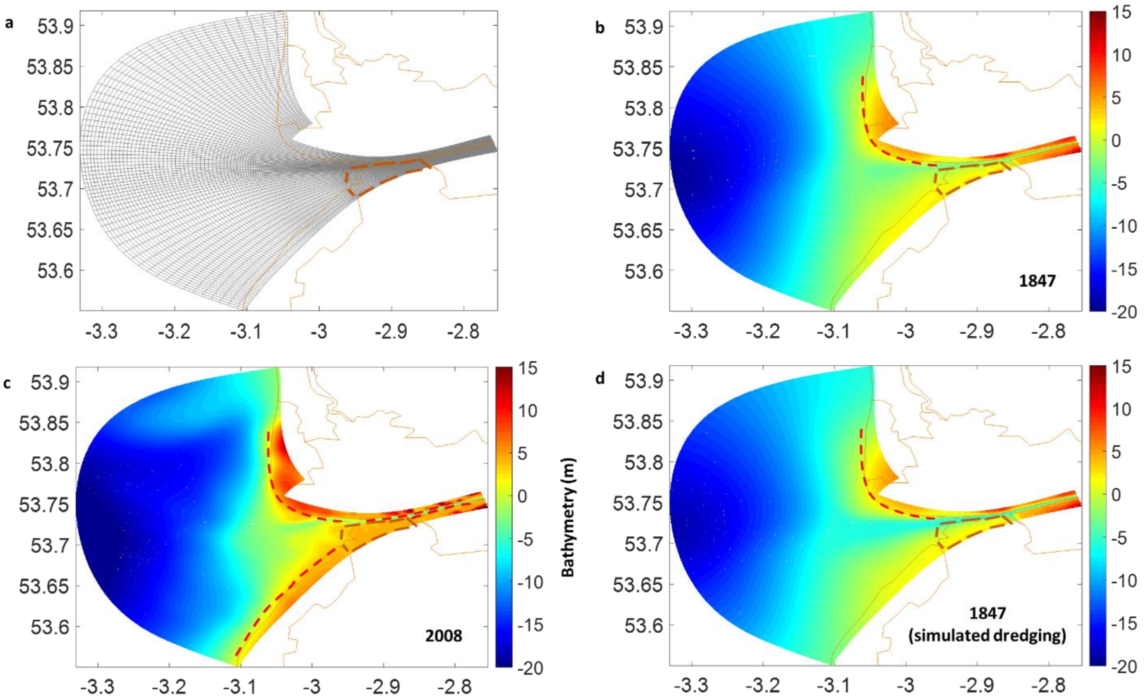

Figure 14. Grid (a) and bathymetries from 1847 (b), 2008 (c) and 1847 with simulated dredging (d), used for the model set-up. The continuous brown lines represent the land boundary. The dashed brown lines enclose the area of the domain used for the sediment budget calculation of Hesketh Out Marsh (i.e., the salt marsh platform). The dashed red lines indicate the position of the embankments at the time of bathymetric survey.

3.6 Results

3.6.1 Marsh evolution and sediment provenance

Figure 15 shows the first two components of the PCA performed on the XRF measurements of the sediments taken from Hesketh Out Marsh, the Irish Sea floor, Southport sand dunes and the Ribble catchment. Component 1 and component 2 summarise 72.5% of the variance in the data, respectively 63.8% and 8.7%. Figure 15 also shows how the parameters are used by each component to separate the samples. Component 1 separates samples rich in salt water (Na and S), shells (Ca and Sr) and silicates (Si) from those rich in silt/clay mineral indicators (e.g., Zr, Ti, Rb, K, Al) and pollutants (e.g., As, Pb, Zn). Component 2 separates samples rich in silicates (Si) with and without shelly materials (Ca and Sr). The samples from Hesketh Out Marsh basal core overlap with the samples from the Irish Sea cores and one sample from the Southport sand dunes. Hesketh Out Marsh upper core is characterised by samples that in part cluster with the marine and basal core samples or form a second cluster by themselves. The samples from the Ribble catchment form a third cluster with two of the samples from the Southport sand dunes. This implies that there is a strong correlation between the geochemical composition of the Irish Sea floor sediments and the Hesketh Out Marsh basal core sediments, while most of the upper core does not show this association; conversely, the sediments collected from the Ribble catchment do not correlate with any of the other two clusters. This suggests that the first 200 cm of sediment deposited on the tidal flat-salt marsh platform was predominantly supplied by the Irish Sea floor, with this input from the seafloor becoming less significant in the sediment deposition captured within the top 100 cm of the core; the river instead provides minimal sediment input to the intertidal flat system.

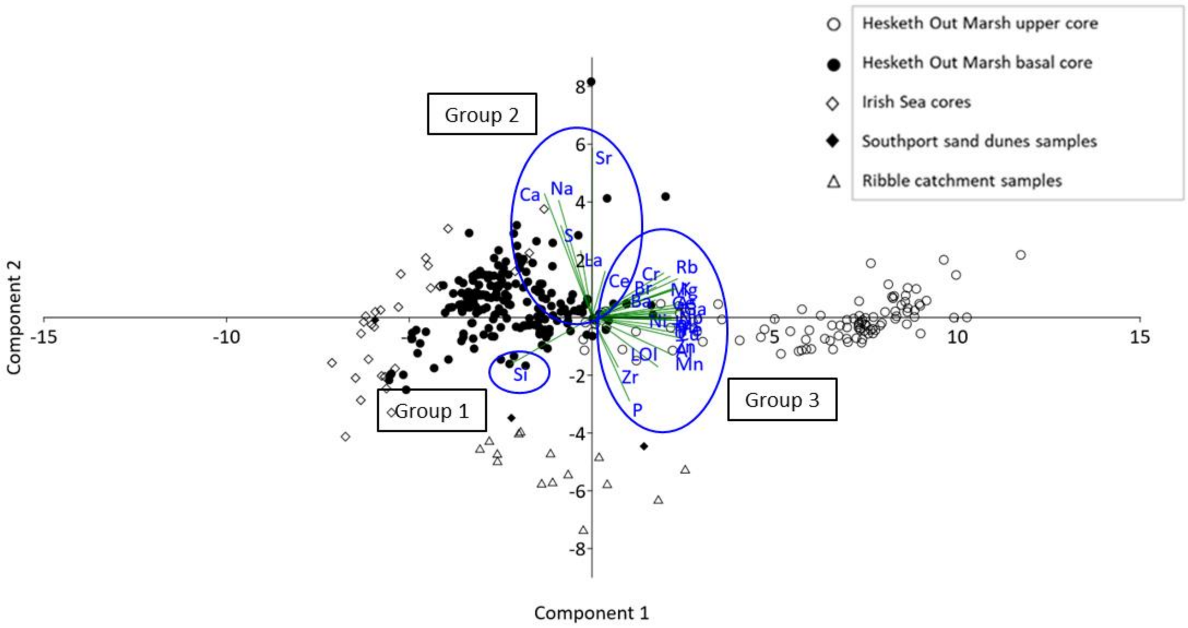

Figure 15. Principal component analysis between the samples collected from the Hesketh Out Marsh core, the samples collected from the Irish Sea cores and the Southport sand dunes, and the surface samples collected from the Ribble catchment. Component 1 and component 2 summarize 72.5% of the variance in the data, respectively 63% and 8.7%. The figure shows the parameters used by each component to separate the samples divided into three groups and the clusters formed by the samples that correlate with each other. Group 1 includes silicates indicators, Group 2 incudes salt water and shell content indicators, and Group 3 includes silt/clay mineral indicators and pollutants.

Figure 16 shows the age-depth distribution of the OSL ages modelled using Bayesian analysis and accretion rates calculated from the modelled ages of Hesketh Out Marsh. The ages between 300 cm and 125 cm overlap within uncertainties between approximately 1734-1806 AD and 1768-1849 AD, with a modelled accretion rate of 4.61 cm yr^{-1}. Between 100 cm and 0 cm, the ages range between 1768-1849 AD and 1926-1986 AD and the modelled accretion rate is 0.83 cm yr^{-1}.

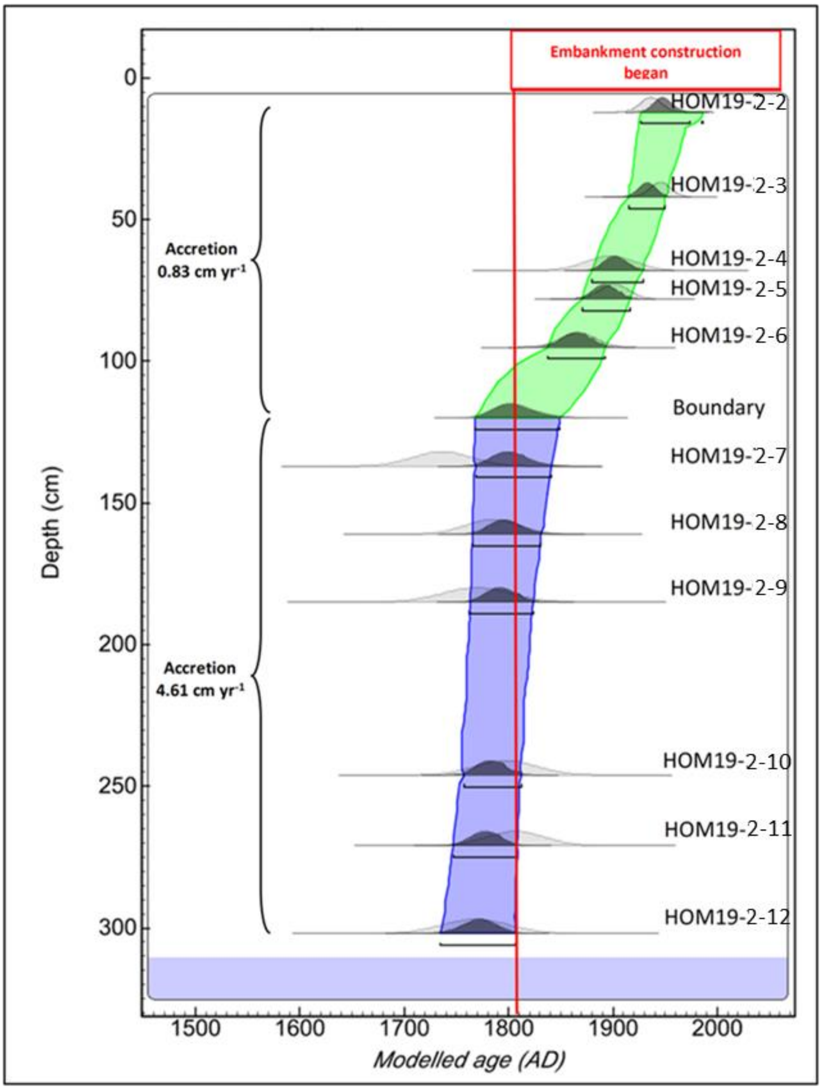

Figure 16. Age-depth profile of optically stimulated luminescence dating (OSL) ages modelled using Bayesian analysis and accretion rates calculated from the modelled ages. The change in colour represents the observed change in core stratigraphy. The OSL ages were entered in the model as a P-sequence using a k parameter which varies between 0.01 and 100. The squared gaps, dark grey and light grey distributions incorporate respectively 68.2%, 95.4% and 99.7% of the total area of the distributions with the highest probability density. Outliers were handled as a student-T distribution using a general outlier model. The final accretion profile uses the probability weighted mean age and 95.4% uncertainties from the Bayesian age-depth model.

The end-member analysis showed that 86% of the variance in the PSDs present in the HOM19-1 core could be explained by four PSD end-members (EM1, EM2, EM3 and EM4). These end members represent the recurring modes detected in the PSDs. Figure 17 a shows that EM1 has a mixed near-symmetrical distribution dominantly clay to silt with a secondary very fine to fine sand mode, EM2 has a fine-skewed to near-symmetrical distribution dominantly very fine to fine sand, EM3 has a bimodal distribution with near-symmetrical clay to silt mode and near-symmetrical to fine skewed very fine to fine sand mode, and EM4 has a fine-skewed to near-symmetrical distribution of fine to coarse sand. Figure 17 b shows that up to 300 cm EM4 and EM2 contribute equally to the PSDs of the core. Between 300 cm and to 150 cm the distribution becomes dominated by EM2 and punctuated by layers of EM4; EM1 and EM3 only give a negligible contribution in this section. Between 150 cm and 100 cm EM1 and EM2 contribute equally to the distribution and dominate this section of the core, however a minor contribution is also given by EM3. From 100 cm up to the top of the core EM1 is the dominant end-member, contributing to 70% of the distribution, while EM3 contributed for about 30%. This suggests that up to 300 cm the particle size distributions were indicative of a high energy environment dominated by infilling of coarser sand through load traction. Between 300 cm and 150 cm the environment became less energetic and dominated by infilling of finer sand occasionally layered by infilling of coarser sand and rarely punctuated by settling of silt-sized material. Between 150 cm and 100 cm the distributions reveal a progressive transition from an environment dominated by infilling through load traction into an environment dominated by accretion through settling. From 100 cm up to the top of the core the environment becomes dominated by settling of silt-sized particles layered with occasional infilling of fine sand.

This suggests that the rapid accretion that occurred between 1734-1806 AD and 1768-1849 AD was caused by an infilling of well-sorted, sand-sized sediment into the estuary accommodation. The slower accretion that characterizes the period comprised between 1768-1849 AD and 1926-1986 AD, on the other hand, was triggered by the deposition of poorly sorted silts.

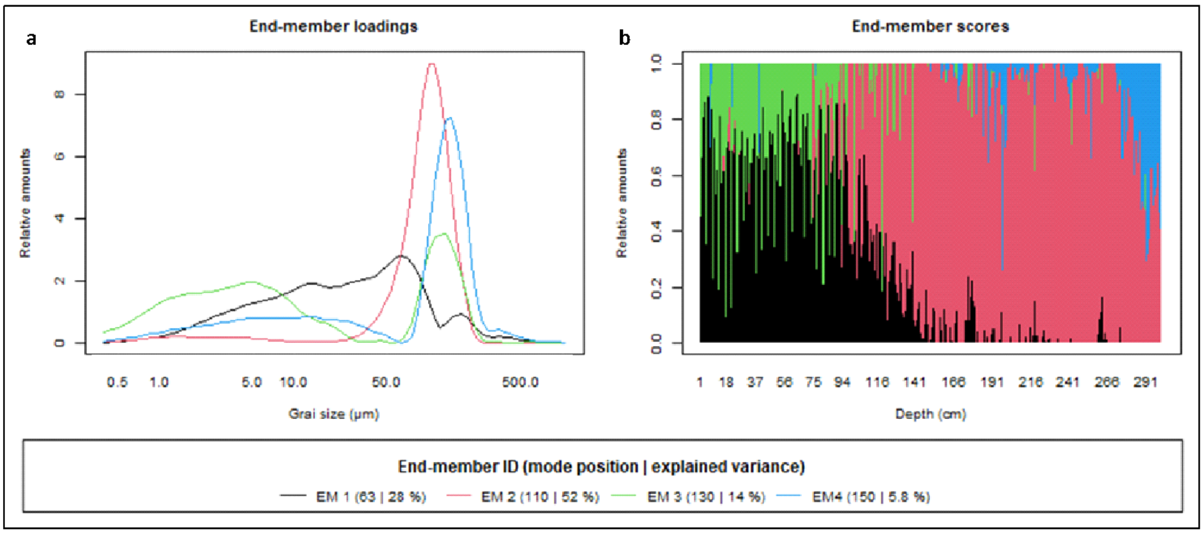

Figure 17. End-members loading (a) and down-core profile of end-members scores (b) for HOM19-1. A fine-skewed to near-symmetrical distribution is typical of traction load delivered by the faster tidal flow velocities (i.e., during flood phase); a near-symmetrical distribution is typical of the suspension load that settles during the turn of the tide (i.e., during ebb phase).

Figure 18 shows that the core is dominated by coarse to very coarse sand up to 150 cm. From 150 cm to 100 cm fine sand becomes dominant. At 100 cm, grains become finer, ranging between fine sand and coarse silt. The grains are mostly well-sorted to moderately sorted up to 100 cm, while the top 100 cm of the core is mainly dominated by poorly to very poorly sorted grains. The grain size distribution is mostly positively skewed up to 150 cm, where near symmetrical distribution starts becoming more common up to 100 cm; from 100 cm to the top of the core the distribution becomes mostly near symmetrical. The core is mostly leptokurtic up to 150 cm. From 150 cm to 100 cm, it becomes mostly mesokurtic. From 100 cm to the top of the core it becomes mostly platykurtic. NIRS analysis suggests that mineral content constitutes more than 90% of the material collected from Hesketh Out Marsh, while shell and organic content together only constitute less than 0.2%. SiO_2 increases consistently up to 50 cm, where it reaches almost 100% of the total composition, and then decreases consistently up to 15 cm, where it drops sharply. $CaCO_3$ behaves in a specular way; it decreases up to 100 cm, where the quantity becomes negligible such that the model stops detecting it, except for a few short sections; it then increases again up to the top of the core; however, the latter increase is likely caused by the biological production of calcium carbonate by plants rather than by an increase in shell content. Humic/Fulvic acid is constant up to 50 cm, where it then starts increasing up to the top of the core. Rb stays constant up to 120 cm, where it starts decreasing up to the top of the core. Ca/K and Si/Al are constant up to 100 cm, where they start decreasing slightly up to 75 cm, and then remain constant up to the top of the core; Ca/K shows a slight increase towards the top which again could be due to biogenic production. Fe/Mn stays constant up to 140 cm, where it then starts decreasing up to 120 cm, after which it remains constant up to the top of the core. LOI is constant up to 100 cm, where it starts to increase up to the top of the core. The clustering analysis statistically shows that the core is divided into two main sections, one extending from the bottom of the core up to 120 cm, dominated by sand-sized, well-sorted grains, shelly material, and reduced conditions, and one extending from 120 cm to the top of the core, dominated by silt-sized, poorly sorted grains, and high mineral and organic content.

Overall, Figure 18 suggests that a sandflat environment dominates the core up to 150 cm, while a transition from sandflat to mudflat occurs between 150 cm and 70 cm. At 70 cm a mudflat environment becomes dominant up to 15 cm, where the transition to a fully vegetated marsh occurs. The most statistically significant change in the down-core composition occurs at c.a. 120 cm, where the sandflat is replaced by a mudflat.

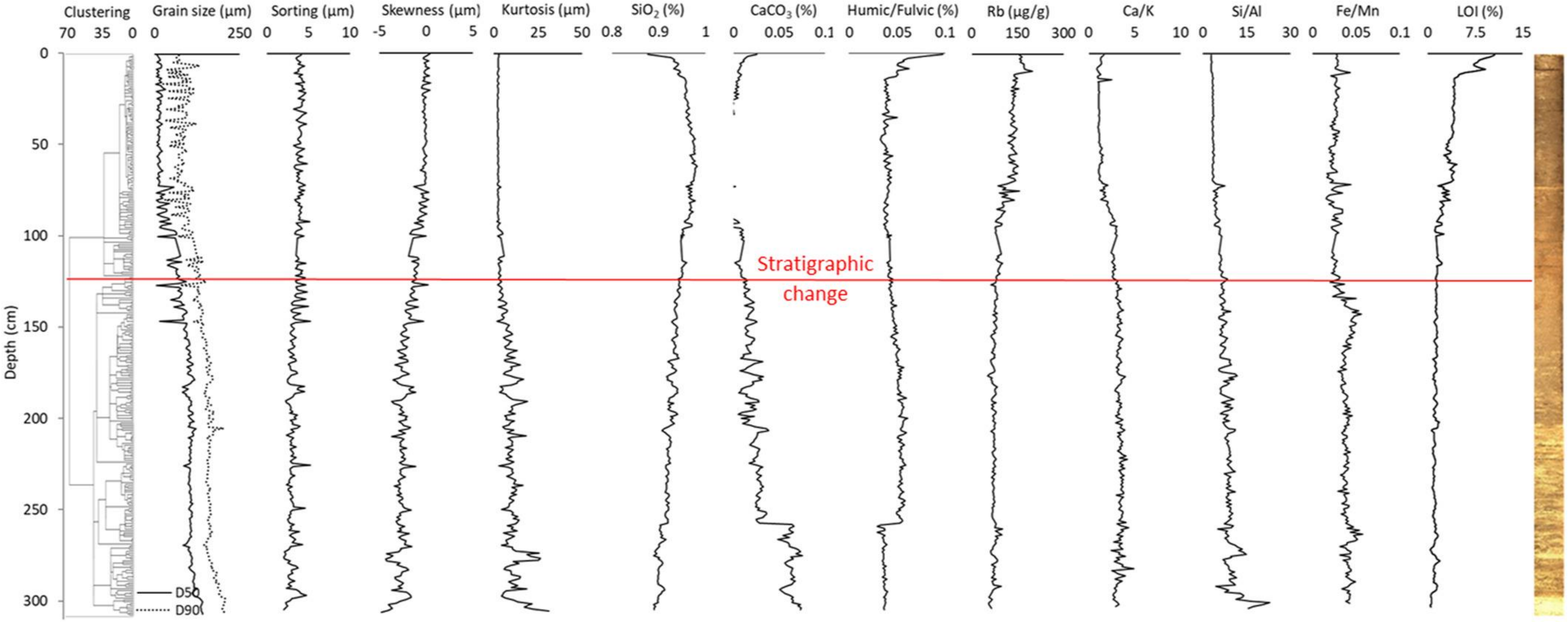

Figure 18. Depth profile of particle size distribution statistical parameters (D50, D90, sorting, skewness, kurtosis), NIRS components (SiO_2, $CaCO_3$, Humic/Fulvic acid), X-Ray Fluorescence parameters (Rb, Ca/K, Si/Al, Fe/Mn) and loss-on-ignition, with relative clusters analysis, for HOM19-1. The red line indicates the statistical division of the core into two main sections.

3.6.2 Modelled scenarios

Figure 19 summarizes the results derived from the sediment budget calculations performed for the numerical simulations. Figure 19 a shows that the sediment budget of Hesketh Out Marsh for present day decreases compared to the sediment budget for the 1847 AD bathymetry; this is true for both scenarios (i.e., with and without embankments). It also shows that, for all simulated bathymetries, the sediment budget decreases when embankments are added. Figure 19 b shows that dredging of the channel causes an increase of 0.5% in the sediment budget when there are no embankments present and an increase of 1.25% when embankments are added.

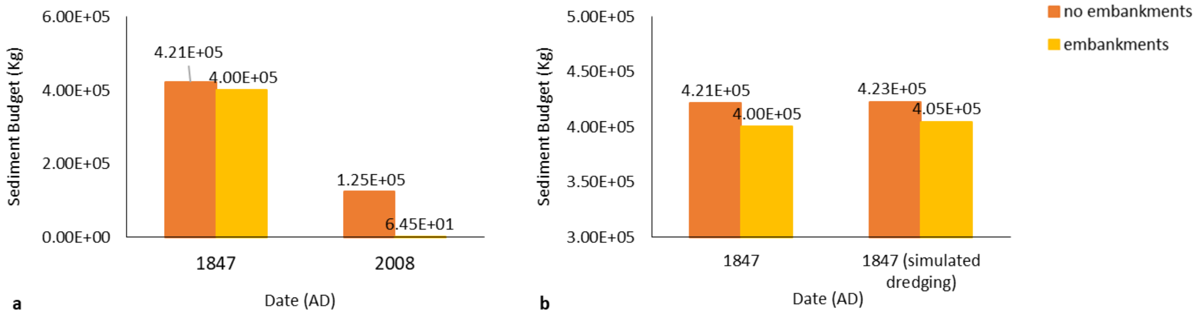

Figure 19. Sediment budget calculated for Hesketh Out Marsh after one year of simulation with and without embankments presence for the years 1847 and 2008 (a); sediment budget calculated for Hesketh Out Marsh after one year of simulation with and without embankments presence for the year 1847 with and without dredged channel (b). The magnitude of the sediment budget is only influenced by the transportation and deposition of the initial suspended sediment input and the constant input of suspended sediment load at ocean and river boundary; the non-erodible bed composition allowed no sediment input generated from the erosion and resuspension of the sea and channel bedload.

Figure 20 shows the tidal analysis performed for each simulated bathymetry. The Ribble Estuary resulted to be overall flood dominated in all simulated years and for both scenarios (i.e., with and without embankments; Figure 20 a, b). In a scenario with no embankments, the flood dominance increases for the present bathymetry with respect to the 1847 AD bathymetry (Figure 20 a). When embankments are added, despite the estuary remaining flood dominated, there is an overall intensification of the ebb currents, particularly near the tidal flat (Figure 20 c). For the 2008 AD bathymetry, the intensification of the ebb currents is significant also in the outer estuary (Figure 20 c). This explains why the sediment budget decreases when embankments are added, since an intensification of ebb currents causes an increase in the sediment export out of the system. Figure 20 (d, e) shows that the increase in ebb dominance follows an increase in the phase of the M2 constituent and a decrease in the phase of the M4 constituent. With channel dredging, the flood dominance near the tidal flat is enhanced in both scenarios (i.e., with and without embankments; Figure 20 a, b). This explains the overall increase in the sediment budget caused by the channel dredging compared to the non-dredged bathymetry, as the enhanced flood dominance near the tidal flat promotes sediment import. When embankments are added, the intensification of the ebb currents near the tidal flat is lower compared to the non-dredged bathymetry (Figure 20 c), which explains why the increase of sediment budget for the dredging scenarios compared to the no-dredging scenarios is greater when embankments are present.

Overall Figures 19 and 20 suggest that embankments promote sediment export and cause a decrease in the sediment budget of the salt marsh.

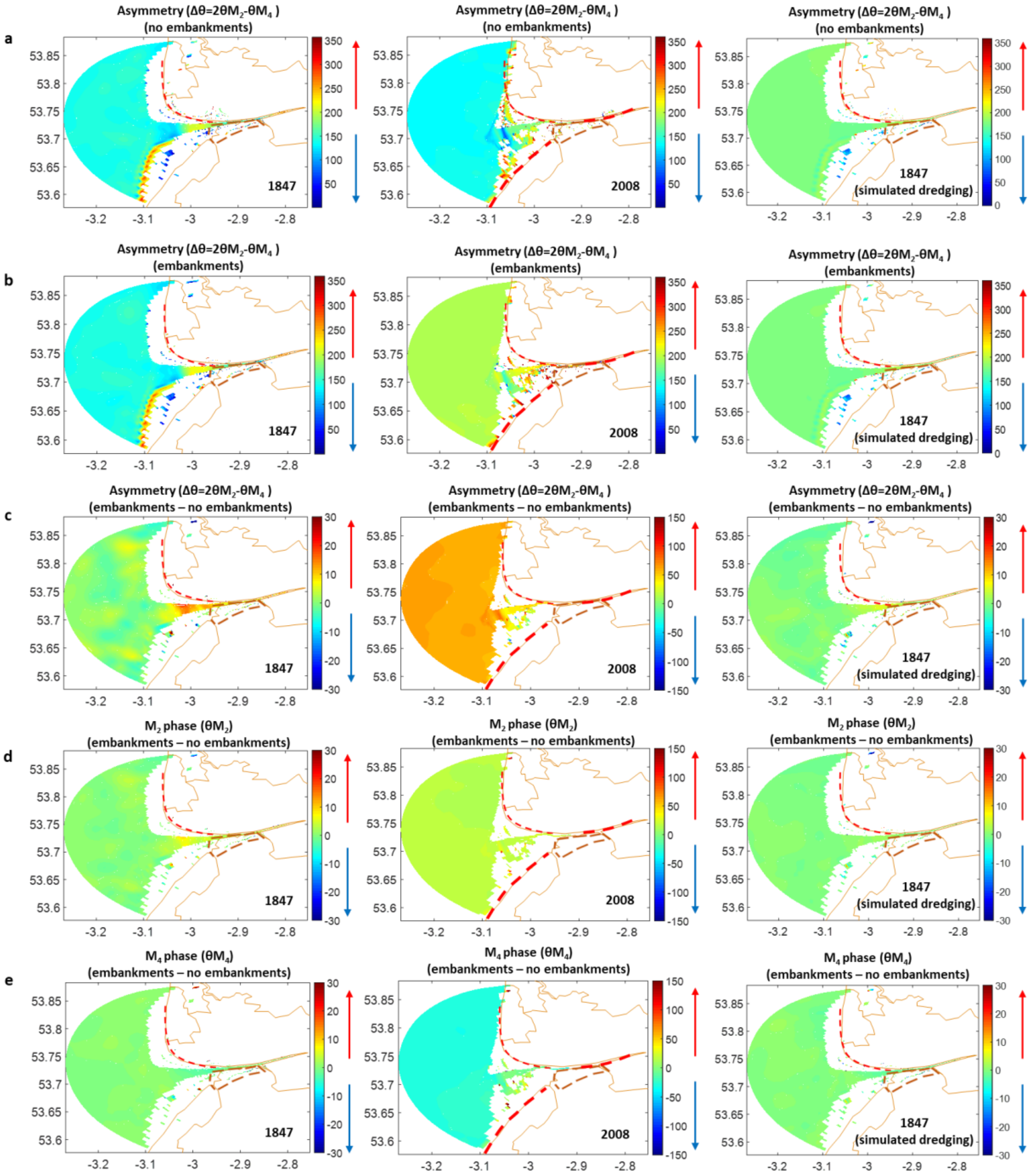

Figure 20. Tidal asymmetry (Δθ) for the scenarios without embankments (a) and with embankments (b). Where Δθ is between 0° and 180° the system is flood dominated (blue arrows), where Δθ is between 180° and 360° the system is ebb dominated (red arrows). Tidal asymmetry (Δθ) (c), M2 phase (θ_{M2}) (d) and M4 phase (θ_{M4}) (e) difference between the scenarios with embankments and the scenarios with no embankments. Where Δθ is positive there is an increase in ebb dominance (red arrows), where it is negative there is an increase in flood dominance (blue arrows). The continuous brown lines represent the land boundary.

The dashed brown lines enclose the area of the domain used for the sediment budget calculation of Hesketh Out Marsh (i.e., the salt marsh platform). The dashed red lines indicate the position of the embankments at the time of bathymetric survey. See Figure S5 in Appendix I for tidal distortion (A_{4-2}), M2 amplitude (A_{M2}) and M4 amplitude (A_{M4}) for the same scenarios.

3.7 Discussion

3.7.1 Sediment provenance

The principal component analysis (Figure 15) showed a correlation between the geochemistry of Hesketh Out Marsh sediments and the geochemistry of the Irish Sea floor sediments, indicating that the provenance of the marsh sediments is predominantly marine. Figures 6 and 7 show the causes that determined the strong correlation between the Irish Sea cores and the lower part of Hesketh Out Marsh core, while the upper 0-1.25 m of salt marsh sediments do not show an association with the seabed sediments. The lower 1.25-3 m of sandflat deposits of the core are characterised by sediments entrained at the seafloor by flood currents and deposited directly in the estuarine accommodation space before a tidal flat was formed, while the upper part is characterised by fine suspended sediments deposited by ebb currents through tidal creeks when a tidal flat was already forming (Rahman and Plater, 2014). Our results agree with the interpretation of Lyons (1997) that sediments are delivered into the estuary mainly by tidal pumping. They further support previous hypotheses that abundant legacy of sediment left during the last glacial cycle (Scourse et al., 2021) and regularly remobilised through the central Irish Sea, often as sediment waves (Van Landeghem et al. 2012), has been the main source of sediment supply to the estuary (Wright et al., 1971).

3.7.2 Changes in marsh accretion

While some studies (e.g., Madsen et al., 2005; Madsen et al., 2007a,b; Davis et al., 2010) have found well-bleached quartz in tidal flats and salt marsh environments, Madsen et al. (2009) found partially bleached quartz in three hurricane deposits made of coarse sandy particles rapidly deposited on Little Sippewissett Marsh. High levels of turbidity characterising the water table during high energy events, which are a major source of sediment supply to the Ribble Estuary (Lyons, 1997), might have contributed to partial bleaching by attenuating the blue end of the daylight spectrum (Berger, 1990; Plater and Poolton, 1992). Moreover, the tidal inundation of Hesketh Out Marsh is semidiurnal, therefore sediment deposition can occur either at daytime or night-time (UKHO, 2019). This means that some grains experience shorter exposure to light if not none, further contributing to partial bleaching (Mauz et al., 2010). However, since the sediments analysed are very young - between 67 ± 9 and 264 ± 26 years old - they might have also suffered incomplete resetting of prior stored charge which can lead to significant offsets in the equivalent dose (Murray and Olley, 2002). The asymmetry in the D_e distribution could alternatively be caused by microdosimetry. It was indeed found that, in sandy environments, K-feldspar can affect quartz dose rate distribution and, as a consequence, the D_e distribution skewness and dispersion of dose rate distributions increase as the number of potassium-rich feldspar grains is decreased relative to the number of quartz grains or if the quartz grain size increases, as this causes an increase in distance between the quartz grains and the source of potassium (Guerin et al., 2015). Nonetheless, regardless of the cause of the asymmetrical D_e distribution, accurate OSL ages can be derived using small aliquots and the MAM (Galbraith and Laslett, 1993).

The Bayesian analysis of the OSL ages shows that between 1734-1806 AD and 1768-1849 AD there was a very rapid accumulation of sediments (ca. 4.61 cm yr^{-1}), followed by a slower accretion (ca. 0.83 cm yr^{-1}) that persisted until 1926-1986 AD (Figure 16). The overlap of the OSL ages between 300 cm and 125 cm was likely to be due the resolution of the technique that is not able to differentiate individual ages in such fast deposition. However, the timeframe of the environmental reconstruction of the historical maps confirms the accuracy of the age intervals at a decadal scale. Indeed, according to the reconstruction of marsh evolution (Figure 18), the first period of fast accretion determined the formation of the sand flat substrate until 1768-1849 AD, when the rate of accretion decreased, and the sandflat progressed into a mudflat. Accordingly, the historical reconstruction shows that in 1840 AD Hesketh Out Marsh area was occupied by a sandflat (Figure 12 b), while between 1890 AD and 1950 AD a mudflat was the dominant environment (Figure 12 c, d, e). The new OSL ages here extend this understanding by providing the first record of sediment dating and the longest record of accretion rates for the Ribble Estuary (Mamas et al., 1995) that then allow us to compare with hydrodynamical modelling to understand the processes involved in salt marsh accretion. The numerical simulations show that the sediment budget of Hesketh Out Marsh decreases towards present day (Figure 19 a); this is true for both scenarios (i.e., with and without embankments). There is an agreement between the trends observed for the sediment budget of the 1847 AD and 2008 AD scenarios and the trends detected in the long-term accretion profile provided by the luminescence ages. The results of the two techniques are therefore comparable.

Historical records of the estuary show that in 1810 AD embankment construction started along the northern bank of the Ribble Estuary. Between 1810 AD and 1850 AD the whole northern bank, from Lytham to Preston, and part of the southern bank, north of Southport, was embanked, with the exception of the coastline surrounding Hesketh Out Marsh area (van der Wal et al., 2002). The period where the majority of embankment construction occurred (1810-

1850 AD) falls within the age intervals given by the OSL ages for the period of the fast sand flat accretion (from 1734-1806 AD to 1768-1849 AD). However, the OSL age intervals suggest that there is a possibility that the rapid sedimentation might have started before the beginning of the 19th century. Moreover, no shift was detected from a slower to a faster accretion rate in the lower part of the core, therefore there is no direct evidence that the embankment construction might have triggered the infilling that caused the rapid sedimentation.

3.7.3 Effects of embankments on marsh sediment budget

The calculation of the sediment budget for all the simulated bathymetries revealed that the final sediment budget for Hesketh Out Marsh is greater when no embankments are present (Figure 19 a). The quantity of sediment entering and exiting an estuary during each tidal cycle is influenced by tidal asymmetry (Guo et al., 2016; Palazzoli et al., 2020; Donatelli et al., 2018). A flood dominance (flood phase shorter and more intense than ebb phase) triggers a net landward sediment import as flood velocities can be sufficiently high to resuspend sediment, while an ebb dominance is responsible for a net export (Van Dongeren and de Vriend, 1994; Lanzoni and Seminara, 2002). Tidal analysis for the Ribble Estuary (Figure 20 a, b, c) showed that, despite the estuary remaining flood dominated, the addition of embankments along the coastline affected the tidal propagation within the system by causing an overall intensification of ebb currents and weakening of flood currents. The Irish Sea, where the Ribble Estuary is located, is influenced by a phenomenon of resonance (Pickering et al., 2012). In San Francisco Bay (Holleman and Stacey, 2014), Yellow River Delta (Pelling et al., 2013) and the Patagonian Shelf (Carless et al., 2016), it has been observed that the introduction of embankments can affect the resonance properties of a basin, causing changes in the amplitude and phase of the M2 and M4 constituents, which result in changes in tidal distortion and asymmetry. In the Ribble Estuary, this increase in ebb dominance when embankments are added, follows an increase in the phase of the M2 constituent and a decrease in the phase of the M4 constituent (Figure 20 d, e).

When the channel is dredged, the areas of the channel adjacent to the tidal flat become flood dominated (Figure 20 a, b). It has been observed that an enhancement of flood dominance following channel dredging is caused by a tidal amplification which increases estuarine circulation (Zhu et al. 2015; Van Maren et al. 2015). Other estuaries, such as the Ems Estuary, located between the Netherlands and Germany, have showed similar behaviour (Van Maren et al. 2015). In the Ribble Estuary, this resulted in a lower intensification of ebb currents when embankments are added (Figure 20 c), hence attenuating the effects of the embankments on the sediment budget (Figure 19 b).

Overall, our numerical modelling shows that embankments enhanced sediment export out of the system (Figures 19 and 20). Embankments begun to be built in 1810 AD; however, the oldest bathymetry available is from 1847 AD (van der Wal et al., 2002; Parsons et al., 2013a). Therefore, we cannot directly discuss changes in sediment transport caused by the beginning of the embankment construction. Luminescence derived accretion rates (Figure 16), in line with historical maps (Figure 12) and later bathymetric studies (van der Wal et al., 2002), show a continuous infilling of the estuary and progressive formation of the tidal flat over the period studied. Accordingly, tidal analysis shows that in 1847 AD the estuary was overall flood dominated despite the presence of the embankments (Figure 20 b). For the 2008 AD bathymetry, with no embankments present, the flood dominance of the Ribble Estuary is greater than it is for the 1847 AD (Figure 20 a). Both in the Ribble Estuary (Li et al., 2018; Chapter 4) and in other sites (e.g., Donatelli et al., 2018; Palmer et al., 2019), it has been observed that an increase in accommodation space promotes ebb dominance; the strengthening of flood dominance for the 2008 AD no-embankment scenario could be therefore caused by more extensive intertidal flats present in the 2008 AD bathymetry, responsible for a decrease in accommodation space. A similar behaviour has been observed in the Tamar Estuary (Australia), where infilling of the accommodation space causes an increase in flood dominance (Palmer et al., 2019). However, when embankments are added, the 2008 AD scenario is characterised by a weakening of the flood currents compared to the 1847 AD scenario which extend also to the outer estuary (Figure 20 b). This indicates that further land reclamation and the addition of more embankments reduced the overall flood dominance of the estuary towards present day, which explains the sharper drop in sediment budget when embankments are added to the 2008 AD bathymetry compared to when they are added to the 1847 AD bathymetry. It further suggests that in 1810 AD the estuary might have been characterised by greater accommodation space and might have already been flood dominated, but the beginning of embankment construction might have already started reducing the natural strengthening of flood dominance driven by the infilling of the accommodation space.

3.7.4 Natural accretion of the marsh

The OSL age intervals suggested that there is a possibility that the rapid sedimentation might have started before the beginning of the 19th century, preceding the start of the embankment construction (Figure 16). Moreover, no shift was detected from a slower to a faster accretion rate in the lower part of the core, showing no direct evidence that the embankment construction might have triggered the rapid sedimentation (Figure 16). The sediment budget and tidal analysis suggest that in the Ribble Estuary, embankments were responsible for an overall intensification of the ebb currents, promoting sediment export and causing a decrease in the sediment budget of the tidal flat-salt marsh platform (Figures 19 and 20). Therefore, embankment construction was unlikely to be responsible for an increase in sedimentation. This suggests that the infilling of the estuary responsible for the high sedimentation rate must have had a different cause.

The particle size distribution analysis (Figure 17) suggests that the rapid accretion, detected by the Bayesian analysis of the OSL ages and occurred between 1734-1806 AD and 1768-1849 AD, was mainly caused by infilling of the estuary with sand-sized sediments during flood tide (Rahman and Plater, 2014) and the reconstruction of Hesketh Out Marsh evolution (Figures 6) suggests that in this period a sandflat was the dominant environment (Plater et al., 2007). In the first period (bottom 300 cm of the core) the Hesketh Out Marsh area was a highly energetic environment that favoured deposition of coarser sand into the estuary; this was then followed by a transition (between 300 cm and 150 cm of the core) in which the environment became less energetic and dominated by infilling of finer sand (Figure 17). Glacial Isostatic Adjustment models show a long-term decrease in relative sea-level in North-West England for the past 2000 years (Tooley, 1974; Shennan et al., 2018). Historical tidal gauge records showed that this was followed by an average increase in mean sea-level of 2 mm yr^{-1} since the beginning of the measurements in 1858 AD (Woodworth et al., 1999; PSMSL, 2019), and Plater et al. (1993) suggested that a secular rise in sea-level characterised the area, increasing the accommodation space. The secular rise in sea-level of the past centuries and consequent increase in accommodation space, might have led to the formation of the estuary, favouring an infilling of the area with marine sediments. The central Irish Sea is characterised by waves of mobile sediments that move up to 70 m per year (Van Landeghem et al. 2012). This high amount of mobile sediment is a legacy of materials left by the former Irish Sea Glacier that is mobilised on the seafloor in the form of sediment waves and sand sheets (Van Landeghem et al. 2012). Wright et al. (1971) suggested that this sediment was the main source of sediment supply to the estuary, and this is confirmed by the analysis of sediment provenance (Figure 15) that shows a strong correlation between the floor sediment of the Irish Sea and the sediment of the initial Hesketh Out Marsh sandflat platform. The progressive increase of the accommodation space and the overall flood dominance of the estuary (Figure 20 a) might have facilitated the deposition of sea-bed sediments transported from the Irish Sea floor into the estuary during flood tide (Plater et al., 1993), therefore explaining such a rapid deposition of sediment into the area. As the platform started increasing in elevation, the deposition of coarse sand was replaced by the deposition of finer sand, which was responsible for the formation of the sandflat (Reed, 1990). The slower accretion that characterized the period comprised between 1768-1849 AD and 1926-1986 AD, on the other hand, was caused by the deposition of poorly sorted silts (Figure 17, Rahman and Plater, 2014). The reconstruction of Hesketh Out Marsh evolution (Figure 18) suggests that the accretion rate decreases with the progression from a sandflat to a mudflat (Plater et al., 2007) and the particle size distribution analysis (Figure 17) suggests that between 150 cm and 100 cm a transition occurred from an environment dominated by infilling through load traction into an environment dominated by accretion through settling, while in the top 100 cm of the core the environment becomes dominated by settling of silt-sized particles layered with occasional infilling of fine sand (Rahman and Plater, 2014). This mode of deposition is typical of mudflat-salt marsh systems. When mudflat platforms reach an elevation which is above sea-level, tidal creeks form and become the main mean through which marine sediments can reach the marsh platform and deposit; they transport silt-sized sediments to the marsh areas of higher elevation during flood tide and deposit them during ebb tide (Reed et al., 1999). The sandy layers that punctuate the upper 100 cm of the core are instead likely to be caused by infilling of fine sand through load traction during occasional flooding of the marsh platform owed to spring tide high waters or storm surges (Chapter 4 and Appendix II). Accordingly, the numerical simulations show that the sediment budget of Hesketh Out Marsh decreases towards present day both for embankments and no-embankments scenarios (Figure 19 a). The 1847 AD bathymetry is characterised by a greater accommodation space preceding the formation of the intertidal flat, whereas the 2008 AD bathymetry was characterised by an established intertidal flat and salt marsh platform. Therefore, it is likely that the increase in elevation of the sandflat platform, following the infilling of the estuary accommodation space, and the conversion into a mudflat-salt marsh platform, was responsible for the decrease in accretion rate detected by OSL around 1768-1849 AD. Hence, the rapid accretion of the Ribble Estuary tidal flat-salt marsh system seems to be a natural evolution of the system that adapted to the high availability of sediments.

3.7.5 Long-term marsh resilience to embankment construction

The numerical simulations showed that the estuary has been flood dominated through the investigated period, but embankments were responsible for an overall intensification of the ebb currents in the system which promoted sediment export. The paleoenvironmental analysis showed that Hesketh Out Marsh has been accreting at a rate of 4.61 to 0.86 cm yr^{-1} over the last ca. 190 years and that the estuary has experienced continuous infilling over the period studied caused by a natural high rate of sediment supply. Furthermore, the modelling showed that the channel dredging reduced the intensification of the ebb currents caused by the construction of the embankments. The combination of these analyses suggests that the effects of the embankment construction on sediment transport did not compromise the long-term resilience of the salt marsh because of the high rates of sediment supply and undergoing river dredging that enhanced flood dominance near the tidal flat.

Part of Hesketh Out Marsh was enclosed by embankments in 1980 AD and managed realigned between 2007 AD and 2017 AD (Tovey et al., 2009). Managed realigned sites have been found to be resilient to rates of sea-level rise below 5 mm yr^{-1} (Orr et al., 2003). The resilience of managed realigned salt marshes has been found to be highly dependent upon the breach design and size of the site (Kiesel et al., 2020; Kiesel et al., 2022) as well as sediment supply, size of sediment supplied to the marsh and tidal range (Xu et al., 2022). It was also observed that the vegetation cover at different stages of marsh maturity and related ability to trap sediments in restored salt marshes are comparable with those of forming marshes (Xu et al., 2022). However, for Hesketh Out Marsh, the effects on the reclamation and subsequent managed realignment on the marsh accretion cannot be discussed in relation to the accretion rates provided by the luminescence analysis, due to the low resolution of the technique that was only able to provide with ages ranging between 1734-1806 AD and 1926-1986 AD with a minimum error of +/-30 years.

Other studies have shown that embankment construction can trigger higher sedimentation rates in certain areas of an estuary. This was observed, for instance, by Pontee (2014) in the Humber Estuary and Lee et al. (2017) in Chesapeake Bay and Delaware Bay, who concluded that, by channelising sediment, embankments can favour the delivery of sediment to a specific area of an estuary accommodation space, inducing siltation of intertidal areas and aiding vertical accretion of tidal flat-salt marsh systems. This suggests that the effects of embankments on sediment deposition can change from case to case depending on the hydrodynamic and morphodynamic feedbacks characteristic of the site and that results for single basin studies cannot be generalised. Along the North-West coast of England, other estuaries of great economic importance and at high flood risk, experience tidal dynamics and rate of sediment supply similar to the Ribble Estuary (Parsons et al., 2013d). Liverpool Bay estuaries – i.e., Dee Estuary and Mersey Estuary – and Morecambe Bay estuaries are all tidally dominated, macrotidal, flood dominated and receive sediments from the central Irish Sea that accumulate in intertidal areas forming extensive tidal flats and salt marsh platforms (Parsons et al., 2013b, 2013c, 2013d). They were also all affected by land reclamation and embankment construction over the past c.a. 200 years (Parsons et al., 2013b, 2013c, 2013d). Hence, the findings of this study could be used to inform about the effects that embankment construction might have on the sediment transport dynamics of these estuaries in relation to sediment availability.

3.8 Conclusions

This study used Hesketh Out Marsh, in the Ribble Estuary, and an integrated approach of paleoenvironmental analysis and numerical modelling to investigate the contribution of embankment construction to long-term salt marsh accretion. OSL analysis showed that Hesketh Out Marsh has been accreting at a rate of 4.61 to 0.86 cm yr^{-1}, and that this rapid accretion responsible for the infilling of the estuary might have started before the beginning of embankment construction in 1810 AD, which is in contrast with previous hypotheses. Moreover, no shift from a slower to a more rapid accretion was noticeable in the trend that could link the beginning of the rapid accretion to the beginning of the embankment construction. Furthermore, the numerical simulations showed that in the Ribble Estuary the addition of embankments is responsible for an overall intensification of the ebb currents, which enhances sediment export. This confirms that embankments cannot be considered responsible for an increase in sedimentation. XRF analysis showed that sediment supply to the Ribble Estuary is predominantly from the Irish Sea and, in conjunction with PSD and NIRS analyses, it showed that the changes in accretion rate detected by OSL were connected to the natural evolution and stabilisation of the system, supporting the hypothesis that the high sediment supply to the Ribble Estuary is likely to be connected to the high availability of mobile sediment in the central Irish Sea that was discharged by the Irish Sea Glacier during the last deglaciation. The rapid sedimentation is, therefore, more likely to be attributed to the natural sediment supply to the estuary. The following decrease in sedimentation is instead attributable to the natural evolution of the mudflat-salt marsh system that reached equilibrium. Despite the numerical modelling showing that embankments promote sediment export, the long-term accretion of the salt marsh was not compromised by the effects of the embankment construction. The numerical modelling showed that the estuary has been flood dominated throughout the studied period and that the infilling of intertidal flats, combined with undergoing river dredging, further enhanced this flood dominance. It is likely that a combination of overall flood dominance, natural high rates of sediment supply, infilling of the accommodation space with this sediment and undergoing river dredging, contributed to the formation and accretion of the salt marsh despite the negative impact of the embankments on the marsh sediment budget.

3.9 Acknowledgements

We acknowledge support from the School of Environmental Sciences, University of Liverpool, which is funding the PhD project of the first Author and the EPRSC support to Prof Leonardi N. (EP/V056042/1). We also acknowledge the support of RSPB for allowing the field work campaign in the Ribble Estuary and the Physical Geography and luminescence laboratories and their technicians and students (Jennifer Bradley, Luke Glascott, Mike O'Connor and Grace Skirrow) for their support with equipment, field work and laboratory analyses. The model for the Ribble Estuary was originally designed as part of the projects 'Adaptation and Resilience of Coastal Energy Supply (ARCoES)' and 'Physical and biological dynamic coastal processes and their role in coastal recovery (BLUE-coast)' and we are grateful for being able to use it; the original model details are presented in Li et al., 2018, 2019 and Dr. Li X. developed the model. We also thank Prof Plater A. for the constructive discussions about the interpretation of the results, Dr. Fenn K. for advice on the OSL related analysis and Dr Matsoukis C. for significant advice on the model running. We ultimately thank three anonymous reviewers and the Associate editor for their constructive feedback on the manuscript.

3.10 Data availability

Data related to this article can be found in the following repository: https://doi.org/10.5281/zenodo.6425788.

Chapter 4

Salt marsh resilience to sea-level rise and increased storm intensity

4.1 Preface

Chapter 3 showed how anthropogenic interventions (e.g., embankment construction and dredging) can change the tidal dynamics and, therefore, the sediment transport dynamics within an intertidal system. Such changes affect sediment delivery to the salt marsh, with implications for marsh accretion, although the extent to which sediment supply to the marsh platform is affected depends on the natural sediment availability within the system. Sediment transport dynamics within an intertidal system, however, can also be affected by natural changes in hydrodynamics (e.g., sea-level rise, occurrence of extreme events). Sea-level and storm intensity are both projected to increase within the next century but, although their separate effects on intertidal sediment dynamics have been widely investigated, their combined effect on sediment transport within an intertidal system has yet not been discussed. Hence, this chapter aims to investigate how combined scenarios of sea-level rise and increases in storm intensity might affect sediment delivery to salt marshes, with implications for future salt marsh resilience. Chapter 3 also demonstrated that sediment budgets estimated from short-term simulations of different scenarios reproducing different bathymetric and hydrodynamic conditions in time are successfully able to represent long-term changes in accretion rates and can, therefore, be useful metrics for evaluating long-term salt marsh resilience. Henceforth, to investigate marsh resilience to sea-level rise and increased storm intensity, this chapter derives sediment budgets from a wealth of sea-level and storm surge scenarios.

4.2 Abstract

Salt marshes are important ecosystems but their resilience to sea-level rise and possible increases in storm intensity is largely uncertain. The current paradigm is that a positive sediment budget supports the survival and accretion of salt marshes while sediment deprivation causes marsh degradation. However, few studies have investigated the combined impact of sea-level rise and increased storm intensity on the sediment budget of a salt marsh. This study investigates marsh resilience under the combined impact of various storm surge (0 m, 0.25 m, 0.5 m, 1.0 m, 2.0 m, 3.0 m and 4.0 m) and sea-level (+0 m, +0.3 m, +0.5 m, +0.8 m and +1.0 m) scenarios by using a sediment budget approach and the hydrodynamic model Delft3D. The Ribble Estuary, North-West England, whose salt marshes have been anthropogenically restored and have a high economic and environmental value, has been chosen as test case. We conclude that storm surges can positively contribute to the resilience of the salt marsh and estuarine system by promoting flood dominance and by triggering a net import of sediment. Conversely, sea-level rise can threaten the stability of the marsh by promoting ebb dominance and triggering a net export of sediment. Our results suggest that storm surges have a general tendency to counteract the decrease in sediment budget caused by sea-level rise. The timing of the storm surge relative to high or low tide, the duration of the surge, the change in tidal range and vegetation presence can also cause minor changes in the sediment budget.

4.3 Introduction

Salt marshes are vegetated wetlands, typical of mid and high latitudes, that are distributed within the upper intertidal zone of low-energy shorelines, such as estuaries, deltas, and barrier islands (Townend et al., 2011). Salt marshes have been widely recognised as valuable coastal defences due to their ability to buffer storm waves (e.g., Möller et al. 1999; Leonardi et al., 2018). There have been a variety of projects around the world to create new salt marshes and/or restore salt marshes that were previously reclaimed for anthropogenic activities to provide long-term and low-cost coastal protection (Temmerman et al., 2013). Salt marshes also provide other valuable ecosystem services, including nutrient removal, habitat provision and high rates of carbon sequestration at geological time scales (Zedler and Kercher, 2005; Barbier et al., 2011). The fate of salt marshes is, however, uncertain as it is still unclear how salt marshes will be affected by the combined impacts of sea-level rise and intensification of storms activity, inducing higher level storm surges (Schuerch et al., 2013; Masson-Delmotte et al., 2018). The sensitivity of tidal flat and salt marsh complexes to changes in hydrodynamics depends on a variety of local features including tidal characteristics, sediment availability, vegetation characteristics and depositional processes (Reed, 1995).

Salt marshes are generally resilient to sea-level rise when sediment supply and organogenic production are high enough to allow marsh accretion or when salt marshes can migrate upland (Kirwan et al., 2010, 2016). The accretion and encroachment of new salt marshes occurs when the delivery of fine sediments from rivers and the sea increases the elevation of marsh platforms and tidal flats relative to the sea-level, and vegetation colonises newly exposed surfaces (Reed, 1990). Sediments that arrive from the sea are delivered during flood tide and sediment deposition is determined by the duration and frequency of tidal inundation (hydroperiod) with more deposition occurring when inundation is longer and more frequent (Reed, 1990). Vegetation supports marsh stability through biomass growth, particle capture by plant stems, and enhanced particle settling caused by a reduction in turbulent kinetic energy of the water flow through the plant canopy (Morris et al. 2002; Neumeier and Ciavola, 2004; Mudd et al., 2010). Increasing rates of sea-level rise can lead to marsh drowning by increasing the accommodation space and the amount of sediment inputs required for marsh stability (FitzGerald et al., 2008; Kirwan et al., 2010; Ganju et al., 2017). Lateral erosion by wind waves can also cause marsh degradation (Marani et al., 2011; Fagherazzi et al., 2013; Leonardi and Fagherazzi, 2014; Leonardi et al., 2018; Li et al., 2019). While waves generated during storms can contribute to salt marsh erosion, there is evidence that overwash by storm surges delivers significant amount of sediments to marsh platforms supporting marsh resilience to sea-level rise (Turner et al., 2006; Walters and Kirwan, 2016; Castagno et al., 2018). Overall, the net sediment budget of a coastal system is a useful metric to evaluate the life-span of salt marshes; a positive sediment budget is frequently associated with the capability of salt marshes to expand, while a negative sediment budget has been linked to marsh degradation (Ganju et al., 2015).

This study investigates the resilience of salt marshes to sea-level rise and storm intensification by focussing on the combined influence of increasing sea-level and storm surge height on the sediment budget of a salt marsh-tidal flat complex using a numerical model of the Ribble Estuary, North-West England. Saltmarshes in the Ribble Estuary are one of Europe's largest systems, which has been restored through managed realignment to provide flood protection (Tovey et al., 2009). A total of 250 numerical simulations representing different storm surge heights and sea-level rise magnitudes were conducted; the timing of occurrence of the surge with respect to high or low tide, the duration of the surge, the change in tidal range and vegetation presence were also considered to understand the influence of these factors on the nature and amplitude of changes in sediment budget.

4.4 Study site

The Ribble Estuary is located on the Lancashire coast, North-West England (Figure 21 c). The estuary is funnel shaped, tidally dominated and macrotidal; the ordinary tidal range is 8.0 m at spring tide and 4.4 m at neap tide (UKHO, 2001). The average marsh platform elevation is approximately 3.5 m above mean sea level. The estuary experiences moderate wave energy owed to waves being generated in the Irish Sea basin (Pye and Neal, 1994). It is thought that the formation of the extensive intertidal sand-silt flats and the salt marsh at the south of the estuary resulted from the combination of infilling of sandy sediments from the bed of the Irish Sea, deposition of the silt and clay-size sediments coming from the River Ribble and a moderate wave climate insufficient to cause significant lateral erosion (van der Wal et al., 2002). Van der Wal et al. (2002) suggested that the river does not significantly influence the sediment supply to the estuary and that the sedimentation is mainly affected by marine sediment. Lyons

(1997) suggested that tidal pumping, especially during high storm surges is the main process introducing sediments into the estuary. Between 2007 and 2017, a scheme was implemented to restore the intertidal habitat previously reclaimed for agricultural purposes and the area has high ecological and economic value (Tovey et al., 2009).

4.5 Methods

4.5.1 The model

The FLOW module of the numerical finite-difference model Delft3D was used to simulate the hydrodynamics and sediment transport of the system. The model calculates non-steady flow and transport phenomena using Navier-Stokes and transport equations (Deltares, 2019a). The model accounts for bed-load and suspended-load of multiple cohesive and non-cohesive sediment fractions, vertical diffusion of sediments due to turbulent mixing and the sediment settling due to gravity. It also accounts for the effect of vegetation on the flow field. The suspended load is evaluated through the advection–diffusion equation and the bed-load transport is computed using the formulation proposed by Van Rijn (1993). The exchange of sediments between the bed and the flow for non-cohesive sediments is computed by evaluating sources and sinks of sediments near the bottom, respectively due to upward diffusion and sediments dropping out from the flow due to their settling velocities (Van Rijn, 1993). For cohesive sediments, the Partheniades–Krone formulations for erosion and deposition are used (Partheniades, 1965). The vegetation presence is computed following the formulation of Baptists (2007). The module accounts for the three-dimensional effect of rigid cylindrical plant structures on drag and turbulence. The first is modelled by adding an extra source term of friction force, caused by the cylindrical plant structures, in the momentum equation; the second is achieved by adding an extra source term of turbulent kinetic energy dissipation, generated by the cylindrical plant structures, in the k-e equations. For more information on the vegetation module, we refer to Deltares (2019a). The design of the domain and the set-up and calibration of the model for this study were performed by Li et al. (2018, 2019). The domain consists of a grid of 344 x 80 cells in the east to west and north to south direction (Figure 21 a), and three equally spaced vertical layers. The bathymetry (Figure 21 b) was obtained from the combination of two datasets: the bathymetric data for the open sea collected from EDINA DIGIMAP and the LiDAR data for the coastal regions downloaded from the Environment Agency's LiDAR data archive. Since the two datasets have different vertical reference levels, Low Astronomical Tide (LAT) and Above Ordnance Datum Newlyn (AODN) respectively, they were adjusted and referred to Mean Sea Level (MSL) following the spatially varying Vertical Offshore Reference Frame (VORF) corrections provided by the UK Hydrographic Office prior to combination. The model is constrained within two open boundaries, one 20 km offshore and one across the River Ribble. Data for the offshore boundary was provided by the Extended Area Continental Shelf Model fine grid (CS3X), which has approximately 12 km resolution, covers an area from 53.55° N to 53.92° N and from -3.33° E to -2.75° E, and uses meteorological data from the UK Met Office Operational model, consisting of hourly water level and current simulation values. Data for the river boundary was collected from the National River Flow Archive and consists of a time series of daily-averaged river discharge values; a constant discharge of 44 m^3 s^{-1} was estimated using the mean discharge for the simulated period. Measurements of suspended sediment concentration performed in the Ribble Estuary by Wakefield et al. (2011) were used to estimate a constant sediment discharge from the river of 0.29 kg m^{-3} s^{-1}. A restricted area of the domain was selected for the sediment budget calculation (Figure 21). For more information on model setup and calibration we refer to Li et al. (2018, 2019).

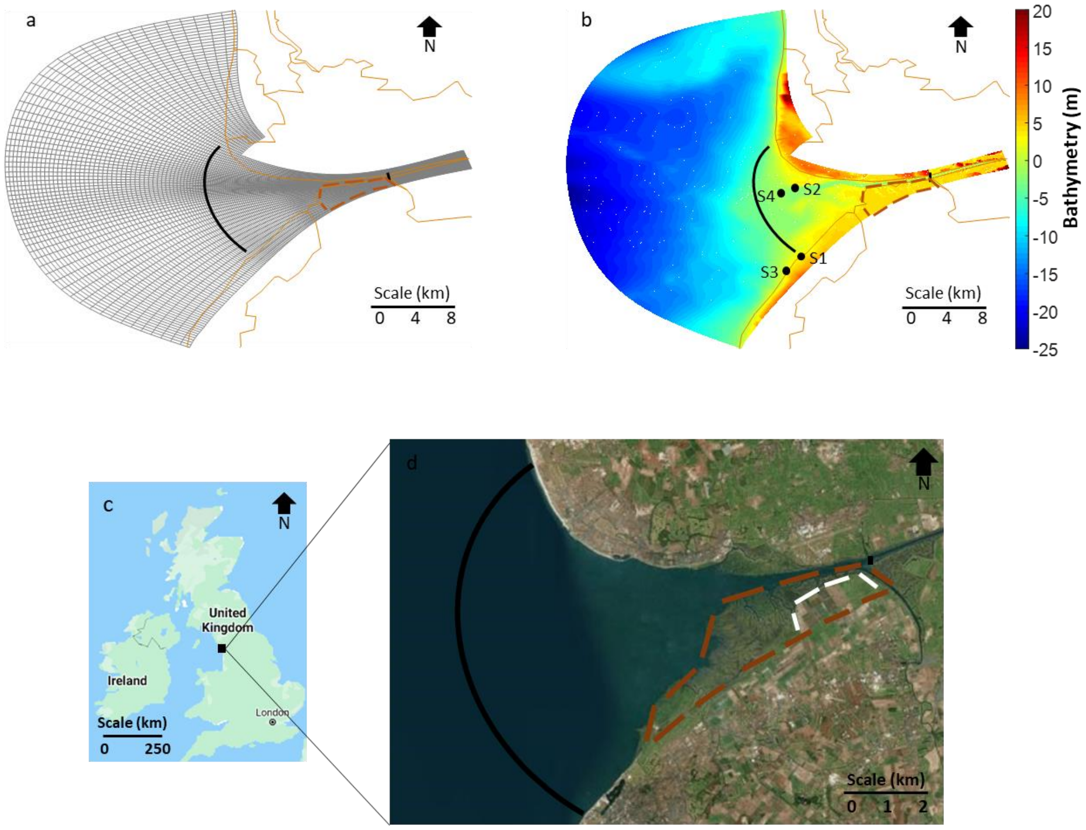

Figure 21. Grid (a), bathymetry (b) and map (c, d) of the domain. The continuous brown lines represent the land boundary. The area enclosed by the black curved lines and the area enclosed by the brown dashed lines (panel a, b and d) are respectively the restricted domain and the salt marsh used for the calculation of the cumulative sediment deposition. The area enclosed by the white dashed lines (panel d) is now part of the saltmarsh as it was restored in 2017 (RSPB, 2019). In panel b, the yellow shade corresponds to the tidal flat and nearshore area, the green shade corresponds to the inner estuary and the light blue shade corresponds to the outer estuary (© Google Earth Pro, 2020).

4.5.2 Simulation scenarios and tidal analysis

A total of 250 simulations were conducted (Table 2). Each simulation was run for a month from January 1st until January 31st 2008. The maximum spring and neap high tides in this period reach respectively 4.2 m and 3.2 m above mean sea-level and the minimum spring and neap low tides reach respectively 3.8 m and 2.5 m below mean sea-level. Storm surges that characterise mid-high latitudes have a typical duration of 2-5 days (von Storch et al., 2015). To understand the impact of the storm duration on the sediment budget, gaussian functions with duration 48 hours (σ = 6 hours), 72 hours (σ = 9 hours) and 120 hours (σ = 15 hours) were added to the initial water level time series at the offshore boundary. Extreme value analysis of storm surge residuals along the UK coastline, presented in Table S3, showed surge heights up to 3 m for exceedance probabilities $p = 0.01$. Values at regular intervals within the range of these observations were chosen to simulate storm surges of different heights: 0 m, 0.25 m, 0.5 m, 1.0 m, 2.0 m, 3.0 m and 4.0 m (Figure 22 a and 22 b). To understand the role of the timing of the surge with respect to tidal levels, for each surge height, two runs were conducted, one with the peak of the surge coinciding with the peak of high tide and one with the peak of the surge coinciding with the peak of low tide. To understand the role of tidal range, these scenarios were simulated for both spring and neap tide. The storm surge was introduced after 11 days of simulation for the spring tide scenario and after 18 days for the neap tide scenario, to avoid any interference with the initial spin-up time. To simulate different sea-level scenarios, the bathymetry was lowered by 0 m, 0.3 m, 0.5 m, 0.8 m and 1.0 m (Figure 22 c). These values were chosen as regular intervals within the range of the IPCC scenarios (Masson-Delmotte et al., 2018). The whole bathymetry was modified, without accounting for morphodynamic evolution. This has been done in previously published papers to simulate scenarios of higher sea-level (e.g., Zhang et al., 2020). Storm surges and sea-level scenarios were then combined to investigate the integrated effects on the sediment budget; the 48 hours scenarios occurring during spring tide were used for this purpose. The Ribble Estuary experiences moderate wave energy (Pye and Neal, 1994). However, for simplicity, the effects of wind waves have been neglected in this study to investigate exclusively the distinct effects of surges and sea-level. There is evidence that vegetation affects sediment deposition not only directly, by capturing particles and enhancing particle settling, but also indirectly, by changing the water flow direction and increasing the flood velocity, hence causing sediment resuspension (Temmermann et al., 2005). Simulations were conducted with and without vegetation presence to test how it affects sediment deposition and, ultimately, the sediment budget. A plant density of 512 stems m^{-2} was used for the vegetated scenarios to simulate a high level of vegetation cover (Li et al., 2018). The cumulative sediment deposition across the marsh area and estuarine system within the restricted domain was used as an estimate of the sediment budget and describes the amount of accretion (positive values) or erosion (negative values) of the bed for each cell of the domain. The net accretion/erosion on the whole marsh and restricted domain can be calculated by multiplying the cumulative deposition of each cell for the cell area and summing them, making it a useful proxy to determine the amount of sediment stored within the system.

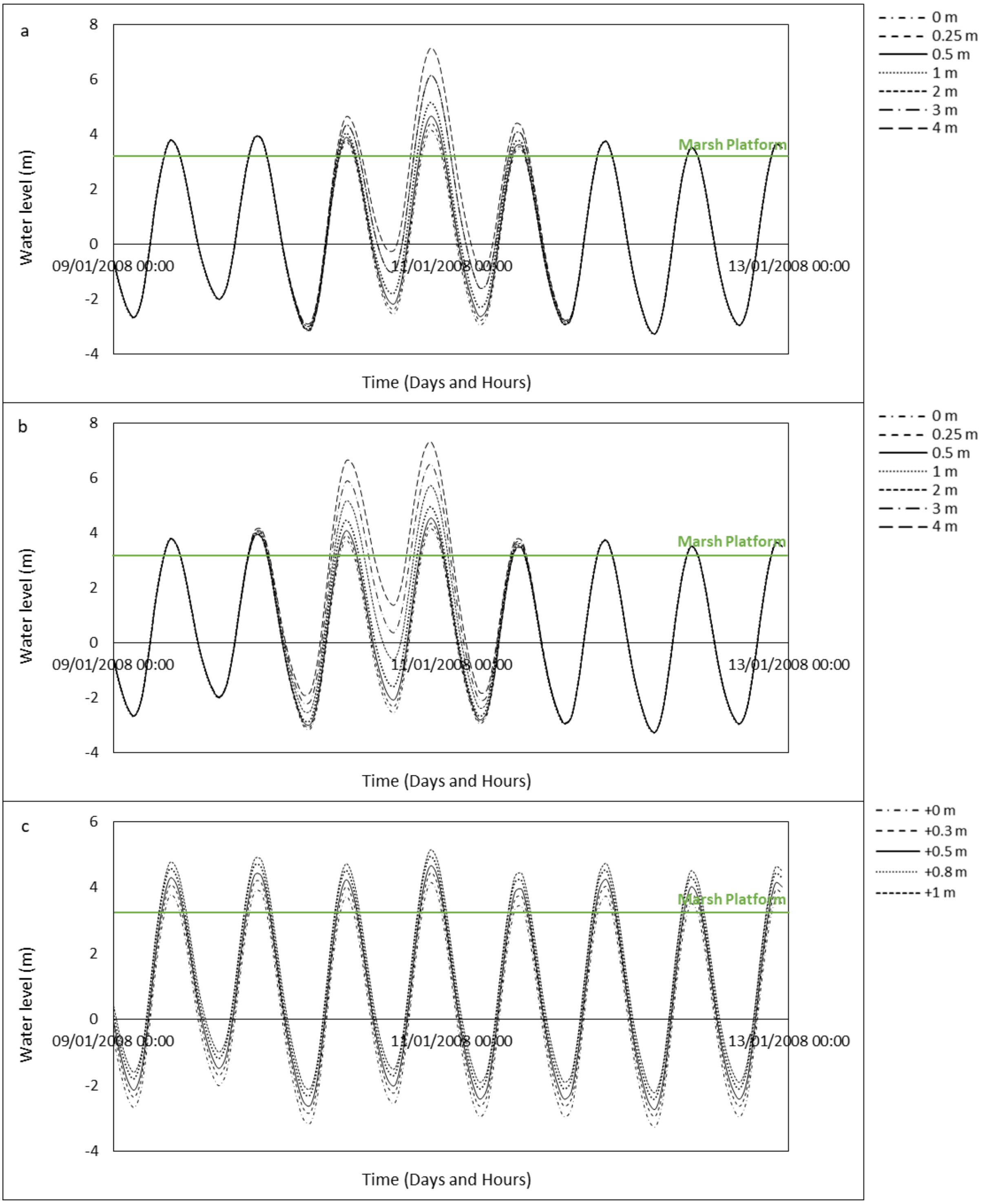

Figure 22. Water level for scenarios of surges peaking at high (a) and low (b) tide; the 48 h scenarios occurring during spring tide are used for the illustration. Water level for scenarios of different sea-levels (c); five days during spring tide were selected for the illustration. The water level is calculated as an average of all water levels at the ocean open boundary.

Table 2. Combinations of simulated scenarios of sea-level and storm surges. These were repeated for different durations (48 h, 72 h and 120 h), with and without vegetation, for different timing of the storm surge with respect to tidal level (peak of the surge corresponding with HT or LT peak) and for different tidal ranges (surge occurring during spring or neap tide).

Sea-level scenarios	Storm surges scenarios at HT and LT peak (for durations of 48 hr, 72 hr, 120 hr)						
0 m	0 m	0.25 m	0.5 m	1 m	2 m	3 m	4 m
0.3 m	0 m	0.25 m	0.5 m	1 m	2 m	3 m	4 m
0.5 m	0 m	0.25 m	0.5 m	1 m	2 m	3 m	4 m
0.8 m	0 m	0.25 m	0.5 m	1 m	2 m	3 m	4 m
1 m	0 m	0.25 m	0.5 m	1 m	2 m	3 m	4 m

Tidal asymmetry has been recognised as one of the main factors controlling the net import/export of sediments and the large-scale morphological evolution of estuaries (Guo et al., 2016; Leonardi and Plater, 2017; Palazzoli et al., 2020) and there is evidence that changes in water level affect the tidal signal (Parker, 2007). It has been observed that, in shallow water, wind generated storm surges with period longer than the tidal period can cause an increase in water depth (when water level is raised by an onshore wind) and change the tidal dynamics by increasing the tidal range, causing a non-linear tidal distortion affecting the asymmetric non-linear terms that involve elevation for the period of the surge duration (Parker, 2007). Parker et al. (2007) suggests that these changes in the non-linear terms modify the harmonic constants since a greater tidal range leads to a maximum wave propagation velocity and minimum attenuation at crest and the opposite at through, causing an asymmetric distortion of the tide and generating second harmonics (e.g., M4). Sea-level is also known to cause modifications of the harmonic constants, as it causes changes in reflection and resonance of the tidal signal (van Maanen et al., 2013). To investigate the effect of storm surges and sea-level on the tidal signal, Fourier analysis was conducted for each scenario; changes in the tidal signal discussed for storm surge scenarios refer to time-limited modifications occurring during the period of the storm, while for sea-level scenarios the whole month was analysed. The MATLAB package T-TIDE was used to conduct the analysis (Pawlowicz et al., 2002); for storm surges, the 48 hours scenarios occurring during spring tide was used for this purpose. The distortion and asymmetry of the tidal signal were analysed using the principal lunar semi-diurnal constituent M2 and the largest shallow water constituent M4; the distortion was calculated using the ratio $A_{4-2}=A_{M4}/A_{M2}$ where A is the amplitude of the tidal height and the asymmetry was calculated using $\Delta\theta=2\theta_{M2}-\theta_{M4}$ where θ is the phase of the tidal height (Friedrichs and Aubrey, 1988; Blanton et al., 2002). When Δθ is between 0° and 180° the flood phase dominates, whereas when it is between 180° and 360° the ebb phase dominates; the magnitude of A_{4-2} is representative of the significance of the dominance (Friedrichs and Aubrey, 1988). The harmonic analysis was not performed on dry cells and on salt marsh or tidal flat cells intermittently covered by water.

4.6 Results

4.6.1 Sediment budget

Figure 23 shows that for spring tide scenarios the cumulative sediment deposition increases overall in both the restricted domain and on the marsh platform when the surge height increases. For the 48 hours scenario, in the restricted domain, for higher surges, deposition is more substantial when the peak of the surge coincides with the high tide peak. On the marsh platform, the rise is more pronounced when the peak of the surge coincides with the low tide peak. For longer durations (72 hours and 120 hours scenarios), this difference decreases visibly and becomes negligible. Similarly, these trends remain comparable when a decrease in tidal range is applied (i.e. neap tide scenarios), but the difference between deposition driven by surges peaking at high tide and surges peaking at low tide becomes less significant (Figure S6). For all durations at spring tide (Figure 23), when vegetation is added, the trends show a variation both in the restricted domain and on the marsh. In the restricted domain, the deposition in the vegetated scenario is greater than the hypothetical non-vegetated scenario for surges up to 2 m and lesser for surges >2 m. Conversely, on the saltmarsh, the deposition in the vegetated scenario is lesser for surges up to 1 m and greater for surges >1 m compared to the non-vegetated scenario. For neap tide scenarios (Figure S6), this inversion in the trends does not occur or it only occurs for surges >3 m. With an increase in sea-level (Figure 24), the cumulative sediment deposition decreases both in the restricted domain and on the marsh. When vegetation is added, no significant difference is noticeable in the trend.

When the surge and sea-level scenarios are combined, the trends in deposition caused by the increase in surge height remain similar in all sea-level scenarios (Figure 25). The main visible difference is a decrease in the difference between deposition during surges occurring at low tide and high tide in the restricted domain (Figure 25 a), whereas on the marsh the difference increases (Figure 25 b). However, there is an overall decrease in the magnitude of deposition with the increase in sea-level. Overall, it seems that the effects of storm surges mask the effects of sea-level rise on the sediment budget, both in the restricted domain and on the marsh platform; this is especially true for surges with the highest intensities (>3 m).

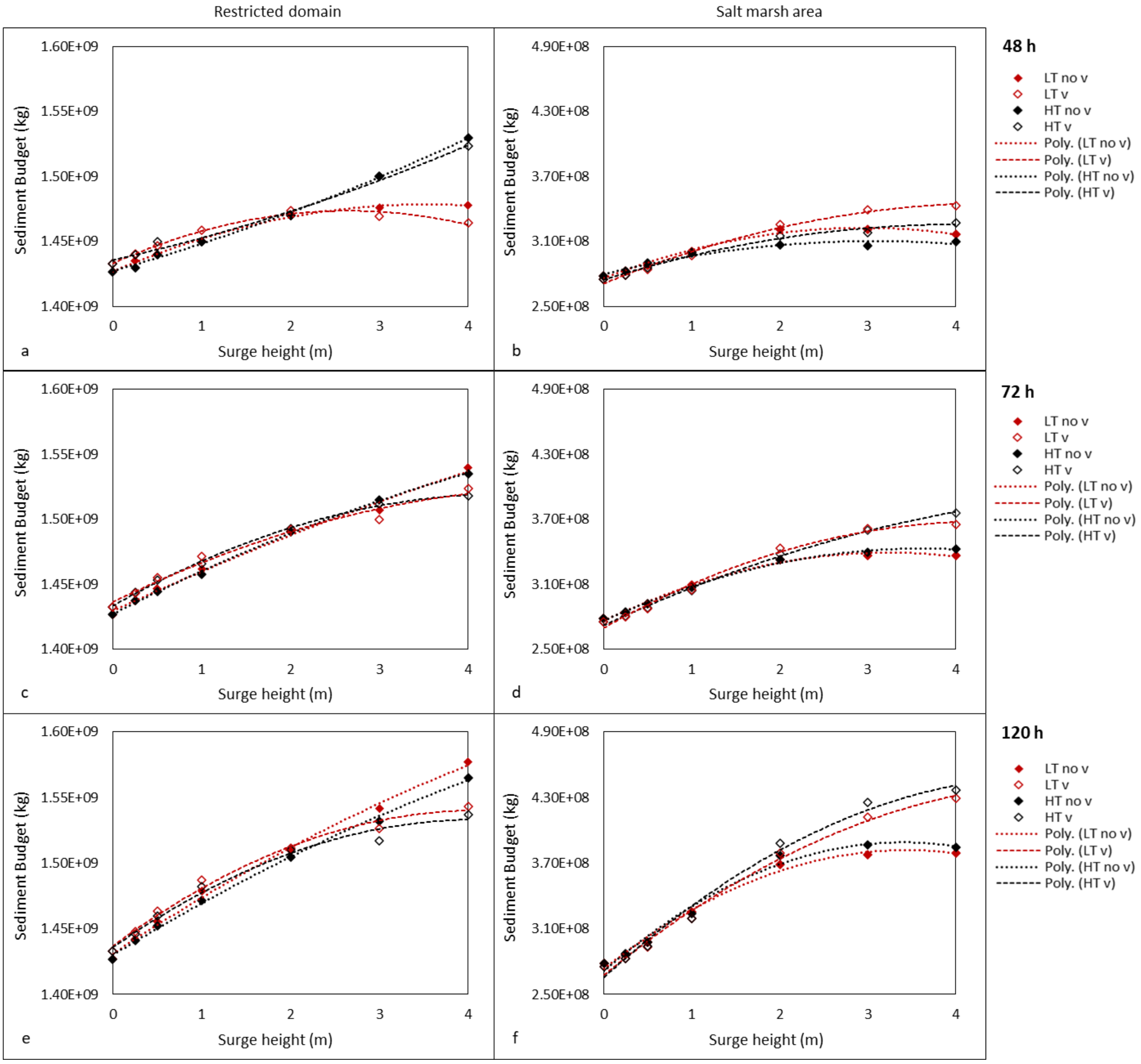

Figure 23. Sediment budget integrated across the entire area of the restricted domain (a, c, e) and the saltmarsh (b, d, f) for each surge height, for surges occurring at high tide (HT) and low tide (LT) without vegetation (no v) and with vegetation (v), for surges of different durations occurring at spring tide (see Figure S6 in Appendix II for surges occurring at neap tide); scenarios run using an ideal only-mud bed composition.

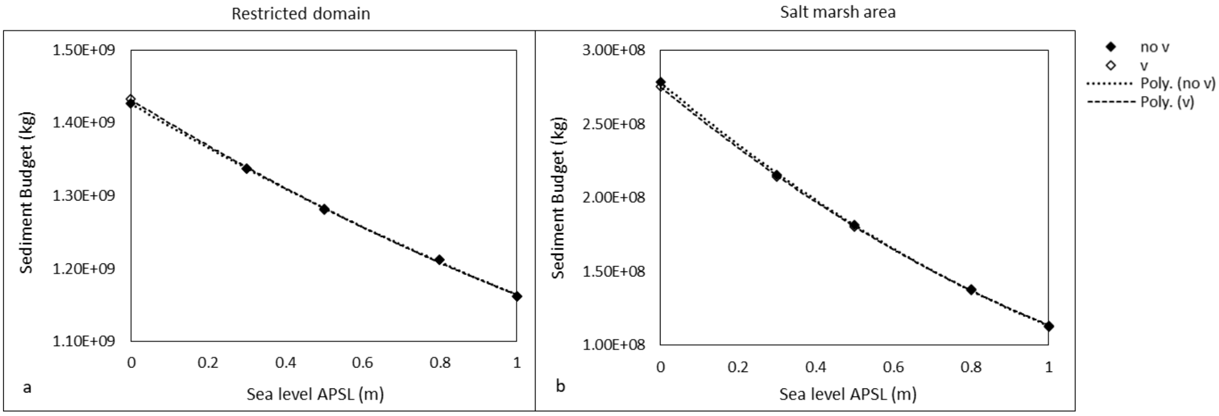

Figure 24. Sediment budget integrated across the entire area of the restricted domain (a) and the saltmarsh (b) for each sea-level scenario, without vegetation (no v) and with vegetation (v); scenarios run using an ideal only-mud bed composition.

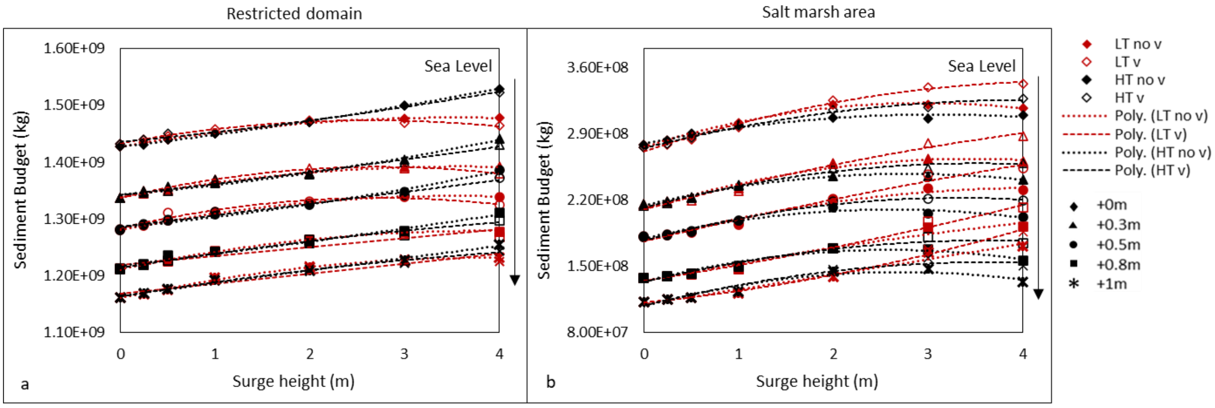

Figure 25. Sediment budget integrated across the entire area of the restricted domain (a) and the saltmarsh (b) for each combination of surge height and sea-level scenarios, for surges occurring at high tide (HT) and low tide (LT) without vegetation (no v) and with vegetation (v); scenarios run using an ideal only-mud bed composition. The analysis was performed using the 48 h scenarios occurring at spring tide.

4.6.2 Tidal analysis

At present-day sea-level and no surges, the estuary is characterised by a dominance of the flood phase (Figure 26). Flood dominance decreases landward, accompanied by an initial increase in distortion, as tides move from the deeper to the shallower portion of the estuary, which then reduces again around the shallower tidal flat areas (Figure 26). The overall flood dominance explains the positive sediment budget characterizing the system in a no sea-level rise and no surge scenario.

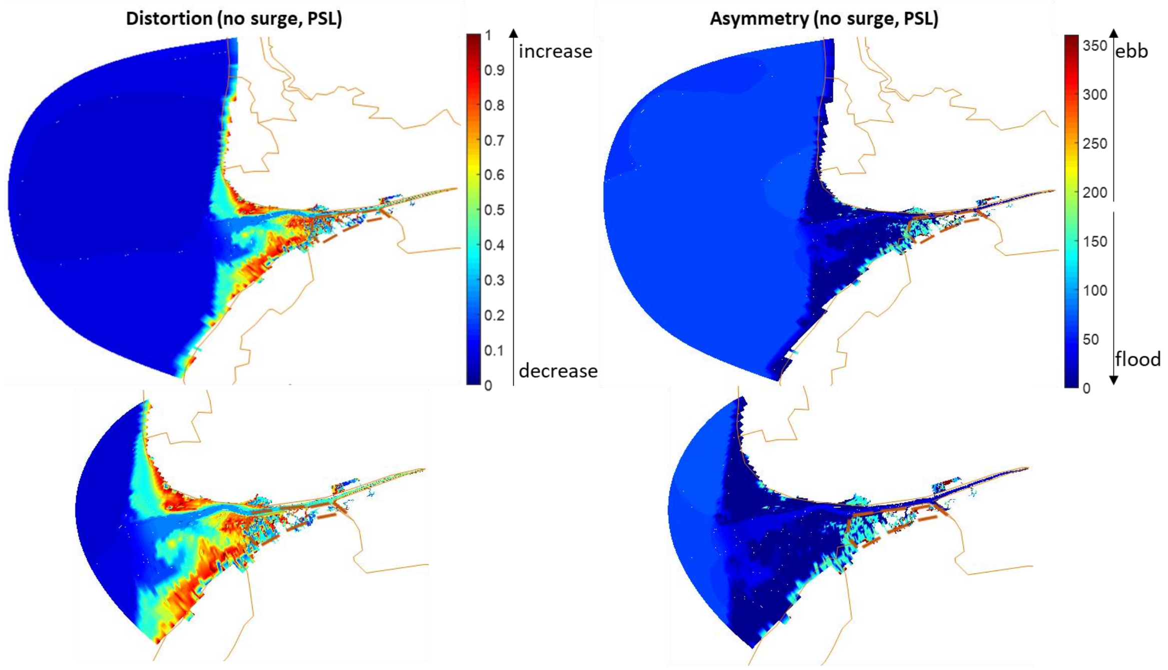

Figure 26. Tidal distortion (A_{4-2}) and asymmetry ($\Delta\theta$) at present sea-level (PSL) with no surges. Entire domain above and zoom on the inner estuary and tidal flat areas below. When $\Delta\theta$ is between 0° and 180° the flood phase dominates, when it is between 180° and 360° the ebb phase dominates; when the magnitude of A_{4-2} increases, the degree of the asymmetry is more significant and vice versa. The continuous brown lines correspond to the land boundary. The area enclosed by the brown dashed lines is the salt marsh.

In the presence of storm surges and for locations near the coastline (Figure 21, S1), the flood dominance and tidal distortion are strongly enhanced as the surge height increases (Figures 27 and 28). Conversely, further away from the coast (Figure 21, S2), the tidal signal is characterised by a reduction in distortion and a slight shift towards ebb dominance (Figures 27 and 28). The significant increase in distortion and flood dominance explains the increase in sediment deposition in the system seen in Figure 23 (above) and in Figure S6. The ebb shift offshore is slightly more pronounced when the surge occurs at low tide peak for higher surges (Figure 27). This can explain the differences in deposition between surges occurring at high and low tide peak seen in the 48 hours scenarios at spring tide for the restricted domain (Figure 23 a). On the salt marsh, for the same scenarios, the higher deposit caused by the surges occurring at low tide, compared to the surges occurring at high tide (Figure 23 b), is likely to depend on the duration of the flooding, since in the first case the surge covers two high tide peaks, enhancing two flood events, whereas in the second case the surge covers only one high tide peak, enhancing only one flood event (Figures 22 a and 22 b). This difference becomes negligible for longer durations (Figure 23 c, d, e, f), since the number of tidal cycles covered by the surge increases enough to reduce the effect of the tidal harmonic on the amplification of the surge and the influence of surge timing. The same principle is applied for lower tidal ranges (i.e. neap tide scenarios, Figure S6); with a decrease in the amplitude of the tidal harmonic, there is a consequent reduction in the surge amplification.

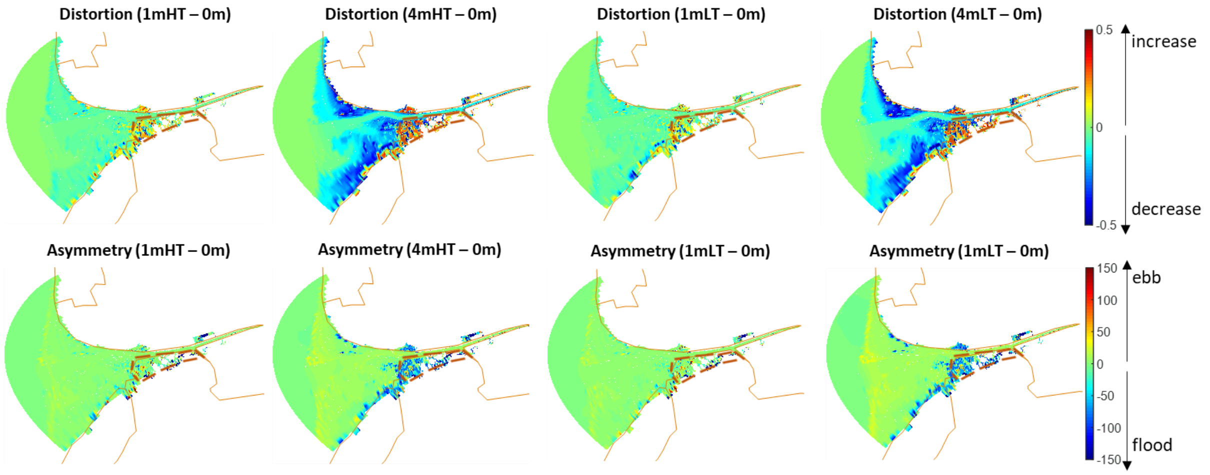

Figure 27. Difference between tidal distortion (A_{4-2}) and asymmetry ($\Delta\theta$) of 1 m and 4 m surge scenarios and the no surge scenario at current sea-level (see Figure S7 in Appendix II for the rest of the surge scenarios). When $\Delta\theta$ is positive there is an increase in ebb dominance with respect to the no surge scenario, when it is negative there is an increase in flood dominance; when A_{4-2} is positive, the degree of the asymmetry is more significant, vice versa when it is negative. The analysis was performed using the 48 h scenarios occurring during spring tide. The continuous brown lines correspond to the land boundary. The area enclosed by the brown dashed lines is the salt marsh.

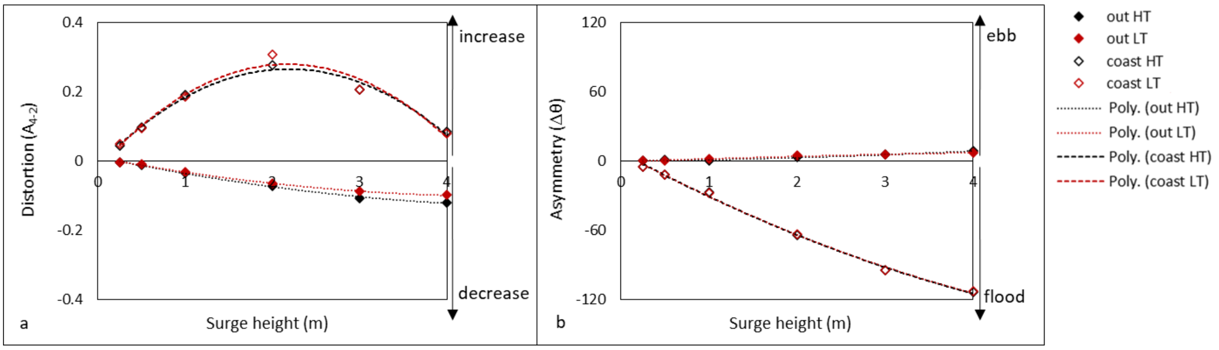

Figure 28. Difference between tidal distortion (A_{4-2}) (a) and asymmetry ($\Delta\theta$) (b) of all surge scenarios and the no surge scenario at current sea-level for one point along the coastline (coast) 53.64° N -3.02° E (Figure 21, S1) and one further away from the coast (out) 53.73° N -3.03° E (Figure 21, S2). When $\Delta\theta$ is positive there is an increase in ebb dominance with respect to the no surge scenario, when it is negative there is an increase in flood dominance;

when A_{4-2} *is positive, the degree of the asymmetry is more significant, vice versa when it is negative. The analysis was performed using the 48 h scenarios occurring during spring tide.*

When different sea-level scenarios are applied, as sea-level rises, locations near the coastline are characterised by an increasing ebb dominance (Figure 21, S3), which seems to be more significant on the deeper areas of the tidal flats, while it becomes less significant on the shallower areas of the tidal flats, where distortion decreases (Figures 29 and 30). This increase in ebb dominance explains the decrease in sediment deposition seen in the system in Figure 24. Conversely, further away from the coast (Figure 21, S4) an increase in distortion is associated to a strengthening of the flood dominance (Figures 29 and 30). The difference in deposition between surges occurring at high and low tide peak seen in the restricted domain for the 48 hours scenario at spring tide (Figure 23 a) decreases with sea-level rise (Figure 25 a); this can be explained by the offshore increase in flood dominance caused by sea-level rise (Figure 29) offsetting the difference in ebb dominance between surges occurring at high tide peak and surges occurring at low tide peak (Figure 27).

For the same scenarios, the difference in deposition between surges occurring at low tide peak and surges occurring at high tide peak on the marsh (Figure 23 b) increases with sea-level rise, since greater water depth enhances inundation for two high tide peaks in the first case but only one high tide peak in the second case (Figures 22 a and 22 b). Overall, the impact of increasing storm surge heights on distortion and asymmetry is higher near the coastline (Figure 28), while the effect of sea-level rise is more pronounced in the outer estuary (Figure 30).

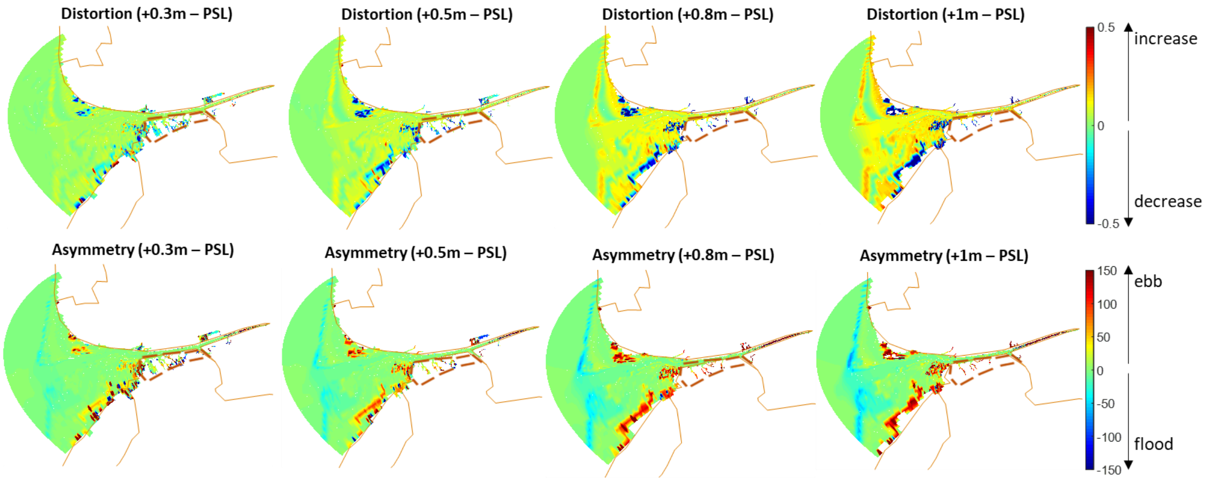

Figure 29. Difference between tidal distortion (A_{4-2}) and asymmetry ($\Delta\theta$) of all sea-level scenarios and the current sea-level scenario. When $\Delta\theta$ is positive there is an increase in ebb dominance with respect to the present sea-level scenario, when it is negative there is an increase in flood dominance; when A_{4-2} is positive, the degree of the asymmetry is more significant, vice versa when it is negative. The continuous brown lines correspond to the land boundary. The area enclosed by the brown dashed lines is the salt marsh.

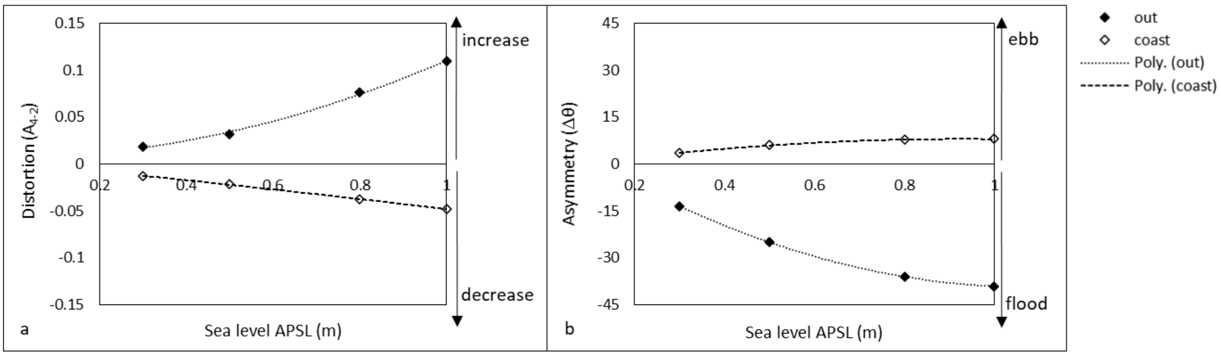

Figure 30. Difference between tidal distortion (A_{4-2}) (a) and asymmetry ($\Delta\theta$) (b) of all sea-level scenarios and the current sea-level scenario for one point along the coastline (coast) 53.63° N-3.06° E (Figure 21, S3) and one further away from the coast (out) 53.72° N-3.07° E (Figure 21, S4). When $\Delta\theta$ is positive there is an increase in ebb dominance with respect to the present sea level scenario, when it is negative there is an increase in flood dominance; when A_{4-2} is positive, the degree of the asymmetry is more significant, vice versa when it is negative.

4.6.3 Vegetation effect in storm surge scenarios

When vegetation is added, there is a change in current velocities in comparison to the hypothetical non-vegetated scenarios (Figure 31). In the spring tide scenarios, for the no surge scenario and for surges up to 1 m, as the surge height increases, on the marsh platform there is a consistent increase in flood velocity within the tidal creeks, whereas along the edge of the marsh there is a consistent decrease. This favours resuspension within the marsh area and deposition in the periphery, therefore leading to less deposition on the marsh platform but more in the restricted domain. During higher surges, the marsh platform is mainly characterised by lower velocities, whereas in the peripheric areas the higher velocities dominate. This favours deposition on the marsh area and excavation in the periphery, leading to more deposition on the marsh platform but less in the restricted domain. For the neap tide scenarios, this inversion does not occur at all or it only occurs for surges >3 m (Figure S6). During neap tide, the water level is lower during flood phase, when the marsh is inundated, therefore the velocity profile typical of lower water depths persists for higher surges.

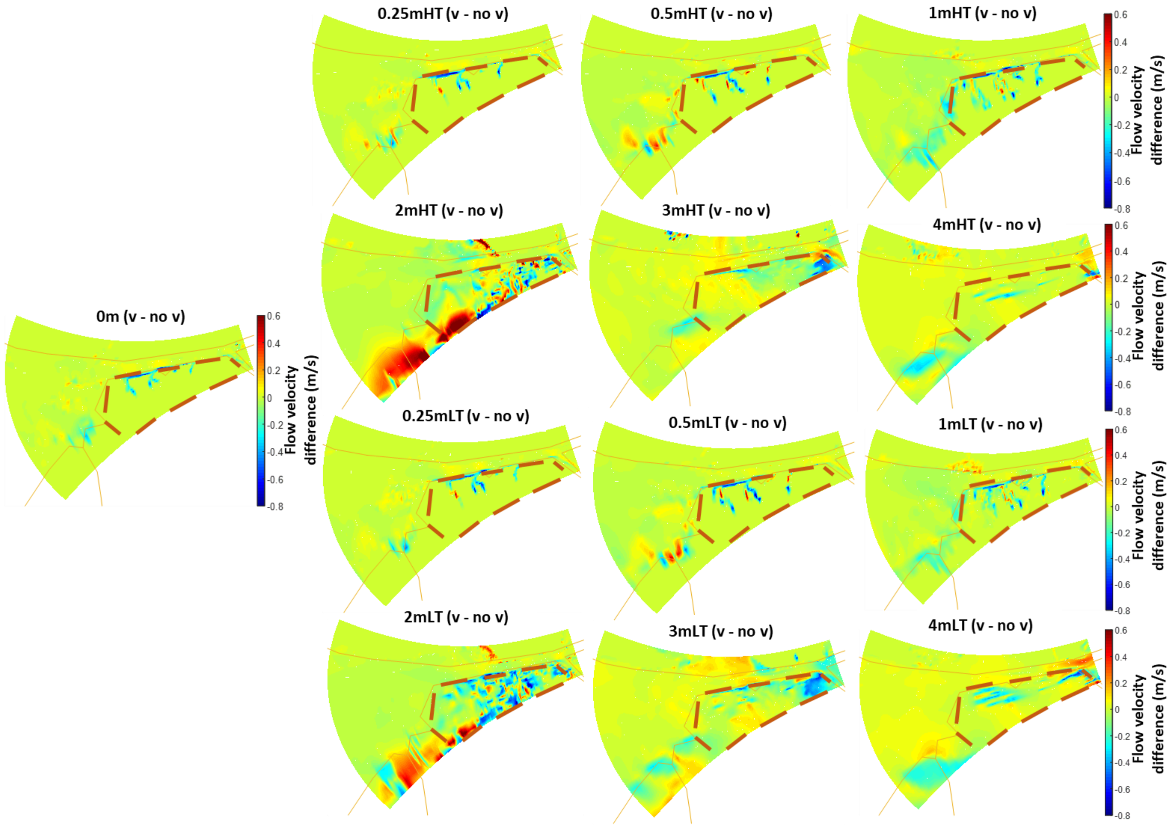

Figure 31. Difference between maximum current velocity during flood phase of vegetated (v) and hypothetical non-vegetated (no v) scenarios for all surge scenarios. The analysis was performed using the 48 h scenarios occurring at spring tide. The continuous brown lines correspond to the land boundary. The area enclosed by the brown dashed lines is the salt marsh.

4.7 Discussion

The sediment budget of estuaries and saltmarshes depends on the quantity of sediment entering and exiting the system during each tidal cycle, and this is influenced by tidal asymmetry and distortion (Guo et al., 2016; Palazzoli et al., 2020). When there is a flood dominance (flood phase shorter and more intense than ebb phase), flood velocities can be sufficiently high to resuspend sediment and promote a net landward sediment import, and vice versa in the case of ebb dominance (Van Dongeren and de Vriend, 1994; Lanzoni and Seminara, 2002).

For a no-sea-level rise and no-surge scenario, the system is overall flood dominated (Figure 26) with a positive sediment budget both in the restricted domain and on the marsh platform (Figure 23). The flood dominance significantly decreases for shallower tidal flats and marsh areas. This decrease is likely to be caused by a landward increase in friction, which reduces the velocity of the incoming tide (Friedrichs and Aubrey, 1988; Wang et al., 2002; Parker, 2007). This phenomenon has been observed in some of the major estuaries around the world, where the friction effect is dominant in the upper estuary – e.g., the Severn Estuary in UK (Lyddon et al., 2018) and the Westerschelde estuary in the Netherlands (Wang et al., 2002).

4.7.1 Storm surges

Storm surge presence enhances the flood dominance near the coastline and causes a slight ebb dominance offshore (Figures 27, 28 and S7). The most important term affecting the non-linear interaction between storm surges and tides in shallow water is the non-linear bottom friction term (Zenghao and Yihong, 1996; Parker, 2007). When a storm surge causes an increase in water level and has period longer than the tidal period, the water depth increases due to the effect of the surge, reducing the bottom friction (Figure S8) and, therefore, increasing the propagation speed of the tidal wave which is depth dependent (Rossiter, 1961; Wolf, 1981; Parker, 2007). This leads to an increase in the speed of the flood phase, as the crest of the tide partially overtakes the trough; hence the enhancement of flood dominance near the coastline caused by the increase in surge height (Friedrichs and Aubrey, 1988; Olbert, 2013). The non-linear interaction between tide and storm surge has been well observed for several years (eg. Rossiter, 1961; Wolf, 1981; Parker, 1991). For instance, Parker (1991) described a tidal signal several locations along Delaware Bay (USA) with shorter and faster flood phase compared to the predicted signal during the occurrence of a subtidal storm surge.

In deeper water, where the effect of the bottom friction is less prevalent, the symmetric relationship of tide and velocity might be the dominant factor that controls the phase dominance (Savenije, 2012). Therefore, the increase in water level caused by the increase in surge height could be responsible for the offshore increase in ebb dominance (Wang et al., 2002; Moore et al., 2009). This is, for instance, observed in the Dee Estuary (UK) where the tidal flats are mainly characterised by a distorted flood dominated tidal signal, while in the deeper channel the signal is less distorted and the ebb phase results to be dominant (Moore et al., 2009). This also explains the more pronounced offshore ebb dominance when the surge peaks at low tide compared to when it peaks at high tide (as observed for the 48 hours scenarios at spring tide but not for the longer durations or the reduced tidal range). In the first case the surge covers two high tide peaks, therefore, the ebb phase offshore is enhanced two times, whereas in the second case the surge covers only one high tide peak, enhancing the ebb phase only once (Figures 22 a and 22 b), but as the number of tidal cycles increases or the amplitude of the tidal signal decreases, the amplification of this effect is reduced. This reduced differences between deposition produced by surges occurring at high tide and surges occurring at low tide peak has been observed in microtidal regimes. This is the case of most US Atlantic bays where the tidal range is about 20 cm - e.g., Virginia Bay (Castagno et al., 2018). The results of this study show that, overall, storm surges contribute to make the salt marsh and estuarine system more resilient, in agreement with other studies (Turner et al., 2006; Walters and Kirwan, 2016; Castagno et al., 2018).

4.7.2 Sea-level

An increase in sea-level causes ebb dominance near the coastline and enhanced flood dominance offshore (Figures 29 and 30). The increase in water level caused by sea-level rise is responsible for an increase in the tidal prism (i.e., volume of the water flowing into the estuary) which in turn causes an increase in the velocity of the incoming tide across the mouth of the estuary (Sinha et al., 1997; Liu et al., 2020; Zhang et al., 2020); this can explain the enhanced flood dominance offshore. Several estuaries around the world have shown a similar behaviour. For example, this phenomenon has been found to be responsible for a decrease in ebb dominance in the whole estuarine system and consequent rejuvenation of the Tairua Estuary, New Zealand (Liu et al., 2020).

However, in the nearshore, the estuary becomes more ebb dominated as sea-level rises (Figures 29 and 30). The Irish Sea, where the Ribble Estuary is located, is influenced by a phenomenon of resonance, and it has been shown that an increase in sea-level can produce changes in resonance properties that are negligible in deep water but can be observed in shallow water (Pugh, 1987). Several studies have been conducted on the effect of sea-level rise on tidal constituents in the European Shelf, including the Irish Sea, and they showed that a rise in sea-level affects the resonance of the basin causing an increase in the M2 component (Pickering et al., 2012; Idier et al., 2017). This could be responsible for the ebb dominance that characterises the inner estuary and the tidal flat areas. Other estuaries on the European Shelf have been found to behave in the same way e.g., the Bristol Channel in UK and the Gulf of St. Malo in France (Pickering et al., 2012; Idier et al., 2017).

This study showed that sea-level rise might threaten the stability of the salt marsh, in agreement with the results of previous studies (FitzGerald et al., 2008; Kirwan et al., 2010; Ganju et al., 2017). Nevertheless, the data presented here show that storms have a general tendency to increase marsh resilience to sea-level rise by counteracting the decrease in sediment budget caused by sea-level rise (Figure 25). This is particularly true for storms with the highest intensity (>3 m surges), in agreement with Schuerch et al. (2013). In terms of relative contribution, Figure 25 shows that, on the marsh platform, storm surges of 48 hours occurring at spring tide can cause up to 65% reduction in sediment loss driven by sea-level rise; in the restricted domain this reduction can reach 7%. Trends in Figure 23 suggest that an increase in duration could amplify this reduction, while Figure S6 shows that a decrease in tidal range could minimize it. Wang et al. (2020) found that a similar level of contribution is provided by storms to the resilience of deltas experiencing erosion driven by high river discharge; here they help reduce the sediment loss induced by riverine flows by over 50%. It is, however, significant to highlight that storm surges with height up to 2 m have substantially lower return period (between 2 and 100 years), while surges >3 m are much less frequent (between 100 years and 1000 years return period) (see Table S3). This suggests that the effects related to the surges of height up to 2 m have greater probability to be detected in reality, while the effects of >3 m surges are rarer to observe.

4.7.3 Vegetation effect

The addition of vegetation does not significantly modify the trends of deposition caused by the storm surges and the increase in sea-level. However, it causes minor changes in the deposit of different storm surge scenarios (Figure 23). Vegetation enhances sediment deposition through particle capture by plant stems and enhanced particle settling caused by a reduction in turbulent kinetic energy of the water flow through the plant canopy (Neumeier and Ciavola, 2004; Mudd et al., 2010). However, it also affects sediment deposition indirectly by channelizing water and increasing flood velocity within tidal creeks and off-site, favouring excavation (Temmermann et al., 2005).

In the spring tide scenarios, for the no surge scenario and for surges up to 1 m, when vegetation is present, the water level is not high enough to overflow the tidal creeks since the vegetation on the marsh platform acts as a barrier (Figure S9); this enhances the velocities of the incoming tide, causing excavation and preventing deposition, hence, there is lower deposition on the marsh platform compared to the hypothetical non-vegetated scenarios (Figure 23 b, d, f). Along the edge of the marsh, where the water is not constrained (Figure S9), the frictional effect of the vegetation causes a decrease in velocity (Figure 31), favouring particle settling on the periphery of the marsh, hence, the higher deposition in the restricted domain compared to the non-vegetated scenarios (Figure 23 a, c, e). During higher surges, the water level is high enough to overflow the tidal creeks despite vegetation (Figure S9), therefore the vegetation present on the marsh platform enhances particle settling, as showed by the dominance of the lower velocities (Figure 31), leading to sediment deposition being higher in vegetated scenarios (Figure 23 b, d, f). Outside the tidal flat areas, the higher velocities dominate (Figure 31). The frictional effect of the vegetation might not be effective on the high-water depths on the edge of the marsh (Beudin et al., 2017), whereas the off-site water channelization might dominate, causing excavation. Therefore, leading to less deposition in the restricted domain compared to the non-vegetated scenarios (Figure 23 a, c, e). The neap tide scenarios show similar trends (Figure S6), but the inversion does not occur at all or it only occurs for surges >3 m. During neap tide, the water level is lower during flood phase, when the marsh is inundated, therefore the channelling effect caused by vegetation on the marsh platform persists for higher surges. In the rest of the domain, where water is not channelised, the water level remains low enough to allow particle settling on the periphery of the marsh, even for greater surges.

With a rise in sea-level, there is no difference in the sediment budget between the vegetated and the hypothetical non-vegetated scenario. Sea-level rise produces an increase in water depth (Figure 22 c). This increase leads to a rise in water level in the tidal creeks and along the edge of the marsh, during flood phase, which produces water depth profiles similar to the ones observed for surges up to 1 m (Figure S9). However, since storm surges trigger a net import of sediment, the quantity of suspended sediment in the system during these events is high enough to allow vegetation to contribute towards accretion/erosion of the different areas of the marsh platform. Conversely, sea-level rise is responsible for sediment export, therefore with sea-level higher than present day the quantity of suspended sediment in the system is never high enough to allow a contribution by vegetation that can be easily observed in the trends (Chapters 1 and 3).

Overall, when an interaction between the tidal channels and the marsh platform is considered (Temmerman et al., 2005; D'Alpaos et al., 2007; Kirwan and Murray, 2007), vegetation does not seem to significantly affect the trends, and this agrees with the observations of Li et al. (2018).

4.7.4 Further considerations

The period used for this study is January 2008. However, it is worthwhile to consider that the ultimate sediment budget can change slightly depending on the period of the year considered and the relative river discharge. The river flow, which is in the direction of the tidal current during ebb phase and in its opposite direction during flood phase, causes a bottom friction effect and non-linearly interacts with the tide, enhancing ebb velocities and reducing flood velocities (Parker, 2007). During flood periods, when river discharge increases, this effect is enhanced, promoting more sediment export (Parker, 1984).

The Ribble Estuary experiences moderate wave energy (Pye and Neal, 1994). However, for simplicity, the effects of wind waves have been neglected in this study to define the distinct effects of surges and sea-level. Even though several studies have shown that storm waves can contribute to marsh erosion (Marani et al., 2011; Fagherazzi et al., 2013; Leonardi and Fagherazzi, 2014; Leonardi et al., 2016; Li et al., 2019), others have also shown that wind waves can resuspend sediments from the seabed, which can then be transported into the estuarine system by tidal currents, contributing to deposition (Fernández-Mora et al., 2015; Brooks et al., 2017) and potentially supporting marsh maintenance. The effect of wind waves in the scenarios analysed above will be investigated in further studies.

Finally, it must be considered that in this manuscript the effects of sea-level rise and storm surges were analysed by looking at the response of sediment fluxes to changing hydrodynamic forcing over a timescale of 30 days. In reality, changes in sea-level would occur within the time scale of decades to century during which salt marshes can undergo intrinsic morphological transformations. Salt marshes adapt to hydrodynamic changes, such as sea-level rise, in a timeframe of c.a. 10-100 years (e.g., Kirwan and Murray, 2008; D'Alpaos et al., 2011), while sediment delivered by storm surge events are deposited instantaneously on the marsh platform, allowing marshes to rapidly accrete by steps (e.g., Schuerch et al., 2018). This suggests that the offsetting of sea-level rise effects on the sediment budget caused by storm surges might be even more amplified in reality.

4.8 Conclusions

This study investigated the resilience of salt marshes to the combined influence of sea-level rise and increasing storm surge intensity on the sediment budget of a salt marsh-tidal flat complex using a numerical model of the Ribble Estuary, North-West England. Different storm surges and sea-level rise magnitudes were simulated and the influence of storm duration and local factors (i.e. the timing of occurrence of the surge with respect to tidal levels, tidal range and vegetation) on the nature and amplitude of changes in sediment budget were also considered. The study concluded that storm surges could contribute to salt marsh and estuarine resilience by causing a shift towards a more flood dominated system and by triggering a net import of sediment. The degree of deposition can change slightly depending on the timing of the surge peak for short durations (48 hours) and high tidal range, while it is reduced if the duration increases (72 hours and 120 hours) or the tidal range decreases. Conversely, sea-level rise will threaten the stability of the marsh by causing a shift towards an ebb dominated system, triggering a higher export of sediment. It seems that storm surges might contribute to increase saltmarsh resilience to sea-level rise by masking the effects of sea-level rise on the sediment budget; this is particularly true for storms with highest intensities (>3 m surges). The sediment loss driven by sea-level rise can be reduced by up to 65% on the marsh platform and by up to 7% in the restricted domain when surges occur at spring tide and last 48 hours, with further reduction when surge duration increases, but lower reduction when tidal range decreases. Nevertheless, since storm surges with height up to 2 m have a lower return period, the effects related to these surges have higher probability to be detected, while surges >3 m occur less frequently, meaning that their effects are rarer to observe. The addition of vegetation caused no variations to the trends produced by the sea-level analysis and only minimal variations to the trends produced by surge height analysis; the latter is due to the ability of vegetation canopy to modify flow velocity.

4.9 Acknowledgements

We acknowledge support from the School of Environmental Sciences, University of Liverpool which is funding the PhD project of the first Author. This model for the Ribble Estuary was originally designed as part of the projects 'Adaptation and Resilience of Coastal Energy Supply (ARCoES)' and 'Physical and biological dynamic coastal processes and their role in coastal recovery (BLUE-coast)' and we are grateful for being able to use the model. The model is also presented in Li et al., 2018, 2019. We thank two anonymous reviewers for their constructive feedback on the manuscript.

4.10 Data availability

Data related to this article can be found in the following repository: https://doi.org/10.5281/zenodo.4511397.

Chapter 5

Storm sediment contribution to salt marsh accretion and expansion

5.1 Preface

Chapter 4 showed that storm surges might contribute to increase salt marsh resilience to sea-level rise by masking the effects of sea-level rise on marsh sediment budget. However, although a sediment budget study is useful to understand marsh response, it is also necessary to understand the transport pathways of storm delivered sediments to fully evaluate how salt marshes respond to storm sediment input and to what extent storms enhance marsh resilience. This chapter uses field measurements and sediment analyses conducted at high spatial resolution to understand how storms influence the sediment supply to different marsh areas and whether storms can deliver new material onto the salt marsh platform which would otherwise not be sourced in fair-weather conditions. Chapter 4 neglected the effects of wind waves to focus on the distinct effects of surges and sea-level on the sediment transport dynamics and ultimately on the marsh sediment budget. However, although several studies have shown that storm waves can contribute to marsh erosion, others have also shown that storm waves can contribute to sediment supply to marsh. Hence, to clarify the respective contributions of storm surges and storm waves in storm sediment supply to the salt marsh, this chapter considers both hydrodynamic parameters.

5.2 Abstract

Salt marshes are ecosystems with significant economic and environmental value. However, the accelerating rate of sea-level rise is a significant threat to these ecosystems. Storms significantly contribute to the sediment budget of salt marshes, playing a critical role in salt marsh survival to sea-level rise. There are, however, uncertainties on the extent to which storms contribute sediments to different areas of marsh platforms (e.g., outer marsh vs marsh interior) and on the sediment sources that storms draw on (e.g., offshore vs nearshore). This study uses field analyses from an eight-month field campaign in the Ribble Estuary, North-West England,

to understand storms' influence on the sediment supply to different marsh areas and whether storms can deliver new material onto the salt marsh platform which would otherwise not be sourced in fair-weather conditions. Field data from sediment traps indicate that storm activity caused an increase in inorganic sediment supply to the whole salt marsh platform, especially benefitting the marsh interior. Geochemistry and particle size distribution analysis indicate that the majority of the sediment supplied to the salt marsh platform during the stormy periods was generated by an increase in erosion and resuspension of mudflat and tidal creek sediments, while only a minimal contribution was given by the sediments transported from outside the intertidal system. This suggests that, in the long term, storms will promote salt marsh vertical accretion but might simultaneously reduce the overall larger-scale sediment availability with implications for the marsh lateral retreat.

5.3 Introduction

Salt marshes are environments of significant value, as they provide numerous ecosystem services (Zedler and Kercher, 2005; Barbier et al., 2011). Salt marshes are also effective nature-based solutions for coastal protection against flooding and erosion (Temmerman et al., 2013), as they can buffer storm waves and stabilise sediments (e.g., Möller et al. 1999; Feagin et al., 2009). However, increasing rates of salt marsh loss have been recorded worldwide (e.g., Bakker et al., 1993; Environment Agency, 2011), despite the global effort in creating new vegetated intertidal areas and/or restoring wetlands previously reclaimed for anthropogenic purposes (Temmerman et al., 2013). Understanding the geomorphic processes that promote salt marsh resilience is, therefore, necessary for the effective management of these ecosystems.

Salt marshes form when the input of sediments from rivers and the sea to estuarine accommodation space allows tidal flats to reach a threshold elevation relative to sea level that permits vegetation growth (Morris et al., 2002). Encroachment and survival of salt marshes are possible if vertical accretion and lateral expansion of the salt marsh can keep pace with sea-level rise (Mariotti and Carr, 2014; Ma et al., 2014; Mitchell et al., 2017). Increasing rates of sea-level rise can lead to marsh drowning and lateral retreat, as sea-level rise creates new accommodation space, increasing the amount of sediment input required to guarantee marsh stability (FitzGerald et al., 2008; Kirwan et al., 2010; Ganju et al., 2017; Fagherazzi et al., 2020; Leonardi et al., 2018), and promotes near-shore ebb dominance, enhancing sediment export from the intertidal system (Carrasco et al., 2018; Zhang et al., 2020; Chapter 4). Vertical accretion and lateral expansion are determined by sediment supply and organogenic production (Kirwan et al., 2010, 2016; Donatelli et al., 2020). However, the ongoing decrease in sediment supply to the coastlines, caused seawards by river dredging and damming and landwards by the enhanced sediment export, is currently exacerbating the vulnerability of salt marshes to increasing sea levels (Donatelli et al., 2018; Ganju et al., 2017).

Field and numerical investigations have shown that storms play a significant role in salt marsh accretion, as overwash by storm surges delivers a considerable amount of sediment to marsh platforms supporting marsh growth (Turner et al., 2006; Castagno et al., 2018; Tognin et al., 2021). Further studies have shown that the contribution of storm sedimentation to the salt marsh sediment budget allows salt marshes to keep pace with sea-level rise and is therefore critical for marsh survival (Schuerch et al., 2013; Chapter 4). Despite the numerous studies that have investigated the roles of storm surges in salt marsh resilience, there are still uncertainties on the degree to which storms enhance the accretion of salt marsh platforms – i.e., to what extent storm sediment supply benefits different areas of marsh platforms (e.g., outer marsh vs marsh interior) and what are the sediment sources that storms draw on (e.g., offshore vs nearshore).

Sediment supply to the marsh platform depends on the hydroperiod (duration and frequency of tidal inundation), which decreases with distance from the water sources (i.e., sea and tidal creeks) (Reed, 1990). Therefore, while the outer marsh experiences marine sediment inputs regularly, the inner marsh areas only experience marine sediment inputs when they are inundated by high spring tides and/or storm surges (Roberts and Plater, 2005). Determining how storm sediment supply affects different areas of the marsh platform is, therefore, crucial for understanding to what extent salt marsh vertical accretion can benefit from storm activity. Nonetheless, vertical accretion must be compensated by lateral expansion to avoid the collapse of the platform edge (Mariotti and Fagherazzi, 2013; Fagherazzi et al., 2013). Marine sediments delivered to marsh platforms, however, originate mostly from the erosion of the adjacent intertidal areas, thus promoting vertical accretion but enhancing the lateral retreat of the salt marsh (Roner et al., 2021). Hence, understanding if storms can deliver to the marsh platform sediments from outside the intertidal system allows for determining whether these sediments can also benefit marsh lateral expansion.

This study uses field analyses conducted during the 2021-2022 storm season in the Ribble Estuary, North-West England, to understand: i) how storm activity affects sediment supply to different areas of the marsh platform; and ii) whether storm sediment supply has a different origin than sediment delivered to the marsh platform in fair-weather conditions. The Ribble Estuary was chosen as a case study due to its ecological and economic value (Tovey et al., 2009) and because of the critical role that storm deposits have on the survival of its salt marshes and intertidal flats (Lyons, 1997; Chapter 4 and Appendix II). The concentration of suspended sediments collected from Hesketh Out Marsh after stormy and non-stormy periods was analysed to assess how storm activity changes the spatial variability of sediment supply across the marsh platform. The geochemistry and particle size distributions of the salt marsh sediments collected after stormy and non-stormy periods were then compared with each other and to the geochemistry and particle size distributions of surface sediments collected onshore, nearshore, and offshore to determine the sources of sediment supply in stormy and fair-weather conditions.

5.4 Study site

The Ribble Estuary is located on the Lancashire coast of North-West England (Figure 33 a). It is a funnel-shaped, tidally dominated and macro-tidal estuary (Wakefield et al., 2011) with an ordinary tidal range of 8.0 m at spring tide and 4.4 m at neap tide (UKHO, 2001). It only experiences moderate wave energy, owing to waves generated in the Irish Sea basin predominantly by southerly and westerly winds (Pye and Neal, 1994). The average marsh platform elevation is approximately 3.5 m above mean sea level at Ordinance Datum. The formation of the extensive intertidal sand-silt flats and salt marshes lying along the riverbanks (Figure 33 b) resulted from the combination of infilling of sandy sediments from the bed of the Irish Sea and the deposition of silt and clay-sized sediments coming from the River Ribble (van der Wal et al., 2002). The accretion of the intertidal flat and salt marsh platform might have been further aided by the moderate wave climate characterising the estuary, which is insufficient to cause significant lateral erosion (van der Wal et al., 2002). The majority of the sediment supplied to the marsh platform is marine in provenance (Wright et al., 1971; Chapter 3), with tidal pumping being the main process introducing sediments into the estuary (Lyons, 1997). Sediment supplied by storm surges has a crucial role in the accretion and expansion of the salt marsh and tidal flats, increasing the sediment budget of the system with increasing storm surge intensity and duration (Chapter 4 and Appendix II). Between 2007 and 2017, a two-phase scheme was implemented to restore the intertidal habitat, previously reclaimed for agricultural purposes, to enhance the protection of coastal infrastructures against flooding (Tovey et al., 2009).

5.5 Methods

5.5.1 Detection of storm activity

Sediments were collected approximately every 30 days from Hesketh Out Marsh from 15th November 2021 to 5th July 2022, with the same frequency both during stormy and non-stormy periods, with the exception of the first period (15th November 2021 to 12th January 2022) as sediments were collected after approximately 60 days for logistics reasons. For the identification of storm events, water level and significant wave height records measured respectively at the Liverpool Gladstone Dock tide gauge station (Figure 32 a; BODC, 2021) and at the Liverpool Bay WaveNet Site wave buoy (Figure 32 b; Cefas, 2022) were collected for the period studied. BODC and Cefas perform regular checks on the performance of the gauges and data are routinely processed and quality controlled. The water level data has been adjusted to Ordinance Datum (OD) using the conversion parameters provided by the National Tidal and Sea Level Facility and the values flagged as unreliable by BODC were removed from the time series. The residual water level was calculated by subtracting the predicted tide for the period studied from the total water level, and the predicted tide was calculated by combining the tidal constituents derived from the total water level of the period studied, using the MATLAB package T-Tide (Pawlowicz et al., 2002). Stormy periods were identified as periods in which residual water level and significant wave height increased above the 95th percentile (Figure 32). This is a threshold commonly associated with storm activity (e.g., Matulla et al., 2008; Lyddon et al., 2018). Only periods in which both residual water level and significant wave height increased above the 95th percentile were associated with storm activity.

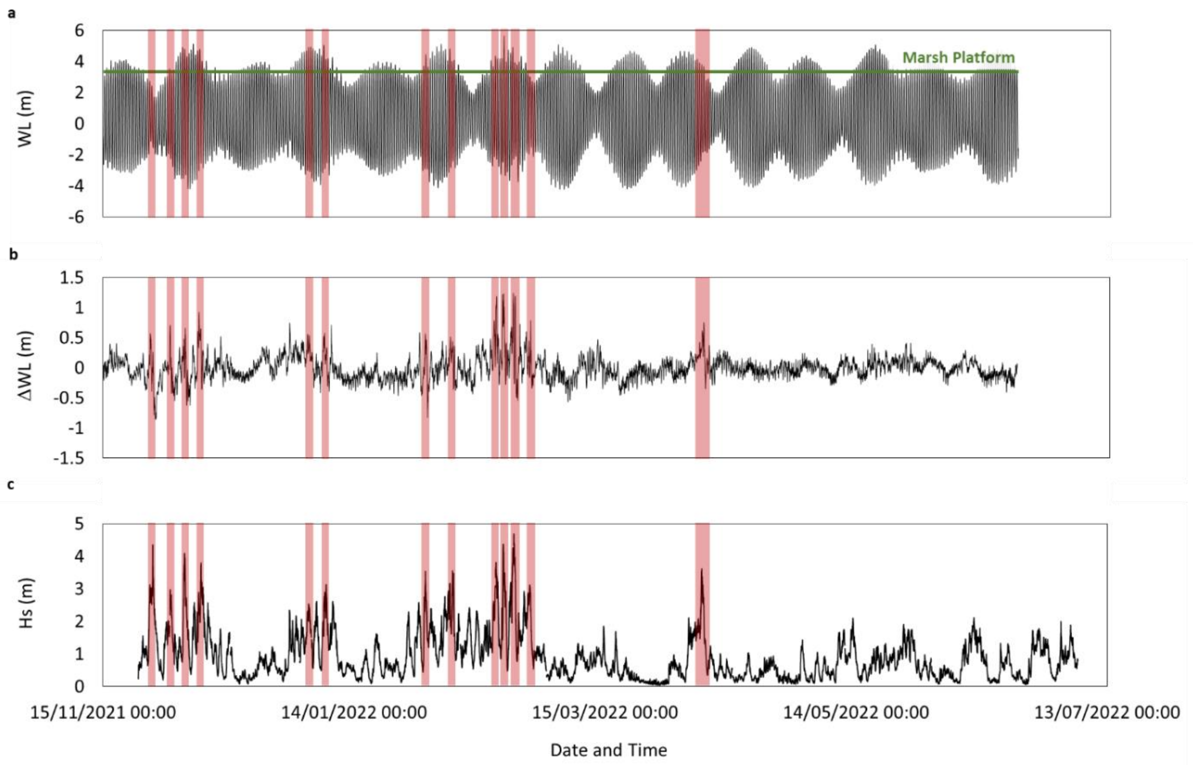

Figure 32. Total water level (WL) (a), residual water level (ΔWL) (b) and significant wave height (Hs) (c) measured from 15th November 2021 to 5th July 2022. The red bands highlight periods in which both residual water level and significant wave height are higher than the 95th percentile (i.e., stormy periods). The water level data has been adjusted to Ordnance Datum (OD).

5.5.2 Sediment supply

There is evidence that sediment supply to salt marshes is strongly controlled by the concentration of suspended sediment in the source water (Temmerman et al., 2004; Willemsen et al., 2021). Hence, to assess how storm activity affects sediment supply over the marsh platform, suspended sediments were collected across Hesketh Out Marsh (Figure 33 e) during stormy and non-stormy periods, using sediment traps. Two transects 100 m in length were set up on the salt marsh with traps placed at 15 m intervals, one orthogonal to the marsh edge and one orthogonal to the bank of one of the biggest tidal creeks (Figure 33 f). To ensure that there were no significant topographic constraints on the sediment supply to the sediment traps, transects profiles were produced using a TOPCON HIPER II RTK GPS with ~ 10 mm + 1 ppm horizontal accuracy and ~ 15 mm + 1 ppm vertical accuracy. The overall transects elevation has been adjusted to Ordnance Datum (OD) using the LiDAR-derived Digital Elevation Model (DEM) relative to the RTK base-station position as the reference point (Figure 33 g). The traps consisted of 50 mL plastic tubes which were placed at ground level and at 30 cm from the ground to capture the SSC vertical profile and to compare the trends at different levels to ensure internal consistency (Figure 33 h). Multiple stormy and non-stormy periods were assessed to further ensure consistency between trends relative to periods with similar hydrodynamic conditions (Figures 34 and S12). The samples were centrifuged to remove excess water and freeze-dried to remove any moisture before being weighed.

The availability of suspended sediment in the water column is controlled by current velocities and wave energy, responsible for sediment resuspension and transport (Rose and Thorne, 2001; Zhang et al., 2019). Storms cause an increase in water level and wave height, enhancing current velocities and wave energy (Bertin et al., 2017), thus increasing the availability of suspended sediment within the system (Duvall et al., 2019). As the storm period increases, the availability of suspended sediment also increases (Chapter 4 and Appendix II). Hence, to assess how storms control the sediment delivery to different areas of the marsh platform, a regression analysis was performed between the suspended sediment concentration measured across both transects over stormy and non-stormy periods and the hydrodynamic variables estimated for the same periods – i.e., mean residual water level and significant wave height above the 95th percentile (representative of storm intensity) and total period during which residual water level and significant wave height are above the 95th percentile (representative of the total period of storminess). To facilitate comparison between all stormy and non-stormy periods, the total suspended sediment concentration measured at the end of each period was normalized to daily rates and the total storm period was measured in days per month with one month being defined as 30 days. The regression analysis was then used to calculate coefficients of determination (R^2) to investigate how the control of each hydrodynamic parameter on the SSC varies spatially across the marsh platform.

5.5.3 Sediment composition and provenance

Chapter 3 showed that the inorganic sediment input to Hesketh Out Marsh is predominantly marine in provenance, while the riverine influence is minimal. As the marine provenance of the inorganic sediments was ascertained, to assess the spatial extent of marine sediment supply to the marsh platform during stormy and fair-weather conditions, the geochemical composition of the sediments collected from the salt marsh after stormy and non-stormy periods and the geochemical composition of the sediments collected from potential marine sources were determined using X-Ray Fluorescence (XRF) analysis and compared. Geochemistry is, indeed, widely used as a proxy to reconstruct the composition of marshland sediments (e.g., Kolditz et al., 2012; Hazermoshar et al., 2016).

As the estuary is infilled with marine sediments, the nearshore and offshore areas of the estuary are expected to be similar in sediment composition; thus, geochemical analysis is insufficient to discern which marine source the inorganic sediments are transported from. Particle size distributions (PSDs) analysis, on the other hand, can detect differential modes of sediment deposition, indicative of different levels of energy, that characterise the salt marsh in different hydrodynamic conditions, and can be used to speculate on the distance travelled by sediments before deposition (Rahman and Plater, 2014; Chapter 6). Fine-skewed to near-symmetrical distributions characterised by well-sorted, sand-sized sediment are typical of traction load delivered by the fast tidal flow velocities (i.e., during the flood phase) and are found in substrates with low elevation and high energy levels (e.g., sandflats). Near-symmetrical distributions characterised by fine to very fine, poorly sorted silts are typical of the suspension load that settles during the turn of the tide (i.e., during the ebb phase) and are found in substrates with high elevation and low energy levels (e.g., salt marsh platforms). Mudflats, which are transitional environments, typically have a mixed distribution. As salt marshes are low energy environments, the suspension load that dominates their PSDs is mostly eroded and transported by tidal currents and waves from adjacent mudflats and tidal creeks (Zhang et al., 2019; Roner et al., 2021). If storm flooding significantly enhances the energy levels over the marsh platform, the PSD of the salt marsh sediments are expected to change and resemble the PSD of the mudflat sediments, as higher energy levels allow sediment supply to the marsh platform through infilling as well as settling. A significant increase in energy levels would further imply that sediments can be transported over longer distances, thus suggesting that storms could transport significant amount of sediments from further marine sources (i.e., sandflat, sand dunes and offshore region) in addition to eroding the adjacent mudflat areas and tidal creeks (Cahoon et al., 1995). On the contrary, if storm flooding does not cause a significant increase in the energy level over the marsh platform, it would be unlikely that sediments are be transported from sources further than the adjacent mudflat and tidal creeks, and the PSD of the sediments supplied to the salt marsh by storms are expected be similar to the PSD of the sediments supplied in fair-weather conditions.

To show how PSDs can detect differential modes of sediment deposition, PSD analysis was first performed on the sediments collected from the potential onshore, nearshore and offshore sources, to characterise the landward change in energy levels. The same analysis was then performed on the sediments collected from the salt marsh platform during stormy and non-stormy periods to assess any change in energy levels caused by storm activity and relative change in sediment transport pathways. To characterise the onshore sediments, three samples were collected from the coastal aeolian dunes near Southport (Figure 33 c). To characterise the nearshore sediments, a set of nine samples (three per location) were collected from the mudflat and tidal creek adjacent to the marsh platform (Figure 33 f), and the sandflat at the south of the Ribble Estuary (Figure 33 d). The offshore sediments were characterised by analysing three sediment cores collected at 2 km spacing across the Irish Sea ~ 20 km offshore in 28-30 m water depths (Pearce et al., 2011); only the top 1 m of the cores (originally 6 m long) was subsampled (at 0.1 m intervals, resulting in 30 samples in total), with these depths characterising the more mobile surface sediments of the eastern Irish Sea (Figure 33 b).

5.5.3.1 Sediment composition

The geochemical composition of the sediments collected from Hesketh Out Marsh and potential marine sediment sources was measured by X-Ray fluorescence (XRF) using a XEPOS 3 Energy-dispersive XRF. All samples were hand ground, pressed and then measured under a He atmosphere under combined Pd and Co excitation radiation and using a high resolution, low spectral interference silicon drift detector. The XEPOS 3 undergoes daily standardisation procedure and has accuracies verified routinely using 18 certified reference materials (Boyle et al., 2015). Light elements were corrected for organic content, using loss-on-ignition (LOI) values measured by heating the samples at 105°C overnight to evaporate all moisture content and then igniting them in a furnace at 450°C for 4.5 hours to combust all organic matter (Boyle, 2000).

Principal component analysis was performed using PAST3 (Hammer, 2019) to explore the geochemical compositions of the samples and to assess any association between the salt marsh sediments and the potential marine sources. The parameters selected for this PCA were: coarse mineral (Si (mg/g), Zr (µg/g)) and shell content (Ca (mg/g), Sr (µg/g)) indicators, salt water (Na (mg/g)) and organic content (LOI (%), S (mg/g), Br (µg/g)) indicators, fine mineral indicators (K (mg/g), Al (mg/g), Ti (µg/g), Rb (µg/g), Nb (µg/g)), post-depositional diagenesis indicators (Fe (mg/g), Mn (µg/g)), pollutants (Mg (mg/g), P (mg/g), As (µg/g), Pb (µg/g), Zn (µg/g), Ni (µg/g), Cu (µg/g), V (µg/g), Cr (µg/g), Ga (µg/g), Ge (µg/g), Ba (µg/g), I (µg/g)) and the rare elements (Y (µg/g), La (µg/g), Ce (µg/g)) (Boyle, 2000; Plater, 2000).

5.5.3.2 Particle size distribution analysis

Particle size distributions (PSDs) were measured for the sediments collected at the marsh edge and from the potential sources using a Coulter LS 13 320 Single-Wavelength Laser Diffraction Particle Size Analyser that determines the dimensions of individual particles 0.375-2000 µm. Only the sediments trapped at marsh edge at ground level were used for the PSD analysis, as they are the most likely to show a mixed distribution if any infilling has occurred (Rahman and Plater, 2014). Subsamples were digested in 6% concentrated H_2O_2 (50 ml of H_2O_2 per 10 ml of sample) to remove any organic component, with the samples then dispersed and sonicated in $Na_6O_{18}P_6$ and analysed under sonicating measurement conditions. The resulting PSDs are the average of three repeats after the elimination of outliers. The Coulter LS 13 320 undergoes regular calibration checks using samples with known size distributions. End-member modelling analysis (EMMA) was conducted using the EMMAgeo R package to statistically derive the dominant modes in the PSDs of the marsh and potential marine source sediments (Dietze et al., 2012). The maximum number of end-members that the model could detect was set as seven, as identified by Clarke et al. (2013) and Clarke et al. (2014). Particle size categories with several zero values were combined to enable an end-member analysis of the entire data set. A robustness test was performed to check on each end-member (Figure S11 a). The model showed that 85% of the variance in the PSDs could be explained by two PSD end-members (Figure S11 b). The loading of the end-members explaining most of the variance was plotted to characterise the dominant modes in the PSDs of the marsh edge and potential marine source sediments. The end-members scores relative to the salt marsh and potential sources were then plotted to observe any similarities between the modes characterising the salt marsh sediments during stormy and non-stormy periods and the modes characterising the potential marine sources.

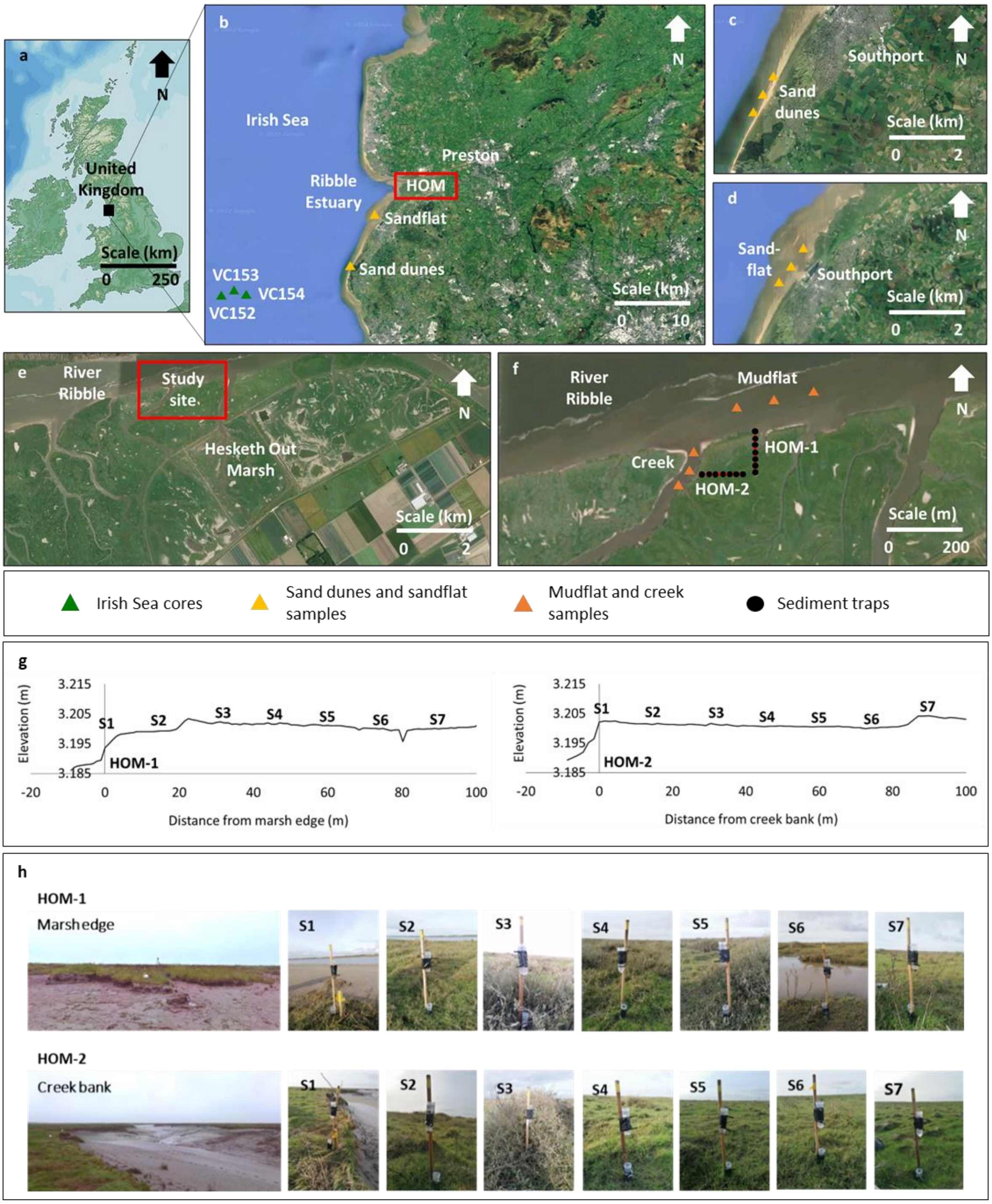

Figure 33. Location of the Ribble Estuary (a); location of Hesketh Out Marsh (HOM), the Irish Sea coring sites (VC153, VC154, VC152), and the sand dunes and sandflat sampling sites (© Google Earth Pro, 2022) (b); high-resolution view of the sand dunes (c) and sandflat (d)

sampling sites (© Google Earth Pro, 2022); high-resolution view of Hesketh Out Marsh and location of the study site (© Google Earth Pro, 2022) (e); high-resolution view of the mudflat and creek sampling sites and transects location (© Google Earth Pro, 2022) (f); transects profiles and location of the sediment traps (g); panoramic of the starting points of the transects HOM-1 (marsh edge) and HOM-2 (creek bank) obtained with a FARO 3D laser scanner Focus X330 and photos displaying the locations of the sediment traps along each transect (see Figure S10 in Appendix III for zoomed-in photos) (h).

5.6 Results

5.6.1 Sediment supply

Both at ground level and at 30 cm from the ground, suspended sediment concentration (SSC) decayed non-linearly with distance from the marsh edge and the creek bank, similarly during stormy and fair-weather periods, but was overall higher across both transects during stormy periods (Figures 34 and S12).

Close to the marsh edge, SSC reached up to 0.2 g/day at ground level and up to 0.04 g/day at 30 cm from the ground in fair-weather conditions, while it reached up to 0.7 g/day at ground level and up to 0.2 g/day at 30 cm from the ground in stormy conditions (Figure 35 c, d). Close to the creek bank and at 30 m from the marsh edge and creek bank, SSC was consistently lower than 0.01 g/day in fair-weather conditions, both at ground level and at 30 cm from the ground, while it reached up to 0.07 g/day at ground level and up to 0.04 g/day at 30 cm from the ground in stormy conditions (Figure 35 e, d). Thus, in stormy periods, SSC at the marsh edge increased by up to 250% at ground level and by up to 400% at 30 cm from the ground; in the marsh interior, however, it increased up to 600% at ground level and up to 300% at 30 cm from the ground. Hence, in relative terms, the increase in SSC caused by storm activity was more significant for the interior of the marsh than it was for the marsh edge.

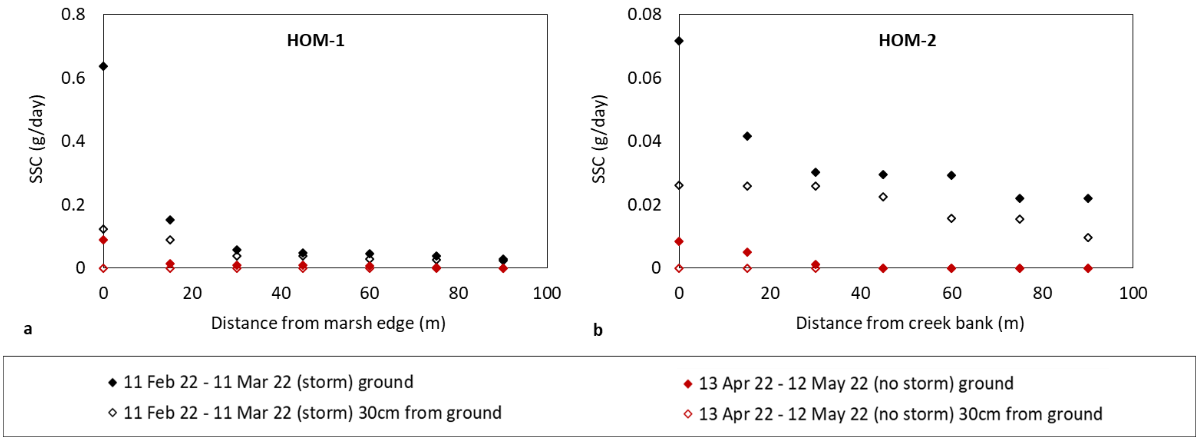

Figure 34. SSC (g/day) profile with distance from the marsh edge (a) and the creek bank (b), at ground level and at 30 cm from the ground, relative to a stormy and a non-stormy period (see Figure S12 in Appendix III for the profiles relative to the other periods studied).

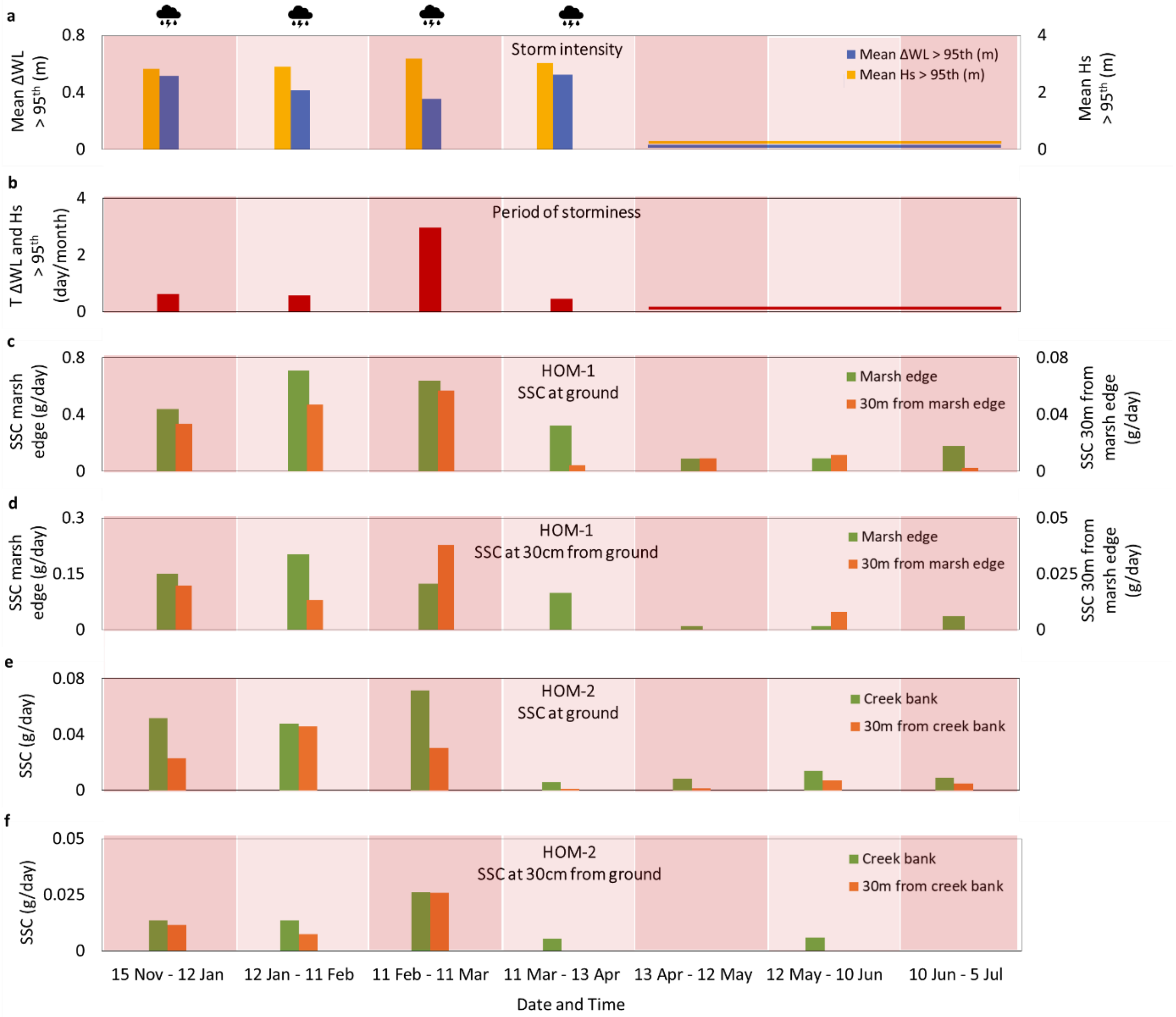

Figure 35. Mean residual water level (ΔWL) (m) and significant wave height (Hs) (m) above the 95th percentile (a); total period (T) during which residual water level (ΔWL) and significant wave height (Hs) are above the 95th percentile (b); SSC (g/day) at ground level, at the marsh edge and at 30 m from the marsh edge (c); SSC (g/day) at 30 cm from the ground, at the marsh edge and at 30 m from the marsh edge (d); SSC (g/day) at ground level, at the creek bank and at 30 m from the creek bank (e); SSC (g/day) at 30 cm from the ground, at the creek bank and at 30 m from the creek bank (f); for each period studied between 15th November 2021 and 5th July 2022. The cloud symbols indicate the periods characterised by storm activity.

The increase in SSC during stormy periods corresponds to an increase in the residual water level and significant wave height, both of which consistently increased above the 95th percentile; the mean residual water level above the 95th percentile ranged between 0.35 m and 0.53 m, while the significant wave height above the 95th percentile ranged between 2.8 m and 3.2 m (Figure 35 a, b). Overall, across both transects, SSC shows a positive correlation with all three hydrodynamic variables, increasing with an increase in storm intensity (i.e., mean residual water level and significant wave height above the 95th percentile) and storm duration (i.e., total period during which residual water level and significant wave height are above the 95th percentile), similarly at ground level and at 30 cm from the ground (Figure 36). The control of the hydrodynamic variables on the SSC, however, is not uniform across the salt marsh platform (Figure 37). Results show that variations in water level and wave height cause the greatest changes in SSC at the marsh edge, while their influence decreases with distance from marsh edge and creek bank. Nevertheless, wave height has a stronger control on SSC compared to water level. Storm duration, on the other hand, is more influential over the marsh interior and has, overall, the strongest control on the total sediment availability above the marsh platform.

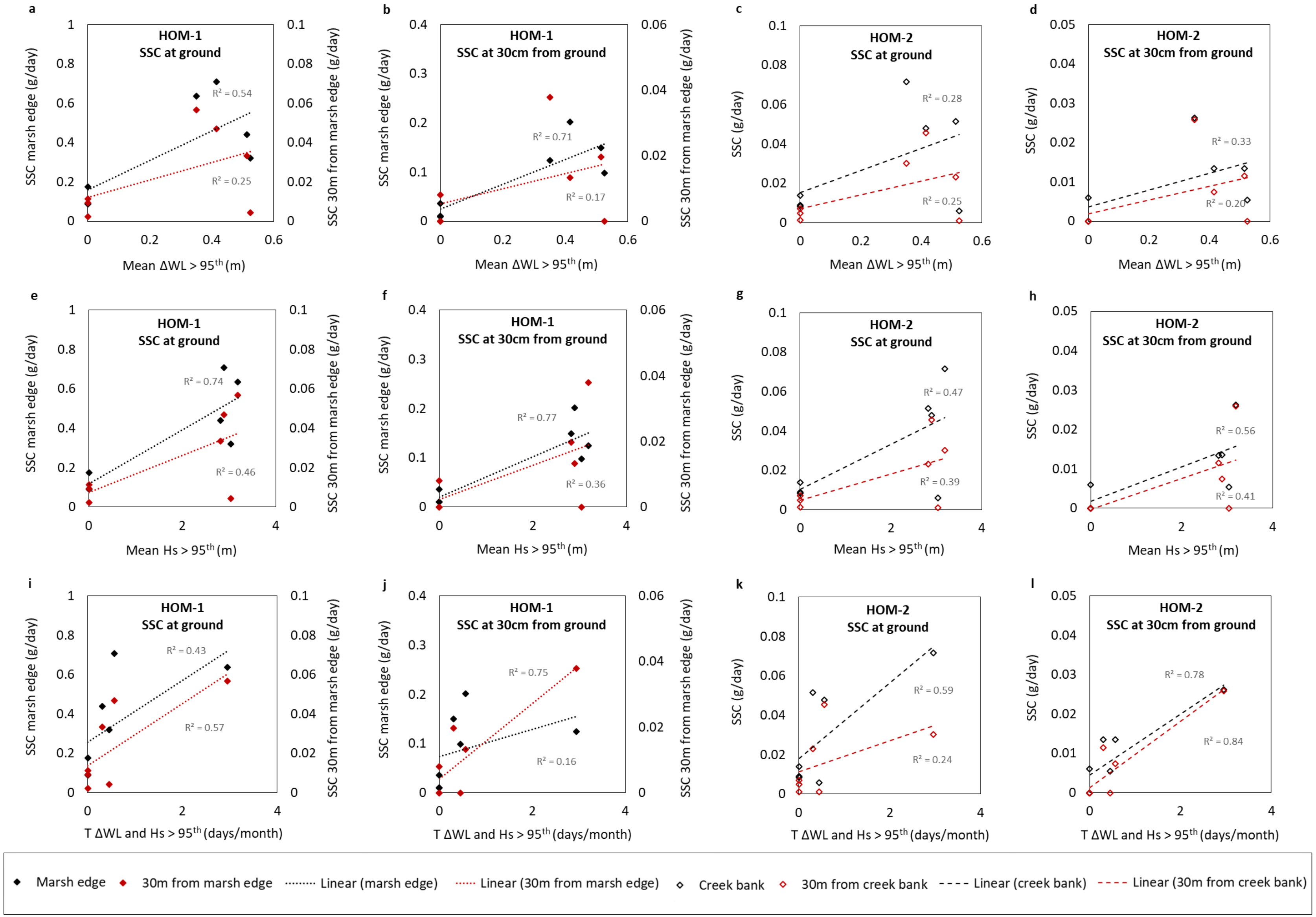
a
HOM-1
SSC at ground
SSC marsh edge (g/day)
SSC 30m from marsh edge (g/day)
R² = 0.54
R² = 0.25
Mean ΔWL > 95th (m)
b
HOM-1
SSC at 30cm from ground
SSC marsh edge (g/day)
SSC 30m from marsh edge (g/day)
R² = 0.71
R² = 0.17
Mean ΔWL > 95th (m)
c
HOM-2
SSC at ground
SSC (g/day)
R² = 0.28
R² = 0.25
Mean ΔWL > 95th (m)
d
HOM-2
SSC at 30cm from ground
SSC (g/day)
R² = 0.33
R² = 0.20
Mean ΔWL > 95th (m)
e
HOM-1
SSC at ground
SSC marsh edge (g/day)
SSC 30m from marsh edge (g/day)
R² = 0.74
R² = 0.46
Mean Hs > 95th (m)
f
HOM-1
SSC at 30cm from ground
SSC marsh edge (g/day)
SSC 30m from marsh edge (g/day)
R² = 0.77
R² = 0.36
Mean Hs > 95th (m)
g
HOM-2
SSC at ground
SSC (g/day)
R² = 0.47
R² = 0.39
Mean Hs > 95th (m)
h
HOM-2
SSC at 30cm from ground
SSC (g/day)
R² = 0.56
R² = 0.41
Mean Hs > 95th (m)
i
HOM-1
SSC at ground
SSC marsh edge (g/day)
SSC 30m from marsh edge (g/day)
R² = 0.43
R² = 0.57
T ΔWL and Hs > 95th (days/month)
j
HOM-1
SSC at 30cm from ground
SSC marsh edge (g/day)
SSC 30m from marsh edge (g/day)
R² = 0.75
R² = 0.16
T ΔWL and Hs > 95th (days/month)
k
HOM-2
SSC at ground
SSC (g/day)
R² = 0.59
R² = 0.24
T ΔWL and Hs > 95th (days/month)
l
HOM-2
SSC at 30cm from ground
SSC (g/day)
R² = 0.78
R² = 0.84
T ΔWL and Hs > 95th (days/month)
◆ Marsh edge
◆ 30m from marsh edge
Linear (marsh edge)
Linear (30m from marsh edge)
◇ Creek bank
◇ 30m from creek bank
Linear (creek bank)
Linear (30m from creek bank)

Figure 36. Linear regression analysis performed between SSC (g/day), mean residual water level (ΔWL) (m) and significant wave height (Hs) (m) above the 95th percentile, and the total period (T) during which residual water level (ΔWL) and significant wave height (Hs) are above the 95th percentile (days/month); at ground level at the marsh edge and at 30 m from the marsh edge (a, e, i), at 30 cm from the ground at the marsh edge and at 30 m from the marsh edge (b, f, j), at ground level at the creek bank and at 30 m from the creek bank (c, g, k), and at 30 cm from the ground at the creek bank and at 30 m from the creek bank (d, h, l).

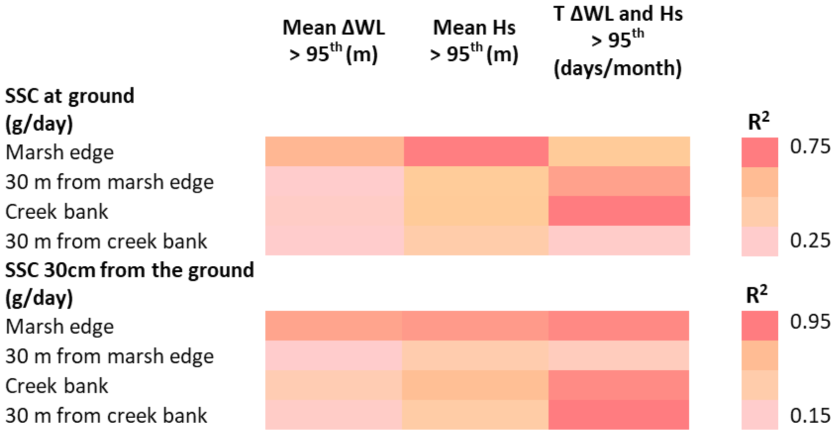

Figure 37. Coefficients of determination (R^2) relative to the linear regression analysis performed between SSC (g/day), mean residual water level (ΔWL) (m) and significant wave height (Hs) (m) above the 95th percentile, and the total period (T) during which residual water level (ΔWL) and significant wave height (Hs) are above the 95th percentile (days/month); at ground level at the marsh edge and at 30 m from the marsh edge, at 30 cm from the ground at the marsh edge and at 30 m from the marsh edge, at ground level at the creek bank and at 30 m from the creek bank, and at 30 cm from the ground at the creek bank and at 30 m from the creek bank.

5.6.2 Sediment composition and provenance

The first two components of the PCA performed on the XRF measurements of the sediments collected from Hesketh Out Marsh, the Irish Sea floor, Southport sand dunes, and the intertidal areas summarise 76% of the variance in the data, respectively 43% and 33% (Figure 38). Component 2 separates samples rich in shells (Ca and Sr) and silt-sand sized minerals (Si and Zr) from those rich in organic content (LOI, S and Br). Component 1 separates samples rich in organic content from those rich in minerals and pollutants. The marsh sediments collected after stormy periods are mostly characterised by shells and silt-sand sized minerals, with some contribution from finer minerals, and have similar composition to some of the marine samples. The sediments collected after non-stormy periods are mostly characterised by organic content with minimal contribution from finer minerals, with the exception of the sediments collected at the edge of the marsh platform, which are richer in shells and silt-sand sized minerals and have stronger association with the stormy sediments and some of the marine samples.

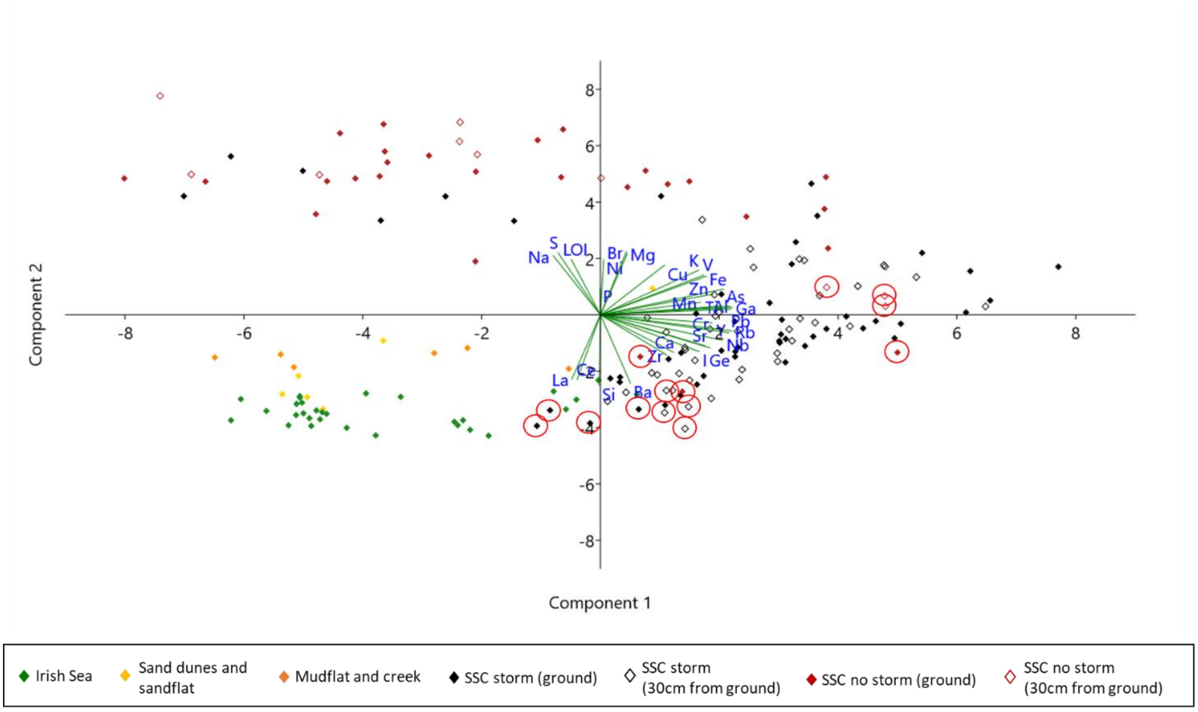

Figure 38. Principal component analysis between samples collected from Hesketh Out Marsh, sand dunes and sandflat, mudflat and creek adjacent to the salt marsh, and the Irish Sea cores. Component 1 and component 2 summarise 76% of the variance in the data, respectively 43% and 33%. The figure shows the parameters used by each component to separate the samples and the clusters formed by the samples that correlate with each other. The red circles highlight the samples collected at the marsh edge.

The EMMA analysis (Figure 39) shows two dominant end-members characterising the PSDs variance: EM1 is characterised by a mixed near-symmetrical to fine-skewed distribution of silt to fine sand with a secondary near-symmetrical mode dominantly clay to silt and EM2 is characterised by a fine-skewed to near-symmetrical distribution of fine to coarse sand. The Irish Sea, sand dunes and sandflat sediments have PSDs dominated by EM2, with only minimal contribution (up to 30%) from EM1. Progressing landwards, however, the EM1 mode becomes dominant, characterising between 40% and 100% of the mudflat and creek PSDs. The samples collected from the salt marsh edge after the stormy periods do not differ statistically from the samples collected after non-stormy periods; their PSDs are both dominated by the EM1 mode.

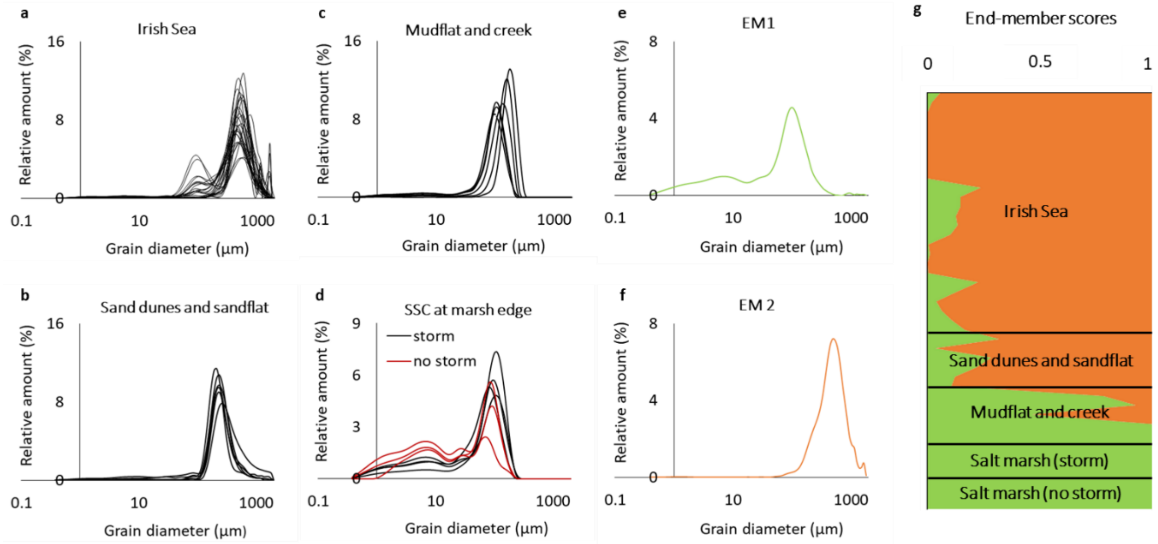

Figure 39. PSDs of sediments from Irish Sea (a), sand dunes and sandflat (b), mudflat and creek (c) and Hesketh Out Marsh (d); end-member loading for EM1 (e) and EM2 (f); end-member scores for salt marsh and potential sediment sources (g).

5.7 Discussion

5.7.1 Sediment supply

Suspended sediment concentration decreased with distance from the marsh edge and the creek bank, similarly during stormy and fair-weather periods (Figures 34 and S12). This non-linear decrease resembles trends already showed for other sites by modelling (Zhang et al., 2019; Zhu and Wiberg, 2022) and field (Temmerman et al., 2003; Duvall et al., 2019) studies. Sediments are transported over the marsh platform by flood currents and waves, which are dependent of water depth. Close to the water sources (i.e., at the marsh edge and creek bank), where water depths are higher, flood currents and waves are stronger due to lower friction and deliver higher concentrations of sediments. With increasing distance from the water sources (i.e., in the marsh interior), water depth decreases and so does the strength of the flood currents and waves; thus, decreasing the sediment supply to the areas of the marsh further from the water sources (Temmerman et al., 2003; Duvall et al., 2019; Zhang et al., 2019).

Sediment supply over the marsh platform, however, was overall higher across both transects during stormy periods (Figures 34 and S12). Storms cause an increase in both water level and wave height (Figure 35 a; Bertin et al., 2017). When a storm causes an increase in water level (i.e., positive surge), the water depth increases and enhances the propagation speed of the tidal wave, leading to an increase in the speed of the flood currents (Bertin et al., 2017). Simultaneously, storms also cause an increase in wave height, which is responsible for an increase in wave energy (Bertin et al., 2017). This increase in current velocities and wave energy contributes to higher bottom shear stress resulting in higher sediment resuspension and enhance sediment transport within the system (Mariotti et al., 2010; Carniello et al., 2010), also affecting areas of the inner marsh platform which are not flooded in fair-weather conditions (Kirwan and Murray, 2007; D'Alpaos et al., 2007). As showed by the regression analysis (Figure 36), this resulted in a positive correlation between SSC and the hydrodynamic parameters, with SSC increasing with increasing storm intensity (i.e., mean residual water level and significant wave height above the 95th percentile) and storm duration (i.e., period during which mean residual water level and significant wave height are above the 95th percentile). The uneven influence of the hydrodynamic parameters on the spatial distribution of sediment supply across the salt marsh platform observed in Figure 37 is due partially to the increase of vegetation and topographic constraints with increasing distance from marsh edge (Neumeier and Ciavola, 2004; Mudd et al., 2010; Yang et al., 2012) and partially to the differential increase in settling time over different marsh areas (Temmerman et al., 2003; Duvall et al., 2019; Zhang et al., 2019). Water level and wave height cause the greatest changes at the marsh edge, while their influence decreases with distance from marsh edge and creek bank. While above the outer marsh an increase in water level and wave height directly corresponds to an increase in tidal current velocities and wave energy, with increasing distance from marsh edge and creek bank, the increased friction caused by vegetation and topographic variations buffers tidal currents and waves, hence inhibiting their influence above the inner marsh areas (Neumeier and Ciavola, 2004; Mudd et al., 2010; Yang et al., 2012). Wave height, however, seems to have a stronger control on sediment supply than water level, in agreement with results from other field (Duvall et al., 2019) and modelling (Zhu and Wiberg, 2022) studies. Duvall et al. (2019) observed that water level is responsible for the regulation of the marsh inundation, which influences sediment delivery, while waves are responsible for most of the sediment resuspension on the tidal flat, which controls sediment availability; hence, waves are ultimately responsible for the amount of sediments that can be transported from the mudflat to the salt marsh platform. Storm duration, on the other hand, is more influential over the marsh interior and has, overall, the strongest control on the total sediment availability above the marsh platform. Although an increase in storm duration is responsible for longer inundation of the marsh platform and consequent higher overall sediment supply (Chapter 4 and Appendix II), close to the marsh edge, where water depths are already high, the increase in settling time caused by increased water levels is higher than in the marsh interior (Temmerman et al., 2003; Duvall et al., 2019; Zhang et al., 2019); hence, an increase in storm duration has lower control on the sediment deposition closer to the water sources. The higher settling time (due to increased water depth) at the marsh edge compared to the marsh interior is also responsible for the lower rates of change in sediment supply that characterise the outer marsh, as observed in Figure 35. Indeed, although sediment supply was overall higher at the marsh edge than it was in the marsh interior, the increase in sediment supply at ground level during stormy periods was more significant for the inner marsh (up to 600%) than it was for the marsh edge (up to 400%). This differential increase in settling time was also detected by the SSC vertical profile. At the marsh edge, the storm-driven increase in SSC at ground level was lower than the increase at 30 cm from the ground; however, over the marsh interior, the increase at ground level was higher than the increase at 30 cm from the ground (Figure 35).

Overall, results showed that storm activity causes an increase in sediment supply to the whole salt marsh platform, and that this increase is especially significant for the marsh interior.

5.7.2 Sediment composition and provenance

The PCA analysis (Figure 38) suggests that, in fair-weather conditions, inorganic sediments transported from marine sources only reach the outer portion of the marsh platform up to 30 m from the marsh edge; most of the sedimentation beyond that point is caused by in-situ organogenic processes (Boyle, 2000; Plater, 2000), as those areas of the marsh are not regularly flooded (Kirwan and Murray, 2007; D'Alpaos et al., 2007). During storm events, on the other hand, as water level and wave height increase (Bertin et al., 2017) and further inland portions of the salt marsh experience flooding (Kirwan and Murray, 2007; D'Alpaos et al., 2007), marine sediments reach both outer and inner marsh areas covering, in the majority of the cases, the whole extent of the transects (Boyle, 2000; Plater, 2000). Similar trends have been observed in other sites (Stumpf et al., 1983; Marani et al., 2013; Morris et al., 2016; Tognin et al., 2021).

The EMMA analysis (Figure 39) shows, as expected (Rahman and Plater, 2014; Chapter 6), that the particle size distributions (PSDs) of the sediments collected from the Irish Sea basin, sand dunes and sandflat are dominated by the EM2 mode (fine-skewed to near-symmetrical distribution of fine to coarse sand typical of energetic environments where sedimentation occurs through infilling), with only minimal contribution from EM1, while the mudflat and tidal creeks have PSDs which progressively become dominated by the EM1 mode (mixed near-symmetrical to fine-skewed distribution of silt to fine sand with a secondary near-symmetrical mode dominantly clay to silt typical of low energy environments where sedimentation occurs through settling). Interestingly, the EMMA analysis also shows that the PSDs of the sediments collected from the salt marsh edge after the stormy periods do not differ statistically from the PSDs of the sediments collected after non-stormy periods, as they are both dominated by the

EM1 mode. The sediment supplied to salt marshes is mostly suspension load that is transported by flood tides from adjacent mudflats and tidal creeks and settles on the marsh platforms during the turn of the tide (Rahman and Plater, 2014; Zhang et al., 2019; Roner et al., 2021; Chapter 6). The lack of significant change in the PSDs of the salt marsh sediments between fair-weather and stormy periods suggests that the increase in energy levels caused by the storms was not high enough to change the mode of sediment deposition (Rahman and Plater, 2014); hence, even in stormy conditions, the majority of the sediments supplied to the salt marsh platform are likely to be resuspended from the tidal creeks and the mudflats adjacent to the marsh (Zhang et al., 2019; Roner et al., 2021). It is indeed reasonable that, since sediment availability is strongly dependent on resuspension (Figure 37; Duvall et al., 2019), the majority of the sediments are transported from shallow areas, where waves and currents can generate shear stresses (Mariotti et al., 2010; Carniello et al., 2010). This interpretation also agrees with the trends observed in Chapter 4, which modelled the effects of increasing storm intensity on the sediment budget of the Ribble Estuary. The model showed that even the most intense storms (surges up to 4 m) would increase the sediment budget of the salt marsh platform by up to 67% but would only contribute to an increase in the sediment budget of the inner estuary by up to 7%. Such a difference in rates suggests that, although a minimal contribution from further sources is probable, the majority of the sediments transported by storms onto the salt marsh platform must come from within the inner estuary, thus confirming our interpretation of the PSDs results.

5.7.3 Implications

With the ongoing decrease in sediment supply to the coastlines (Darby et al., 2020; Tamura et al., 2020; Wei et al., 2020), the contribution of storm sedimentation to the salt marsh sediment budget is thought to be critical for marsh survival to sea-level rise (Schuerch et al., 2013;

Chapter 4). Salt marsh resilience to sea-level rise depends on their ability to accrete vertically and expand laterally (Mariotti and Carr, 2014; Ma et al., 2014; Mitchell et al., 2017). While vertical accretion prevents salt marshes from drowning, lateral expansion is crucial to avoid collapse of the platform edge (Mariotti and Fagherazzi, 2013; Fagherazzi et al., 2013).

Results showed that storm activity causes an overall increase in sediment supply to the salt marsh platform, and that this increase is especially significant for the marsh interior. This suggests that storms are especially beneficial to the vertical accretion of the inner marsh areas, which rarely experience minerogenic supply (Stumpf et al., 1983; Marani et al., 2013; Morris et al., 2016; Tognin et al., 2021). Nonetheless, results also showed that the majority of the sediment supplied to the salt marsh platform by storms is likely generated by an increase in erosion and resuspension of mudflat and tidal creek sediments (Zhang et al., 2019; Roner et al., 2021), while only a minimal contribution is given by sediment transported from outside the system (Cahoon et al., 1995). This suggests that, in the long-term, storms will promote salt marsh vertical accretion, but might simultaneously reduce the overall larger-scale sediment availability with implications for the lateral retreat of the marsh platform (Roner et al., 2021).

5.8 Conclusions

This study aimed at understanding how storm activity affects sediment supply to different marsh areas and whether storm sediment supply has different origin to the marine sediment delivered to marsh platforms during fair-weather conditions. Suspended sediment concentrations were analysed across Hesketh Out Marsh, North-West England, during the 2021-2022 storm season, during stormy and non-stormy periods to assess how storm activity changes the spatial variability of sediment supply across the marsh platform. Geochemical and particle size distribution analyses were then conducted on sediments from the salt marsh and potential onshore, nearshore and offshore sources of sediments to determine whether storms deliver any new material onto the salt marsh platform which would not be delivered in fair-weather conditions. Results showed that storm activity causes an increase in inorganic sediment supply to the whole salt marsh platform and that this increase is especially significant for the marsh interior. However, the majority of the sediment supplied to the salt marsh platform by storms is produced by an increase in erosion and resuspension of mudflat and tidal creek sediments, while the sediments transported from outside the intertidal system only contribute minimally. This suggests that, in the long-term, storms will promote salt marsh vertical accretion but might simultaneously reduce the overall larger-scale sediment availability with implications for the marsh lateral retreat.

5.9 Acknowledgements

We acknowledge support from the School of Environmental Sciences, University of Liverpool, which is funding the PhD project of the first author, the RGS-IBG for funding the field campaign and the first author time on this project (project title: Building coastal resilience one sediment grain at the time: field measurements and community engagement on nature-based solutions for coastal protection, PI Prof. Nicoletta Leonardi, RGS-IBG Environment and Sustainability Research Grant) and EPSRC support to Prof. Nicoletta Leonardi (EP/V056042/1). We also acknowledge Prof. Chiverrell R. for providing us with the Irish Sea cores. We further acknowledge the support of the RSPB for allowing the fieldwork campaign in the Ribble Estuary and the Geography laboratories and their technicians and students (Jennifer Bradley, Luke Glascott, Mike O’Connor, Richard Clark, Joshua Hicks, and Molly Spater) for their support with equipment, fieldwork and laboratory analyses. We ultimately thank Dr. Kirwan M. and Dr. Hein C. for the insightful discussions held at the early stages of this study during an AGU conference and two anonymous reviewers for their constructive feedback on the manuscript.

5.10 Data Availability

Data related to this article can be found in the following repository: https://doi.org/10.5281/zenodo.7590233.

Chapter 6

Novel luminescence diagnosis of storm deposition across intertidal environments

6.1 Preface

Chapters 4 and 5 showed how and to what extent storms contribute to salt marsh resilience. None of the chapters, however, have analysed the contribution of storm frequency to long-term marsh resilience. The choice of not investigating storm frequency is determined by the inconsistencies in long-term storm activity records which are necessary for validating and informing long-term modelling studies, as high-resolution gauge measurements are often short-term and traditional paleoenvironmental reconstruction techniques are not able to detect all storm events (i.e., those which do not cause a change in stratigraphy and sediment composition). Therefore, this chapter aims to develop a new approach for diagnosing storm activity in geological records that does not rely solely upon a change in sediment composition and stratigraphy. Since luminescence has the potential to detect different degrees of sediment processing without relying on change in composition, this chapter tests whether K-feldspar luminescence signals can detect differential modes of deposition in intertidal settings and can therefore diagnose storm activity within an intertidal system.

6.2 Abstract

Salt marshes provide valuable nature-based, low-cost defences protecting against coastal flooding and erosion. Storm sedimentation can improve the resilience of salt marshes to accelerating rates of sea-level rise, which poses a threat to salt marsh survival worldwide. It is therefore important to be able to accurately detect the frequency of storm activity in longer-term sediment records to quantify how storms contribute to salt marsh resilience. Luminescence is able to infer how long mineral grains were exposed to sunlight prior to burial (e.g., the presence or absence of sediment processing). This study used sediment cores collected from the Ribble Estuary, North West England, to show that luminescence properties of sand-sized K-feldspar grains can diagnose the differential modes of deposition across intertidal

settings (i.e., sandflat, mudflat and salt marsh) in longer-term sediment records by detecting the variability in sediment bleaching potential between settings (i.e., sediment exposure to sunlight), thus establishing a framework for the interpretation of luminescence properties of intertidal sediments. It then used modern sediment samples collected before and after a storm event to show how such properties can diagnose changes in sediment processing (i.e., bleaching potential) of mudflat sediments caused by storm activity, despite no changes in sediment composition being recorded by geochemical and particle size distribution analyses. This new luminescence approach can be applied to longer-term sediment records to reveal (and date) changes in the environment of deposition and/or depositional dynamics where there is no obvious stratigraphic evidence of such.

6.3 Introduction

Salt marshes provide valuable nature-based, longer-term, low-cost defences protecting against coastal flooding and erosion (e.g., Möller et al., 1999; Temmerman et al., 2013; Leonardi et al., 2018). Storm sedimentation can improve the resilience of salt marshes to accelerating rates of sea-level rise and decreasing sediment discharges of rivers (Mariotti and Fagherazzi, 2010; Schuerch et al., 2013; Yang et al., 2020; Chapter 4), which pose a threat to salt marsh survival worldwide (e.g., Bakker et al., 1993; Environment Agency, 2011). Understanding the processes and longer-term frequency of storms that promote salt marsh resilience to sea-level rise is, therefore, a fundamental goal to ensure effective management of coastlines in the future (e.g., McCloskey and Liu, 2012; Walters and Kirwan, 2016; Bianchette et al., 2022). Salt marsh platforms do not record storm deposits uniformly, due to spatial constraints on sediment deposition caused by vegetation and topographic features characteristic of salt marsh surfaces. Tidal flats, conversely, represent a good archive for storm activity as there are fewer topographic and no vegetation constraints on sediment deposition. However, many storms process sediment locally rather than providing fresh input to the intertidal area (Grant et al., 1997; Wesselman et al., 2017; Brooks et al., 2017), causing no change in the tidal flat sediment composition (e.g., in particle size distribution or geochemistry); thus, existing techniques are not always able to detect storm activity in longer sediment records (Cundy et al., 1997). Solving this challenge requires a new approach to diagnosing storm activity in the geological record that does not rely upon a change in sediment composition.

The luminescence properties of mineral grains have been successfully used as a diagnostic tool of sediment dynamics (Gray et al., 2019), and deployed thus far as a sediment tracer to identify sediment sources and transport pathways in both coastal and fluvial settings (Sawakuchi et al., 2011, 2012, 2018; Ahmed et al., 2014; Haddadchi et al., 2016; Gray et al. 2017, 2018). Luminescence is based upon the principle that, when minerals (e.g., K-feldspars) are stimulated by light, heat or pressure, electrons that were stored in the crystal lattice are released, i.e. the luminescence signal is reset (or bleached) (see reviews by Smedley, 2018 and Murray et al., 2021). When subsequently buried, the minerals are exposed for a period of time to natural radiation (termed environmental dose-rate), which re-traps electrons within the crystal lattice and restores a luminescence signal (measured in the laboratory as equivalent dose, or D_e). In environments where sediments were exposed to sufficient duration and intensity of sunlight prior to burial, the luminescence signals of all of the grains are reset (i.e., well bleached) prior to burial. Where sunlight exposure prior to burial was insufficient, the luminescence signals reset partially (i.e., partially bleached). By determining D_e values from each sample, it is possible to determine how well bleached the mineral grains were before they were buried, and thus infer the nature of the bleaching environment (e.g., the presence or absence of sediment processing). The infra-red stimulated luminescence (IRSL) signals of K-feldspar have the potential to be used as a diagnostic tool of sediment dynamics due to the relative differences in bleaching rates of the multiple-elevated temperature (MET) post-infra-red infra-red stimulated luminescence (post-IR IRSL) signals measured at 50°C (termed IR_{50}), 150°C (termed $pIRIR_{150}$)

and 225°C (termed pIRIR$_{225}$) (e.g., Reimann et al., 2015; Chamberlain et al., 2017; Gray et al., 2017, 2018).

The aim of this study is to assess whether the luminescence properties of K-feldspars can be used to infer changes in sedimentation modes that have occurred in an intertidal setting. The Ribble Estuary, North West England, is used as a case study due to its ecological and economic value, and because storm surge deposits here are significant for the resilience of this salt marsh to sea-level rise (Lyons, 1997; Chapter 4 and Appendix II). First, we test whether changes in sedimentation modes characteristic of the different intertidal settings (sandflat, mudflat and salt marsh) can be detected by the luminescence properties using a well-constrained, long-term, multi-proxy evolutionary analysis of the marsh platform (Chapter 3). Secondly, we use modern analogues collected before and after a storm event to assess whether luminescence can diagnose the greater opportunity for sunlight exposure (i.e., bleaching potential) caused by sediment processing from a storm event, which could be used to detect the storm activity preserved in sediment records that would otherwise go undetected using existing techniques.

6.4 Study site

The Ribble Estuary is a funnel-shaped, hypertidal estuary located in North West England (Figure 40 a), with an ordinary tidal range of 8.0 m at spring tide and 4.4 m at neap tide (UKHO, 2001). The marsh platform reaches 3 km at its widest and stands between ~ + 3.2 m OD and ~ + 4.7 m OD, while the intertidal flat reaches 2 km at its widest and stands between ~ + 2 m OD and ~ + 3 m OD. The extensive intertidal sand-silt flats and the salt marsh at the south of the estuary (Figure 40 b) resulted from the combination of infilling of sandy sediments from the bed of the Irish Sea and deposition of the silt and clay-size sediments coming from the River Ribble (van der Wal et al., 2002), with the majority of the sediment supply being marine in provenance (Wright et al., 1971; Chapter 3). The bed of the central Irish Sea is characterised by waves of mobile sediments that move up to 70 m per year (Van Landeghem et al., 2012), which can only be sustained because of the large sediment volumes deposited by ice retreating northwards up the Irish Sea during the last deglaciation (Van Landeghem and Chiverrell, 2020; Scourse et al., 2021). Tidal pumping, especially during high storm surges, is the main process introducing sediments into the estuary, increasing the sediment budget of the salt marsh with increasing storm surge intensity and duration (Lyons, 1997; Chapter 4 and Appendix II). The moderate wave climate of the Ribble Estuary (Pye and Neal, 1994), that is insufficient to cause significant lateral erosion, is thought to have favoured the accretion of the marsh platform (van der Wal et al., 2002). Glacial Isostatic Adjustment models show a long-term decrease in the rate of relative sea-level rise in North West England for the past 2000 years (Tooley, 1974; Shennan et al., 2018). However, sea-level reconstructions and historical tidal gauge records show that, for the past ca. 240 years, the rate of sea-level rise has been increasing again (from ca. 0.39 mm yr^{-1} to ca. 2 mm yr^{-1}), thus causing an increase in the accommodation space (Plater et al., 1993; Woodworth et al., 1999; PSMSL, 2019). The salt marsh is covered predominantly by *Puccinellia maritima* and *Spartina townsendii*; the latest was planted in 1932 to aid the accretion of the marsh to favour land reclamation for agricultural purposes (van der Wal et al., 2002). Hesketh Out Marsh was reclaimed in 1980 and, between 2007 and 2017, a two-phase scheme was implemented to restore the intertidal habitat, to enhance the protection of coastal infrastructures against flooding (Tovey et al., 2009).

6.5 Methods

6.5.1 Sampling strategy

To analyse the changes in bleaching potential in relation to salt marsh evolution and modes of deposition, Hesketh Out Marsh was cored using a percussion corer with a gouge 1 m long and 7.5 cm in diameter (Chapter 3). Two replicate cores 3.2 m long (HOM19-1 and HOM19-2) were extracted from the middle salt marsh next to one another at ~ +3.5 m OD (Figure 40 c). The middle salt marsh location provided a stratigraphic record from the formation of the sandflat through to a mature salt marsh, which was characterised by an accumulation rate spanning from 4.61 cm yr^{-1} in the sandflat to 0.83 cm yr^{-1} in the mature marsh. Core HOM19-1 was extracted in the sunlight and used for the analysis of the geochemical composition, organic content and particle size distribution. Core HOM19-2 was extracted into opaque sleeves to prevent sunlight contamination prior to luminescence analysis. Stratigraphic analysis showed that both cores contained similar stratigraphic patterns and were therefore comparable (Figure 40 d).

To assess whether luminescence properties could be used to diagnose the presence or absence (i.e. fair-weather conditions) of storm deposition across intertidal wetlands, modern analogues (Figure 40 c) were collected from the mudflat (~ +3 m OD) and lower salt marsh (~ +3.2 m OD) approximately one month before (HOM21-1 and HOM21-2) and after (HOM22-1 and HOM22-2) a storm event (Storm Barra as defined by the UK Met Office and Met Éireann). The storm hit the coast of North West England from 7th to 8th December 2021, during the transition from spring to neap tide, with wind gusts between 93 and 111 km h^{-1} in west-to-east direction (UK Met Office, 2021) that generated a storm surge of 0.5-0.9 m (BODC, 2021). The lower salt marsh and mudflat were chosen as the most suitable sampling locations based on the bleaching profile provided by the IRSL analysis performed on the core HOM19-2 (Figure 41 f). Each sample was combined from three superficial sub-samples (0.5-1.5 cm depths below the surface) collected using opaque tubes (10 cm in diameter) from 50 cm apart from each other to capture some of the spatial variability that could characterise this setting. Previous observations have shown that an ~ 1 m storm surge (comparable to the 0.5-0.9 m surge of Storm Barra) re-worked sediment down to ~ 15 cm below the mudflat surface in an unvegetated surface (de Vet et al., 2020); thus, the sampled sediment at 0.5-1.5 cm depths would avoid contamination from surface material that would have been exposed to sunlight since deposition while still preserving the signature of the storm activity.

All cores and samples are named according to the coring/sampling location (i.e., Hesketh Out Marsh) and year of the relative field campaign (i.e., 2019, 2021 and 2022).

6.5.2 Characterising different depositional environments

To characterise the geochemical composition and modes of deposition typical of each type of depositional environment (i.e., sandflat, mudflat or salt marsh), geochemical and particle size distribution (PSD) analyses were performed on core HOM19-1 in Chapter 3. Identical geochemical and PSD analyses were then performed on the modern analogues (both pre- and post- storms) in this study for comparison to core HOM19-1. A PSD model (Rahman and Plater, 2014) was used to infer whether sediment deposition was driven by accretion due to sea-level rise or infilling. Fine-skewed to near-symmetrical distributions characterised by well-sorted, sand-sized sediment are typical of traction load delivered by the fast tidal flow velocities (i.e., during the flood phase) and are attributable to infilling. Near-symmetrical distributions characterised by fine to very fine, poorly sorted silts are typical of the suspension load that settles during the turn of the tide (i.e., during the ebb phase) and is attributable to gradual accretion. Sandflats have low elevation and are flooded during high tide and so sediment deposition occurs through infilling as a result of the delivery of traction load during the flood phase. Salt marshes have high elevation; therefore, sediment deposition occurs as a result of the settling of suspension load during the turn of the tide. Mudflats are transitional environments characterised by a combination of the two processes. Principal component analysis (PCA) was performed using PAST3 (Hammer, 2019) using the correlation matrix to explore the geochemical compositions of the samples and to assess any association between the salt marsh core and the pre- and post- storm samples. The parameters selected for this PCA were: coarse mineral indicators (Si (mg/g), Zr (µg/g)), salt water (Na (mg/g)) and shell content indicators (Ca (mg/g), Sr (µg/g)), organic content indicators (LOI (%), S (mg/g), Br (µg/g)), silt/clay mineral indicators (K (mg/g), Al (mg/g), Ti (µg/g), Rb (µg/g), Nb (µg/g)), post-depositional diagenesis indicators (Fe (mg/g), Mn (µg/g)), pollutants (Mg (mg/g), P (mg/g), As (µg/g), Pb (µg/g), Zn (µg/g), Ni (µg/g), Cu (µg/g), V (µg/g), Cr (µg/g), Ga (µg/g), Ge (µg/g), Ba (µg/g), I (µg/g)) and the rare elements (Y (µg/g), La (µg/g), Ce (µg/g)) (Boyle, 2000; Plater et al., 2000).

To provide a robust evolutionary profile for the salt marsh platform alongside the depth profile of the PSDs, the PSD-derived median particle-size (D50), and the chosen geochemical elements (Si/Al as sand indictor, Ca/K as shell indicator, Rb as fine mineral matter indicator and loss-on-ignition (LOI) as organic content indicator), Chapter 3 also derived a long-term accretion rate of the marsh platform from core HOM19-2 using luminescence dating of quartz. For further details on the conduction of these analyses see Chapter 3.

6.5.3 Luminescence properties

Luminescence analyses were performed on sand-sized grains of K-feldspar extracted from the 12 core samples (HOM19-2) and the four modern analogue samples (HOM21-1/2 and HOM22-1/2). Each of the visible changes in core stratigraphy were sampled to capture the changing intertidal settings. At least 50 mm of the outer portion of each core sample was removed to prevent sunlight contamination. For the analysis of the modern analogues, three sub-samples per sample were extracted and combined for analysis, each from 0.5-1.5 cm depths below the surface to avoid contamination from surface material that would have been exposed to sunlight since deposition, but close enough to the surface to still allow the signature of storm activity to be recorded. The degree of bleaching of the K-feldspar grains discussed here is intended as the cumulative product of pre-, during and post- depositional bleaching.

To isolate the coarse feldspar grains for equivalent dose (D_e) measurement, all samples were treated with a 10% (v/v) dilution of 37% HCl to dissolve carbonates and with a 10% (v/v) dilution of H_2O_2 to remove organic content. Dry sieving was used to extract grains 90-150 µm in diameter for samples HOM19-2-2 and HOM19-2-4 and 90-125 µm for the rest of the samples. Density separation using sodium polytungstate was performed to isolate the K-feldspar fraction. However, no coarse-grained K-feldspar was recovered for sample HOM19-2-1 (top of the core) and so no analyses could be performed on this sample.

Grains were mounted as 2 mm-diameter multiple-grain aliquots on to 9.8 mm-diameter aluminium discs for analysis. The luminescence measurements were made using an automated Risø TL/OSL DA-15 reader equipped with a $^{90}Sr/^{90}Y$ source (Bøtter-Jensen et al., 2003). Infra-red (IR) light emitting diodes (LEDs) were used to stimulate the K-feldspar grains and the luminescence signals were detected in blue wavelengths using 2-mm thick Schott BG39 and Corning 7-59 filters. A single aliquot regeneration dose (SAR) protocol was used for determining D_e values, where the IRSL signal was recorded using a multiple-elevated post-IR IRSL protocol at 50°C (termed the IR_{50}), 150°C (termed the $pIRIR_{150}$) and 225°C (termed the $pIRIR_{225}$) (Wallinga et al., 2000; Thomsen et al., 2008; Li and Li, 2011). Stimulation was for a total of 100 s, where the initial and background signals were summed for the first 3 s and final 40 s, respectively. Individual aliquots were screened for reliability of D_e determination based on the following screening criteria (considering the associated uncertainties): the test dose response was >3 ʃ above the background; the test dose uncertainty was <20%; the recycling ratio was ±20%; and recuperation was <5% of the response from the largest regenerative dose (7-8 Gy). Dose-recovery experiments performed on sample HOM19-2-6 using IR_{50} (ratio of 0.89 ± 0.00), $pIRIR_{150}$ (ratio of 0.91 ± 0.00) and $pIRIR_{225}$ (0.91 ± 0.03) signals showed that the measurement protocol was appropriate for luminescence analysis. Consequently, the central age model (CAM; Galbraith et al., 1999) was calculated from D_e distributions (Figure S13, S14 and S15) determined for each sample to give an indication of the bleaching potential prior to burial. D_e is measured in Gy (J kg^{-1}).

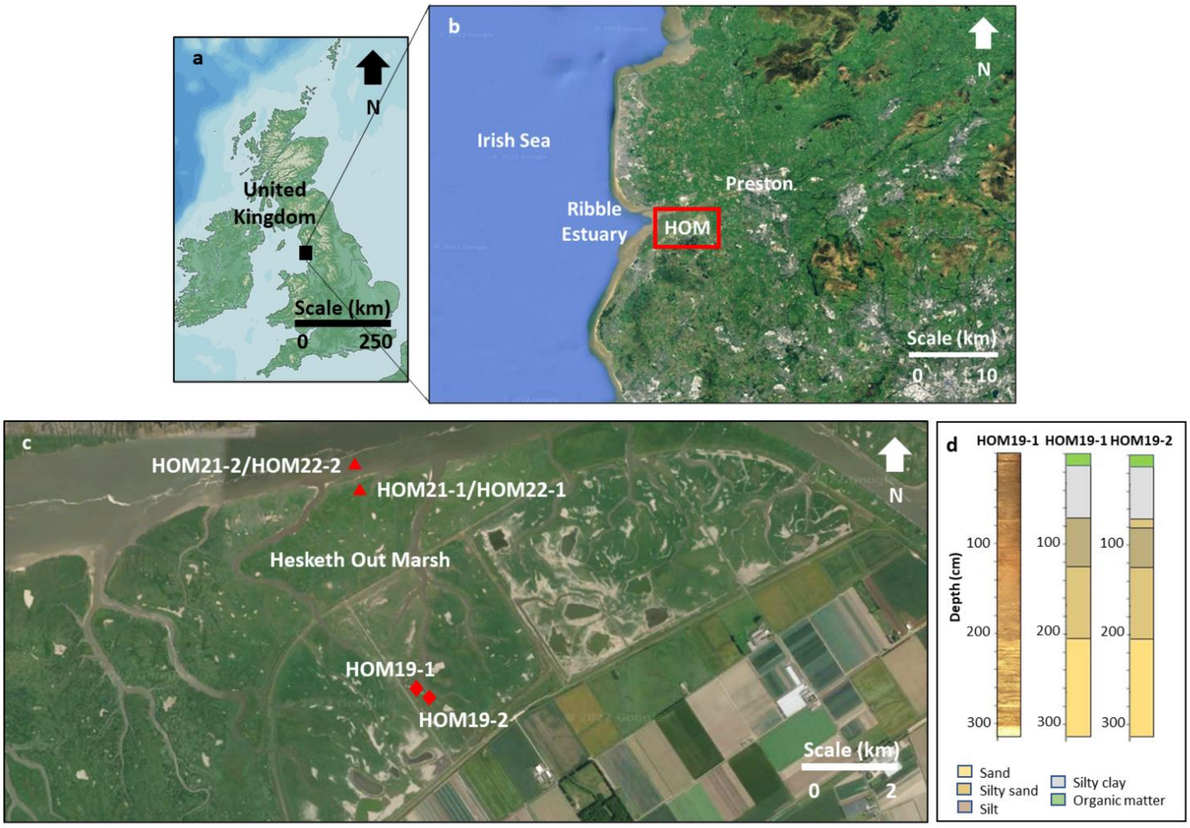

Figure 40. Location of the Ribble Estuary (a); location of Hesketh Out Marsh (HOM) (b) (© Google Earth Pro, 2022); location of the cores HOM19-1 and HOM19-2 and the modern analogues collected before (HOM21-1 and HOM21-2) and after (HOM22-1 and HOM22-2) the storm event (c) (© Google Earth Pro, 2022); photographic analysis of the core HOM19-1 and stratigraphic analysis of the cores HOM19-1 and HOM19-2 (d).

6.6 Results

6.6.1 Luminescence properties of intertidal settings

The luminescence properties reflect the extent of sediment processing characterising each intertidal setting before sediment deposition. Overall, the multi-proxy analysis (Figure 41; Chapter 3) shows that a sandflat environment dominates the lower part of the core up to 150 cm, while a transition from sandflat to mudflat occurs between 150 cm and 70 cm, followed by the mudflat gradually transitioning into a fully vegetated salt marsh. This is revealed by the Si/Al and Ca/K concentrations (indicators of shell and sand content, respectively, Figure 41 b) as well as the median particle-size (D_{50}, Figure 41 c), which are constant up to 100 cm, but decrease slightly up to 75 cm, before remaining constant to the top of the core. Also, the Rb concentrations (an indicator of fine mineral concentration) are constant up to 120 cm, but then decrease to the top of the core (Figure 41 b). Finally, loss on ignition (LOI) (an indicator of organic content concentration) is constant up to 100 cm, but then increases to the top of the core (Figure 41 b). Furthermore, the luminescence-derived accretion rates (from quartz; Chapter 3) show that up to 120 cm, the sequence experienced more rapid accretion (4.61 cm yr^{-1}) than the slower accretion (0.83 cm yr^{-1}) from 120 cm to the top of the core (Figure 41 a).

End-member analysis of the particle size distributions (PSDs) (Chapter 3) showed that 86% of the variance present in core HOM19-1 could be explained by four PSD end-members (EM1, EM2, EM3 and EM4; Figure 41 d), each in different proportions within different samples from the core (Figure 41 e). These end-members represent the recurring modes detected in the PSDs: EM1 has a mixed near-symmetrical distribution dominated by clay to silt with a secondary very fine to fine sand mode; EM2 has a fine-skewed to near-symmetrical distribution dominantly very fine to fine sand; EM3 has a bimodal distribution with near-symmetrical clay to silt mode and near-symmetrical to fine skewed very fine to fine sand mode; and EM4 has a fine-skewed to near-symmetrical distribution of fine to coarse sand.

The PSD data empirically confirms that in the sandflat (300-150 cm depths) sediment deposition was mainly characterised by infilling of sand-sized particles through load traction (Figure 41 e). Here, the luminescence properties of all three luminescence signals (i.e., the D_e values) were constant (Figure 41 f), where the D_e density distributions (representative of the degree of bleaching of the mineral grains) were symmetrical (i.e., well-bleached grains) (Figure S13). As the sandflat progressed into a mudflat (150-70 cm depths), the sediment deposition was progressively dominated by more accretion through particle settling (Figure 41 e). Here, the luminescence properties increased (120-70 cm depths; Figure 41 f), where the D_e distributions were symmetrical for the IR_{50} signal but were near-symmetrical (i.e., well-bleached grains co-existing with poorly bleached grains) for the $pIRIR_{150}$ and $pIRIR_{225}$ signals (Figure S13); thus, indicating a reduction in bleaching potential prior to burial of the sediment compared to the sandflat. Lastly, as the mudflat progressed into a salt marsh (70-0 cm depths), the sediment deposition was dominated by the settling of silt-sized particles (Figure 41 e). Here, the luminescence properties showed an increase first, followed by a non-linear decrease (Figure 41 f), suggesting an initial further decrease in the bleaching potential of the sediment followed by an increase once again. The D_e distributions were near-symmetrical (for the IR_{50} and $pIRIR_{150}$ signals) and symmetrical (for the $pIRIR_{225}$); however, the symmetrical nature of the $pIRIR_{225}$ may be due to the relatively smaller population for this signal.

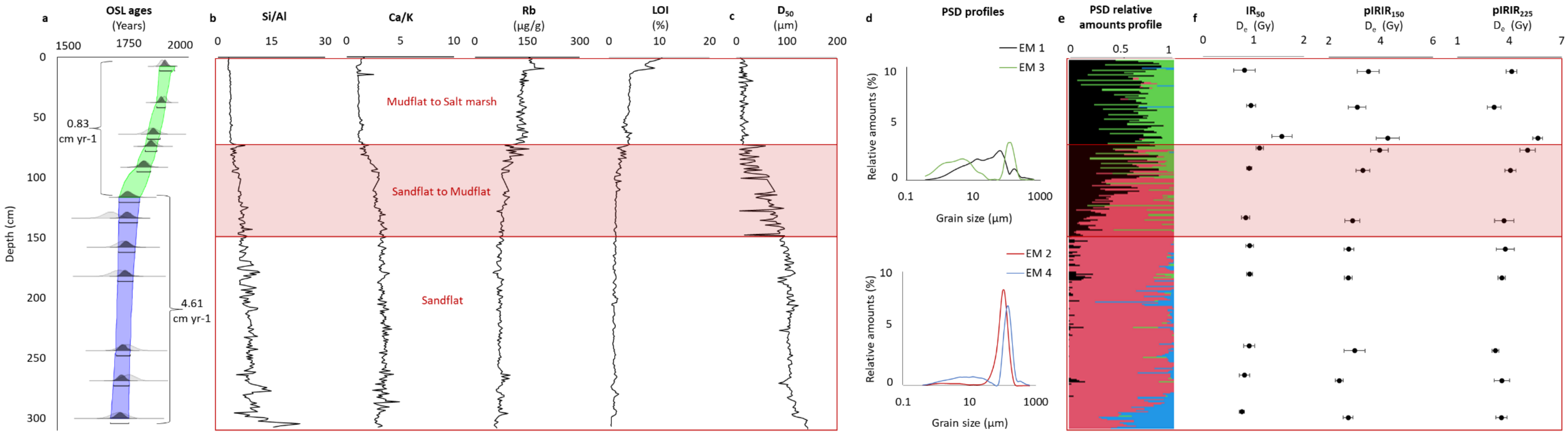

Figure 41. Depth profile (core HOM19-2) of OSL ages with derived accretion rates (a); depth profile (core HOM19-1) of geochemical proxies (Si/Al, Ca/K, Rb) and organic content (LOI) (b); depth profile (core HOM19-1) of median particle-size (D50) (c); EMMA-derived PSD profiles (d) and depth profile (core HOM19-1) of the PSD relative amounts (e); depth profile (core HOM19-2) of D_e *(equivalent dose measured in Gy (J* kg^{-1}*)) values calculated for* IR_{50}, $pIRIR_{150}$ *and* $pIRIR_{225}$ *signals (f).*

6.6.2 Luminescence properties of pre- and post-storm deposits

Figure 42 shows the first two components of the PCA performed on the geochemical properties of the salt marsh and mudflat samples. Component 1 and component 2 summarise 76.9% of the variance in the data, respectively 66.4% and 10.5%. Based on correlation, the PCA analysis shows that the pre- and post-storm samples form a single cluster (i.e., the geochemical composition of the pre-storm sediments is statistically indistinguishable from the composition of the post-storm sediment), and that the composition of the modern samples differs from that of the core largely due to the absence of historical heavy metal pollution post-depositional diagenesis.

Overall, Figure 43 shows that the luminescence properties of the sediments collected post-storm were different to those collected pre-storm, likely reflecting the greater extent of sediment processing that occurs during a storm and agree with the trends observed in the down-core profile.

For the salt marsh sample, there is a small change in the shape of the PSD profile after the storm surge (Figure 43 a). Before the storm, the salt marsh sample exhibits a near-symmetrical distribution characterised by fine to very fine silts but with a wider range than the post-storm sample, which exhibits fine-skewed to near-symmetrical distribution. For all three luminescence signals, the D_e values of the salt marsh sample collected before the storm and after the storm are all statistically indistinguishable, i.e. mean D_e values and relative uncertainties of the two samples overlap for all signals. The D_e density distributions for the pre- and post-storm salt marsh samples do not differ significantly as they are predominantly symmetrical to near-symmetrical in both cases (Figure S14).

For the mudflat sample, both the pre- and post-storm PSD profiles exhibit very similar fine-skewed to near-symmetrical distributions characterised by coarse to fine silts, with the post-storm PSD profile only showing slightly higher kurtosis (Figure 43 a). Interestingly, the post-storm PSD profile for the mudflat was very similar to the salt marsh, demonstrating that the mudflat and salt marsh experienced the same depositional dynamics from the storm. There was little difference in the IR_{50} signal before and after the storm on the mudflat as the D_e value of the post-storm sample was slightly higher than the pre-storm sample but overlapped within uncertainties. In contrast, the D_e values of the post-storm samples were lower than the D_e values of the pre-storm samples for both the $pIRIR_{150}$ and $pIRIR_{225}$ signals. This suggests that sediments in a mudflat setting experience more bleaching from sediment processing during a storm surge than during fair weather conditions, which is not recorded on the lower salt marsh. The mudflat samples had symmetrical to near-symmetrical D_e density distributions in both cases, however, the post-storm distributions become wider in for all three signals, suggesting that a small proportion of grains with larger D_e distribution was incorporated into the sediment post-storm, in addition to the overall reduction in CAM D_e value.

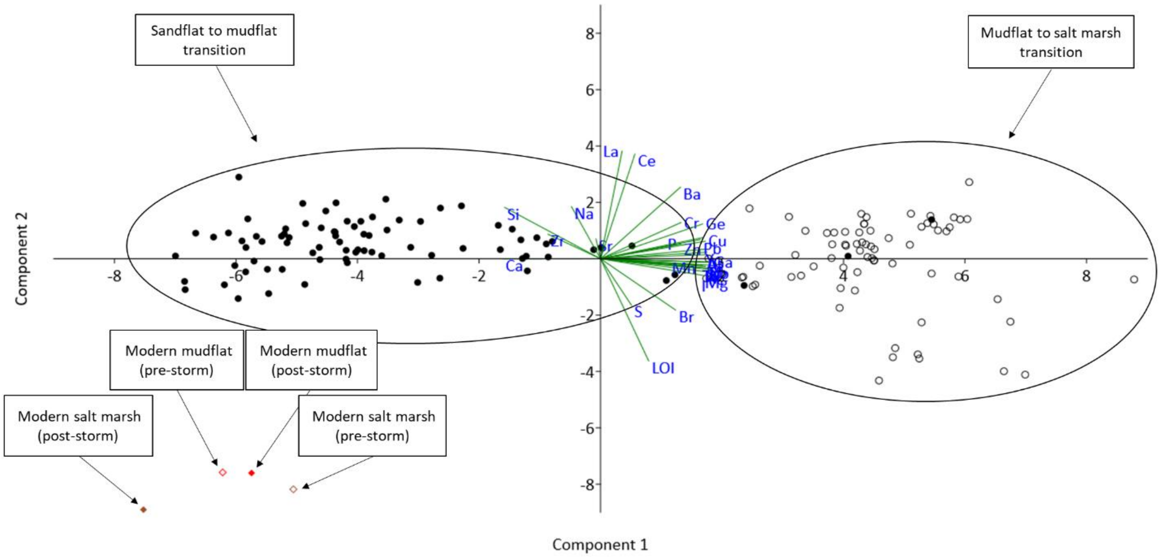

Figure 42. PCA performed on the salt marsh and mudflat modern analogues collected before (HOM21-1/2) and after (HOM22-1/2) the storm and the core (HOM19-1) intervals showing sandflat-to-mudflat (150–70 cm depths) and mudflat-to-salt marsh (70–0 cm) transitions. Component 1 and component 2 summarise 76.9 % of the variance in the data, respectively 66.4 % and 10.5 %. The figure shows the parameters used by each component to separate the samples. The modern mudflat and salt marsh deposits differ from their paleo counterparts due to lower concentrations of heavy metals.

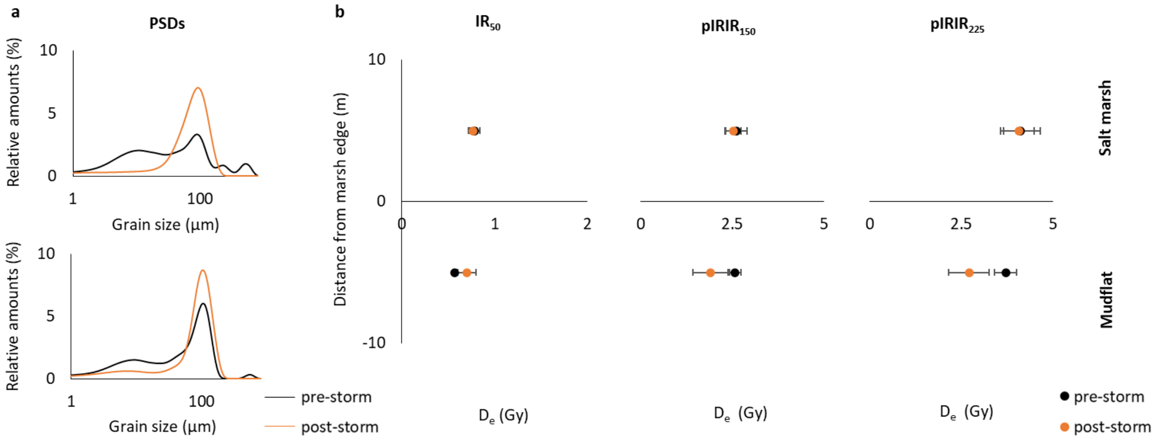

Figure 43. EMMA-derived PSD profiles (a) and D_e (equivalent dose measured in Gy (J kg^{-1})) values relative to the IR_{50}, $pIRIR_{150}$ and $pIRIR_{225}$ signals (b) for the salt marsh and mudflat modern analogues collected before (HOM21-1/2) and after (HOM22-1/2) the storm.

6.7 Discussion

6.7.1 Sediment processing in intertidal settings

Luminescence properties were used to diagnose the changes in sediment processing characteristic of different intertidal settings (sandflat, mudflat, salt marsh) based on the bleaching potential of the feldspar grains present in intertidal sediments (Reimann et al., 2015). In the sandflat environment (300-120 cm; Figure 41 b, c), the luminescence properties (i.e., the D_e values calculated for the IR_{50}, $pIRIR_{150}$ and $pIRIR_{225}$ signals) were constant (Figure 41 f) and the average accretion rate was higher than the upper sequence (4.61 cm yr^{-1}; Figure 41 a). With the transition from the sandflat into a mudflat (120-70 cm depths; Figure 41 b, c), the average accretion rate decreased (0.83 cm yr^{-1}; Figure 41 a) and the luminescence properties showed progressive increases in D_e values (Figure 41 f). Between 70 cm and the top of the core, where the well-established mudflat transitions into the fully-vegetated salt marsh (Figure 41 b, c) (Plater et al., 2007), the average accretion rate was maintained (0.83 cm yr^{-1}; Figure 41

a) and the luminescence properties showed an initial further increase followed by progressive decreases in D_e values similar to the sandflat (Figure 41 f).

The luminescence properties showed that the bleaching potential was high in the sandflat, where the extent of sediment processing is large. It then decreased with the formation of a mudflat and transition into a vegetated salt marsh environment but increased again with the transition into a mature marsh, where sediments are directly exposed to sunlight for long periods of time. These changes in the bleaching potential of the sediments were also reflected in the D_e density distributions (Figure S13), which were representative of the degree of bleaching of the mineral grains. The D_e distributions for all three signals for the sandflat were symmetrical, indicating well-bleached grains. The D_e distribution for the IR_{50} signal for the mudflat was symmetrical but bimodal, and near-symmetrical for the $pIRIR_{150}$ and $pIRIR_{225}$ signals, suggesting poorer bleaching of the grains. Finally, in the salt marsh, the D_e distributions were near-symmetrical to symmetrical again for all three signals, indicating that the grains were again better bleached (Wallinga, 2002a).

PSD analysis of the core (Figure 41 d, e) shows that from 300-150 cm, the two dominant modes (EM4 and EM2) exhibit fine-skewed to near-symmetrical distributions characterised by well-sorted sand-sized sediment. Sandflats have an elevation low enough to allow the platform to be permanently flooded and experience the fastest tidal currents (Reed, 1990); hence, sediment deposition occurs through infilling resulting from the delivery of traction load by the fast tidal flow velocities during the flood phase (Rahman and Plater, 2014). When the sandflats evolve into mudflats, the elevation of the platform increases, and they start experiencing slower tidal currents (Reed, 1990). Therefore, deposition gradually progresses from being dominated by infilling of sand-sized sediment to being dominated by silt-sized particles that are transported by the fast tidal flow velocities during the flood phase and deposited through settling during the turn of the tide (Rahman and Plater, 2014). This is reflected in the down-core PSDs profile, which shows that at 150 cm EM4 (fine-skewed to near-symmetrical distribution of fine to coarse sand) is replaced by EM1 (mixed near-symmetrical distribution dominated by clay to silt with a secondary very fine to fine sand mode), and the mode of deposition becomes dictated by EM2 (fine-skewed to near-symmetrical distribution dominantly very fine to fine sand) and EM1, with EM1 becoming more influential towards the top of the section.

Salt marsh platforms have higher elevation with respect to mudflats where the frequency and duration of inundation depend on the level of maturity of the salt marsh platform and distance from the marsh edge (van Proosdij et al., 2006), with mature marshes being inundated only a few times a year due to very high spring tides or storm surges (Roberts and Plater, 2005). Hence, sediment deposition occurs mainly from the settling of the suspension load during the turn of the tide (Rahman and Plater, 2014). This is reflected in the down-core PSDs profile, which shows the mode of deposition being dictated by EM3 (bimodal distribution with near-symmetrical clay to silt mode and near-symmetrical to fine skewed very fine to fine sand mode) and EM1 (mixed near-symmetrical distribution dominated by clay to silt with a secondary very fine to fine sand mode), both characterised by a near-symmetrical clay to silt mode, representative of the sediment settling, and near-symmetrical to fine skewed, very fine to fine sand mode, representative of the infilling events.

The bleaching potential of K-feldspar grains depends on the duration and intensity of sunlight exposure (Godfrey-Smith et al., 1988). In turbulent water columns, this can be affected by the degree of sediment processing in the water column during deposition (Wallinga, 2002b). This suggests that the different elevations and modes of deposition characteristic of each type of intertidal environment (sandflat, mudflat and salt marsh) are responsible for the different degrees of bleaching of the K-feldspar grains. Figure 44 shows a schematic of how the bleaching potential of intertidal sediments varies with the evolution of the intertidal substrate in proportion to the hydroperiod, the waves and tidal currents induced shear stress, and the duration of sunlight exposure during the period of sub-aerial exposure. The duration and frequency of flooding on the intertidal platform (i.e., hydroperiod) and the sheer stress magnitude are higher for a sandflat with low elevation, and they decrease with the increase in elevation of the platform (Roberts and Plater, 2005; Zhang et al., 2019), up to a point when a mature marsh forms, which is inundated only a few times a year by very high spring tides or storm surges (Pethick, 1981). Direct exposure to sunlight during the period of sub-aerial exposure conversely increases with an increase in elevation of the intertidal platform as it reaches its maximum when the hydroperiod and shear stress are at their minimum.

In the sandflat, where the magnitude of the hydroperiod and the shear stress is high (Zhang et al., 2019), the traction load deposited on the platform can be re-entrained and resuspended within the water column for multiple tidal cycles before being buried by new sediment. This continuous re-entrainment allows sediments to be exposed to sunlight for a period of time long enough for the luminescence signal to reset to zero, and it is recycled several times on a series of tides (Wallinga, 2002b). When the sandflat progresses into a mudflat and the platform elevation increases, the hydroperiod and shear stress decrease (Zhang et al., 2019), which causes less re-entrainment and resuspension of the traction load and reduces the recycling of sediment on each tide. Moreover, as the mudflat increases in elevation, the suspension load that settles during the turn of the tide progressively replaces the traction load transported by the flood tide. This causes less opportunity for the sediment to be re-entrained and re-suspended by the fast tidal currents before being buried by new sediments, leading to less sunlight exposure, and therefore less potential for the luminescence signal to have been well bleached prior to burial (Wallinga, 2002b). Turbidity caused by mud in suspension can further promote partial bleaching of the luminescence signals by attenuating the blue wavelengths of the daylight spectrum, inhibiting the bleaching of the grains (Berger, 1990).

As the mudflat progresses into a lower salt marsh, the influence of the hydrodynamics on the resetting of the luminescence signal becomes minimal, as the presence of vegetation attenuates the resuspension caused by waves and currents (Neumeier and Ciavola, 2004; Mudd et al., 2010; Yang et al., 2012), and the sediments are mainly deposited during the turn of the tide, thus causing a further decrease in bleaching potential. Finally, on the mature salt marsh, where there is no inundation and sediments are continuously exposed to sunlight, grains reach their maximum bleaching potential (Godfrey-Smith et al., 1988). Overall, the long-term analysis suggests that luminescence properties can detect the different sedimentation modes balanced across the bleaching potential and sediment processing potential typical of each intertidal setting.

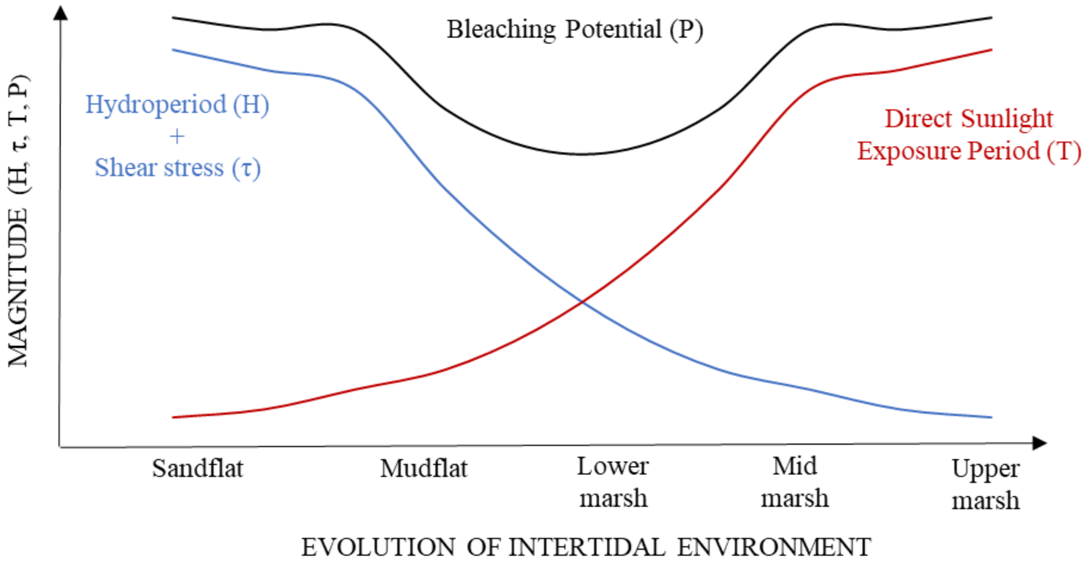

Figure 44. Schematic of variation in bleaching potential of intertidal sediments (P) in relation to the evolution of the intertidal environment, hydroperiod (H), wave and tidal current induced shear stress (τ), and period of direct exposure to sunlight after deposition (T).

6.7.2 Sediment processing during storm events

The luminescence properties of the down-core profile show that the mudflat and lower salt marsh are the environments with the lowest bleaching potential (Figure 41 f). Therefore, since storms are responsible for longer inundation and higher potential sediment resuspension compared to ordinary conditions (Chapter 4 and Appendix II), mudflat and lower salt marsh (where topography and vegetation allow deposition) sediments are expected to be the most likely to show an increase in bleaching during stormy conditions (Brill et al., 2018). Hence, they have been selected in this study as locations for the sampling of the modern analogues (Figure 40 c). Both mudflat and salt marsh sediments show no significant difference in the geochemical composition (Figure 42) and a slight variability in the gross depositional energy (Figure 43 a) between the pre- and post- storm samples, providing a weak inference of the storm event from the lower salt marsh but none from the mudflat.

The storm occurred during spring tide and caused a surge of 0.5-0.9 m (BODC, 2021). During spring high tide, the water depth above the lower marsh platform at Hesketh Out Marsh can reach up to 3 m in fair-weather conditions and a surge of 0.5 m can cause an increase in the depth of the water level of 0.5 m (Appendix II). This suggests that the storm-enhanced inundation of the salt marsh caused an increase in the extreme water level by at least 0.5 m, potentially reaching up to at least 3.5 m during high tide. Furthermore, the surge peak occurred towards the lower end of the tide, coinciding with the rising flood tide, thus promoting the most optimal conditions for sediment re-entraining and recycling (Chapter 4). Despite that, the luminescence properties of the salt marsh sample collected before and after the storm were indistinguishable (Figure 43 b; Figure S14), suggesting that the storm surge did not cause any significant change in the bleaching potential of the lower marsh sediment. The long-term multi-proxy analyses showed that the lower salt marsh was suitable for detecting a possible increase in the resetting of the luminescence signal caused by a storm surge (Brill et al., 2018), due to its low natural bleaching potential. However, it must be considered that vegetation causes a reduction in the turbulent kinetic energy of the water flow, causing a considerable reduction in shear stresses produced by the combined action of waves and currents, therefore reducing the potential for sediment re-suspension (Neumeier and Ciavola, 2004; Mudd et al., 2010; Yang et al., 2012; Temmerman et al., 2022). This might have prevented sediment re-entrainment and recycling during the inundation of the lower marsh and inhibited the bleaching of the grains.

For the mudflat, there was a difference between the sediments collected before and after the storm surge for the higher temperature signals (pIRIR$_{150}$ and pIRIR$_{225}$ signals), but not for the IR$_{50}$ signal (Figure 43 b). The IR$_{50}$ signal bleaching rate is on the order of seconds to minutes (Godfrey-Smith et al. 1988), while the pIRIR$_{150}$ and pIRIR$_{225}$ signals can take up to hours to completely reset according to laboratory measurements (e.g., Smedley et al. 2015; Colarossi et al. 2015). This suggests that the IR$_{50}$ signal is likely to reset completely even if sediments do not spend a long period in suspension within the water column (Brill et al., 2018), whereas the pIRIR$_{150}$ and pIRIR$_{225}$ signals are more likely to show partial resetting if sediments are not exposed to sunlight for a sufficient duration of time (Reimann et al., 2015). As such, the IR$_{50}$ signal is likely to reset in both ordinary and stormy conditions, while the pIRIR$_{150}$ and pIRIR$_{225}$ signals are likely to bleach faster in stormy conditions when sediments are resuspended in the water column for longer or transported for longer distances. The pIRIR$_{150}$ and pIRIR$_{225}$ signals are therefore likely to be more reliable in diagnosing changes in the bleaching potential of the grains with respect to the IR$_{50}$ signal. The change in bleaching potential characterising the mudflat after the storm event is also evident in the D$_e$ density distributions of single aliquots (Figure S14), which shows a widening of the distributions for all three signals. The overall reduction in D$_e$ values suggests that autochthonous sediments could have bleached better in stormy conditions because the longer inundation maintained them in re-suspension longer than in fair-weather conditions, or that allochthonous well-bleached sediments were transported onto the mudflat platform while they were maintained in suspension within the water column (Brill et al., 2018). The small proportion of grains with larger D_e density distributions could have come from sediments unlikely to have been exposed to sunlight where the enhanced mud re-suspension caused by the storm is likely to have enhanced turbidity, potentially preventing the exposure to sunlight (i.e. bleaching) of those grains (Berger, 1990). Regardless of the provenance and/or composition of the well-bleached sediment (i.e., autochthonous, or allochthonous), the D_e distributions are able to detect the increase in bleaching rate caused by the storm.

Overall, the modern analogues have shown that the samples collected after the storm event on the mudflat were characterised by no significant change in sediment composition, but the post-storm sediments exhibited higher bleaching potential than the pre-storm samples, which suggests a greater extent of sediment processing; thus, luminescence could be used to diagnose the storm deposition on the mudflat where the sediment composition could not. In contrast, there was no difference in the bleaching potential pre- and post-storm on the lower salt marsh.

6.7.3 Implications

There is evidence that increasing rates of sea-level rise can threaten salt marsh survival (FitzGerald et al., 2008; Kirwan et al., 2010; Ganju et al., 2017; Fagherazzi et al., 2020), while storm-sedimentation can support salt marsh resilience to sea-level rise (Mariotti and Fagherazzi, 2010; Schuerch et al., 2013; Chapter 4). To provide effective management of these natural coastal defences and ecosystems, it is essential to quantify the contribution of sea level and storm activity to long-term marsh accretion and survival (Walters and Kirwan, 2016) and to derive long-term records of storm frequency that can contextualise the changes observed by recent climate change (McCloskey and Liu, 2012; Bianchette et al., 2022). Traditional techniques used to detect sedimentary records of storm activity (i.e., geochemical and particle size analysis) in mudflat settings cannot detect storm-driven changes in hydrodynamics when no change in sediment composition has occurred, as recorded during Storm Barra. Therefore, longer-term sediment grain size and geochemical composition records cannot readily provide accurate records of the frequency of storm activity. The new luminescence approach shown here can reveal (and date) changes in the extent of sediment processing (e.g., storm activity) where there is no obvious stratigraphic evidence of such that could be revealed by the existing techniques (e.g., the sediment composition). Applying this luminescence approach, and associated dating, to established sedimentary archives of coastal change in estuary and deltaic depositional contexts (e.g., Yangtze Estuary, Rhine-Meuse lowlands) would therefore more accurately constrain the contribution and significance of storms in moderating coastal change over the long term, e.g. during periods of sea-level rise throughout the last interglacial and the Holocene. This has far-reaching consequences for projecting future coastal response to sea-level rise and changes in storm activity by providing an improved assessment of the resilience of populated coastal lowlands to climate change.

6.8 Conclusions

To conclude, this study has shown how luminescence properties can be used to diagnose the differential modes of deposition across intertidal settings, and therefore the presence of storm activity in the longer-term sediment records where no changes in sediment composition occurred. The luminescence signals of K-feldspars measured at different temperatures (50, 150 and 225 °C) reset at inherently different rates and so were used to assess the extent of sediment processing (i.e., the bleaching potential) in an environment during deposition. Analysis of a long-term, multi-proxy evolutionary model of the marsh platform showed that the luminescence properties of mineral grains can be used to diagnose changes in sedimentation modes characteristic of the different intertidal settings (sandflat, mudflat and salt marsh) by detecting the variability in sediment bleaching potential between settings (i.e., sediment exposure to sunlight), thus establishing a framework for the interpretation of luminescence properties of intertidal sediments. Modern analogue samples showed that post-storm sediments exhibited higher bleaching potential detectable by the $pIRIR_{150}$ and $pIRIR_{225}$ signals (i.e., more sediment processing) on the mudflat prior to burial in comparison to the pre-storm samples, despite no significant change in sediment composition being recorded by the geochemical and particle size distribution analyses. This new luminescence approach is more sensitive than existing techniques at detecting the intertidal response to sea level and/or storms, and so can accurately identify periods of change that were previously undetectable in apparently monotonous minerogenic sequences. This offers the potential to revise established sedimentary archives of coastal change and determine with more accuracy the significance of storms in controlling coastal change over the longer-term during climate warming, e.g. the Holocene and the last interglacial.

6.9 Acknowledgements

We acknowledge support from the School of Environmental Sciences, University of Liverpool, which is funding the PhD project of the first author, the EPSRC support to Prof. Nicoletta Leonardi (EP/V056042/1) and the RGS-IBG for funding part of the field campaign (project title: Building coastal resilience one sediment grain at the time: field measurements and community engagement on nature-based solutions for coastal protection, PI Prof. Nicoletta Leonardi). We also acknowledge the support of the RSPB for allowing the fieldwork campaign in the Ribble Estuary and the Physical Geography and luminescence laboratories and their technicians and students (Jennifer Bradley, Luke Glascott, Mike O’Connor, Richard Clark, Grace Skirrow and Molly Spater) for their support with equipment, fieldwork and laboratory analyses.

6.10 Data availability

Data related to this article can be found in the following repository: https://doi.org/10.5281/zenodo.7378526.

Chapter 7

Conclusions

7.1 Project summary

Salt marsh survival largely depends on the equilibrium between sea-level variations and sediment availability, but the amount of sediments that can reach salt marsh platforms depend on sediment transport dynamics, which can be influenced by anthropogenic and climate forcings. With an accelerating rate of sea-level rise, changes in storm activity and increasing land reclamation, it is not clear whether salt marshes will be able to retain their resilience. Firstly, although there is evidence that embankments can affect tidal propagation, hence sediment transport, their impact on marine sediment supply to salt marsh platforms is still very poorly understood. Secondly, there are still large uncertainties on the impact that the combined action of future sea-level rise and increase in storm intensity will have on salt marsh resilience, and on the extent to which storms enhance salt marsh accretion and expansion, despite the individual impacts of storms and sea-level have been widely investigated. Ultimately, while long-term human activity and sea-level records derived from well-established proxies are available from around the globe to study, there are still inconsistencies in long-term storm activity records, as traditional paleoenvironmental techniques rely on abrupt changes in stratigraphy and composition for the reconstruction of extreme events, which do not always occur during storm activity; hence, the impact of storm frequency on salt marsh survival is still difficult to predict. To address these knowledge gaps, this study aimed to:

i) better understand salt marsh resilience to changes in climate forcings and sea defences implementation, by

O1. investigating the effects of embankment construction on long-term salt marsh accretion,

O2. exploring estuarine and salt marsh response to the combined impact of sea-level rise and increased storm intensity, O3. quantifying storm sediment contribution to different areas of marsh platforms and determining the sediment sources that storms draw on;

ii) develop a new luminescence-based approach for the detection of storm activity across intertidal environments which is stratigraphy and sediment composition independent, by

O1. testing whether luminescence signals can diagnose differential modes of deposition across intertidal settings,

O2. testing whether these signals can detect storm activity across intertidal environments that remain undetectable with existing techniques that depend on sediment composition.

The Ribble Estuary, North-West England, was used as test case due to its environmental and economic importance, in addition to its exposure to escalating climate hazards and extensive anthropogenic interventions, which make it suitable for the investigation of salt marsh response to climate and anthropogenic forcings. To investigate the contribution of embankment construction to long-term marsh accretion, Chapter 3 integrated numerical modelling and paleoenvironmental analysis. First, accretion rates derived using optically stimulated luminescence (OSL) dating were combined with a multi-proxy paleoenvironmental investigation on sediment cores extracted from the salt marsh, the mobile seafloor of the central Irish Sea and the river catchment area, to provide the first evolutionary perspective on the Ribble Estuary preceding any management interventions. The paleoenvironmental analyses were then compared to simulations conducted using the coupled hydrodynamic-morphodynamic model Delft3D to investigate the effects of embankment construction on estuarine hydrodynamics and morphodynamics of the salt marsh over the period constrained by the OSL dating. As Chapter 3 demonstrated that sediment budgets estimated from short-term simulations of different scenarios reproducing different bathymetric and hydrodynamic conditions in time are successfully evaluate long-term salt marsh resilience, Chapter 4 then investigated the combined impact of projected sea-level rise and increased storm intensity on salt marsh resilience deriving sediment budgets from a wealth of sea-level and storm surge scenarios simulated using Delft3D. Chapter 5 then investigated how both storm surges and storm waves influence the sediment supply to different marsh areas and whether storms can deliver new material onto the salt marsh platform which would otherwise not be sourced in fair-weather conditions. Sediment supply was investigated from field measurements of suspended sediment concentrations above the salt marsh platform conducted at high spatial resolution during the 2021-2022 storm season, while sediment provenance was investigated using a multi-proxy analysis of the suspended sediments collected from the salt marsh, surface sediments collected from the adjacent mudflat and tidal creeks and the more distant sandflats and sand dunes, and cores collected from the Irish Sea floor. Ultimately, Chapter 6 tested the suitability of K-feldspar luminescence signals for diagnosing storm activity in geological records without relying upon a change in sediment composition and stratigraphy. It first tried to diagnose the differential modes of deposition across intertidal settings in longer-term sediment records by detecting the variability in sediment bleaching potential between settings, to establish a framework for the interpretation of luminescence properties of intertidal sediments. It then used modern sediment samples collected before and after a storm event to test whether such properties can diagnose changes in sediment processing of intertidal sediments caused by storm activity.

7.2 Key findings of the study

7.2.1 Salt marsh response to anthropogenic disturbance and climate change

Numerical simulations and paleoenvironmental analyses (Chapter 3) showed that in the Ribble Estuary, the construction of embankments along the estuary shorelines, which were started in 1810, enhanced ebb dominance across the intertidal system and intensified sediment export. Results, however, also showed that the long-term accretion of the Ribble marshes has not been compromised by embankment construction because of the high rates of marine sediment supply, supported by the high availability of mobile sediments in the central Irish Sea legacy of the Irish Sea Glacier, and the 60 years of channel dredging, both of which enhanced the flood dominance of the tide near the tidal flat and favoured infilling. Numerical analyses (Chapter 4) have also showed that sea-level rise can further threaten estuary and marsh stability by promoting ebb dominance and triggering a net sediment export. Conversely, storm surges promote flood dominance and trigger sediment import, aiding marsh resilience. Results further showed that storm surges might contribute to increase salt marsh resilience to sea-level rise by masking the effects of sea-level rise on the sediment budget; this is particularly true for storms with the highest intensities (>3 m surges). This reduction in sediment loss, however, can reach up to 65% on the marsh platform but only up to 7% in the inner estuary (for 4 m surges occurring at spring tide and lasting 48 hours). This discrepancy is explained by the results of a field monitoring campaign conducted during the 2021-2022 storm season (Chapter 5). Field measurements of suspended sediment concentrations above the salt marsh platform showed that storms mostly enhanced salt marsh vertical accretion, especially benefitting the marsh interior. The multi-proxy analysis of the salt marsh sediments and the sediments collected from the potential sources, however, showed that the majority of the storm sediment supplied to the salt marsh platform were generated by an increase in erosion and resuspension of the adjacent mudflat and tidal creek sediments, suggesting that, in the long term, medium-intensity storms might reduce the overall larger-scale sediment availability with implications for marsh lateral retreat.

7.2.2 A new tool for detecting storm activity in intertidal environments

The luminescence tests (Chapter 6) performed on sediment cores demonstrated that luminescence signals of K-feldspars (IR_{50}, $pIRIR_{150}$ and $pIRIR_{225}$) can diagnose differential modes of deposition across intertidal settings (i.e., sandflat, mudflat and salt marsh) in longer-term sediment records by detecting the variability in sediment bleaching potential between settings (i.e., sediment exposure to sunlight), thus establishing a framework for the interpretation of luminescence properties of intertidal sediments. The same tests run on modern sediment samples collected before and after a storm event further showed that the two elevated temperature signals ($pIRIR_{150}$ and $pIRIR_{225}$) can successfully detect storm activity across intertidal environments that remain undetectable with existing techniques that depend on sediment composition, as post-storm sediment samples exhibited higher bleaching potential (i.e., more sediment processing) on the mudflat prior to burial in comparison to the pre-storm samples, despite no significant change in sediment composition being recorded by the geochemical and particle size distribution analyses.

7.3 Implications

7.3.1 Research perspectives

7.3.1.1 Understanding the true fate of coastal wetlands

This thesis investigated salt marsh resilience to anthropogenic disturbance and climate change. Through the analysis of the impact of embankment construction and dredging operations on salt marsh sediment budget, Chapter 3 demonstrated that both hard and soft engineering activities can have an effect on sediment transport dynamics of intertidal systems, ultimately impacting the development and encroachment of tidal flats and vegetated wetlands, although the influence of anthropogenic activities on marsh stability is still poorly investigated. Chapter 4 also showed how analysing the impact of different forcings in combination (e.g., sea level and storms) can provide a more comprehensive perspective on the extent to which they can influence sediment transport dynamics within and intertidal system, hence the resilience of tidal flats-salt marsh complexes. Overall, the key findings of this thesis suggest that the effects of anthropogenic disturbance on salt marsh resilience should be more widely investigated and that, to truly understand the fate of coastal wetlands, all forcings (natural and anthropogenic) that can influence sediment dynamics should be studied in combination. Further research should, for instance, investigate how sea-level rise and enhanced storm activity might influence salt marsh response to the implementation of sea defences.

7.3.1.2 A framework for assessing salt marsh response to anthropogenic disturbance and climate change

Some of the results of this study showed how the response of intertidal systems and salt marsh platforms can change from case to case depending on the hydrodynamic and morphodynamic feedbacks characteristic of the site. For instance, Chapter 3 found that embankments enhanced sediment export within the Ribble Estuary; however, other studies, such as Pontee (2014) in the Humber Estuary (UK) and Lee et al. (2017) in Chesapeake Bay and Delaware Bay (USA), concluded that, by channelizing sediments, embankments can favour the delivery of sediments to a specific area, inducing siltation of intertidal basins. Conversely, other results from this study agreed with studies performed in other sites. For instance, Chapter 4 found that sea-level promotes ebb dominance and triggers a net sediment export, similarly to what was found by Carrasco et al. (2018) in Ria Formosa Lagoon (Portugal) and by Zhang et al. (2020) in Plum Island Sound (USA). Furthermore, Chapter 4 also found that storm surges trigger sediment import, comparably to what was found by Turner et al. (2006) in the Mississippi River and by

Castagno et al. (2018) in the Virginia Coast Reserve. Ultimately, Chapter 5 discovered spatial trends of sedimentation across the marsh platform similar to the trends observed by Temmerman et al., (2003) in the Scheldt Estuary (Belgium) and by Zhu and Wiberg (2022) in Hog Bay (USA). However, regardless of the trends observed, the main outcome of this study is that anthropogenic activities and climate forcings affect salt marsh resilience in a similar way, i.e. by changing the sediment dynamics of an intertidal system, as a consequence of their effects on tidal and wave dynamics. Henceforth, although the sensitivity of tidal flat and salt marsh complexes to changes in hydrodynamics depends on a variety of local features (Reed, 1995), this study provides a framework to assess natural and anthropogenic influence on salt marsh resilience by outlining what are the fundamental hydro-morphodynamic feedbacks, common to most estuaries (e.g., Van Dongeren and de Vriend, 1994; Rose and Thorne, 2001; Lanzoni and Seminara, 2002; Zhang et al., 2019), that are affected by anthropogenic activities and climate forcings; framework which can therefore be applied to any estuary regardless of local variability.

7.3.1.3 Integrating numerical and field analyses for the optimum understanding of intertidal sediment dynamics

In addition to the results produced, this study also showcased that, studying intertidal sediment dynamics using a multidisciplinary approach, as suggested by Fagherazzi et al. (2020), can provide a more comprehensive understanding of the processes involved than studies that use only numerical or field analyses. In this study, numerical modelling was employed to simulate different scenarios at multiple spatial and temporal scales and provided information about hydrodynamic-morphodynamic feedbacks characterising the intertidal environment which field analyses alone would have not been able to produce in the same period of time. For example, it was able to simulate estuary and salt marsh response to projected sea-level rise (Chapter 4). On the other hand, paleoenvironmental reconstructions were useful for analysing the long-term accretion dynamics of the salt marsh over a timescale which spanned over 200 years – unreachable by current hydrodynamic models (Chapter 3), while field surveys were able to provide an understanding of hydrodynamic-morphodynamic feedbacks associated with storm dynamics at a resolution higher than what can be sustained by most models (Chapter 5). Finally, luminescence analyses were able to provide novel tools for informing modelled storm scenarios (Chapter 6). Hence, this study demonstrated that integrating numerical and field techniques for the study of sediment dynamics at multiple time and spatial scales is achievable and that it is indeed necessary for the optimum understanding of intertidal systems.

7.3.2 Tools and knowledge for informing coastal management

Despite the advances that still have to be made in the understanding of intertidal systems and coastal wetlands dynamics, the findings of this study have significant implications for current and future salt marsh management. Loss of salt marsh areas has been occurring at increasing rates worldwide in the past decades, with 1,453 km^2 lost globally only over the last 20 years (Campbell et al., 2022). As a response to these losses, numerous projects around the world have been conducted to create new salt marshes and/or restore salt marshes that were previously reclaimed for anthropogenic activities (Temmerman et al., 2013), such as in the Ribble Estuary (Tovey et al., 2009) and in San Francisco Bay (Williams and Faber, 2001). Salt marsh restoration aims at re-establishing the natural functions of salt marshes that have been degraded by natural processes (e.g., sea-level rise, wave erosion) and/or human activities (Billah et al., 2022), while the creation of new salt marsh areas involves the anthropogenic modification of intertidal substrates to favour the development and encroachment of salt marsh areas in locations which are suitable for their growth but where they have not naturally developed yet (Baptist et al., 2021). Restoration and development projects include a variety of interventions such as managed realignment, land raising above the mean water level to allow wetland plants to colonise or to contrast erosion processes which are degrading wetland areas, and water ways diversion or creation to allow water flowing in favourable paths (Billah et al., 2022). The success of these interventions depends on their life-spans, which in turn depends on the long-term response of the salt marsh to anthropogenic disturbance and climate forcings (Billah et al., 2022). Even unmanaged intertidal systems, however, need to be assessed in the light of projected sea-level rise and increases in storm intensity (Masson-Delmotte et al., 2018) and widespread engineering interventions (Floerl et al., 2021). Many unmanaged coastal wetlands might be experiencing degradation or they might experience it in the future (e.g., Tognin et al., 2021) but, due the lack of a comprehensive assessment of all the climatic and anthropogenic factors influencing marsh resilience, mitigation measures are often not implemented or implemented too late (Campbell et al., 2022). Hence, by quantifying salt marsh resilience to anthropogenic disturbance and climate forcings, this study provided a more comprehensive framework for assessing long-term resilience of salt marshes and intertidal systems, which can help maximise the results of marsh creation and restoration projects as well as prevent future salt marsh losses.

References

Ahmed, M.T., Sato, S., Tajima, Y., 2014. Quantitative estimation of longshore sediment transport based on thermoluminescence: Two case studies around Tenryu and Nile River Mouths. Journal of Coastal Research, 30 (3), 537-547. https://doi.org/10.2112/JCOASTRES-D-13-00050.1

Aitken, M.J., 1985. Thermoluminescence Dating: Past progress and future trends. London, Orlando: Academic Press.

Bakker, J.P., de Leeuw, J., Dijkema, K.S., Leendertse, P.C., Prins, H.H., Rozema, J., 1993. Salt marshes along the coast of the Netherlands, Hydrobiologia, 265, 73. https://doi.org/10.1007/BF00007263

Ballarini, M., Wallinga, J., Murray, A.S., van Heteren, S., Oost, A.P., Bos, A.J.J., van Eijk, C.W.E., 2003. Optical dating of young coastal dunes on a decadal time scale. Quaternary Science Review, 22, 1011-1017. https://10.1016/S0277-3791(03)00043-X

Baptist, M.J., Babovic, V., Uthurburu, J.R., Keijzer, M., Uittenbogaard, R.E., Mynett, A., Verwey, A., 2007. On inducing equations for vegetation resistance. Journal of Hydraulic Research, 45 (4), 435-450. https://doi.org/10.1080/00221686.2007.9521778

Baptist, M.J., Dankers, P., Cleveringa, J., Sittoni, L., Willemsen, P.W.J.M., van Puijenbroek, M.E.B., de Vries, B.M.L., Leuven, J.R.F.W., Coumou, L., Kramer, H., Elschot, K., 2021. Salt marsh construction as a nature-based solution in an estuarine social-ecological system. Nature-Based Solutions, 1, 100005. https://doi.org/10.1016/j.nbsj.2021.100005

Barbier, E.B., Hacker, S.D., Kennedy, C., Koch, E.W., Stier, A.C., Silliman, B.R., 2011. The value of estuarine and coastal ecosystem services. Ecological Monographs, 81 (2), 169-193. https://doi.org/10.1890/10-1510.1

Berger, G.W., 1990. Effectiveness of natural zeroing of the thermoluminescence in sediments. Journal of Geophysical Research, 95, 12375-12397. https://doi.org/10.1029/JB095iB08p12375

Berry, A., Plater A.J., 1998. Rates of tidal sedimentation from records of industrial pollution and environmental magnetism: the Tees estuary, north-east England. Water, Air, Soil Pollution, 106 (3-4): 463-479. https://doi.org/10.1023/A:1005012813142

Bertin, X., Olabarrieta, M., McCall, R., 2017. Hydrodynamics under storm conditions. Ciavola, P., Coco, G., Coastal Storms: Processes and Impacts. https://doi.org/10.1002/9781118937099.ch2

Bertness, M.D., Ewanchuk, P.J., Silliman, B.R., 2002. Anthropogenic modification of New England salt marsh landscapes. PNAS., 99, 1395-1398. https://doi.org/10.1073/pnas.022447299

Beudin, A., Kalra, T.S., Ganju, N.K., Warner, J.C., 2017. Development of a coupled wave-flow-vegetation interaction model. Computers & Geosciences, 100, 76-86. https://doi.org/10.1016/j.cageo.2016.12.010

Bianchette, T.A., Liu, K., McCloskey, T.A., 2022. A 4000-year paleoenvironmental reconstruction and extreme event record from Laguna Nuxco, Guerrero, Mexico. Palaeogeography, Palaeoclimatology, Palaeoecology, 594, 110933. https://doi.org/10.1016/j.palaeo.2022.110933

Billah, M., Bhuiyan, M.A., Islam, M.A., Das, J., Hoque, R.A.T.M., 2022. Salt marsh restoration: an overview of techniques and success indicators. Environmental Science and Pollution Research, 29, 15347-15363. https://doi.org/10.1007/s11356-021-18305-5

Blanton, J.O., Lin, G.Q., Elston, S.A., 2002. Tidal current asymmetry in shallow estuaries and tidal creeks. Continental Shelf Research, 22 (11-13), 1731-1743. https://doi.org/10.1016/s0278-4343(02)00035-3

Blott, S.J., Pye, K., 2001. GRADISTAT: a grain size distribution and statistics package for the analysis of unconsolidated sediments. Earth Surface Processes and Landforms, 26 (11), 1237-1248. https://doi.org/10.1002/esp.261

BODC, 2021. British Oceanographic Data Centre. Liverpool: National Oceanography Centre. https://www.bodc.ac.uk

Booij, N., Ris, R.C., Holthuijsen, L.H., 1999. A third-generation wave model for coastal regions, 1. Model description and validation. Journal of Geophysical Research, 104 (C4), 7649-7666. https://doi.org/10.1029/98JC02622

Bøtter-Jensen, L., Andersen, C.E., Duller, G.A.T., Murray, A.S., 2003. Developments in radiation, stimulation and observation facilities in luminescence measurements. Radiation Measurements, 37, 535-541. https://doi.org/10.1016/S1350-4487(03)00020-9

Boyle, J.F., Chiverrell, R.C., Schillereff, D., 2015. Approaches to Water Content Correction and Calibration for µXRF Core Scanning: Comparing X-ray Scattering with Simple Regression of Elemental Concentrations. In Croudace, I.W., Rothwell, R.G., Micro-XRF Studies of Sediment Cores, pp. 373-390. Springer Netherlands. http://doi10.1007/978-94-017-9849-5_14

Boyle, J.F., 2000. Rapid elemental analysis of sediment samples by isotope source XRF. Journal of Paleolimnology, 23, 213-221. https://doi.org/10.1023/A:1008053503694

Brill, D., Reimann, T., Wallinga, J., May, S.M., Engel, M., Riedesel, S., Brückner, H, 2018. Testing the accuracy of feldspar single grains to date late Holocene cyclone and tsunami deposits. Quaternary Geochronology, 48, 91-103. https://doi.org/10.1016/j.quageo.2018.09.001

Bronk Ramsey, C., 1995. Radiocarbon Calibration and Analysis of Stratigraphy: The OxCal Program. Radiocarbon, 37 (2), 425-430. https://doi.org/10.1017/S0033822200030903

Bronk Ramsey, C., 2009. Dealing with outliers and offsets in radiocarbon dating. Radiocarbon, 51 (3), 1023-1045. https://doi.org/10.1017/S0033822200034093

Brooks, S.M., Spencer, T., Christie E.K., 2017. Storm impacts and shoreline recovery: Mechanisms and controls in the southern North Sea. Geomorphology, 283, 48-70. https://doi.org/10.1016/j.geomorph.2017.01.007

Cahoon, D.R., Reed, D.J., Day, J.W., Steyer, G.D., Boumans, R.M., Lynch, J.C., McNally, D., Latif, N., 1995. The Influence of Hurricane Andrew on Sediment Distribution in Louisiana Coastal Marshes. Journal of Coastal Research, 21, 280-94. http://www.jstor.org/stable/25736015

Campbell, A.D., Fatoyinbo, L., Goldberg, L., Lagomasino, D., 2022. Global hotspots of salt marsh change and carbon emissions. Nature, 612, 701-706. https://doi.org/10.1038/s41586-022-05355-z

Capotondi, A., Jacox, M., Bowler, C., Kavanaugh, M., Lehodey, P., Barrie, D., Brodie, S., Chaffron, S., Cheng, W., Dias, D.F., Eveillard, D., Guidi, L., Iudicone, D., Lovenduski, N.S., Nye, J.A., Ortiz, I., Pirhalla, D., Pozo Buil, M., Saba, V., Sheridan, S., Siedlecki, S., Subramanian, A., de Vargas, C., Di Lorenzo, E., Doney, S.C., Hermann, A.J., Joyce, T., Merrifield, M., Miller, A.J., Not, F., Pesant, S., 2019. Observational Needs Supporting Marine Ecosystems Modeling and Forecasting: From the Global Ocean to Regional and Coastal Systems. Frontiers in Marine Science, 6. https://doi.org/10.3389/fmars.2019.00623

Carless, S.J., Green, J.A.M., Pelling, H.E., Wilmes, S.-B., 2016. Effects of future sea-level rise on tidal processes on the Patagonian Shelf. Journal of Marine Systems, 163, 113-124. https://doi.org/10.1016/j.jmarsys.2016.07.007

Carniello, L., Defina, A., D’Alpaos., A., 2010. Modeling sand-mud transport induced by tidal currents and wind-waves in shallow microtidal basins: Application to the Venice Lagoon (Italy). Estuarine, Coastal and Shelf Science, 102-103: 105-115. https://doi.org/10.1016/j.ecss.2012.03.016

Carrasco, A.R., Plomaritis, T., Reyns, J., Ferreira, Ó., Roelvink, D., 2018. Tide circulation patterns in a coastal lagoon under sea-level rise. Ocean Dynamics, 68 (9), 1121-1139. https://doi.org/10.1007/s10236-018-1178-0

Castagno, K.A., Jimenez-Robles, A.M., Donnelly, J.P., Wiberg, P.L., Fenster, M.S., Fagherazzi, S., 2018. Intense Storms Increase the Stability of Tidal Bays. Geophysical Research Letters, 45 (11), 5491-5500. https://doi.org/10.1029/2018gl078208

Cefas, 2022. Centre for Environment, Fisheries and Aquaculture Science. https://www.cefas.co.uk/

Chamberlain, E.L., Wallinga, J., Reimann, T., Goodbred, S.L. Jr., Steckler, M.S., Shen, Z., Sincavage, R., 2017. Luminescence dating of delta sediments: Novel approaches explored for the Ganges-Brahmaputra-Meghna Delta. Quaternary Geochronology, 41, 97-111. http://dx.doi.org/10.1016/j.quageo.2017.06.006

Clarke, D.W., Boyle, J.F., Chiverrell, R.C., Lario, J., Plater, A.J., 2014. A sediment record of barrier estuary behaviour at the mesoscale: interpreting high-resolution particle size analysis. Geomorphology, 221, 51-68. https://doi.org/10.1016/j.geomorph.2014.05.029

Clarke, D.W., Boyle, J.F., Lario, J., Plater, A.J., 2013. Meso-scale barrier estuary disturbance, response and recovery behaviour: Evidence of system equilibrium and resilience from high-resolution particle size analysis. HOLOCENE, 24 (3), 357-369. https://doi.org/10.1177/0959683613518597

Colarossi, D., Duller, G.A.T., Roberts, H.M., Tooth, S., Lyons, R., 2015. Comparison of paired quartz OSL and feldspar post-IR IRSL dose distributions in poorly bleached fluvial sediments from South Africa. Quaternary Geochronology, 30, 233-238. http://dx.doi.org/10.1016/j.quageo.2015.02.015

Costanza, R., Pérez-Maqueo, O., Martinez, M.L., Sutton, P., Anderson, S.J., Mulder, K., 2008. The value of coastal wetlands for hurricane protection, AMBIO. Journal of Human Environment, 37 (4), 241-248. https://doi.org/10.1579/0044-7447(2008)37[241:TVOCWF]2.0.CO;2

Cundy, A.B., Croudace, I.W., Thomson, J., Lewis, J.T., 1997. Reliability of Salt Marshes as "Geochemical Recorders" of Pollution Input: A Case Study from Contrasting Estuaries in Southern England. Environmental Science and Technology, 31 (4), 1093-1101. https://doi.org/10.1021/es960622d

D'Alpaos, A., Lanzoni, S., Marani, M., Rinaldo A., 2007. Landscape evolution in tidal embayments: Modeling the interplay of erosion, sedimentation, and vegetation dynamics. Earth Surface, 112, F01008. https://doi.org/10.1029/2006JF000537

D'Alpaos, A., Mudd, S. M., Carniello L., 2011. Dynamic response of marshes to perturbations in suspended sediment concentrations and rates of relative sea level rise. Earth Surface, 116 (F24). https://doi.org/10.1029/2011JF002093

Darby, S.E., Appeaning Addo, K., Hazra, S., Rahman, M.M., Nicholls, R.J., 2020. Fluvial Sediment Supply and Relative Sea-Level Rise. In Nicholls, R., Adger, W., Hutton, C., Hanson, S., Deltas in the Anthropocene, pp. 103-126. Palgrave Macmillan. https://doi.org/10.1007/978-3-030-23517-8_5

Davis, F., Duller, G.A.T., Roberts H.M., 2010. Testing the use of feldspars for optical dating of hurricane overwash deposits. Quaternary Geochronology, 5, 125-130. https://doi.org/10.1016/j.quageo.2009.03.001

de Vet, P.L.M., van Prooijen, B.C., Colosimo, I., Steiner, N., Ysebaert, T., Herman, P.M.J., Wang, Z.B., 2020. Variations in storm-induced bed level dynamics across intertidal flats. Scientific Reports, 10, 12877. https://doi.org/10.1038/s41598-020-69444-7

Deltares, 2019a. Delft3D-FLOW User Manual: Simulation of multi-dimensional hydrodynamic flows and transport phenomena, including sediments. https://content.oss.deltares.nl/delft3d4/Delft3D-FLOW_User_Manual.pdf

Deltares, 2019b. Delft3D-WAVE User Manual: Simulation of short-crested waves with SWAN. https://content.oss.deltares.nl/delft3d4/Delft3D-WAVE_User_Manual.pdf

Dietze, E., Hartmann, K., Diekmann, B., IJmker, J., Lehmkuhl, F., Opitz, S., Stauch, G., Wünnemann, B., Borchers, A., 2012. An end-member algorithm for deciphering modern detrital processes from lake sediments of Lake Donggi Cona, NE Tibetan Plateau, China. Sedimentary Geology, 243-244, 169-180. https://doi.org/10.1016/j.sedgeo.2011.09.014

Donatelli, C., Ganju, N.K., Zhang, X., Fagherazzi, S., Leonardi, N, 2018. Salt marsh loss affects tides and the sediment budget in shallow bays. Journal of Geophysical Research: Earth Surface, 123 (10), 2647-2662. https://doi.org/10.1029/2018JF004617

Donatelli, C., Zhang, X., Ganju, N.K., Aretxabaleta, A.L., Fagherazzi, S., Leonardi, N., 2020. A nonlinear relationship between marsh size and sediment trapping capacity compromises salt marshes’ stability. Geology, 48 (10), 966-970. https://doi.org/10.1130/G47131.1

Duller, G.A.T., 2008. Luminescence dating – Guidelines on using luminescence dating in archaeology. English Heritage, 44pp. https://pure.aber.ac.uk/ws/portalfiles/portal/19677465/download.pdf

Durcan, J.A., King, G.E., Duller, G.A.T., 2011. DRAC: Dose Rate and Age Calculator for trapped charge dating. Quaternary Geochronology, 28, 54-61. https://doi.org/10.1016/j.quageo.2015.03.012

Duvall, M.S., Wiberg, P.L., Kirwan, M.L., 2019. Controls on Sediment Suspension, Flux, and Marsh Deposition near a Bay-Marsh Boundary. Estuaries and Coasts, 42, 403-424. https://doi.org/10.1007/s12237-018-0478-4

Elias, E.P.L., Gelfenbaum, G., Van der Westhuysen, A.J., 2012. Validation of a coupled wave-flow model in a high-energy setting: The mouth of the Columbia River. Journal of Geophysical Research: Oceans, 117 (C9). https://doi.org/10.1029/2012JC008105

Elmilady, H., van der Wegen, M., Roelvink, D., van der Spek, A., 2021. Modeling the Morphodynamic Response of Estuarine Intertidal Shoals to Sea-Level Rise. Journal of Geophysical Research: Earth Surface, 127 (1), e2021JF006152. https://doi.org/10.1029/2021JF006152

Engelhart, S.E., Horton, B.P., 2012. Holocene sea level database for the Atlantic coast of the United States. Quaternary Science Reviews, 54, 12-25. https://doi.org/10.1016/j.quascirev.2011.09.013

Engelhart, S.E., Horton, B.P., Kemp, A.C., 2011. Holocene Sea Level Changes Along the United States' Atlantic Coast. Oceanography, 24 (2), 70-79. https://doi.org/10.5670/oceanog.2011.28

Environment Agency, 2011. The Extent of Saltmarsh in England and Wales: 2006-2009. Environment Agency, Bristol. https://assets.publishing.service.gov.uk/government/uploads/system/uploads/attachment_data/file/291573/LIT_5799_a4e627.pdf

Fagherazzi, S., Kirwan, M.L., Mudd, S.M., Guntenspergen, G.R., Temmerman, S., D'Alpaos, A., van de Koppel, J., Rybczyk, J.M., Reyes, E., Craft, C., Clough, J., 2012. Numerical models of salt marsh evolution: Ecological, geomorphic, and climatic factors. Reviews of Geophysics, 50 (1). https://doi.org/10.1029/2011RG000359

Fagherazzi, S., Mariotti, G., Leonardi, N., Canestrelli, A., Nardin, W., Kearney, W. S., 2020. Salt marsh dynamics in a period of accelerated sea level rise. Journal of Geophysical Research: Earth Surface, 125 (8), e2019JF005200. https://doi.org/10.1029/2019JF005200

Fagherazzi, S., Mariotti, G., Wiberg, P.L., McGlathery, K.J., 2013. Marsh Collapse Does Not Require Sea Level Rise. Oceanography, 26 (3), 70-77. https://doi.org/10.5670/oceanog.2013.47

Feagin, R.A., Lozada-Bernard, S.M., Ravens, T.M., Möller, I., Yeager, K.M., Baird, A.H., 2009. Does vegetation prevent wave erosion of salt marsh edges?. PNAS, 106 (25), 10109-10113. https://doi.org/10.1073/pnas.0901297106

Fernández-Mora, A., Calvete, D., Falqués, A., Swart H.E., 2015. Onshore sandbar migration in the surf zone: New insights into the wave-induced sediment transport mechanisms. Geophysical Research Letters, 42 (8), 2869-2877. https://doi.org/10.1002/2014GL063004

Fernández-Fernández, S., Ferreira, C.C., Silva, P.A., Baptista, P., Romão, S., Fontán-Bouzas, Á., Abreu, T., Bertin,, X., 2019. Assessment of Dredging Scenarios for a Tidal Inlet in a High-Energy Coast. Journal of Marine Science and Engineering, 7 (11), 395. https://doi.org/10.3390/jmse7110395

FitzGerald, D.M., Fenster, M.S., Argow, B.A., Buynevich, I.V., 2008. Coastal impacts due to sea-level rise. Annual Review of Earth and Planetary Sciences, 36, 601-647. https://doi.org/10.1146/annurev.earth.35.031306.140139

Fitzsimmons, K.E., 2011. An assessment of the luminescence sensitivity of Australian quartz with respect to sediment history. Geochronometria, 38 (3), 199-208. https://doi.org/10.2478/s13386-011-0030-9

Floerl, O., Atalah, J., Bugnot, A.B., Chandler, M., Dafforn, K.A., Floerl, L., Zaiko, A., Major, R., 2021. A global model to forecast coastal hardening and mitigate associated socioecological risks. Nature Sustainability, 4, 1060-1067. https://doi.org/10.1038/s41893-021-00780-w

Friedrichs, C.T., Aubrey, D.G., 1988. NON-LINEAR TIDAL DISTORTION IN SHALLOW WELL-MIXED ESTUARIES - A SYNTHESIS. Estuarine Coastal and Shelf Science, 27 (5), 521-545. https://doi.org/10.1016/0272-7714(88)90082-0

Galbraith, R.F., Laslett, G.M., 1993. Statistical models for mixed fission track ages. Nuclear Tracks and Radiation Measurements, 21, 459-470. https://doi.org/10.1016/1359-0189(93)90185-C

Galbraith, R.F., Roberts, R.G., Laslett, G.M., Yoshida, H., Olley, J.M., 1999. Optical dating of single and multiple grains of quartz from Jinmium rock shelter, northern Australia: Part I, Experimental design and statistical models. Archaeometry, 41 (2), 339-364. https://doi.org/10.1111/j.1475-4754.1999.tb00987.x

Ganju, N.K., Defne, Z., Kirwan, M.L., Fagherazzi, S., D'Alpaos, A., Carniello, L., 2017. Spatially integrative metrics reveal hidden vulnerability of microtidal salt marshes. Nature Communications, 8. https://doi.org/10.1038/ncomms14156

Ganju, N.K., Kirwan, M.L., Dickhudt, P.J., Guntenspergen, G.R., Cahoon, D.R., Kroeger, K.D., 2015. Sediment transport-based metrics of wetland stability. Geophysical Research Letters, 42 (19), 7992-8000. https://doi.org/10.1002/2015gl065980

Gao C., Adcock T.A.A., 2016. The characteristics of storm surges in the Bristol channel. The 26th International Ocean and Polar Engineering Conference, International Society of Offshore and Polar Engineers. https://users.ox.ac.uk/~spet1235/2016-TPC-0536__Gao.pdf

Garzanti, E., Barbarano, M., Andò, S., Lenzi, M., Deng, K., Yanget, S., 2020. Provenance of Neogene sandstones in western Taiwan traced with garnet geochemistry and zircon geochronology. Basin Research, 33 (3), 2069-2088. https://doi.org/10.1111/bre.12548

Godfrey-Smith, D.I., Huntley, D.J., Chen, W.H., 1988. Optical dating studies of quartz and feldspar sediment extracts. Quaternary Science Reviews, 7, 373-380. https://doi.org/10.1016/0277-3791(88)90032-7

Grant, J., Turner, S.J., Legendre, P., Hume, T.M., Bell, R.G., 1997. Patterns of sediment reworking and transport over small spatial scales on an intertidal sandflat, Manukau Harbour, New Zealand. Journal of Experimental Marine Biology and Ecology, 216, 33-50. PII S0022-0981(97)00089-0

Gray, H.J., Jain, M., Sawakuchi, A.O., Mahan, S.A., Tucker, G.E., 2019. Luminescence as a sediment tracer and provenance tool. Reviews of Geophysics, 57. https://doi.org/10.1029/2019RG000646

Gray, H.J., Tucker, G.E., Mahan, S.A., 2018. Application of a luminescence-based sediment transport model. Geophysical Research Letters, 45, 6071-6080. https://doi.org/10.1029/2018GL078210

Gray, H.J., Tucker, G.E., Mahan, S.A., McGuire, C., Rhodes, E.J., 2017. On extracting sediment transport information from measurements of luminescence in river sediment. Journal of Geophysical Research: Earth Surface, 122, 654-677. https://doi.org/10.1002/2016JF003858

Guerin, G., Jain, M., Thomsen, K.J., Murray, A.S., Mercier, N., 2015. Modelling dose rate to single grains of quartz in well-sorted sand samples: The dispersion arising from the presence of potassium feldspars and implications for single grain OSL dating. Quaternary Geochronology, 27, 52-65. https://doi.org/10.1016/j.quageo.2014.12.006

Guerin, G., Mercier, N., Adamiec, G., 2011. Dose-rate conversion factors: Update. Ancient TL, 29 (1), 5-8. https://www.aber.ac.uk/en/media/departmental/dges/ancienttl/pdf/vol29no1/guerin_atl29(1)_5-8.pdf

Guerin, G., Mercier, N., Nathan, R., Adamiec, G., Lefrais, Y., 2012. On the use of the infinite matrix assumption and associated concepts: A critical review. Radiation Measurements, 47 (9), 778-785. http://dx.doi.org/10.1016/j.radmeas.2012.04.004

Gunnell, G.R., Rodriguez, A.B., McKee, B.A., 2013. How a marsh is built from the bottom up. Geology, 41 (8), 859-862. https://doi.org/10.1130/G34582.1

Guo, L.C., van der Wegen, M., Wang, Z.B., Roelvink, D., He, Q., 2016. Exploring the impacts of multiple tidal constituents and varying river flow on long-term, large-scale estuarine morphodynamics by means of a 1-D model. Journal of Geophysical Research: Earth Surface, 121 (5), 1000-1022. https://doi.org/10.1002/2016jf003821

Haddadchi, A., Olley, J., Pietsch, T., 2016. Using LM-OSL of quartz to distinguish sediments derived from surface-soil and channel erosion. Hydrological Processes, 30 (4), 637-647. https://doi.org/10.1002/hyp.10646

Hammer, O., 2019. PAST, Paleontological Statistics Version 3.25, Reference manual. Natural History Museum, University of Oslo. https://www.nhm.uio.no/english/research/resources/past/downloads/past4manual.pdf

Hazermoshar, A., Lak, R., Espahbood, M.R., Ghadimvand, N.K., Farajzadeh, R., 2016. Geochemical, Sedimentological and Mineralogical Characterization of Surficial Sediments in Eynak Marsh (North of Iran). Open Journal of Geology, 6, 640-659. https://doi.org/10.4236/ojg.2016.67050

Hillen, M.M., Geleynse, N., Storms, J.E.A., Walstra, D.J.R., Stive, M.J.F., 2009. Morphology and stratigraphy of a degrading delta. Proceedings of Coastal Dynamics, 1-12. https://doi.org/10.1142/9789814282475_0137

Holleman, R.C., Stacey, M.T., 2014. Coupling of Sea Level Rise, Tidal Amplification, and Inundation. American Meteorological Society, 44 (5), 1439-1455. https://doi.org/10.1175/JPO-D-13-0214.1

Hopkinson, C S., Morris, J.T., Fagherazzi, S., Wollheim, W.M., Raymond, P.A., 2018. Lateral marsh edge erosion as a source of sediments for vertical marsh accretion. Journal of Geophysical Research: Biogeosciences, 123, 2444-2465. https://doi.org/10.1029/2017JG004358

Idier, D., Paris, F., Le Cozannet, G., Boulahya, F., Dumas, F., 2017. Sea-level rise impacts on the tides of the European Shelf. Continental Shelf Research, 137, 56-71. https://doi.org/10.1016/j.csr.2017.01.007

Kennish, M.J., 2001. Coastal Salt Marsh Systems in the U.S.: A Review of Anthropogenic Impacts. Journal of Coastal Research, 17 (3), 731-748. http://www.jstor.org/stable/4300224

Kiesel, J., MacPherson, L.R., Schuerch, M., Vafeidis, A.T., 2022. Can Managed Realignment Buffer Extreme Surges? The Relationship Between Marsh Width, Vegetation Cover and Surge Attenuation. Estuaries and Coasts 45, 345-362. https://doi.org/10.1007/s12237-021-00984-5

Kiesel, J., Schuerch, M., Christie, E.K., Möller, I., Spencer, T., Vafeidis, A.T., 2020. Effective design of managed realignment schemes can reduce coastal flood risks. Estuarine, Coastal and Shelf Science, 242, 106844. https://doi.org/10.1016/j.ecss.2020.106844

Lepofsky, D., Kirch, P.V., Lertzman, K.P., 1996. Stratigraphic and Paleobotanical Evidence for Prehistoric Human-Induced Environmental Disturbance on Mo'orea, French Polynesia. Pacific Science, 50 (3), 253-273. http://hdl.handle.net/10125/2899

Kirwan, M. L., Murray A. B., 2008. Tidal marshes as disequilibrium landscapes? Lags between morphology and Holocene sea level change. Geophysical Research Letters, 34 (24), L24401. https://doi.org/10.1029/2008GL036050

Kirwan, M.L., Guntenspergen, G.R., D'Alpaos, A., Morris, J.T., Mudd, S.M., Temmerman, S., 2010. Limits on the adaptability of coastal marshes to rising sea level. Geophysical Research Letters, 37. https://doi.org/10.1029/2010gl045489

Kirwan, M.L., Murray A.B., 2007. A coupled geomorphic and ecological model of tidal marsh evolution. PNAS, 104 (15), 6118-6122. https://doi.org/10.1073/pnas.0700958104

Kirwan, M.L., Temmerman, S., Skeehan, E.E., Guntenspergen, G.R., Fagherazzi, S., 2016. Overestimation of marsh vulnerability to sea level rise. Nature Climate Change, 6 (3), 253-260. https://doi.org/10.1038/nclimate2909

Kolditz K., Dellwig O., Barkowski J., Badewien T. H., Freund H., Brumsack H.-J., 2012. Geochemistry of salt marsh sediments deposited during simulated sea-level rise and consequences for recent and Holocene coastal development of NW Germany. Geo-Marine Letters, 32 (1): 49 -60. https://doi.org/10.1007/s00367-011-0250-2

Lanzoni, S., Seminara, G., 2002. Long-term evolution and morphodynamic equilibrium of tidal channels. Journal of Geophysical Research - Oceans, 107 (C1). https://doi.org/10.1029/2000jc000468

Lee, S.B., Li, M., Zhang, F., 2017. Impact of sea level rise on tidal range in Chesapeake and Delaware Bays. Journal of Geophysical Research: Oceans, 122, 3917-3938. http://doi.org/10.1002/2016JC012597

Leonardi, N., Carnacina, I., Donatelli, C., Ganju, N.K., Plater, A.J., Schuerch, M., Temmerman, S., 2018. Dynamic interactions between coastal storms and salt marshes: A review. Geomorphology, 301, 92-107. https://doi.org/10.1016/j.geomorph.2017.11.001

Leonardi, N., Fagherazzi, S., 2014. How waves shape salt marshes. Geology, 42 (10), 887-890. https://doi.org/10.1130/g35751.1

Leonardi, N., Ganju, N.K., Fagherazzi, S., 2016. A linear relationship between wave power and erosion determines salt-marsh resilience to violent storms and hurricanes. PNAS, 113 (1), 64-68. https://doi.org/10.1073/pnas.1510095112

Leonardi, N., Plater, A.J, 2017. Residual flow patterns and morphological changes along a macro- and meso-tidal coastline. Advances in Water Resources, 109, 290-301. https://doi.org/10.1016/j.advwatres.2017.09.013

Leonardi, N., Canestrelli, A., Sun, T., Fagherazzi, S., 2013. Effect of tides on mouth bar morphology and hydrodynamics. Journal of Geophysical Research: Oceans, 118 (9), 4169-4183. https://doi.org/10.1002/jgrc.20302

Lesser, G.R., Roelvink, J.A., van Kester, J.A.T.M., Stelling, G.S., 2004. Development and validation of a three-dimensional morphological model, Coastal Engineering, 51, (8-9), 883-915. https://doi.org/10.1016/j.coastaleng.2004.07.014

Li, B., Li, S.-H., 2011. Luminescence dating of K-feldspar from sediments: A protocol without anomalous fading correction. Quaternary Geochronology 6, 468-479. https://doi.org/10.1016/j.quageo.2011.05.001

Li, M., Zhang, F., Guo, Y., Wang, X., 2020. Probabilistic Projections of High-Tide Flooding for the State of Maryland in the Twenty-First Century. In: Lyubchich, V., Gel, Y.R., Kilbourne, K.H., Miller, T.J., Newlands, N.K., Smith A.B., Evaluating Climate Change Impacts. https://doi.org/10.1201/9781351190831

Li, X.R., Leonardi, N., Plater, A.J, 2019. Wave-driven sediment resuspension and salt marsh frontal erosion alter the export of sediments from macro-tidal estuaries. Geomorphology, 325, 17-28. https://doi.org/10.1016/j.geomorph.2018.10.004

Li, X.R., Plater, A., Leonardi, N., 2018. Modelling the Transport and Export of Sediments in Macrotidal Estuaries with Eroding Salt Marsh. Estuaries and Coasts, 41 (6), 1551-1564. https://doi.org/10.1016/j.geomorph.2017.11.001

Liu, Z.C., de Lange, W.P., Bryan, K.R., 2020. Estuary rejuvenation in response to sea level rise: an example from Tairua Estuary, New Zealand. Geo-Marine Letters, 40 (2), 269-280. https://doi.org/10.1007/s00367-019-00603-0

Lyddon, C., Brown, J.M., Leonardi, N., Plater, A.J., 2018. Flood Hazard Assessment for a Hyper-Tidal Estuary as a Function of Tide-Surge-Morphology Interaction. Estuaries and Coasts, 41 (6), 1565-1586. https://doi.org/10.1007/s12237-018-0384-9

Lyons, M.G., 1997. The dynamics of suspended sediment transport in the Ribble estuary. Water Air and Soil Pollution, 99 (1-4), 141-148. https://doi.org/10.1023/a:1018388517409

Ma, Z., Ysebaert, T., van der Wal, D., de Jong, D.J., Li, X., Herman, P.M.J., 2014. Long-term salt marsh vertical accretion in a tidal bay with reduced sediment supply. Estuary, Coastal and Shelf Science, 146, 14-23. https://doi.org/10.1016/j.ecss.2014.05.001

Madsen, A.T., Duller, G.A.T., Donnelly, J.P., Roberts, H.M., Wintle, A.G., 2009. A chronology of hurricane landfalls at Little Sippewissett Marsh, Massachusetts, USA, using optical dating. Geomorphology 109, 36-45. https://doi.org/10.1016/j.geomorph.2008.08.023

Madsen, A.T., Murray, A.S., Andersena, T.J., Pejrupa, M., Breuning-Madsenaet, H, 2005. Optically stimulated luminescence dating of young estuarine sediments: a comparison with 210Pb and 137Cs dating. Marine Geology, 214, 251-268. https://doi.org/10.1016/j.margeo.2004.10.034

Madsen, A.T., Murray, A.S., Andersn, T.J., Pejrup, M., 2007a. Temporal changes of accretion rates on an estuarine salt mash during the late Holocene e reflection of local sea level changes? The Waddden Sea, Denmark. Marine Geology, 242, 221-233. https://doi.org/10.1016/j.margeo.2007.03.001

Madsen, A.T., Murray, A.S., Andersn, T.J., Pejrup, M., 2007b. Optical dating of young tidal sediments in the Danish Wadden Sea. Quaternary Geochronology, 2, 89-94. https://doi.org/10.1016/j.quageo.2006.05.008

Mamas, C.J.V., Earwaker, L.G., Sokhi, R.S., 1995. An estimation of sedimentation rates along the Ribble Estuary, Lancashire, UK, based on radiocaesium profiles preserved in intertidal sediments. Environment International, 21 (2), 151-165. https://doi.org/10.1016/0160-4120(95)00005-4

Marani, M., Da Lio, C., D’Alpaos, A., 2013. Vegetation engineers marsh morphology through multiple competing stable states. PNAS, 110 (9) 3259-3263. https://doi.org/10.1073/pnas.1218327110

Marani, M., D'Alpaos, A., Lanzoni, S., Santalucia, M., 2011. Understanding and predicting wave erosion of marsh edges. Hydrology and Land Surface Studies, 38 (21), L21401. https://doi.org/10.1029/2011GL048995

Mariotti, G., Carr, J., 2014. Dual role of salt marsh retreat: Long-term loss and short-term resilience. Water Resources Research, 50, 2963-2974. https://doi.org/10.1002/2013WR014676

Mariotti, G., Fagherazzi, S., 2013. Critical width of tidal flats triggers marsh collapse in the absence of sea-level rise. PNAS, 110 (14) 5353-5356. https://doi.org/10.1073/pnas.1219600110

Mariotti, G., Fagherazzi, S., Wiberg, P.L., McGlathery, K.J., Carniello, L., Defina, A., 2010. Influence of storm surges and sea level on shallow tidal basin erosive processes. Journal of Geophysical Research: Oceans, 115 (C11). https://doi.org/10.1029/2009JC005892

Masson-Delmotte, V., Zhai, P., Pörtner, H.-O., Roberts, D., Skea, J., Shukla, P.R., Pirani, A., Moufouma-Okia, W., Péan, C., Pidcock, R., Connors, S., Matthews, J.B.R., Chen, Y., Zhou, X., Gomis, M.I., Lonnoy, E., Maycock, T., Tignor M., Waterfield T., 2018. Summary for Policymakers. In: Global Warming of 1.5°C. An IPCC Special Report on the impacts of global warming of 1.5°C above pre-industrial levels and related global greenhouse gas emission pathways, in the context of strengthening the global response to the threat of climate change, sustainable development, and efforts to eradicate poverty. In Press. https://www.ipcc.ch/2018/10/08/summary-for-policymakers-of-ipcc-special-report-on-global-warming-of-1-5c-approved-by-governments/

Matulla, C., Schöner, W., Alexandersson, H., 2008. European storminess: late nineteenth century to present. Climate Dynamics, 31, 125-130. https://doi.org/10.1007/s00382-007-0333-y

Mauz, B., Baeteman, C., Bungenstock, F., Plater, A.J., 2010. Optical dating of tidal sediments: Potentials and limits inferred from the North Sea coast. Quaternary Geochronology, 5, 667-678. https://doi.org/10.1016/j.quageo.2010.05.004

McCloskey T.A., Liu, K., 2012. A 7000 year record of paleohurricane activity from a coastal wetland in Belize. The Holocene, 23 (2), 278-291. https://doi.org/10.1177/0959683612460782

Mcowen, C.J., Weatherdon, L.V., Bochove, J.V., Sullivan, E., Blyth, S., Zockler, C., Stanwell-Smith, D., Kingston, N., Martin, C.S., Spalding, M., Fletcher, S., 2017. A global map of saltmarshes. Biodiversity Data Journal, 5, e11764. https://doi.org/10.3897/BDJ.5.e11764

Mitchell, M., Herman, J., Bilkovic, D.M., Hershner, C., 2017. Marsh persistence under sea-level rise is controlled by multiple, geologically variable stressors. Ecosystem Health Sustainability, 3, 10. https://doi.org/10.1080/20964129.2017.1396009

Möller, I., Spencer, T., French, J.R., Leggett, D.J., Dixon, M., 1999. Wave transformation over salt marshes: A field and numerical modelling study from north Norfolk, England. Estuarine Coastal and Shelf Science, 49 (3), 411-426. https://doi.org/10.1006/ecss.1999.0509

Moore, R.D., Wolf, J., Souza, A.J., Flint, S.S., 2009. Morphological evolution of the Dee Estuary, Eastern Irish Sea, UK: A tidal asymmetry approach. Geomorphology, 103 (4), 588-596. https://doi.org/10.1016/j.geomorph.2008.08.003

Morris, J.T., Barber, D.C., Callaway, J.C., Chambers, R., Hagen, S.C., Hopkinson, C.S., Johnson, B.J., Megonigal, P., Neubauer, S.C., Troxler, T., Wigand, C., 2016. Contributions of organic and inorganic matter to sediment volume and accretion in tidal wetlands at steady state. Earth's Future, 4, 110-121. https://doi.org/10.1002/2015EF000334

Morris, J.T., Sundareshwar, P.V., Nietch, C.T., Kjerfve, B., Cahoon, D.R., 2002. Responses of coastal wetlands to rising sea level. Ecology, 83 (10), 2869-2877. https://doi.org/10.2307/3072022

Mudd, S.M., D'Alpaos, A., Morris, J.T., 2010. How does vegetation affect sedimentation on tidal marshes? Investigating particle capture and hydrodynamic controls on biologically mediated sedimentation. Journal of Geophysical Research-Earth Surface, 115. https://doi.org/10.1029/2009jf001566

Mullarney, J.C., Henderson, S. M., 2010. Wave-forced motion of submerged single-stem vegetation. Journal of Geophysical Research: Oceans, 115 (C12). https://doi.org/10.1029/2010JC006448

Murray, A.S., Arnold, L.J., Buylaert, J-P., Guerin, G., Qin, J., Singhvi, A.K., Smedley, R.K., Thomsen, K.J., 2021. Optically stimulated luminescence dating using quartz. Nature Reviews Methods Primer, 1, 72. https://doi.org/10.1038/s43586-021-00068-5

Murray, A.S., Olley, J.M., 2002. Precision and accuracy in the optically stimulated luminescence dating of sedimentary quartz: a status review. Geochronometria, 21, 1-16.

Murray, A.S., Wintle, A.G., 2000. Luminescence dating of quartz using an improved single-aliquot regenerative-dose protocol. Radiation Measurements, 32, 57-73. https://doi.org/10.1016/S1350-4487(99)00253-X

Natural England, 2019. Designated Sites View. https://designatedsites.naturalengland.org.uk/

NASA, 2020. New Update to SEDAC’s Gridded Population of the World (GPW). https://www.earthdata.nasa.gov/news/new-gpw-release

Neumeier, U., Ciavola, P., 2004. Flow resistance and associated sedimentary processes in a Spartina maritima salt-marsh. Journal of Coastal Research, 20 (2), 435-447. https://doi.org/10.2112/1551-5036(2004)020[0435:fraasp]2.0.co;2

Olbert, A.I., Nash, S., Cunnane, C., Hartnett, M., 2013. Tide-surge interactions and their effects on total sea levels in Irish coastal waters. Ocean Dynamics, 63 (6), 599-614. https://doi.org/10.1007/s10236-013-0618-0

Orr, M., Crooks, S., Williams, P.B., 2003. Will Restored Tidal Marshes Be Sustainable? San Francisco Estuary and Watershed Science, 1, 1. https://doi.org/10.15447/sfews.2003v1iss1art5

Palazzoli, I., Leonardi, N., Jimenez-Robles, A.M., Fagherazzi, S., 2020. Velocity skew controls the flushing of a tracer in a system of shallow bays with multiple inlets. Continental Shelf Research, 192. https://doi.org/10.1016/j.csr.2019.104008

Palmer, K., Watson, C., Fischer, A., 2019. Non-linear interactions between sea-level rise, tides, and geomorphic change in the Tamar Estuary, Australia. Estuarine, Coastal and Shelf Science, 225, 106247. https://doi.org/10.1016/j.ecss.2019.106247

Parker, B.B., 1984. Frictional Effect on the Tidal Dynamics of a Shallow Estuary. Ph.D. Dissertation, The Johns Hopkins University, Baltimore, Maryland, pp. 292.

Parker, B.B., 1991. The relative importance of the various nonlinear mechanisms in a wide range of tidal interactions. In Tidal Hydrodynamics, pp. 237-268. John Wiley & Sons.

Parker, B.B, 2007. Tidal analysis and prediction. Silver Spring, MD: NOAA NOS Center for Operational Oceanographic Products and Services. http://dx.doi.org/10.25607/OBP-191

Parsons, A., Allan, E., Pontee, N., Pye, K., 2013a. North-West Estuaries Processes Reports – Ribble Estuary.

Parsons, A., Allan, E., Pontee, N., Pye, K., 2013b. North-West Estuaries Processes Reports – Mersey Estuary.

Parsons, A., Allan, E., Pontee, N., Pye, K., 2013c. North-West Estuaries Processes Reports – Dee Estuary.

Parsons, A., Allan, E., Pontee, N., Pye, K., 2013d. North-West Estuaries Processes Reports – Overview Report.

Partheniades, E., 1965. Erosion and deposition of cohesive soils. Journal of the Hydraulics Division, 91 (1), 105-139. https://cedb.asce.org/CEDBsearch/record.jsp?dockey=0013640

Pawlowicz, R., Beardsley, B., Lentz, S., 2002. Classical tidal harmonic analysis including error estimates in MATLAB using T-TIDE. Computers & Geosciences, 28 (8), 929-937. https://doi.org/10.1016/s0098-3004(02)00013-4

Pearce, A., Johnson, M., White, J., 2011. GEOTECHNICAL REPORT - LABORATORY AND IN SITU DATA WESTERN HVDC LINK MARINE CABLE ROUTE SURVEY GEOTECHNICAL FIELDWORK - SHALLOW SAMPLING (VIBROCORING) AND CONTINUOUS PIEZOCONE PENETRATION TESTING (PCPT).

Pearson, S.G., van Prooijen, B.C., Elias, E. P.L., Vitousek, S., Wang, Z.B., 2020. Sediment Connectivity: A Framework for Analyzing Coastal Sediment Transport Pathways. Journal of Geophysical Research: Earth Surface, 125, e2020JF005595. https://doi.org/10.1029/2020JF005595

Pelling, H. E., Uehara K., Green J. A. M., 2013. The impact of rapid coastline changes and sea level rise on the tides in the Bohai Sea, China. Journal of Geophysical Research: Oceans, 118 (7), 3462-3472. https://doi.org/10.1002/jgrc.20258

Pendleton, L, Donato, D.C., Murray, B.C., Crooks, S., Jenkins, W.A., Sifleet, S., Craft, C., Fourqurean, J.W., Kauffman, J.B., Marbà, N., Megonigal, P., Pidgeon, E., Herr, D., Gordon, D, Baldera A., 2012. Estimating Global "Blue Carbon" Emissions from Conversion and Degradation of Vegetated Coastal Ecosystems. PLOS ONE, 7 (9), e43542. https://doi.org/10.1371/journal.pone.0043542

PSMSL, 2019. Permanent Service for Mean Sea Level. https://www.psmsl.org/

Pethick, J., 1981. Long-term accretion rates on tidal salt marshes. Journal of Sedimentary Research, 51 (2), 571-577. https://doi.org/10.1306/212F7CDE-2B24-11D7-8648000102C1865D

Pickering, M.D., Wells, N.C., Horsburgh, K.J., Green, J.A.M., 2012. The impact of future sea-level rise on the European Shelf tides. Continental Shelf Research, 35, 1-15. https://doi.org/10.1016/j.csr.2011.11.011

Plater, A.J., Huddart, D., Innes, J.B., Pye, K., Smith, A.J., Tooley, M.J., 1993. Coastal and sea-level changes. In Atkinson, D., Houston, J., The Sand Dunes of the Sefton Coast, pp. 23-34. NMGM.

Plater, A.J., Poolton, N.R.J., 1992. Interpretation of Holocene sea level tendency and intertidal sedimentation in the Tees estuary using sediment luminescence techniques: a variability study. Sedimentology, 39, 1-15. https://doi.org/10.1111/j.1365-3091.1992.tb01020.x

Plater, A.J., Ridgway, J., Rayner, B., Shennan, I., Horton, B.P., Haworth, E.Y., Wright, M.R., Rutherford, M.M., Wintle, A.G., 2000. Sediment provenance and flux in the Tees Estuary: the record from the Late Devensian to the present. Geological Society, 166, 171-195. https://doi.org/10.1144/GSL.SP.2000.166.01.10

Plater, A.J., Stupples, P., Roberts, H.M., 2007. The depositional history of the Dungeness Foreland. In Long, A.J., Walker, M.P., Plater, A.J., The late Holocene evolution of the Romney Marsh/Dungeness Foreland depositional complex, UK. Oxbo Books.

Pontee, N., 2014. Accounting for siltation in the design of intertidal creation schemes. Ocean & Coastal Management, 88, 8-12. https://doi.org/10.1016/j.ocecoaman.2013.10.014

Pratolongo, P., Leonardi, N., Kirby, J.R., Plater, A., 2019. Chapter 3 - Temperate Coastal Wetlands: Morphology, Sediment Processes, and Plant Communities. In Perillo, G.M.E., Wolanski, E., Cahoon, D.R., Hopkinson, C.S., Coastal Wetlands: An Integrated Ecosystem Approach (Second Edition), pp. 105-152. https://doi.org/10.1016/B978-0-444-63893-9.00003-4

Prescott, J.R., Hutton, J.T., 1994. Cosmic ray contributions to dose rates for luminescence and ESR dating: Large depths and long-term time variations. Radiation Measurements, 23 (2-3), 497-500. https://doi.org/10.1016/1350-4487(94)90086-8

Pugh, D., 1987. Tides, Surges and Mean Sea-Level. Chichester: John Wiley & Sons Ltd.

Pye, K., Neal, A., 1994. COASTAL DUNE EROSION AT FORMBY POINT, NORTH MERSEYSIDE, ENGLAND - CAUSES AND MECHANISMS. Marine Geology, 119 (1-2), 39-56. https://doi.org/10.1016/0025-3227(94)90139-2

R Core Team, 2013. R: a language and environment for statistical computing. R Foundation for statistical Computing, Vienna, Austria. http://www.R-project.org/

Rahman, R., Plater, A.J., 2014. Particle-size evidence of estuary evolution: A rapid and diagnostic tool for determining the nature of recent saltmarsh accretion. Geomorphology, 213, 139-152. https://doi.org/10.1016/j.geomorph.2014.01.004

Ray, R.D., 1999. A global ocean tide model from Topex/Poseidon altimetry: GOT99.2, NASA Tech. Memo. 209478, pp. 58, Goddard Space Flight Center, Greenbelt, MD.

Reed, D.J., 1990. THE IMPACT OF SEA-LEVEL RISE ON COASTAL SALT MARSHES. Progress in Physical Geography, 14 (4), 465-481. https://doi.org/10.1177/030913339001400403

Reed, D.J., 1995. THE RESPONSE OF COASTAL MARSHES TO SEA-LEVEL RISE - SURVIVAL OR SUBMERGENCE. Earth Surface Processes and Landforms, 20 (1), 39-48. https://doi.org/10.1002/esp.3290200105

Reed, D.J., Spencer., T., Murray, A.L., French, J.R., Leonard, L., 1999. Marsh surface sediment deposition and the role of tidal creeks: Implications for created and managed coastal marshes. Journal of Coastal Conservation, 5 (1), 81-90. https://doi.org/10.1007/BF02802742

Reimann, T., Notenboom, P.D., De Schipper, M.A., Wallinga, J., 2015. Testing for sufficient signal resetting during sediment transport using a polymineral multiple-signal luminescence approach. Quaternary Geochronology, 25, 26-36. https://doi.org/10.1016/j.quageo.2014.09.002

Reimer, P., Austin, W., Bard, E., Bayliss, A., Blackwell, P., Bronk Ramsey, C., Butzin, M., Cheng, H., Edwards, R., Friedrich, M., Grootes, P., Guilderson, T., Hajdas, I., Heaton, T., Hogg, A., Hughen, K., Kromer, B., Manning, S., Muscheler, R., Palmer, J., Pearson, C., van der Plicht, J., Reimer, R., Richards, D., Scott, E., Southon, J., Turney, C., Wacker, L., Adolphi, F., Büntgen, U., Capano, M., Fahrni, S., Fogtmann-Schulz, A., Friedrich, R., Köhler, P., Kudsk, S., Miyake, F., Olsen, J., Reinig, F., Sakamoto, M., Sookdeo, A., Talamo, S., 2020. The IntCal20 Northern Hemisphere radiocarbon age calibration curve (0–55 cal kBP). Radiocarbon, 62, 4. https://doi.org/10.1017/RDC.2020.41

Roberts, H.M., Plater, A.J., 2005. Optically Stimulated Luminescence (OSL) dating of sands underlying the gravel beach ridges of Dungeness and Camber, southeast England, UK. Centre for Archaeology Report, 27. https://doi.org/10.5284/1000031

Roner, M., Ghinassi, M., Finotello, A., Bertini, A., Combourieu-Nebout, N., Donnici, S., Gilli, A., Vannacci, M., Vigliotti, L., Bellucci. L.G., Fedi, M., Liccioli, L., Tommasini, L., D’Alpaos, A., 2021. Detecting the Delayed Signatures of Changing Sediment Supply in Salt-Marsh Landscapes: The Case of the Venice Lagoon (Italy). Frontiers in Marine Science, 8. https://doi.org/10.3389/fmars.2021.742603

Rose, C.P., Thorne, P.D., 2001. Measurements of suspended sediment transport parameters in a tidal estuary. Continental Shelf Research, 21 (15), 1551-1575. https://doi.org/10.1016/S0278-4343(00)00087-X

Rossiter, J.R., 1961. INTERACTION BETWEEN TIDE AND SURGE IN THE THAMES. Geophysical Journal of the Royal Astronomical Society, 6 (1), 29-53. https://doi.org/10.1111/j.1365-246X.1961.tb02960.x

RSPB, 2019. Ribble Estuary Nature Reserve - The RSPB. https://www.rspb.org.uk/

Russell, F., Boyle, J.F., Chiverrell, R.C., 2019. NIRS quantification of lake sediment composition by multiple regression using end-member spectra. Journal of Paleolimnology, 62 (1), 73-88. https://doi.org/10.1007/s10933-019-00076-2

Savenije, H.H.G., 2012. Salinity and Tides in Alluvial Estuaries. Second Completely Revised Edition. Elsevier Science Ltd. https://hubertsavenije.files.wordpress.com/2014/01/salinityandtides2_21.pdf

Sawakuchi, A.O., Blair, M.W., DeWitt, R., Faleiros, F.M., Hyppolito, T., Guedes, C.C.F., 2011. Thermal history versus sedimentary history: OSL sensitivity of quartz grains extracted from rocks and sediments. Quaternary Geochronology, 6 (2), 261-272. https://doi.org/10.1016/j.quageo.2010.11.002

Sawakuchi, A.O., Guedes, C.C.F., DeWitt, R., Giannini, P.C.F., Blair, M.W., Nascimento, D.R., Faleiros, F.M., 2012. Quartz OSL sensitivity as a proxy for storm activity on the southern Brazilian coast during the Late Holocene. Quaternary Geochronology, 13, 92-102. https://doi.org/10.1016/j.quageo.2012.07.002

Sawakuchi, A.O., Jain, M., Mineli, T.D., Nogueira, L., Bertassoli, D.J., Häggi, C., Sawakuchi, H.O., Pupim, F.N., Grohmann, C.H., Chiessi, C.M., Zabel, M., Mulitza, S., Mazoca, C.E.M., Cunha, D.F., 2018. Luminescence of quartz and feldspar fingerprints provenance and correlates with the source area denudation in the Amazon River basin. Earth and Planetary Science Letters, 492, 152-162. https://doi.org/10.1016/j.epsl.2018.04.006

Schuerch, M., Dolch, T., Bisgwa, J., Vafeidis A.T., 2018. Changing Sediment Dynamics of a Mature Backbarrier Salt Marsh in Response to Sea-Level Rise and Storm Events. Frontiers in Marine Science, 5, 155. https://doi.org/10.3389/fmars.2018.00155

Schuerch, M., Vafeidis, A., Slawig, T., Temmerman, S., 2013. Modeling the influence of changing storm patterns on the ability of a salt marsh to keep pace with sea level rise. Journal of Geophysical Research-Earth Surface, 118 (1), 84-96. https://doi.org/10.1029/2012jf002471

Scourse, J.D., Chiverrell, R.C., Smedley, R.K., Small, D., Burke, M.J., Saher, M., Van Landeghem, K.J.J., Duller, G.A.T., Cofaigh, C.Ó, Bateman, M.D., Benetti, S., Bradley, S., Callard, L., Evans, D.J.A., Fabel, D., Jenkins, G.T.H., McCarron, S., Medialdea, A., Moreton, S., Ou, X., Praeg, D., Roberts, D.H., Roberts, H.M., Clark, C.D. (2021). Maximum extent and readvance dynamics of the Irish Sea Ice Stream and Irish Sea Glacier since the Last Glacial Maximum. JOURNAL OF QUATERNARY SCIENCE, 36 (5), 780-804. https://doi:10.1002/jqs.3313

Shennan, I., Bradley, S.L., Edwards, R., 2018. Relative sea-level changes and crustal movements in Britain and Ireland since the Last Glacial Maximum. Quaternary Science Reviews, 188, 143-159. https://doi.org/10.1016/j.quascirev.2018.03.031

Silva, T., Biermann, L., Rees, J., 2016. Suspended Sediment Climatologies around the UK. CEFAS.

Sinha, P.C., Rao, Y.R., Dube, S.K., 1997. Effect of sea-level rise on tidal circulation in the Hooghly Estuary, Bay of Bengal. Marine Geodesy, 20 (4), 341-366. https://doi.org/10.1080/01490419709388114

Smedley, R.K., 2018. Telling the time with dust, sand and rocks. Elements, 14, 9-14. https://doi.org/10.2138/gselements.14.1.9

Smedley, R.K., Duller, G.A.T., Roberts, H.M., 2015. Bleaching of the post-IR IRSL signal from individual grains of K-feldspar: Implications for single-grain dating. Radiation Measurements, 79, 33-42. http://dx.doi.org/10.1016/j.radmeas.2015.06.003

Slaymaker, O., 2003. The sediment budget as conceptual framework and management tool. Hydrobiologia, 494, 71–82. https://doi.org/10.1023/A:1025437509525

Stefani, M., Vincenzi, S., 2005. The interplay of eustasy, climate and human activity in the late Quaternary depositional evolution and sedimentary architecture of the Po Delta system. Marine Geology, 222–223, 19-48. https://doi.org/10.1016/j.margeo.2005.06.029

Stelling, G., 1984. On the Construction of Computational Methods for Shallow Water Flow Problems. Rijkswaterstaat Communication Series, 35, Rijkswaterstaat, The Hague.

Stumpf, R.P., 1983. The process of sedimentation on the surface of a salt marsh. Estuarine, Coastal and Shelf Science, 17 (5), 495-508. https://doi.org/10.1016/0272-7714(83)90002-1

Stupples, P., Plater, A.J., 2007. Statistical analysis of the temporal and spatial controls on tidal signal preservation in late-Holocene tidal rhythmites, Romney Marsh, Southeast England. INTERNATIONAL JOURNAL OF EARTH SCIENCES, 96 (5), 957-976. https://doi.org/10.1007/s00531-006-0134-2

Tamura, T., Nguyen, V.L., Ta, T.K.O., 2020. Long-term sediment decline causes ongoing shrinkage of the Mekong megadelta, Vietnam. Scientific Report, 10, 8085. https://doi.org/10.1038/s41598-020-64630-z

Temmerman, S., Bouma, T.J., Govers, G., Wang, Z.B., De Vries, M.B., Herman, P.M.J., 2005. Impact of vegetation on flow routing and sedimentation patterns: Three-dimensional modeling for a tidal marsh. Journal of Geophysical Research-Earth Surface, 110 (F4). https://doi.org/10.1029/2005jf000301

Temmerman, S., Govers, G., Wartel, S., Meire, P., 2003. Spatial and temporal factors controlling short-term sedimentation in a salt and freshwater tidal marsh, Scheldt estuary, Belgium, SW Netherlands. Earth Surface Processes and Landforms, 28 (7), 739-755. https://doi.org/10.1002/esp.495

Temmerman, S., Horstman, E.M., Krauss, K.W., Mullarney, J.C., Pelckmans, I., Schoutens, K., 2022. Marshes and Mangroves as Nature-Based Coastal Storm Buffers. Annual Review of Marine Science, 15 (9), 1-24. https://doi.org/10.1146/annurev-marine-040422-092951

Temmerman, S., Meire, P., Bouma, T.J., Herman, P.M.J., Ysebaert, T., De Vriend, H.J., 2013. Ecosystem-based coastal defence in the face of global change. Nature, 504 (7478), 79-83. https://doi.org/10.1038/nature12859

Temmerman S., Govers, G., Wartel, S., Meire, P., 2004. Modelling estuarine variations in tidal marsh sedimentation: response to changing sea level and suspended sediment concentrations. Marine Geology, 212 (1-4), 1-19. https://doi.org/10.1016/j.margeo.2004.10.021

Thomsen, K.J., Murray, A., Jain, M., Bøtter-Jensen, L., 2008. Laboratory fading rates of various luminescence signals from feldspar-rich sediment extracts. Radiation Measurements, 43, 1474-1486. https://doi.org/10.1016/j.radmeas.2008.06.002

Tognin, D., D'Alpaos, A., Marani, M., Carniello, L., 2021. Marsh resilience to sea-level rise reduced by storm-surge barriers in the Venice Lagoon. Nature Geoscience, 14 (12), 906-911. https://doi.org/10.1038/s41561-021-00853-7

Tonjes, D.J., 2013. Impacts from ditching salt marshes in the mid-Atlantic and northeastern United States. Environmental Reviews, 21 (2). https://doi.org/10.1139/er-2013-0003

Tooley, M., 1974. Sea level changes during the last 9000 years in northwest England. Journal of Geography, 140, 18-42. https://doi.org/10.2307/1797005

Tovey, E.L., Pontee, N.I., Harvey, R., 2009. Managed Realignment at Hesketh Out Marsh West. Proceedings of the Institution of Civil Engineers-Engineering Sustainability, 162 (4), 223-228. https://doi.org/10.1680/ensu.2009.162.4.223

Townend, I., Fletcher, C., Knappen, M., Rossington, K., 2011. A review of salt marsh dynamics. Water and Environment Journal, 25 (4), 477-488. https://doi.org/10.1111/j.1747-6593.2010.00243.x

Turner, R.E., Baustian, J.J., Swenson, E.M., Spicer, J.S., 2006. Wetland sedimentation from Hurricanes Katrina and Rita. Science, 314 (5798), 449-452. https://doi.org/10.1126/science.1129116

UK MET Office, 2021. Weather and climate. Warnings and advice. UK Strom Centre. https://www.metoffice.gov.uk/weather/warnings-and-advice/uk-storm-centre/index

UKHO, 2001. Admiralty Tide Tables. United Kingdom and Ireland (including European Channel Ports). Taunton: UK Hydrographic Office. https://www.admiralty.co.uk/publications/publications-and-reference-guides/admiralty-tide-tables

UKHO, 2019. Admiralty Tide Tables. United Kingdom and Ireland (including European Channel Ports). Taunton: UK Hydrographic Office. https://www.admiralty.co.uk/publications/publications-and-reference-guides/admiralty-tide-tables

van der Wal, D., Pye, K., Neal, A., 2002. Long-term morphological change in the Ribble Estuary, northwest England. Marine Geology, 189 (3-4), 249-266. https://doi.org/10.1016/s0025-3227(02)00476-0

Van Dongeren, A.R., De Vriend, H.J., 1994. A MODEL OF MORPHOLOGICAL BEHAVIOR OF TIDAL BASINS. Coastal Engineering, 22 (3-4), 287-310. https://doi.org/10.1016/0378-3839(94)90040-X

Van Landeghem, K.J.J., Baas, J., Mitchell, N., Wilcockson, D., Wheeler, A., 2012. Sediment wave migration in the Irish Sea, NW Europe: a reappraisal of the validity of geometry-based predictive modelling and assumptions. Marine Geology, 295-298, 95-112. https://doi.org/10.1016/j.margeo.2011.12.004

Van Landeghem, K.J.J., Chiverrell, R.C., 2020. Bed erosion during fast ice streaming regulated the retreat dynamics of the Irish Sea Ice Stream. QUATERNARY SCIENCE REVIEWS, 245. https://doi:10.1016/j.quascirev.2020.106526

van Maneen, B., Coco., G., Bryan, K.R., Friedrichs, C.T., 2013. Modeling the morphodynamic response of tidal embayments to sea-level rise. Ocean Dynamics, 63, 1249-1262. https://doi.org/10.1007/s10236-013-0649-6

van Maren, D.S., van Kessel, T., Cronin, K., Sittoni, L., 2015. The impact of channel deepening and dredging on estuarine sediment concentration. Continental Shelf Research, 95, 1-14. https://doi.org/10.1016/j.csr.2014.12.010

van Proosdij, D., Davidson-Arnott, R.G.D., Ollerhead, J., 2006. Controls on spatial patterns of sediment deposition across a macro-tidal salt marsh surface over single tidal cycles. Estuarine, Coastal and Shelf Science, 69, 64-86. https://doi.org/10.1016/j.ecss.2006.04.022

Van Rijn, L.C., 1993. Principles of sediment transport in rivers, estuaries and coastal areas. Aqua publications, Amsterdam.

Veeramony J., Condon, A., van Ormondt, M., 2017. Forecasting Storm Surge and Inundation: Model Validation. Weather and Forecasting, 32, 2045-2063. https://doi.org/10.1175/WAF-D-17-0015.1

von Storch, H., Jiang, W., Furmanczyk, K.K., 2015. Chapter 7 - Storm Surge Case Studies. In Shroder, J.F., Ellis, J.T., Sherman, D.J., Coastal and Marine Hazards, Risks, and Disasters, Hazards and Disasters Series, pp. 181-196.

Wakefield, R., Tyler, A.N., McDonald, P., Atkin, P.A., Gleizon, P., Gilvear, D., 2011. Estimating sediment and caesium-137 fluxes in the Ribble Estuary through time-series airborne remote sensing. Journal of Environmental Radioactivity, 102 (3), 252-261. https://doi.org/10.1016/j.jenvrad.2010.11.016

Wallinga, J., 2002a. Detection of OSL age overestimation using single-aliquot techniques. Geochronometria, 21, 17-20.

Wallinga, J., 2002b. Optically stimulated luminescence dating of fluvial deposits: a review. Boreas, 31, 303-322. ISSN 0300-9483

Wallinga, J., Murray, A., Wintle, A., 2000. The single-aliquot regenerative-dose (SAR) protocol applied to coarse-grain feldspar. Radiation Measurements, 32 (5-6), 529-533. https://doi.org/10.1016/S1350-4487(00)00091-3

Walters, D.C., Kirwan, M.L., 2016. Optimal hurricane overwash thickness for maximizing marsh resilience to sea level rise. Ecology and Evolution, 6 (9), 2948-2956. https://doi.org/10.1002/ece3.2024

Wang, J., Dai, Z., Mei, X., Fagherazzi S, 2020. Tropical Cyclones Significantly Alleviate Mega-Deltaic Erosion Induced by High Riverine Flow. Geophysical Research Letter, 47 (19), e2020GL089065. https://doi.org/10.1029/2020GL089065

Wang, Z.B., Jeuken, M., Gerritsen, H., de Vriend, H.J., Kornman, B.A., 2002. Morphology and asymmetry of the vertical tide in the Westerschelde estuary. Continental Shelf Research, 22 (17), 2599-2609. https://doi.org/10.1016/s0278-4343(02)00134-6

Warner, J.C., Armstrong, B., He, R., Zambon, J.B., 2010. Development of a Coupled Ocean–Atmosphere–Wave–Sediment Transport (COAWST) Modeling System. Ocean Modelling, 35 (3), 230-244. https://doi.org/10.1016/j.ocemod.2010.07.010

Wei, X., Cai, S., Ni, P., Zhan, W., 2020. Impacts of climate change and human activities on the water discharge and sediment load of the Pearl River, southern China. Scientific Report, 10 (1), 16743. https://doi.org/10.1038/s41598-020-73939-8

Wesselman, D., de Winter, R., Engelstad, A., McCall, R., van Dongeren, A., Hoekstra, P., Oost, A., van der Vegt, M., 2017. The effect of tides and storms on the sediment transport across a Dutch barrier island. Earth Surface Processes and Landforms, 43 (3), 579-592. https://doi.org/10.1002/esp.4235

Willemsen, P.W.J.M, Smits, B.P., Borsje, B.W., Herman, P.M.J., Dijkstra, J.T., Bouma, T.J., Hulscheret, S.J.M.H., 2021. Modeling Decadal Salt Marsh Development: Variability of the Salt Marsh Edge Under Influence of Waves and Sediment Availability. Water Resources Research, 58, 1, e2020WR028962. https://doi.org/10.1029/2020WR028962

Williams, P., Faber, P.M, 2001. DESIGN GUIDELINES FOR TIDAL WETLAND RESTORATION IN SAN FRANCISCO BAY. https://scc.ca.gov/webmaster/ftp/pdf/pub/tidal_wet_guidelines_report.pdf

Wolf, J., 1981. Surge-tide interaction in the North Sea and River Thames. In Peregrine, D.H., Floods Due to High Winds and Tides. Elsevier, New York, pp. 75-94.

Woodworth, P.L., Tsimplis, M.N., Flather, R.A., Shennan, I., 1999. A review of the trends observed in British Isles mean sea level data measured by tide gauges. Geophysical Journal International 136, 651-670. https://doi.org/10.1046/j.1365-246x.1999.00751.x

Wright, J.E., Hull, J.H., McQuillin, R., Arnold, S.E., 1971. Irish Sea Investigations 1969-71. NERC Institute of Geological Sciences, Report 71/19.

Xu, Y., Kalra, T.S., Ganju, N.K., Fagherazzi, S., 2022. Modeling the dynamics of salt marsh development in coastal land reclamation. Geophysical Research Letters, 49, e2021GL095559. https://doi.org/10.1029/2021GL095559

Yang, S.L., Luo, X., Temmerman, S., Kirwan, M., Bouma, T., Xu, K., Zhang, S., Fan, J., Shi, B., Yang, H., Wang, Y.P., Shi, X., Gaoet, S., 2020. Role of delta-front erosion in sustaining salt marshes under sea-level rise and fluvial sediment decline. Limnology and Oceanography, 65 (9), 1990-2009. https://doi.org/10.1002/lno.11432

Yang, S.L., Shi, BW., Bouma, TJ., Ysebaert, T., Luo, X.X., 2012. Wave Attenuation at a Salt Marsh Margin: A Case Study of an Exposed Coast on the Yangtze Estuary. Estuaries and Coasts, 35, 169-182. https://doi.org/10.1007/s12237-011-9424-4

Zaron E.D., Elipot, S., 2021. An Assessment of Global Ocean Barotropic Tide Models Using Geodetic Mission Altimetry and Surface Drifters. Journal of Physical Oceanography, 51 (1), 63-82. https://doi.org/10.1175/JPO-D-20-0089.1

Zedler, J.B., Kercher, S., 2005. Wetland resources: Status, trends, ecosystem services, and restorability. Annual Review of Environment and Resources, 30, 39-74. https://doi.org/10.1146/annurev.energy.30.050504.144248

Zenghao, Q., Yihong, D., 1996. Numerical Study of Nonlinear Tide-Surge Interaction in the Coastal Waters of Shanghai. Land-Based and Marine Hazards, Advances in Natural and Technological Hazards Research, 7, 139-156. https://doi.org/10.1007/978-94-009-0273-2_9

Zhang, X., Leonardi, N., Donatelli, C., Fagherazzi, S., 2019. Fate of cohesive sediments in a marsh-dominated estuary. Advances in Water Resources, 125, 32-40. https://doi.org/10.1016/j.advwatres.2019.01.003

Zhang, X.H., Leonardi, N., Donatelli, C., Fagherazzi, S., 2020. Divergence of Sediment Fluxes Triggered by Sea-Level Rise Will Reshape Coastal Bays. Geophysical Research Letters, 47 (13). https://doi.org/10.1029/2020gl087862

Zhu, Q., Wiberg, P.L., 2022. The Importance of Storm Surge for Sediment Delivery to Microtidal Marshes. Journal of Geophysical Research: Earth Surface, 127 (9), e2022JF006612. https://doi.org/10.1029/2022JF006612

Zhu, R., Hong, B., Zhu, L., Gong., W., Zhang, H., 2015. Responses of estuarine circulation to the morphological evolution in a convergent, microtidal estuary. Ocean Science, 18, 213-231. https://doi.org/10.5194/os-18-213-2022

Appendix I – Supplementary material to Chapter 3

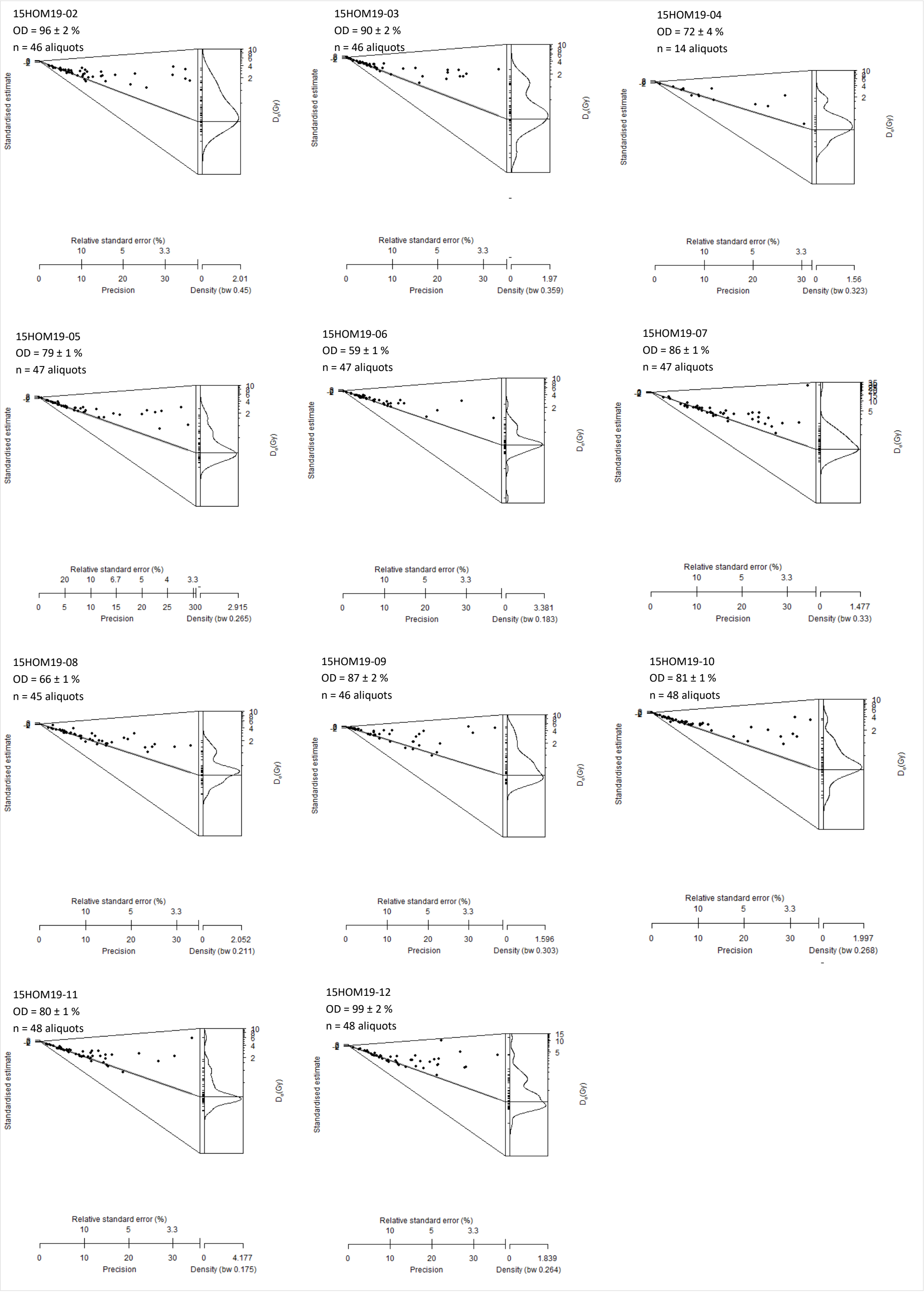

Figure S1. Abanico plots showing D_e values for the 11 OSL samples analysed, incorporating the results of the minimum age model (MAM).

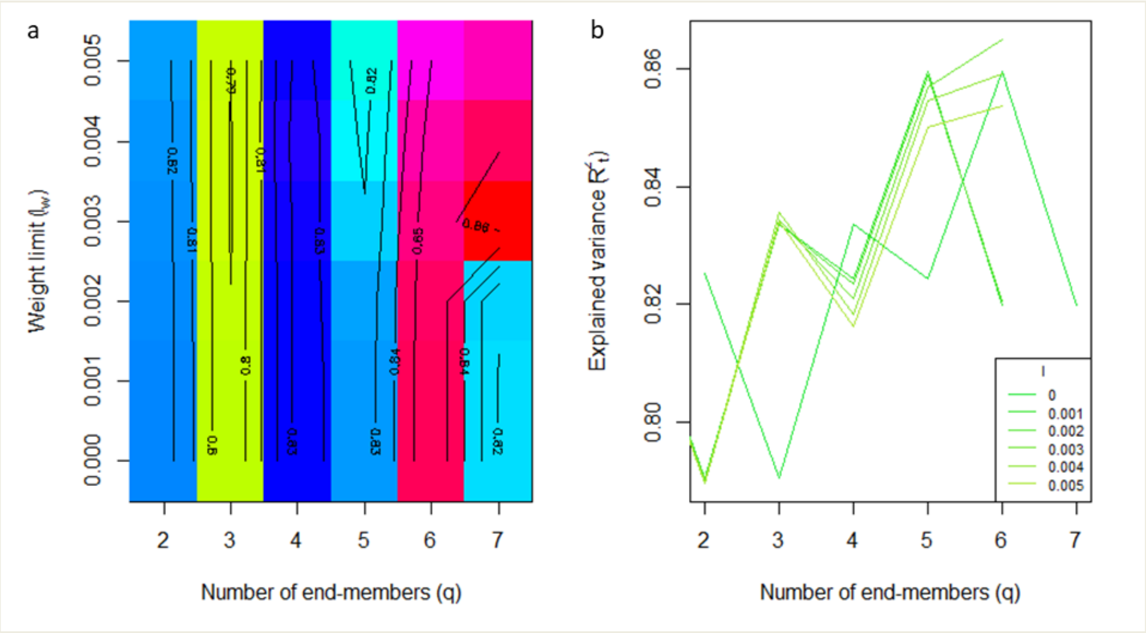

Figure S2. Weight limit (a) and explained variance (b) for the maximum possible number of end-members.

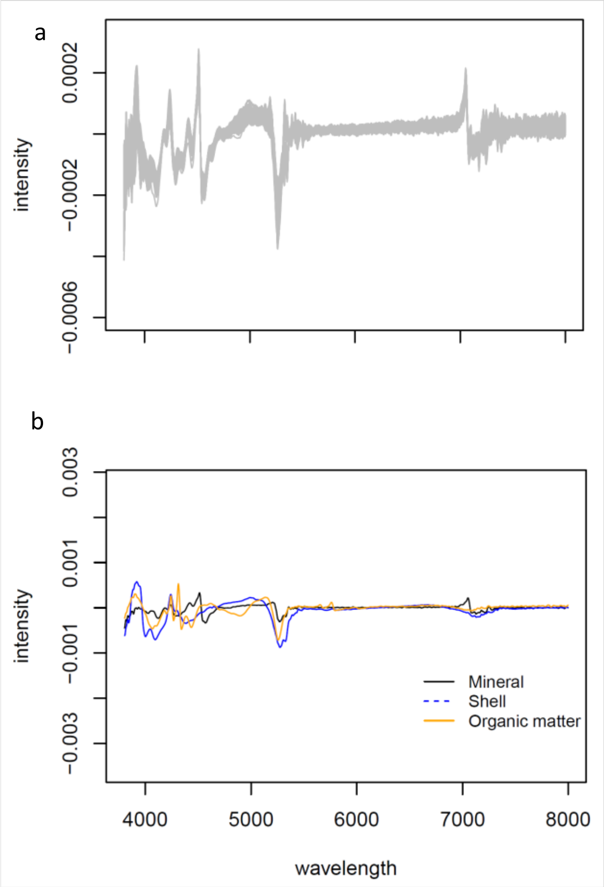

Figure S3. NIRS spectra (a) and coefficients showing the best fit (b).

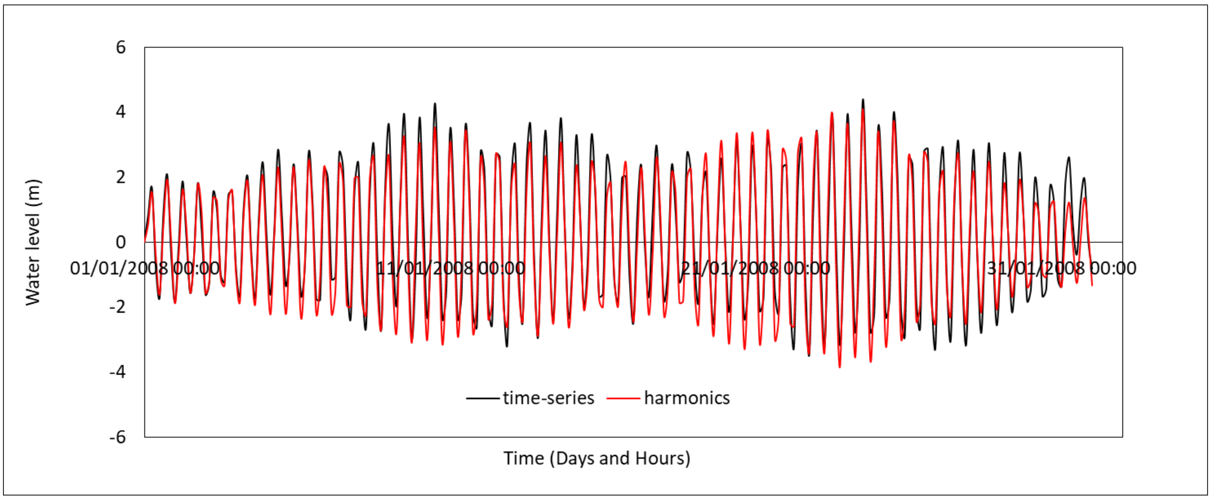

Figure S4. Average water level at ocean boundary for the 2008 scenario forced with time-series and with tidal harmonics.

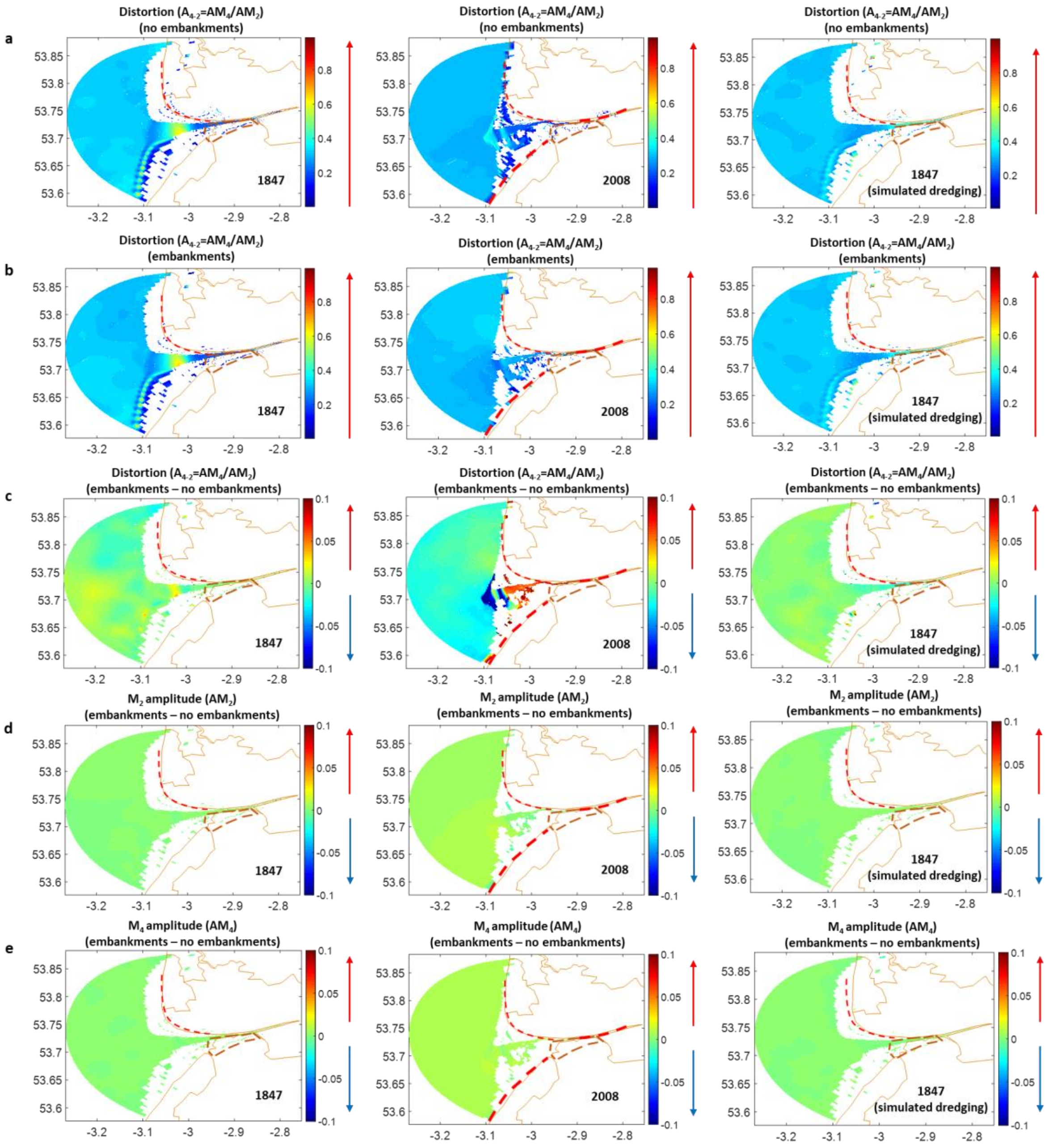

Figure S5. Tidal distortion (A_{4-2}) for the scenarios without embankments (a) and with embankments (b). Where A_{4-2} increases (red arrow), the degree of the asymmetry is more significant. Tidal distortion (A_{4-2}) (c), M2 amplitude (A_{M2}, d) and M4 amplitude (A_{M4}, e) difference between the scenarios with embankments and the scenarios with no embankments. Where A_{4-2} is positive there is an increase in distortion (red arrows) and the degree of the asymmetry change is more significant, where it is negative there is a decrease in distortion (blue arrows) and the degree of the asymmetry change is less significant. The continuous brown *lines represent the land boundary. The dashed brown lines enclose the area of the domain used for the sediment budget calculation of Hesketh Out Marsh (i.e., the salt marsh platform). The dashed red lines indicate the position of the embankments at the time of bathymetric survey.*

Table S1. Radionuclide concentrations, beta and gamma dose-rates, cosmic dose-rate, water content, total dose-rate and Th:U for each OSL sample.

Sample ID	**Depth (m)**	**K (%)**	**U (ppm)**	**Th (ppm)**	**Beta dose-rate (Gy Ka^{-1})**	**Gamma dose-rate (Gy Ka^{-1})**	**Cosmic dose-rate (Gy Ka^{-1})**	**Water content (%)**	**Total dose-rate (Gy Ka^{-1})**
HOM19-2	0.12 ± 0.04	3.82 ± 0.38	15.13 ± 0.32	1.58 ± 0.32	1.40 ± 0.18	1.10 ± 0.07	0.18 ± 0.02	42 ± 2	2.68 ± 0.19
HOM19-3	0.42 ± 0.04	3.85 ± 0.34	13.89 ± 0.28	1.53 ± 0.28	1.45 ± 0.17	1.12 ± 0.06	0.12 ± 0.01	41 ± 2	2.69 ± 0.18
HOM19-4	0.68 ± 0.04	2.78 ± 0.28	11.70 ± 0.30	1.70 ± 0.30	1.34 ± 0.17	0.94 ± 0.06	0.09 ± 0.01	42 ± 2	2.37 ± 0.18
HOM19-5	0.78 ± 0.04	2.24 ± 0.23	9.80 ± 0.24	1.33 ± 0.24	1.09 ± 0.14	0.78 ± 0.05	0.08 ± 0.01	42 ± 2	1.95 ± 0.15
HOM19-6	0.95 ± 0.04	2.19 ± 0.22	8.45 ± 0.22	1.21 ± 0.22	1.07 ± 0.13	0.75 ± 0.05	0.07 ± 0.01	41 ± 2	1.88 ± 0.14
HOM19-7	1.37 ± 0.04	1.64 ± 0.18	6.49 ± 0.19	0.97 ± 0.19	0.82 ± 0.11	0.57 ± 0.04	0.05 ± 0.01	34 ± 2	1.44 ± 0.12
HOM19-8	1.61 ± 0.04	1.70 ± 0.19	5.34 ± 0.18	0.88 ± 0.18	0.76 ± 0.11	0.51 ± 0.04	0.04 ± 0.004	33 ± 2	1.31 ± 0.11
HOM19-9	1.85 ± 0.04	1.51 ± 0.19	5.80 ± 0.20	0.97 ± 0.20	0.82 ± 0.12	0.55 ± 0.04	0.03 ± 0.003	33 ± 2	1.40 ± 0.13
HOM19-10	2.46 ± 0.04	1.30 ± 0.17	4.46 ± 0.18	0.85 ± 0.18	0.71 ± 0.11	0.45 ± 0.04	0.02 ± 0.002	33 ± 2	1.18 ± 0.12
HOM19-11	2.71 ± 0.04	1.12 ± 0.15	4.33 ± 0.18	0.90 ± 0.18	0.71 ± 0.11	0.44 ± 0.04	0.02 ± 0.002	33 ± 2	1.17 ± 0.11
HOM19-12	3.02 ± 0.04	1.11 ± 0.15	4.03 ± 0.17	0.87 ± 0.18	0.71 ± 0.11	0.43 ± 0.04	0.02 ± 0.002	33 ± 2	1.16 ± 0.12

Table S2. Number of aliquots accepted, equivalent dose, total dose-rate and age for each OSL sample.

Sample ID	**Depth (m)**	**Aliquots accepted for D_e/Aliquots measured**	**D_e (Gy)**	**Total dose-rate (Gy Ka^{-1})**	**Age (ka)**	**Age (years ago before 2019)**	**Age (years AD)**
HOM19-2	0.12 ± 0.04	46/48	0.21 ± 0.02	2.68 ± 0.19	0.078 ± 0.009	78 ± 9	1941 ± 9
HOM19-3	0.42 ± 0.04	46/48	0.18 ± 0.02	2.69 ± 0.18	0.067 ± 0.009	67 ± 9	1952 ± 9
HOM19-4	0.68 ± 0.04	14/14	0.27 ± 0.05	2.37 ± 0.18	0.114 ± 0.23	114 ± 23	1905 ± 23
HOM19-5	0.78 ± 0.04	47/48	0.21 ± 0.02	1.95 ± 0.15	0.108 ± 0.013	108 ± 13	1911 ± 13
HOM19-6	0.95 ± 0.04	47/48	0.25 ± 0.02	1.88 ± 0.14	0.133 ± 0.015	133 ± 15	1886 ± 15
HOM19-7	1.37 ± 0.04	47/48	0.38 ± 0.02	1.44 ± 0.12	0.264 ± 0.026	264 ± 26	1755 ± 26
HOM19-8	1.61 ± 0.04	45/48	0.29 ± 0.02	1.31 ± 0.11	0.222 ± 0.025	222 ± 25	1797 ± 25
HOM19-9	1.85 ± 0.04	46/48	0.32 ± 0.03	1.40 ± 0.13	0.229 ± 0.03	229 ± 30	1790 ± 30
HOM19-10	2.46 ± 0.04	48/48	0.24 ± 0.02	1.18 ± 0.12	0.203 ± 0.026	203 ± 26	1816 ± 26
HOM19-11	2.71 ± 0.04	48/48	0.23 ± 0.02	1.17 ± 0.11	0.197 ± 0.026	197 ± 26	1822 ± 26
HOM19-12	3.02 ± 0.04	48/48	0.26 ± 0.02	1.16 ± .12	0.225 ± 0.029	225 ± 29	1794 ± 29

Appendix II – Supplementary material to Chapter 4

Table S3. Exceedance probabilities (p) of storm surge heights along the UK shoreline with return period (RP) of 2 years, 10 years, 25 years, 50 years, 100 years and 500 years. Tidal level records from 1952 to 2015 have been downloaded from the British Oceanographic Data Centre and residuals have been fitted using a generalized extreme values distribution to obtain the heights in the table (Gao and Adcock, 2016).

Station Name	***p*=0.5 (RP=2)**	***p*=0.1 (RP=10)**	***p*=0.04 (RP=25)**	***p*=0.02 (RP=50)**	***p*=0.01 (RP=100)**	***p*=0.002 (RP=500)**
ABERDEEN	0.88	1.11	1.18	1.22	1.25	1.3
AVONMOUTH	1.78	2.37	2.6	2.75	2.89	3.14
BANGOR	1	1.27	1.33	1.36	1.39	1.42
BARMOUTH	1.39	2.05	2.36	2.58	2.8	3.27
BOURNEMOUTH	0.81	1.01	1.08	1.13	1.17	1.25
CROMER	1.53	2.05	2.22	2.32	2.4	2.54
DEVONPORT	0.78	0.93	0.98	1	1.02	1.06
DOVER	1.23	1.55	1.68	1.76	1.84	1.99
FELIXSTOWE	1.58	2.18	2.42	2.59	2.73	3.02
FISHGUARD	0.81	1.06	1.18	1.26	1.35	1.54
HARWICH	1.46	1.88	2.04	2.15	2.24	2.4
HEYSHAM	1.74	2.28	2.45	2.54	2.62	2.74
HINKLEY	1.51	1.95	2.12	2.23	2.33	2.51
HOLYHEAD	0.97	1.24	1.34	1.4	1.44	1.52
ILFRACOMBE	1.07	1.24	1.28	1.29	1.3	1.31
ISLAY	1.07	1.35	1.45	1.52	1.58	1.68

JERSEY	1.07	1.31	1.39	1.44	1.48	1.54
KINLOCHBERVIE	1.06	1.43	1.6	1.73	1.84	2.09
.LEITH	1.06	1.35	1.42	1.46	1.5	1.54
LERWICK	0.57	0.71	0.77	0.81	0.84	0.9
LIVERPOOL	1.76	2.24	2.37	2.44	2.5	2.57
LOWESTOFT	1.52	2.04	2.25	2.4	2.53	2.78
MILFORD HAVEN	0.91	1.19	1.3	1.36	1.42	1.54
MILLPORT	1.35	1.66	1.78	1.86	1.93	2.07
MORAY FIRTH	0.83	1.26	1.61	1.96	2.41	4.01
MUMBLES	1.1	1.56	1.78	1.94	2.1	2.45
NEWLYN	0.69	0.88	0.96	1.02	1.07	1.19
NEWHAVEN	0.87	1.05	1.12	1.16	1.2	1.27
NEWPORT	1.74	2.29	2.58	2.79	3	3.51
PORTPATRICK	1.11	1.44	1.54	1.59	1.63	1.69
PORTRUSH	1.06	1.21	1.24	1.25	1.26	1.26
PORTSMOUTH	0.84	1.08	1.23	1.34	1.47	1.79
SHEERNESS	1.75	2.4	2.63	2.78	2.9	3.11
ST MARY’S	0.6	0.77	0.83	0.87	0.91	0.98
STORNOWAY	0.84	1.07	1.15	1.21	1.26	1.35
TOBERMORY	1.21	1.45	1.5	1.52	1.53	1.54
ULLAPOOL	0.92	1.44	1.79	2.08	2.43	3.42
WEYMOUTH	0.78	0.94	0.99	1.03	1.05	1.1
WHITBY	1.2	1.8	2.2	2.56	2.98	4.2
WICK	0.8	1.01	1.09	1.14	1.18	1.25
WORKINGTON	1.54	1.9	2.05	2.15	2.24	2.42

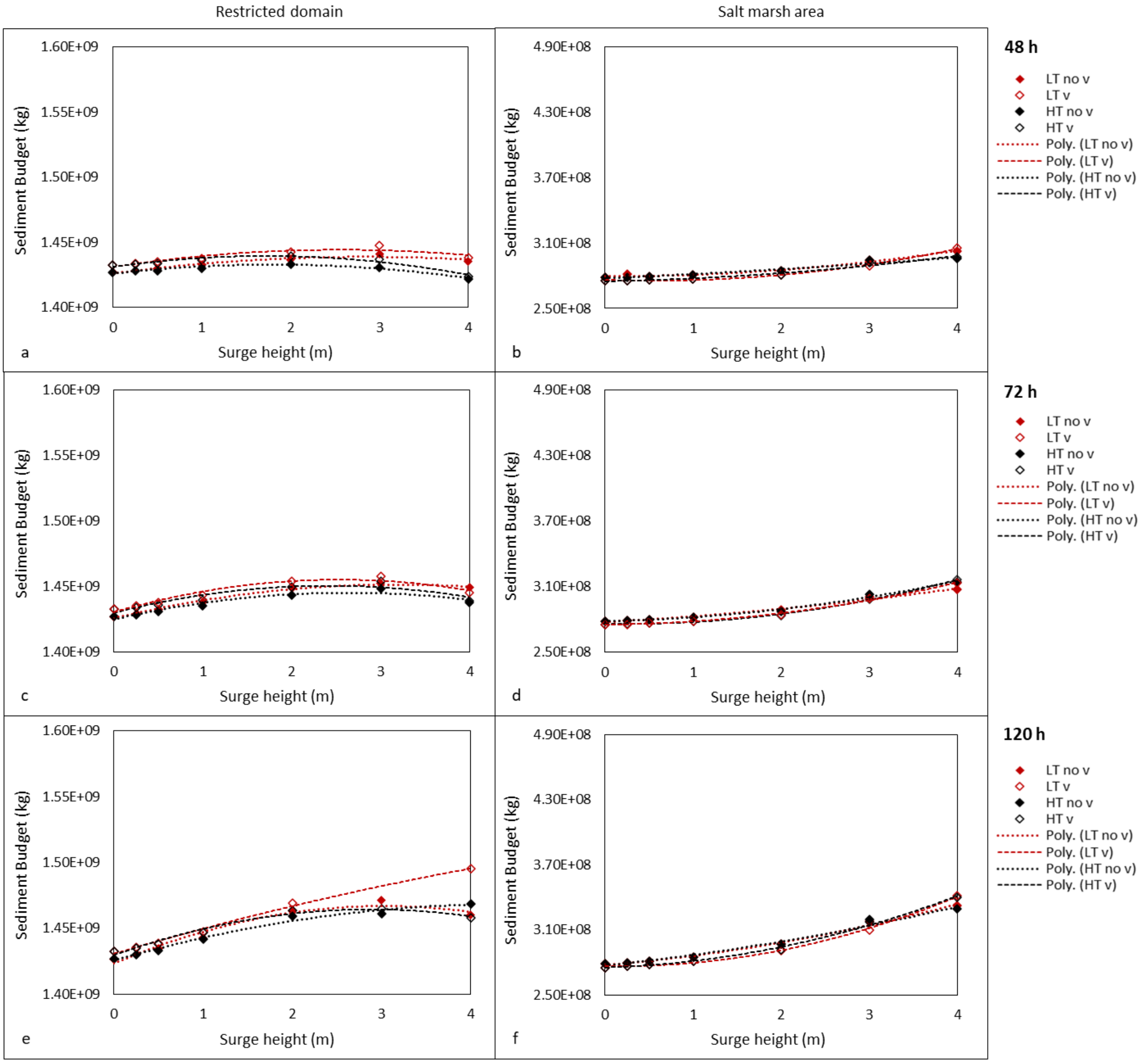

Figure S6. Sediment budget integrated across the entire area of the restricted domain (a, c, e) and the salt marsh (b, d, f) for each surge height, for surges occurring at high tide (HT) and low tide (LT) without vegetation (no v) and with vegetation (v), for surges of different durations occurring at neap tide; (see Figure 23 for surges occurring at spring tide); scenarios run using an ideal only-mud bed composition.

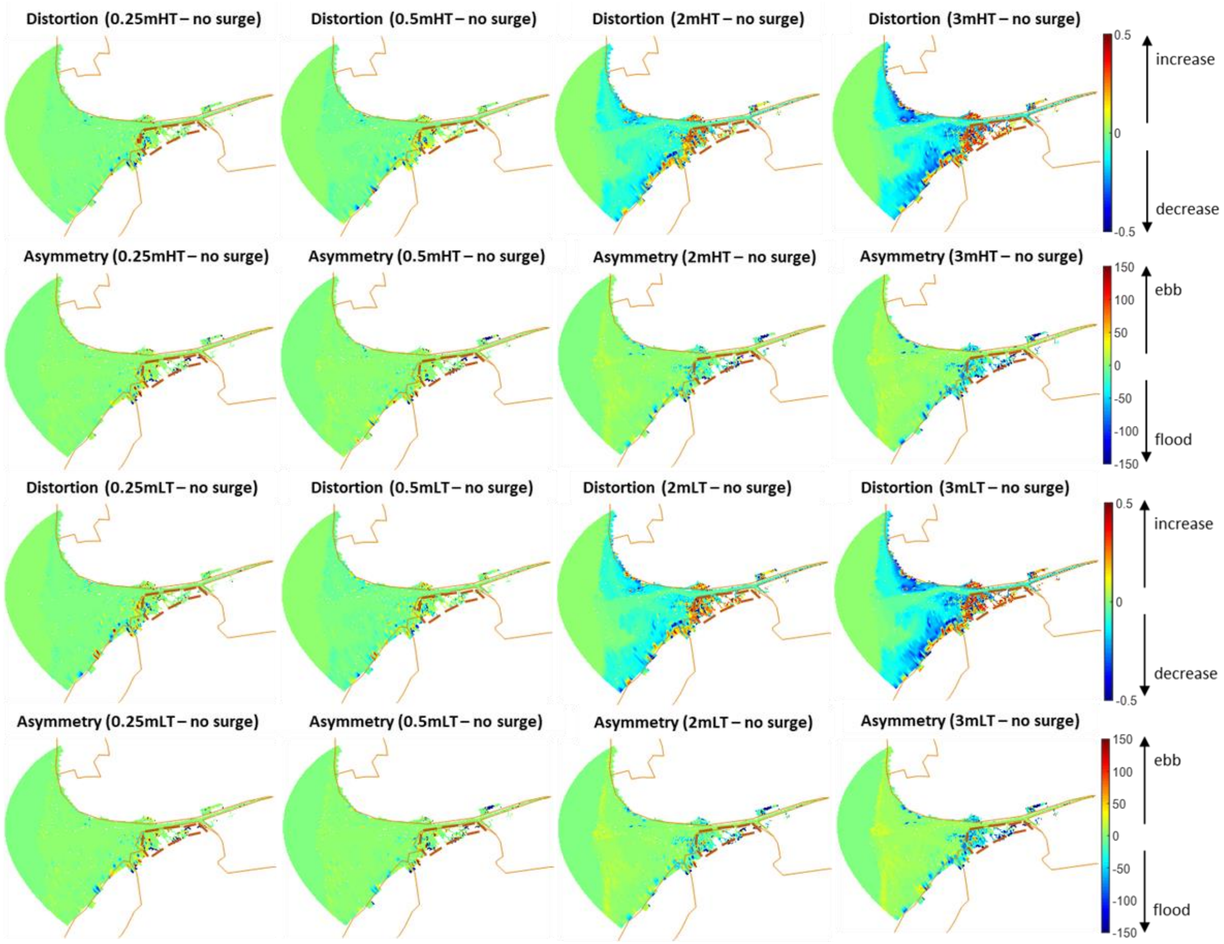

Figure S7. Difference between tidal distortion (A_{4-2}) and asymmetry ($\Delta\theta$) of 0.25 m, 0.5 m, 2 m and 3 m surge scenarios and the no surge scenario at current sea-level (see Figure 27 from for the 1 m and 4 m scenarios). When $\Delta\theta$ is positive there is an increase in ebb dominance with respect to the no surge scenario, when it is negative there is an increase in flood dominance; when A_{4-2} is positive, the degree of the asymmetry is more significant, vice versa when it is negative. The continuous brown lines correspond to the land boundary. The area enclosed by the brown dashed lines is the salt marsh.

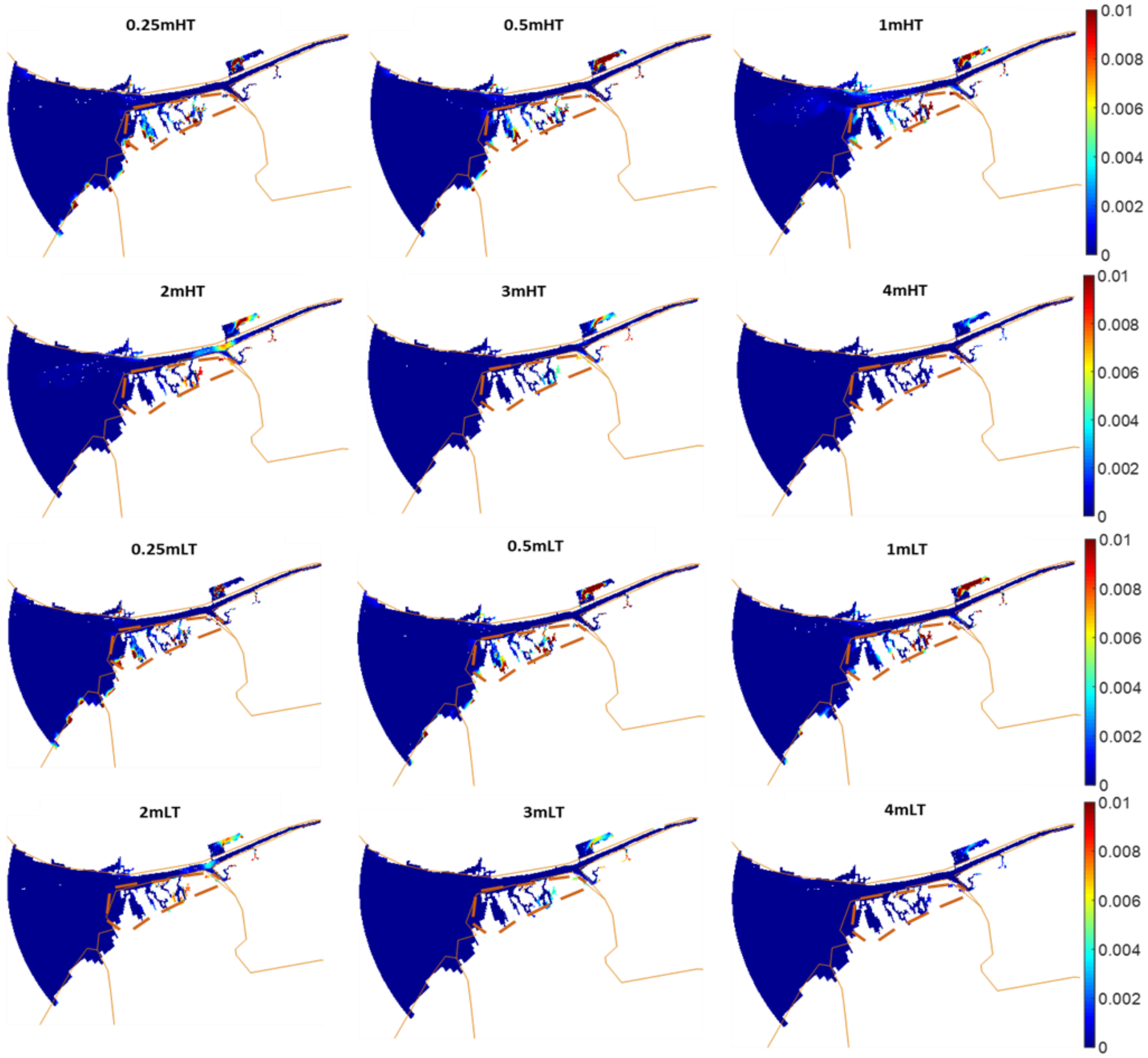

Figure S8. Difference between bottom friction in all surge scenarios and the no surge scenario during flood phase. Calculation of bottom friction followed [*Parker et al. (2007)*]*. The continuous brown lines correspond to the land boundary. The area enclosed by the brown dashed lines is the salt marsh.*

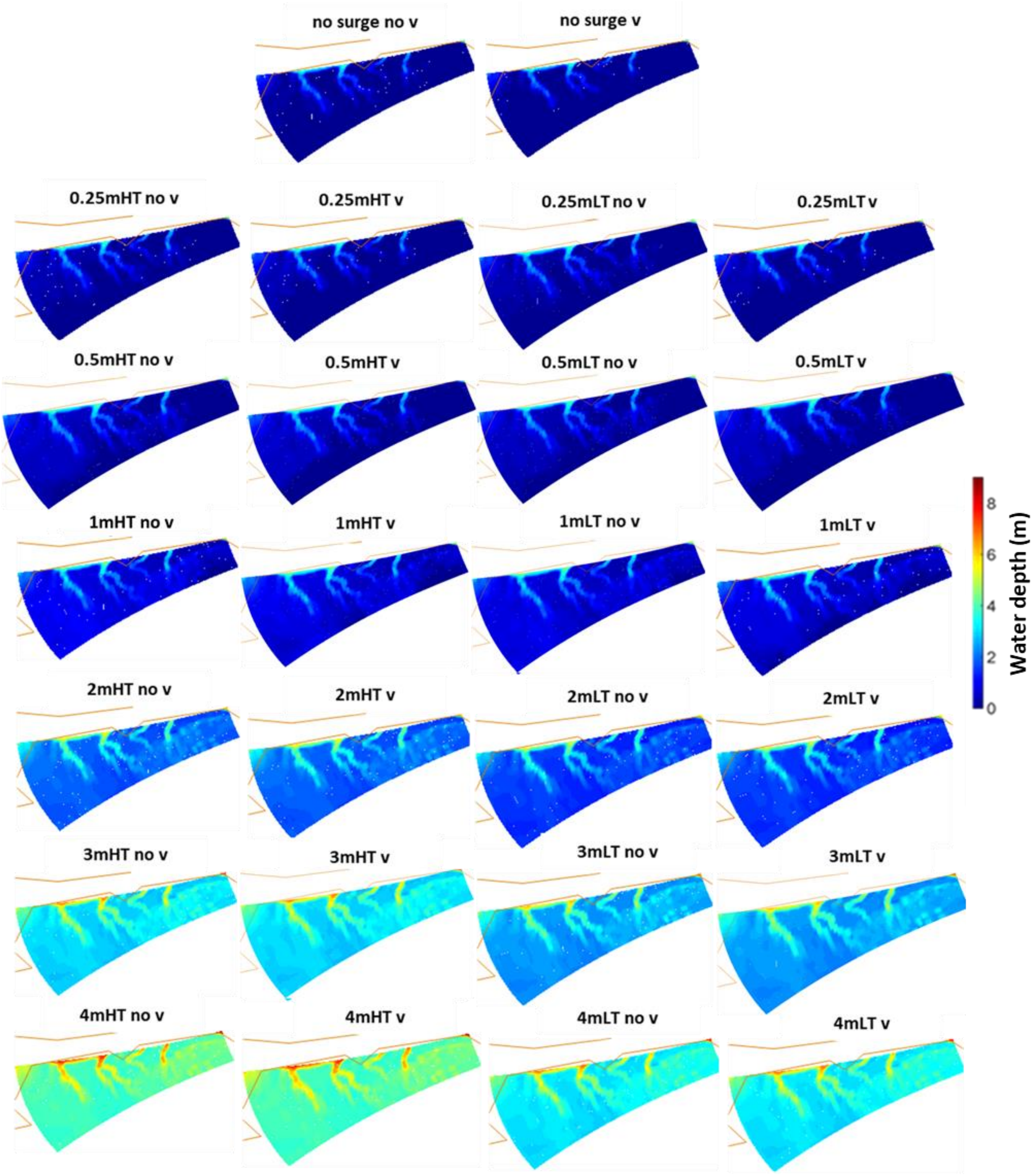

Figure S9. Water depth on the salt marsh platform during flood phase for vegetated and hypothetical non-vegetated scenarios for all surge scenarios. The continuous brown lines correspond to the land boundary.

Appendix III – Supplementary material to Chapter 5

Figure S10. Panoramic of the starting points of the transects HOM-1 (marsh edge) and HOM-2 (creek bank) obtained with a FARO 3D laser scanner Focus X330 and photos displaying the locations of the sediment traps along each transect.

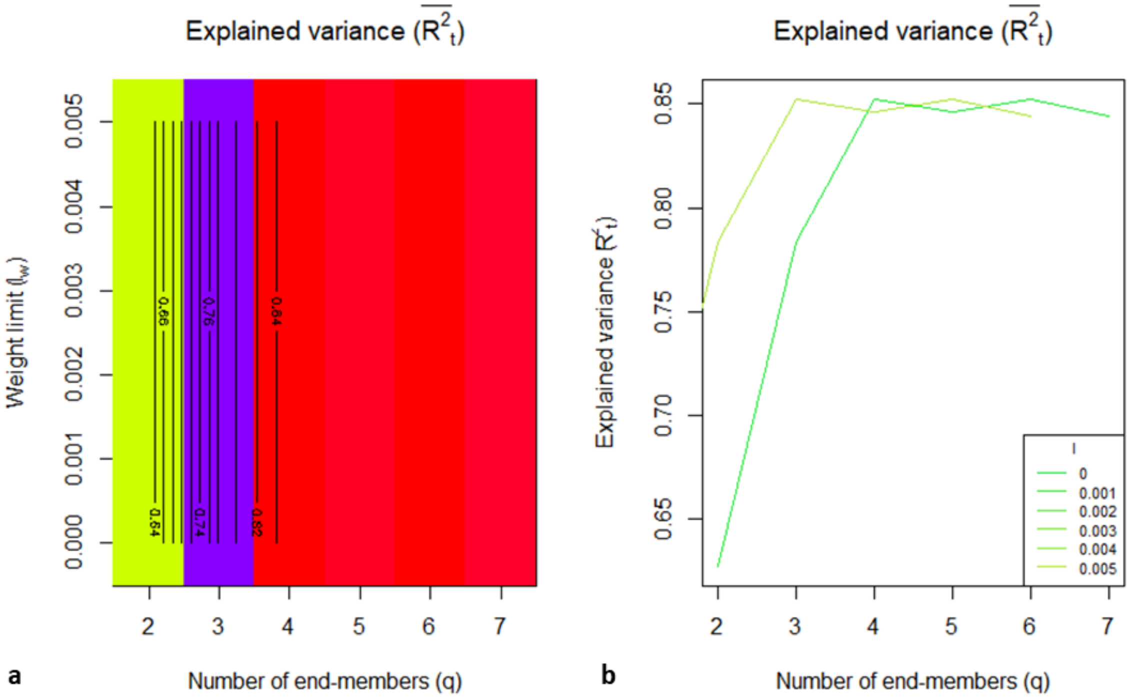

Figure S11. Weight limit (a) and explained variance (b) for the maximum possible number of end-members.

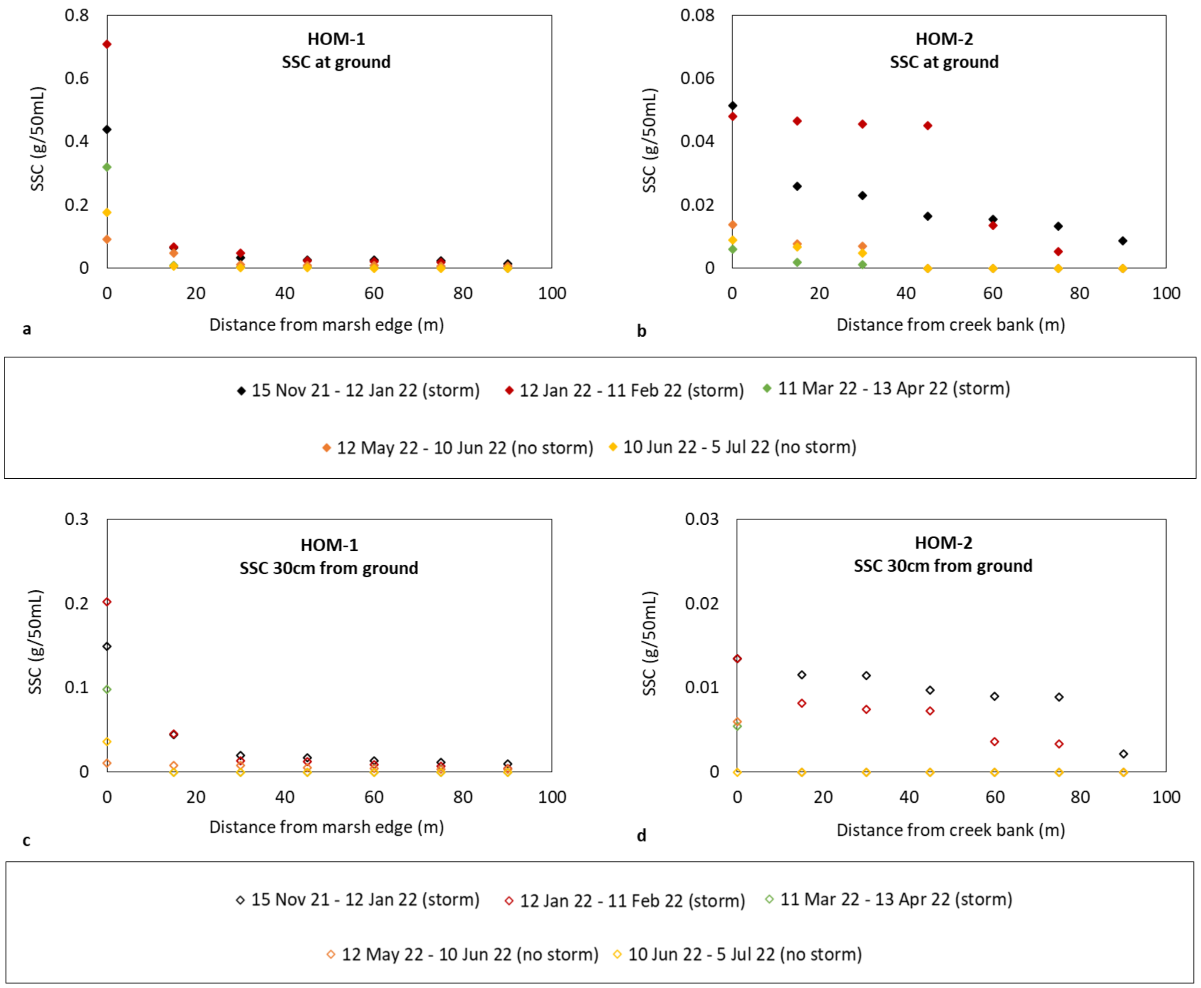

Figure S12. SSC (g/day) profile with distance from the marsh edge (a) and the creek bank (b), at ground level and at 30 cm from the ground, relative to stormy and non-stormy periods (see Figure 34 for the profiles relative to Feb-Mar and Apr-May).

Appendix IV – Supplementary material to Chapter 6

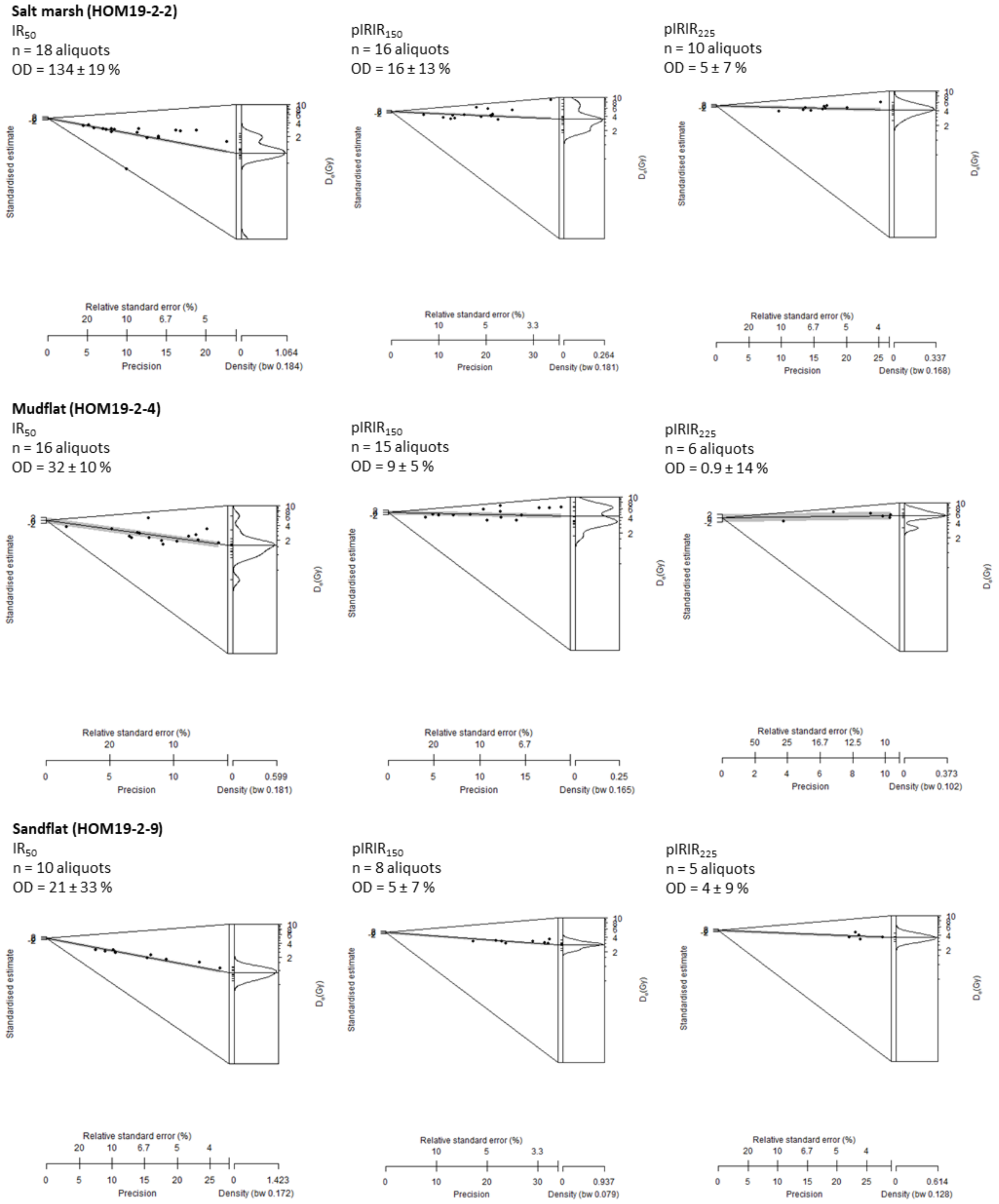

Figure S13. Abanico plots showing representative D_e density distributions of the single aliquots for IR_{50}, $pIRIR_{150}$ and $pIRIR_{225}$ signals of salt marsh, mudflat and sandflat, for selected samples extracted from HOM19-2, incorporating the results of the central age model (CAM).

Marsh pre-storm (HOM21-1)

IR$_{50}$
n = 23 aliquots
OD = 46 ± 17 %

pIRIR$_{150}$
n = 23 aliquots
OD = 20 ± 4 %

pIRIR$_{225}$
n = 15 aliquots
OD = 12 ± 6 %

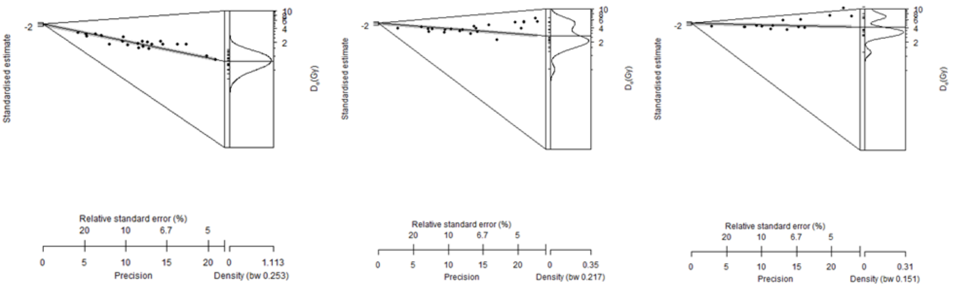

Marsh post-storm (HOM22-1)

IR$_{50}$
n = 24 aliquots
OD = 34 ± 25 %

pIRIR$_{150}$
n = 23 aliquots
OD = 15 ± 3 %

pIRIR$_{225}$
n = 14 aliquots
OD = 9 ± 5 %

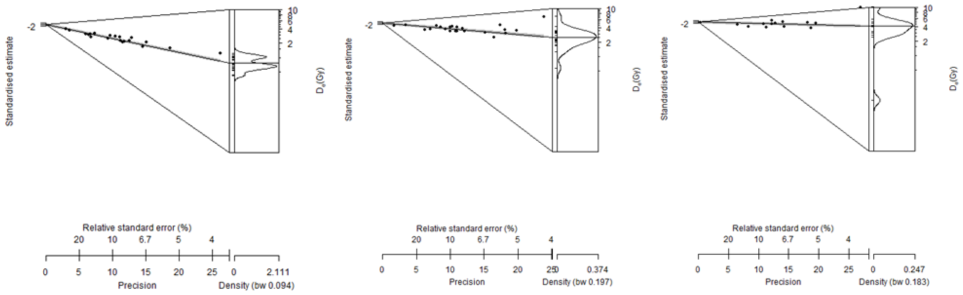

Mudflat pre-storm (HOM21-2)

IR$_{50}$
n = 24 aliquots
OD = 30 ± 50 %

pIRIR$_{150}$
n = 23 aliquots
OD = 11 ± 3 %

pIRIR$_{225}$
n = 15 aliquots
OD = 8 ± 6 %

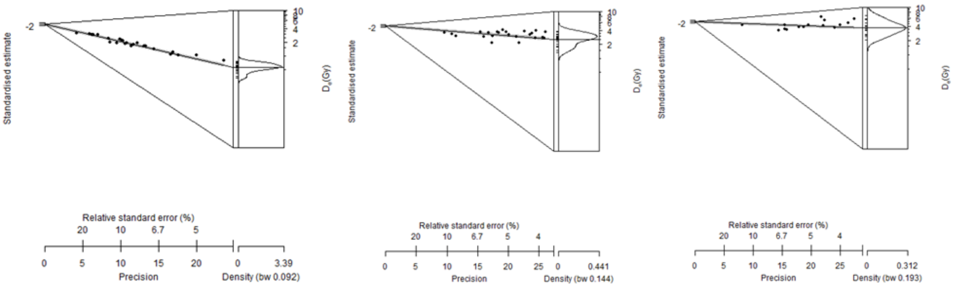

Mudflat post-storm (HOM22-2)

IR$_{50}$
n = 23 aliquots
OD = 93 ± 20 %

pIRIR$_{150}$
n = 20 aliquots
OD = 52 ± 4 %

pIRIR$_{225}$
n = 17 aliquots
OD = 26 ± 7 %

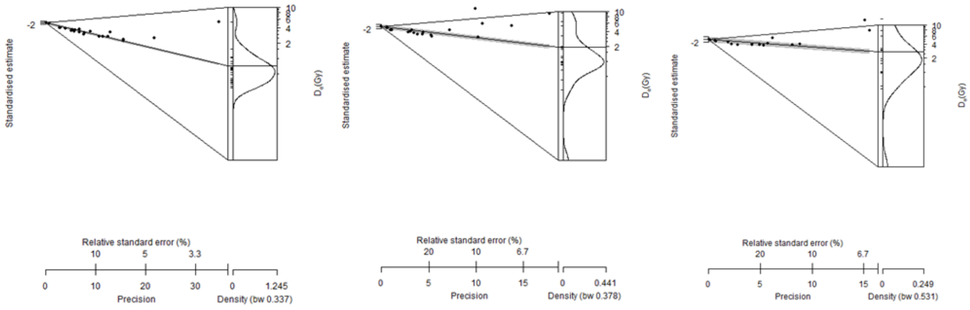

Figure S14. Abanico plots showing D_e density distributions of the single aliquots for IR$_{50}$, pIRIR$_{150}$ and pIRIR$_{225}$ signals of HOM21-1 and HOM21-2 (pre-storm) and HOM22-1 and HOM22-2 (post-storm), incorporating the results of the central age model (CAM).

Salt marsh (HOM19-2-3)

IR$_{50}$
n = 30 aliquots
OD = 49 ± 11 %

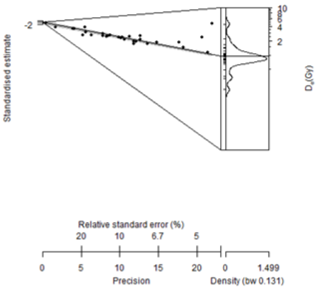

pIRIR$_{150}$
n = 26 aliquots
OD = 18 ± 4 %

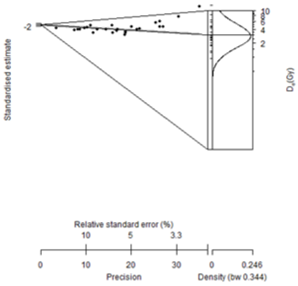

pIRIR$_{225}$
n = 10 aliquots
OD = 12 ± 8 %

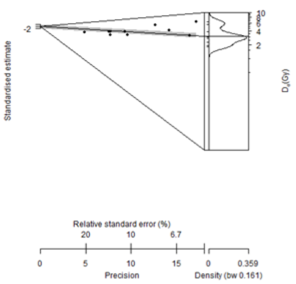

Mudflat (HOM19-2-5)

IR$_{50}$
n = 20 aliquots
OD = 26 ± 14 %

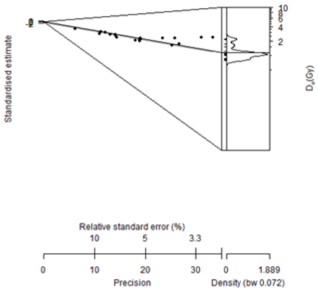

pIRIR$_{150}$
n = 20 aliquots
OD = 10 ± 3 %

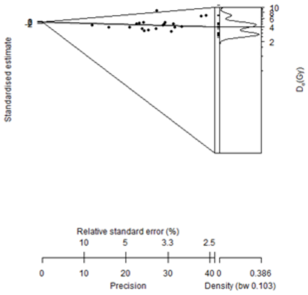

pIRIR$_{225}$
n = 7 aliquots
OD = 4 ± 5 %

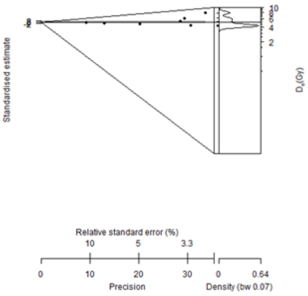

Mudflat (HOM19-2-6)

IR$_{50}$
n = 25 aliquots
OD = 30 ± 20 %

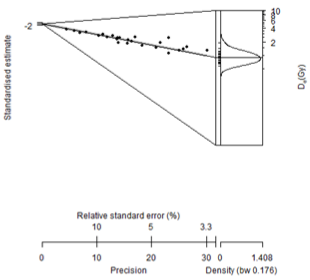

pIRIR$_{150}$
n = 23 aliquots
OD = 12 ± 3 %

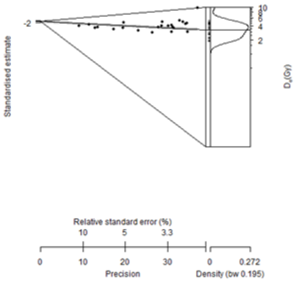

pIRIR$_{225}$
n = 13 aliquots
OD = 7 ± 6 %

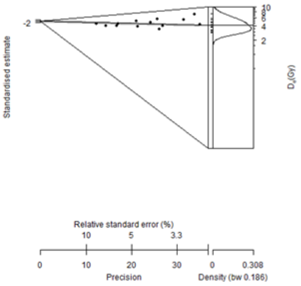

Sandflat (HOM19-2-7)

IR$_{50}$
n = 20 aliquots
OD = 48 ± 25 %

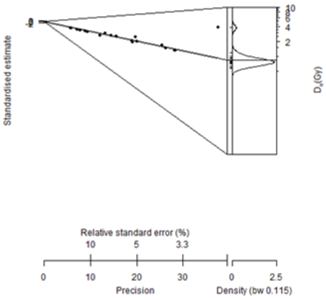

pIRIR$_{150}$
n = 19 aliquots
OD = 15 ± 5 %

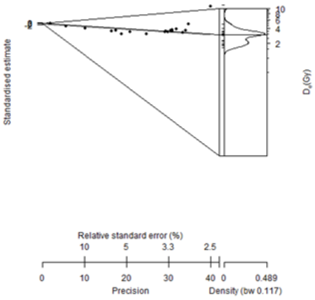

pIRIR$_{225}$
n = 9 aliquots
OD = 12 ± 7 %

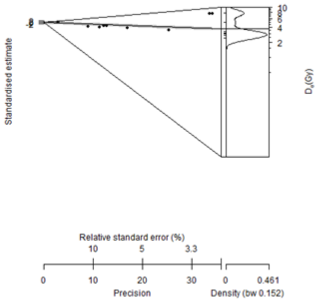

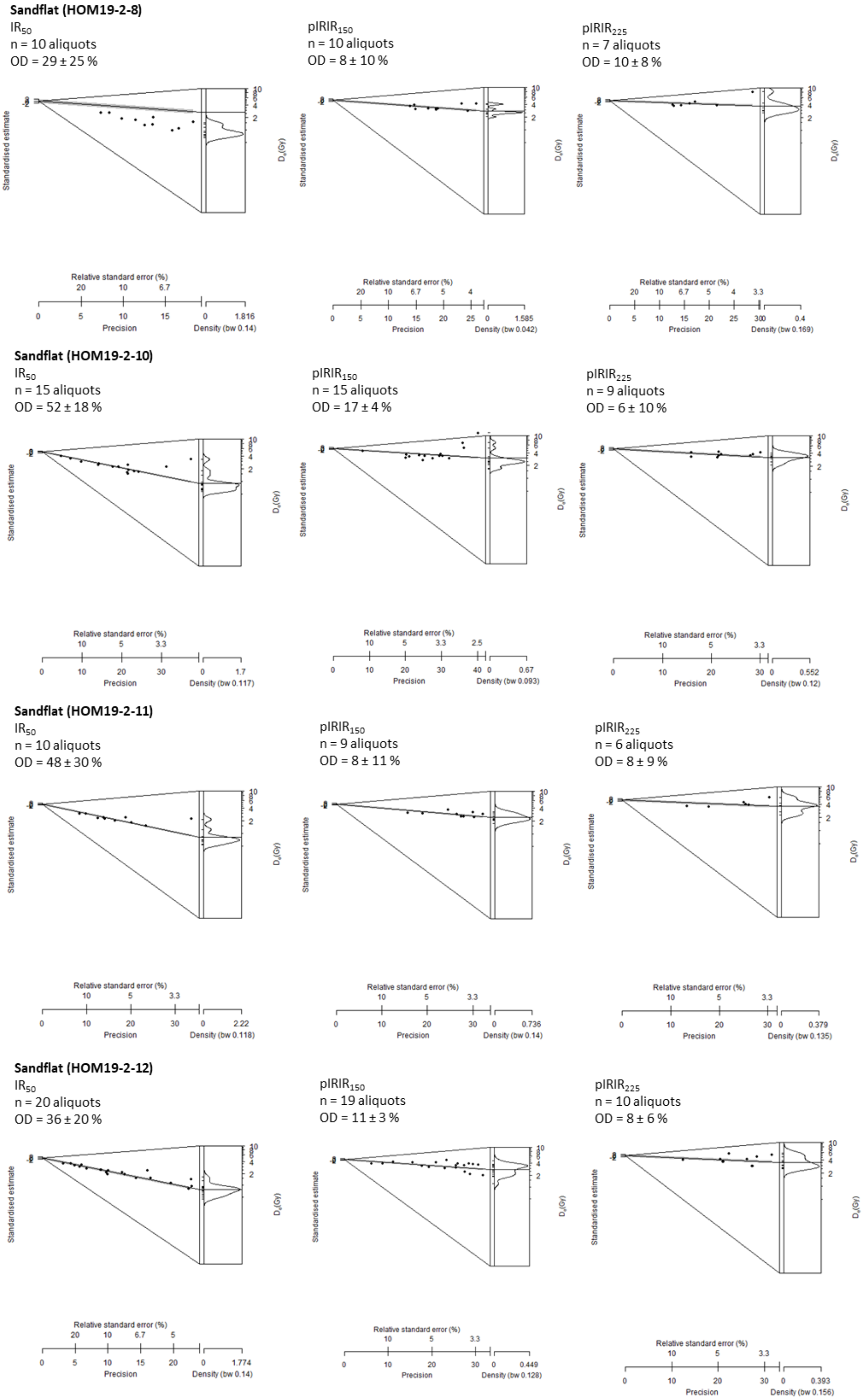

Figure S15. Abanico plots showing D_e distributions of the single aliquots for IR_{50}, $pIRIR_{150}$ and $pIRIR_{225}$ signals for the remaining samples extracted from HOM19-2, incorporating the results of the central age model (CAM).

Appendix V – Research outputs

1. Ongoing research

Pago Pago M., Li X., **Pannozzo N.** et al., 2023. Investigating the effect of managed realignment on estuary circulation with changing climate. (Role: External Advisor on the National Oceanography Centre directed project titled "Co-Opt - Resilient coasts: optimising co-benefit solutions" – numerical modelling sub-division).

Smedley R.K., Plater A.J., **Pannozzo N.**, 2023. OSL and IRSL signals unveil the impact of a tsunami event on the development of a back-barrier salt marsh (Role: Co-Investigator).

Whitworth D., **Pannozzo N.**, 2023. Investigating the effect of storms on salt marshes and sand dunes using drones (Role: External Advisor on RGS funded outreach project).

2. Papers in review/preparation

Pannozzo N., Leonardi N., 2023. Coastal sand dunes response to increasing storminess: lessons from the Sefton Coast, UK, in preparation for submission to *Earth Surface Processes and Landforms*.

Pannozzo N., Leonardi N., 2023. Brief communication: Untangling public knowledge and perception on the implementation of nature-based solutions for coastal protection, submitted to *Natural Hazards and Earth System Sciences*.

3. Published papers

Pannozzo N., Leonardi N., Carnacina I., Smedley R. K., 2023. Storm sediment contribution to salt marsh accretion and expansion. *Geomorphology*, 430: 108670.

Pannozzo N., Smedley R. K., Plater A. J., Carnacina I., Leonardi N., 2023. Novel luminescence diagnosis of storm deposition across intertidal environments. *Science of the Total Environment*, 867: 161461.

Pannozzo N., Smedley R. K., Chiverrell R. C., Carnacina I., Leonardi N., 2022. An integration of numerical modelling and paleoenvironmental analysis reveals the effects of embankment construction on long-term salt marsh accretion. *Journal of Geophysical Research: Earth Surface*, 127: e2021JF006524.

Pannozzo N., Leonardi N., Carnacina I., Smedley R. K., 2021. Dataset of results from numerical simulations of increased storm intensity in an estuarine salt marsh system. *Data in Brief*, 38 (6): 107336.

Pannozzo N., Leonardi N., Carnacina I., Smedley R. K., 2021. Salt marsh resilience to sea-level rise and increased storm intensity. *Geomorphology*, 389 (4): 107825.

- **Nature's Research Highlights**, 2021. *Nature Reviews Earth & Environment*, 2 (7): 448-448.

4. Conference papers

Pannozzo N., Leonardi N., Carnacina I., Smedley R., 2021. An investigation on salt marsh resilience to sea-level rise and increased storm intensity. International Conference on Coastal Dynamics, TU Delft (online).

5. Conference presentations

Pannozzo N., Leonardi N., Carnacina I., Smedley R., 2022. Numerical and field investigations unveil the response of salt marshes to storm sediment input. American Geophysical Union Fall Meeting, Chicago*.

Pannozzo N., Smedley R., Chiverrell R. C., Carnacina I., Leonardi N., 2022. Investigating salt marsh resilience to external disturbance. UK Sea Level and Coasts Meeting. University of Durham (Durham)*.

Pannozzo N., Smedley R., Plater A., Carnacina I., Leonardi N., 2022. Testing the use of luminescence properties as tracer for differential modes of deposition and storm activity in intertidal settings. UK Luminescence and Electron Spin Resonance Dating Conference. Royal Holloway University of London (London)*.

Pannozzo N., Smedley R., Chiverrell R. C., Carnacina I., Leonardi N., 2022. Understanding salt marsh resilience to changes in external disturbance. European Geoscience Union General Assembly, Vienna*.

Pannozzo N., Smedley R., Carnacina I., Leonardi N., 2022. Investigating the resilience of salt marshes to external disturbance. Ocean Sciences Meeting, online*.

Pannozzo N., Smedley R., Carnacina I., Leonardi N., 2021. Understanding the resilience of salt marshes to changes in external forcings. American Geophysical Union Fall Meeting, New Orleans.

Pannozzo N., Smedley R., Plater A., Carnacina I., Leonardi N., 2021. Testing the use of luminescence as sediment tracer in estuarine salt marshes. International Luminescence and Electron Spin Resonance Dating Conference, online.

Pannozzo N., Leonardi N., Carnacina I., Smedley R., 2021. An investigation on salt marsh resilience to sea-level rise and increased storm intensity. International Conference on Coastal Dynamics, TU Delft (online).

Pannozzo N., Leonardi N., Carnacina I., Smedley R., 2021. Salt marsh resilience to sea-level rise and increased storm intensity. European Geoscience Union General Assembly, online.

Pannozzo N., Leonardi N., Carnacina I., Smedley R., 2021. Salt marsh resilience to sea-level rise and increased storm intensity. UK Young Coastal Scientists and Engineers Conference, online*.

Pannozzo N., Smedley R., Chiverrell R. C., Leonardi N., 2019. Salt marshes response to environmental change. UK Luminescence and Electron Spin Resonance Dating Conference, DTU Denmark (Copenhagen).

*This work has been presented in the form of a talk.